UNIVERSIDADE FEDERAL DO RIO GRANDE DO SUL
ESCOLA DE ENGENHARIA
PROGRAMA DE PÓS-GRADUAÇÃO EM ENGENHARIA CIVIL

Hugo Carlos Scheuermann Filho

ADJUSTED POROSITY/CEMENT INDEX: MECHANICAL BEHAVIOR AND MICROSTRUCTURE OVER A WIDE RANGE OF DOSAGES

Porto Alegre
february 2022

HUGO CARLOS SCHEUERMANN FILHO

ADJUSTED POROSITY/CEMENT INDEX: MECHANICAL BEHAVIOR AND MICROSTRUCTURE OVER A WIDE RANGE OF DOSAGES

Thesis presented to the Programa de Pós-Graduação em Engenharia Civil of Universidade Federal do Rio Grande do Sul as part of the requirements for the Degree of Doctor in Engineering

Supervisor: Nilo Cesar Consoli

Porto Alegre
february 2022

HUGO CARLOS SCHEUERMANN FILHO

ADJUSTED POROSITY/CEMENT INDEX: MECHANICAL BEHAVIOR AND MICROSTRUCTURE OVER A WIDE RANGE OF DOSAGES

This Doctoral Thesis was assessed by the Board of Examiners and was considered suitable for the obtainment of the title DOCTOR IN ENGINEERING, in the field of Geotechnical Engineering. Its final version was approved by the supervising professor and the Programa de Pós Graduação em Engenharia Civil (PPGEC) of Universidade Federal do Rio Grande do Sul.

Porto Alegre, 25th February 2022.

Prof. Nilo Cesar Consoli
Ph.D Concórdia University, Canadá
Supervisor

Prof. Lucas Festugato
D. Eng. UFRGS, Brazil
PPGEC/UFRGS Coordinator

BOARD OF EXAMINERS

Profª. Beatrice Baudet
University College London
PhD, City University London, United Kingdom

Prof. Erdin Ibraim
University of Bristol
PhD, INSA/ENTPE Lyon, France

Prof. Lucas Festugato
UFRGS
D. Eng. UFRGS, Brazil

Profª. Monica Prezzi
Purdue University
PhD, University of Carlifornia, Berkeley, USA

ACKNOWLEDGMENTS

This thesis results from major contributions of previous works and, as well, from the aid of several people which have assisted me throughout the whole process. As a reason, I must thank them all and apologize if I have forgotten to mention anyone.

I thank very much professor Nilo Cesar Consoli for all the guidance, assistance and opportunities which I have received since my undergrad period.

I would like to acknowledge professor Lucas Festugato for all the valuable support I have received on the laboratory testing during this entire research and, as well, for the lab's structure which comprehends the finest equipment for geotechnical testing. This applies, as well, to professor Sergio V. Marques.

I shall thank my fellow Gustavo Dias Miguel for assisting me during the soil collection and, as well, throughout the triaxial tests. His work on the laboratory was of prime importance for my research and for several others.

I appreciate the good partnership which I have developed with my friends from LEGG: Gonçalo, Dudi, João Victor, Eclesielter, Mariana Carretta, Lennon, Estéfano, Dionatas, Renato, among others.

I am grateful for all my family support throughout this research and, as well, for the support of my girlfriend Vanessa.

Finally, I shall thank CNPq for the scholarship which was of immense importance during this research.

If I have seen further, it is by standing upon the shoulders
of giants
Isaac Newton

Eu tive que subir
Lá no alto
Para ver
Sebastião Rodrigues Maia

ABSTRACT

The adjusted porosity/cement index has shown to be a useful tool when a rational dosage methodology for soil-cement purposes is sought. It inputs the role of the compactness, through the molding porosity value (η), and the amount of cement, via the volumetric cement content (C_{iv}), into a single dimensionless parameter. Such index, and its derivations, have already been successfully used to model a series of mechanical characteristics of compacted soil-cement specimens, such as unconfined compressive strength, split tensile strength, initial shear modulus and durability. Soils of distinct natures have, so far, being tested through this approach. Moreover, by establishing a specific $\eta/(C_{iv})^c$ value, it is expected that a similar mechanical response can be obtained regardless of the adopted dosage. Still, such assertion has not yet been verified for a broad range of different dosages within specific $\eta/(C_{iv})^c$ values. Present research intends to address this gap by setting seven specific $\eta/(C_{iv})^{0.28}$ values (i.e. 45, 40, 30, 35, 25, 22.5 and 20) for compacted Botucatu residual soil-cement mixtures and establishing, at least, three distinct dosages within each chosen $\eta/(C_{iv})^{0.28}$ by varying the porosity and the cement content. Unconfined compressive strength tests and initial shear modulus tests were carried out for all the 26 defined dosages considering a curing period of 7 days, whereas durability and triaxial tests were conducted for a smaller range of mix designs. Moreover, scanning electron microscope tests and mercury intrusion porosimetry tests were done in for a few dosages The results have shown a great agreement, irrespective of the dosage, between strength, the initial shear modulus and the durability response to the $\eta/(C_{iv})^{0.28}$ index. Yet, the effective stress parameters (ϕ' and c´) could not be correlated to the $\eta/(C_{iv})^{0.28}$ index owing to the dosage-dependance of the strength mobilization mechanisms.

Keywords: *soil-cement, structured soils, porosity/cement index, soil stabilization*

RESUMO

O parâmetro porosidade/teor volumétrico de cimento tem se mostrado conveniente para fins de dosagem de solo-cimento, pois inclui o papel da compactação (η) e da quantidade de cimento (C_{iv}) em um único índice adimensional. Tal abordagem já foi utilizada com êxito em correlações com diferentes propriedades mecânicas de distintos solos cimentados, como resistência à compressão simples, módulo de cisalhamento à pequeníssimas deformações e durabilidade. Dessa forma, ao se estabelecer um valor específico para o índice $\eta/(C_{iv})^c$, espera-se a obtenção de uma resposta mecânica (e.g resistência e rigidez) semelhante a despeito da dosagem adotada. Porém, tal alegação ainda não foi verificada para uma ampla variedade de dosagens dentro de um mesmo valor de $\eta/(C_{iv})^c$. Nesse sentido, a presente pesquisa pretender examinar essa lacuna estabelecendo sete valores específicos do índice porosidade/teor volumétrico de cimento (i.e. 45, 40, 30, 35, 25, 22.5 e 20) para misturas compactadas de solo residual de arenito Botucatu com cimento. Ao menos três dosagens diferentes para cada valor de $\eta/(C_{iv})^c$ foram estipuladas através da variação da porosidade e da quantidade de cimento para um mesmo $\eta/(C_{iv})^c$. Ensaios de resistência à compressão simples e módulo de cisalhamento inicial foram realizados para todas as 26 dosagens estabelecidas considerando-se um período de cura de 7 dias, ao passo que ensaios de durabilidade e ensaios triaxiais foram executados para um número restrito de dosagens. Ademais, ensaios adicionais de microscopia eletrônica de varredura e de porosimetria por intrusão de mercúrio foram realizados em algumas amostras de forma a se caracterizar a microestrutura dessas. Os resultados parciais indicaram uma ótima concordância, independentemente da dosagem adotada, entre o índice $\eta/(C_{iv})^{0.28}$ e a resistência, a rigidez inicial e a durabilidade das misturas estudadas. Porém, os parâmetros efetivos de resistência (ϕ' and c') não puderam ser correlacionados ao índice porosidade/teor volumétrico de cimento devido à dependência da dosagem dos mecanismos de mobilização da resistência.

Palavras-chave: *solo-cimento, solos estruturados, índice porosidade/teor de cimento, estabilização de solos*

LIST OF FIGURES

LIST OF TABLES

LIST OF ABBREVIATIONS

ABNT – Associação Brasileira de Normas Técnicas

ALM – Accumulated Loss of Mass

ASTM – American Society for Testing and Materials

BRS – Botucatu Residual Soil

NCL – Normal Compression Line

PCA – Portland Cement Association

STS – Split Tensile Strength

UCS – Unconfined Compressive Strength

LIST OF SYMBOLS

C – cement content (expressed in relation to dry mass of soil)

c' – effective cohesive intercept

C_{iv} – volumetric cement content

e – void ratio

υ – specific volume (1+e)

E_{sec} – secant Young’s modulus

E_{tan} – tangent Young’s modulus

G_0 – initial shear modulus

M – critical state stress ratio

p' – mean effective stress

P_1 – first yield (onset of bond degradation)

P_2 – second yield (bond’s yield)

q – deviatoric stress

q_t – split tensile strength

q_u – unconfined compressive strength

s' – mean effective stress in the s' versus t plane

t – deviatoric stress in the s' versus t plane

V – total volume of the specimen

V_s – shear wave velocity V_v – volume of voids

τ – shearing stress

ϕ' – effective friction angle

ϕ_{cs}' – critical state friction angle

ϕ_{peak}' –peak friction angle

$\delta\varepsilon_p^p$ or $\delta\varepsilon_v^p$ – increment of plastic volumetric strain

$\delta\varepsilon_q^p$ or $\delta\varepsilon_s^p$ – increment of plastic shear strain

ε_a – axial deformation

ε_r – radial deformation

ε_s – shearing deformation

ε_v – volumetric deformation

γ_d – dry unit weight

η – porosity

η_{cs} – critical state porosity

$\eta/(C_{iv})^c$ – adjusted porosity/cement index

ρ – bulk density

ψ – angle of dilation

w – molding moisture content

SUMMARY

1 INTRODUCTION

The improvement of soils which are not suitable for a specific engineering purpose may be achieved through the employment of techniques that merge the use of densification and incorporation of a specific binder (INGLES & METCALF, 1972; BENHOOD, 2018). Particularly, owing to its practicality and reliability, Portland cement has been worldwide used for decades as this binding agent. As a reason, a variety of researches have already been conducted intending to assess the mechanical behavior of soil-cement mixtures. Specifically, the Post-Graduation Program in Civil Engineering at Federal University of Rio Grande do Sul (PPGEC/UFRGS) has been responsible to major contributions related to this subject. In this regard, Prietto (1996, 2004), Heineck (1998), Rotta (2000, 2003), Schnaid *et al.* (2001), Consoli et al. (1998, 1999, 2000, 2001, 2006, 2007a, 2007b, 2009, 2010, 2011, 2012a, 2012b, 2016, 2017), Foppa (2005, 2016), Cruz (2008), Festugato (2011), Fonini (2012), Floss (2012), Maghous (2014), Marques (2016), Bortolotto (2017), Leon (2018), Carreta (2018), Tomasi (2018), Corte (2020), among others, have studied the role of cementation on the response of a variety of geomaterials through a diversity of laboratory and field tests.

Although complex and influenced by many variables, such as the nature of the geomaterial, the amount of cement and the loading conditions, the overall behavior of cemented-soils can be roughly divided according to the effective state of stress (YUN & SANTAMARINA, 2005; LADE & TRADS, 2014). Under low confinement, the response is cementation controlled and the material exhibits a brittle behavior, presenting an augmented stiffness, a peak strength and a dilatative trend (LEROEIL & VAUGHAN, 1990; FERNANDEZ & SANTAMARINA, 2001; SCHNAID *et al*., 2001). Nonetheless, the shear resistance progressively changes from cohesive to frictional as the strain takes place and the cementing bonds degrade. Under high confining pressures, thus, the cement bonds may have yielded prior to the shearing and the response tends to be controlled by the soil matrix (COOP & ATKINSON, 1993; CUCCOVILLO & COOP, 1999; ROTTA *et al*., 2003).

In the light of numerous geotechnical applications of the soil-cement technique, such as base for shallow foundations, road embankments and slope protection, the response of the geomaterial is usually cemented controlled due to the low confinement stresses that these structures are subjected to (DIAMBRA et al., 2017). Ergo, disregarding the soil's fabric, the overall response of the cemented-soil in these cases is, primarily, a reflection of its cement content and compactness. The latter can be expressed by the porosity (η). In this context, a certain proportionality between strength (or stiffness) and amount of cement is expected (CLOUGH *et al*., 1981; LADE & OVERTON, 1989). On the contrary, an inverse correspondence is awaited amid strength (or stiffness) and the porosity.

Foppa (2005) and Consoli *et al.* (2007) have gathered either the amount of cement, expressed by the volumetric cement content (C_{iv}), and the porosity (η), into a single parameter, the adjusted porosity/cement ratio. The authors have successfully correlated it to the unconfined compressive strength (q_u) of compacted clayey sand-cement mixtures, yielding a single power type relationship. Later, Diambra *et al.* (2017) have proposed a theoretical derivation on such theme. Progressively, the adjusted porosity/cement index, and variations (e.g., the porosity/lime index and the porosity/binder content index) have been applied to a variety of soils and, as well, correlated to other mechanical properties besides the unconfined compressive strength (e.g., split tensile strength, initial shear modulus, durability given by the accumulated loss of mass and vertical swelling).

That being so, the $\eta/(C_{iv})^c$ approach may be accepted as a dosage methodology for artificially cemented soils applications. Theoretically, by the knowledge of a single value of unconfined compressive strength of one specimen molded at a specific $\eta/(C_{iv})^c$ value, the determination of the relationship that controls the strength of the same cemented-soil, for an entire range of porosities and cement contents, is possible (CONSOLI *et al*., 2017). Furthermore, it is virtually feasible the obtainment of the same value of the mechanical response of interest by increasing either the cement content ($\uparrow C$) and the porosity ($\uparrow \eta$), or decreasing both, but maintaining the $\eta/(C_{iv})^c$ constant. That is, depending on the interest, it might be more advantageous to use more cement and less compaction energy (or the opposite) to attain the same pre specified performance.

Accordingly, present research intends to enlarge the comprehension relative to the adjusted porosity/cement index and, as well, establishes boundaries for its correct use based on mechanical and microstructural tests. Specifically, a series of $\eta/(C_{iv})^{0.28}$ values were chosen for compacted Botucatu residual soil-cement mixtures and, within each $\eta/(C_{iv})^{0.28}$, at least three distinct dosages were established to be studied. Unconfined compression tests, split tensile tests, initial shear modulus tests, durability tests and triaxial tests were conducted. In addition, scanning electron microscope tests and mercury intrusion porosimetry tests were performed intending to characterize the microstructure of a few dosages.

1.1 SCOPE AND OBJECTIVES

The major goal of this thesis is to provide an experimental contribution intending to enlarge the comprehension of the $\eta/(C_{iv})^{0.28}$ value on the mechanical response of a cemented clayey sand. Particularly, a clearly understanding of the role of the dosage changing, maintaining a constant $\eta/(C_{iv})^{0.28}$ value, is sought. The following objectives will support this task:

a) Evaluate the overall mechanical response of Botucatu residual soil-cement mixtures assembled at distinct $\eta/(C_{iv})^{0.28}$ values in which, leastwise, two distinct dosages are tested within each adjusted porosity/cement ratio index (i.e. $\uparrow C$ $\uparrow \eta$ and $\downarrow C$, $\downarrow \eta$);

b) Assess the aforementioned results by means of a statistical background in order to check for possible differences amongst each different dosage;

c) Set boundaries (or indicate trends) at which the $\eta/(C_{iv})^{0.28}$ is no longer valid in the determination of effective stress parameters for compacted BRS-cement mixtures;

d) Evaluate the microstructure of some dosages in an attempt to establishes a connection between the microstructure of the studied mixtures and their macro mechanical response.

1.2 CONTENTS OF THE THESIS

This thesis is divided into six chapters. The current chapter presents an introduction relative to the theme of the thesis and, as well, its central objectives.

The **second chapter** contains the literature review, comprehending general aspects of soil stabilization with cement and the mechanical behavior of structured/cemented soils. An insight is given to the main aspects that influence the behavior of soil-cement mixtures.

The **third chapter** presents the research program. Namely, it contains the main tests which have been carried out and indicates the number of tests and the assessed variables.

The **fourth chapter** is relative to the materials and methods employed herein. Thus, it contains the characterization of the materials utilized, as well as the description of the test methods.

The **fifth chapter** introduces the results of the test which have been performed. A discussion of those is presented.

The **sixth chapter** presents the conclusions relative to the thesis results and, likewise, proposes suggestions for future researches.

2. LITERATURE REVIEW

This chapter contextualizes the essential topics regarding the central themes of this thesis. Ergo, general aspects concerning the principles of soil stabilization with cement and the behavior of cemented/structured soils are addressed.

2.1 SOIL STABILIZATION

It is not uncommon in Geotechnical Engineering to encounter unfavorable circumstances owing to the existence of soils which are not suitable for a particular purpose (INGLES & METCALF, 1972). In this regard, Mitchell and Jardine (2002) state five possible options:

(i) deviate from the poor ground by moving to a new site or using deep foundations;
(ii) remove the existing inadequate soil, replacing it with a suitable geomaterial;
(iii) design the structure to accommodate adverse geotechnical conditions;
(iv) improve the poor ground characteristics;
(v) abandon the project.

The fourth alternative concerns the alteration of the soil’s properties in order to meet specific engineering requirements, that is, soil stabilization or ground treatment (INGLES & METCALF, 1972; CHARLES, 2002). There are several possibilities (and combinations of possibilities) which can be used for this purpose that include chemical, thermal and mechanical means. Yet, the choice amongst these numerous options relies on the essence of the problem itself, including the nature of the soil and existing technical limitations. In this regard, one of the most used techniques is the combined used of densification, via mechanical compaction, and the incorporation of a particular binder.

Mechanical compaction of the soil aims to increase the dry density (i.e. diminishes the voids content) of the material and is probably the eldest soil improvement technique (INGLES & METCALF, 1972). Mainly, the overall strength and stiffness increase as the space occupied by voids in the soil declines (CHARLES, 2002). The effect of mixing a certain binder in the soil depends on the soil’s nature and on the binder itself. Clayey soils may promptly flocculate when mixed with hydrated lime owing to cation exchange reactions, implying substantial changes in the soil's workability due to grain size distribution and plasticity alterations (HERZOG & MITCHELL, 1963; MITCHELL & SOGA; 2005). The usage of a certain amount of ordinary Portland cement (OPC), in turn, will ultimately lead to the formation of a bonded structure, irrespective of the initial soil's characteristics, contributing to amend the overall mechanical characteristics of the material (CONSOLI, *et al.*, 2007; ROTTA *et al.*, 2003)

2.1.1 Soil Stabilization Using Cement

According to Ingles and Metcalf (1972), the addition of a binder for a soil stabilization purpose is advisable when a material (or combination of materials) with appropriate mechanical behavior cannot be obtained, or when enhanced strength to water softening is sought. Any cementing material capable to fulfill the minimum performance requirements may be used. Therefore, alternative binders composed by waste and by-products of different sources may be an alternative to ordinary Portland cement (e.g., BEHNOOD, 2018; CONSOLI *et al.*, 2001, 2019a, 2019b; CORRÊA *et al.*, 2021; EKINCI *et al.*, 2021; SALDANHA. *et al.*, 2017; SALDANHA *et al.*, 2018; SALDANHA & CONSOLI, 2016; SCHEUERMANN FILHO *et al.*, 2020; SCHEUERMANN FILHO *et al.*, 2021).

Nonetheless, in spite of the numerous existing alternative binders, ordinary Portland cement is still one of the major materials employed for geomaterials amendment reasons owing to its reliability and practicality. Therefore, it has been broadly employed in road base layers, slope protection for earth dams and embankments, foundation stabilization, channel and ditching linings, liquefaction prevention in granular soils, mine tailings stabilization, amongst other uses (INGLES & METCALF, 1972; CLOUGH *et al.*, 1981; CONSOLI *et al.*, 1998, 2002; SCHNAID *et al*. 2001; FESTUGATO *et al*. 2013).

Naturally, the amount of added cement directly influences the artificially cemented-soil later response and such quantity must be previously selected based on specific requirements. In this regard, the proportion of cement relative to the mass of dry soil is usually inferior to 12% and generally lies within 2% to 7% (PCA, 1995; CONSOLI *et al.*, 2007; CORTE, 2020). Lade and Overton (1989) and Lade and Trads (2014) have called a mixture of soil containing 6% of Portland cement as "soil-cement", whereas the authors have called it a "mortar" when this content was equal to 12%. Clough *et al.* (1981) and Rad and Clough (1982) have classified the strength of the cementation for naturally cemented sands based on its behavior. Yet, considering artificially cemented soils, and regardless minimum strength requirements, a weakly cemented soil may correspond to cement contents up to 3%, a moderately cemented soil to amounts of cement on the range of 4% to 7% and a strongly cemented soil to quantities from 8% up to 12%.

Ordinary Portland cement (OPC) is primarily constituted by four major mineral phases which are present in the clinker (Alite, Belite, Aluminate and Ferrite) and several others that represent a minor amount of its chemical composition such as alkali sulfates and calcium oxide (TAYLOR, 1997). Alite (Ca_3SiO_5) and Belite (Ca_2SiO_4) are the main constituents of the OPC, representing, respectively, around 50-70% and 15-30% of its composition. The first is the primary responsible for the strength development up to 28 days of curing, whereas the latter has a slower hydration rate and contributes to strength gains in a long-term basis. Aluminate ($Ca_3Al_2O_6$) prompts react with water and may cause undesirable setting of the mixture if no set-controlling agent (e.g. gypsum) is used. The rate of reaction of Ferrite ($Ca2AlFeO_5$), in turn, is intimately linked to its particular chemical composition, yet it tends to be elevated in the first phases of hydration (TAYLOR, 1997).

Chemically, the hydration of Portland cement comprehends a series of complex reactions involving the clinker minerals, calcium sulfate and water (ODLER, 2004). These reactions take place simultaneously and successively, at distinct rates and impact each other. An external consequence of the hydration is the setting of the mixture, causing a sudden loss of plasticity, and, afterwards, the hardening which is responsible for the strength development. The major cementitious product yields from both the Alite and Belite hydration and are, in a generical designation, the calcium silicate hydrate (C-S-H). This is a pretty much amorphous cementing product that evolves along the curing and is majorly responsible for the strength and hardening of the mixture. Although similar, the nature of the C-S-H gels formed during the hydration of Alite and Belite are not identical and, besides, the reactions of the first occurs earliest. Calcium hydroxide is a secondary product of both Alite and Belite hydration and may have a certain influence if cement is mixed with soils containing substantial amounts of reactive clay minerals (HERZOG & MITCHELL, 1963; MOH, 1965). The hydration of Aluminate implies the formation of calcium aluminate hydrate gels (C-A-H) which, later on, may partially react with gypsum, allowing the formation of ettringite. The hydration of Ferrite is similar.

2.1.2 Microstructure of Cemented Soils

The interactions developed during the hydration of Portland cement in soil-cement mixtures define the nature of the bonded structure which, ultimately, influences the mechanical response of the cemented soil. For soils containing appreciable amounts of clay minerals, pozzolanic reactions may take place between these and the calcium hydroxide released during the cement hydration (MOH, 1965). Namely, the silica and the alumina from the clay particles dissolve in the high pH environment and combines with the calcium ions, yielding additional cementitious material that further bonds the adjacent clay particles together (HERZOG & MITCHELL, 1963; KAMRUZZAMAN *et al*., 2006). In this regard, Mitchell and El Jack (1966) have affirmed that, after a long period of curing, the mixture of a clayey soil with cement ends up as a homogeneous cemented fabric of indistinguishable components as depicted in Figure 1.

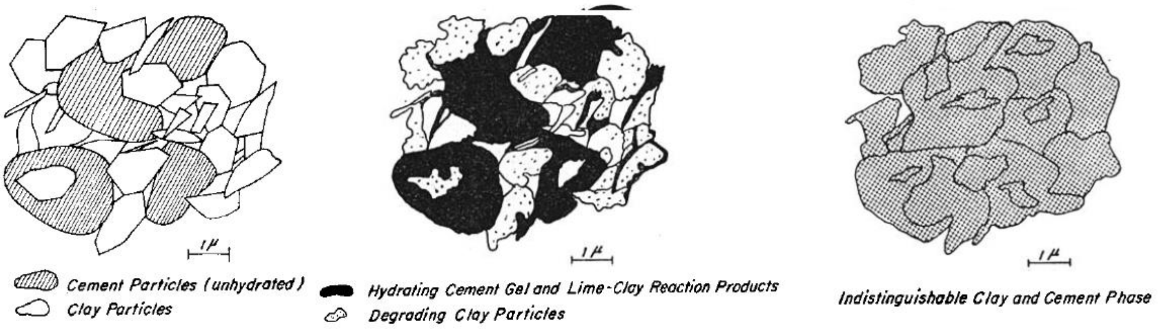

(a) compacted condition (b) after a short curing period (c) after a long curing period

Figure 1 – Effect of cement content on the fabrics of a clayey soil (a) right after compaction (b) after a short curing period (c) after a long period of curing

(MITCHELL; El JACK, 1966).

Considering granular soils in which the clay minerals do not represent a substantial amount and/or in soils that are formed by less reactant clay minerals, the soil matrix may be regarded as inert and the cement bonds only form a structure that bonds the particles together. That is, the cementing material will partially occupy the voids existing between the soil's grains. In this regard, Chang and Woods (1992) have defined a parameter called cementation level (*C*) as the volume of the cementing material over the total volume of the initial voids in a cemented soil specimen. The authors have tested four types of sand at constant relative densities ranging from 60% to 75% and used cementation levels of 10%, 20%, 30%, 45%, 60%, 75% and 90%. The performance of the soil-cement mixtures was assessed by means of the shear modulus measured using a resonant column device. The results are summarized in Figure 2a, in which three zones of behavior (zones I, II and III) were identified according to the impact of the degree of cementation (*C*) on the stiffness of the specimens. Each zone was correlated to different stages of cementation, which are summarized in Figure 2b and are defined as follows:

a) Stage I: cement partially covers the surface of soil particles with some initial bonding (20% - 25% < C).
b) Stage II: cementing of soil particles is substantial at contact points between the soil particles (20% - 25% < C < 60% - 80%).
c) Stage III: cement fills most of the void space between soil particles, being the development of chemical bonds completed C >60% - 80%.

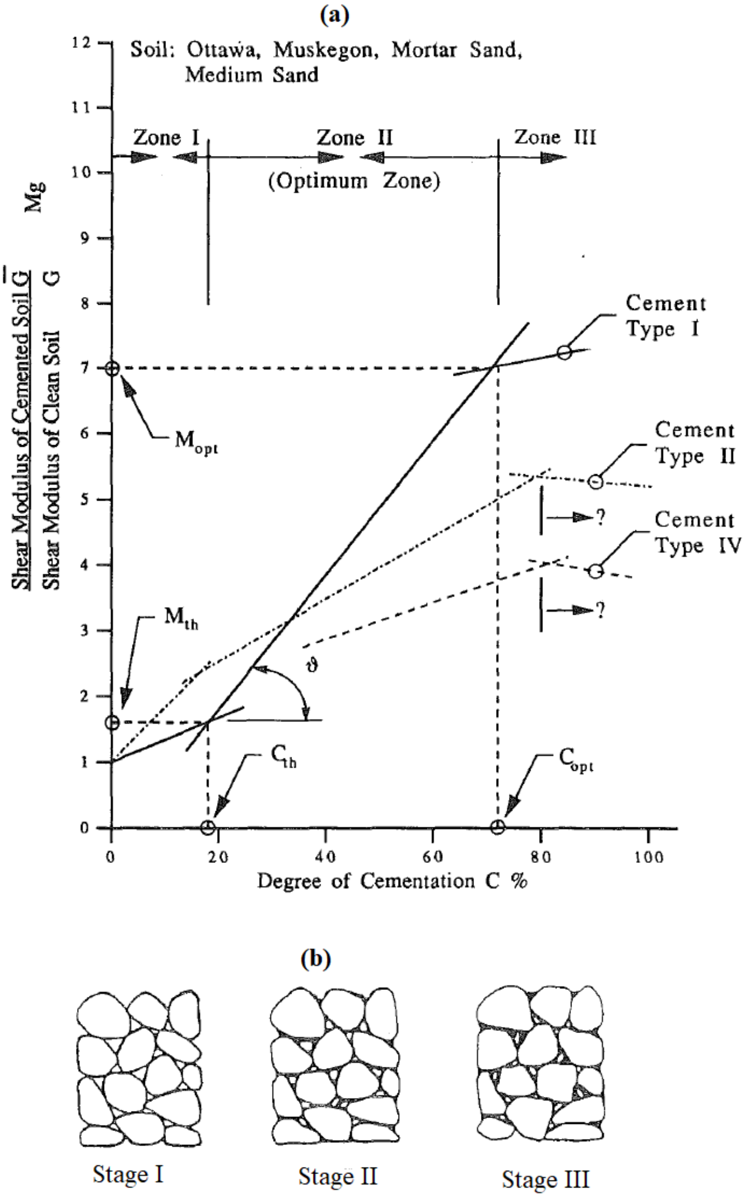

Figure 2 – Effect degree of cementation (a) on the stiffness and (b) on the fabrics of cemented sands

(CHANG & WOODS, 1992).

Regardless of the soil nature, the development of cementing products structurally modifies the pores within the soil-cement specimens. As the curing period progress, changes in the pore size distribution may occur as related by Winslow and Lovell (1981), Wild *et al.* (1987), Kamruzzaman *et al*. (2006), Horpibulsuk *et al.* (2010), Johann (2013), Bhattacharjee (2016), Lee and Shang (2018), Zhang and Zhu (2018), Ranaivomanana and Razakamanantsoa (2018), among others. Horpibulsuk *et al.* (2010) have assessed the pore-size distribution for compacted cemented silty-clay mixtures along the curing period. The results are summarized in Figure 3a. Initially, up to 7 days of curing, the volume of pores smaller than 0.1 μm has substantially decreased while the volume of pores larger than 0.1 μm has marginally increased. This indicates that the cementitious products have filled the pores smaller than 0.1 μm. After this period of 7 days, the volume of pores larger than 0.1 μm has decreased, whereas the volume of pores smaller than 0.1 μm has increased. Hence, the binding compounds have filled the large pores (larger than 0.1 μm), causing the enlargement of the volume of the small pores and an overall decrement in the total pore volume, as prompt perceived in Fig 3b. Johann (2013) has reported a similar trend regarding a silty soil amended with a binder composed by fly ash and hydrated lime. That is, after 28 days of curing, the total volume of pores has decreased.

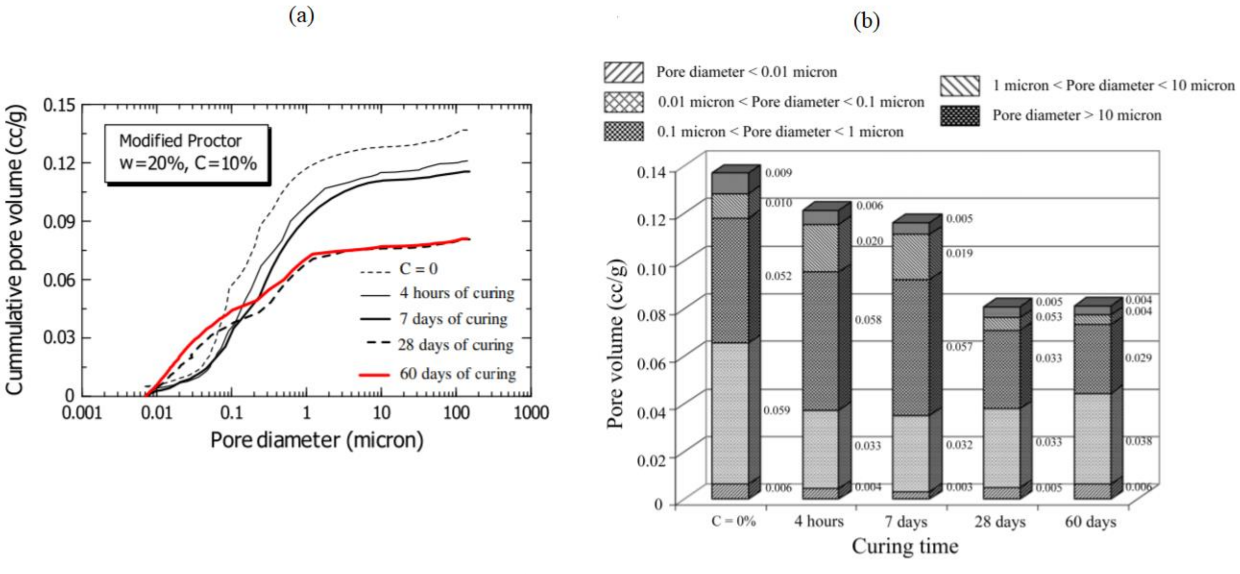

Figure 3 – Pore size distribution as a function of the curing period (a) cumulative pore volume (b) pore volume (HORPIBULSUK *et al.* , 2010).

2.2 FACTORS AFFECTING THE BEHAVIOR OF SOIL-CEMENT MIXTURES

According to Lads and Trads (2014), there are three factors that impact most the stress-strain response and volume change behavior of artificially cemented granular soils, namely: effective confining pressure, initial void ratio and the amount of cementation. Further effects related to the physicochemical properties of the soil, to the soil’s fabric and to the moisture content at the time of compaction can also be highlighted as important aspects in altering the behavior of soil-cement mixtures, regardless the nature of the soil (CUCCOVILO & COOP, 1999; YUN & SANTAMARINA, 2005; CONSOLI *et al.*, 2007a). As a reason, key parameters related to the strength response of compacted soil-cement mixtures are discussed below.

2.2.1 Amount of Cement

Up to a certain threshold value, it is expected that the unconfined compressive strength of compacted soil-cement mixtures increases with the cement content (C) increment, if the void ratio is kept constant, as shown in Figure 4 (INGLES & METCALF, 1972; CONSOLI *et al.*, 2007a, 2012a). In this regard, Horpibulsuk *et al.* (2010) have encountered this limit point for compacted cement-stabilized silty-clay mixtures and, as well, have defined three improvement zones: active, inert and deterioration zone. In the first ($3 < C < 12\%$), substantial strength gains were verified as the cement content increased owing to the decrease of pores smaller than 0.1 μm and the increment in the formation of cementitious products. In the inert zone ($15 < C < 30\%$) negligible improvements in strength were verified, which were accompanied by insignificant changes in either the pore size distribution and in the formation of biding products. In the deterioration zone ($35 < C < 45\%$), the water content was not adequate to hydrate the excessive cement content and an inverse trend between strength and amount of cement was verified. Figure 5 summarizes those findings.

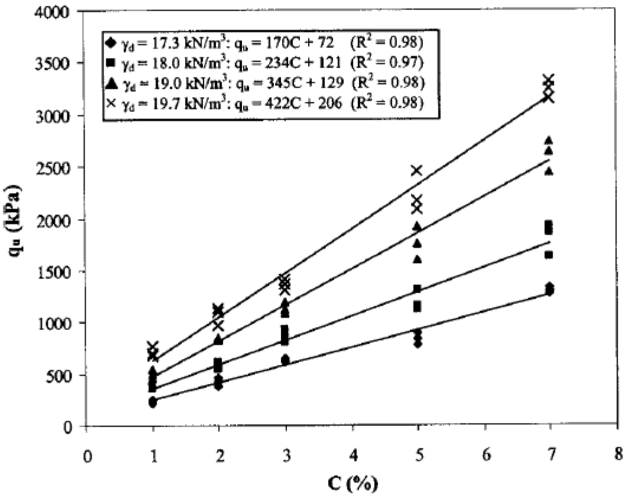

Figure 4 – Effect of cement content on the strength of a cemented silt

(CONSOLI *et al.*, 2007)

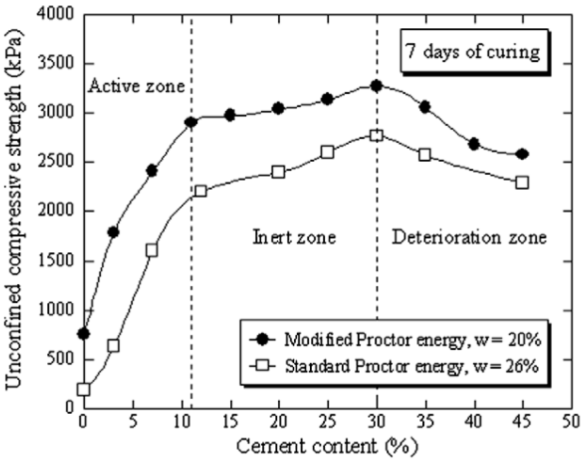

Figure 5 – Strength development zones as a function of cement content

(HORPIBULSUK *et al.*, 2010)

2.2.2 Porosity

The compactness exerts a major influence on the mechanical response of compacted soil-cement specimens as minutely shown by Ingles and Metcalf (1972), Schnaid *et al.* (2001), Consoli *et al*. (2007a, 2012a, 2017, 2018a), Lade and Trads (2014), Maghous *et al.* (2014), Moreira *et al.* (2019), among others. Therefore, it is expected that the unconfined compressive strength increases as the porosity reduces, as depicted in Figure 6 for compacted soil-cement specimens. A denser medium will enhance the interlocking development between its constituent particles and, as well, favor the development of a cementitious matrix owing to augmented contact area between the grains (Saldanha *et al.*, 2017).

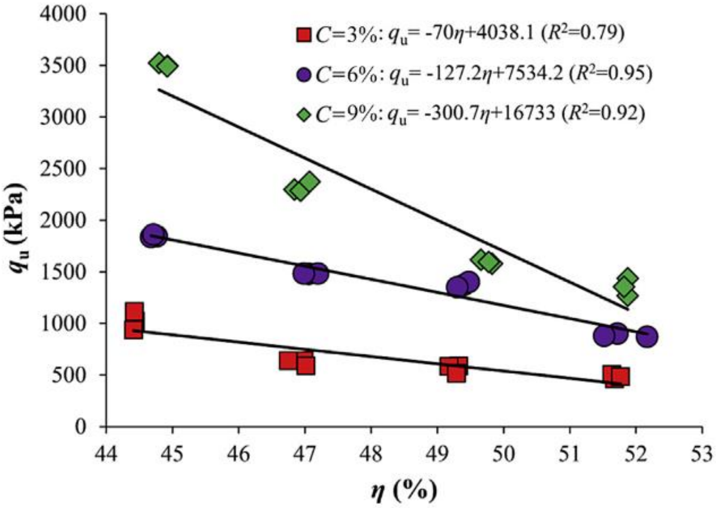

Figure 6 – Effect of porosity on soil-cement mixtures

(MOREIRA *et al*., 2019)

2.2.3 Molding Moisture Content

The amount of liquid within a soil-cement mixture influences its response to compaction efforts as certain dry densities may only be obtained at particular moisture contents due to the interaction between solid particles, voids and liquid (INGLES & METCALF, 1972). Specifically, the maximum dry density value for an individual compaction effort is related to a single moisture content (i.e. optimum moisture content). Such density value separates the compaction curve into “dry” and “wet” sides. In the dry side, the porosity diminishes as the water content increases up to the maximum dry density is reached. From this point beyond, this trend reverses and the dry density decreases as the water content increments.

Regarding soil-cement mixtures, a minimum water content is needed for cement hydration, which depends on the amount of cement (TAYLOR, 1997; HORPIBULSUK *et al.*, 2010 BECKETT & CIANCIO, 2014). Once this minimum amount is satisfied, water in excess may be deleterious to the strength development as demonstrated by Ribeiro *et al*. (2016) for a silty-sand containing 13% of Portland cement (Figure 7a). In this regard, Consoli *et al*. (2007a) have observed that the unconfined compressive was independent on the moisture content when 2% of cement was used to treat a silty soil (Figure 7b). Nonetheless, it has influenced the strength for higher cement contents (9% and 12%).

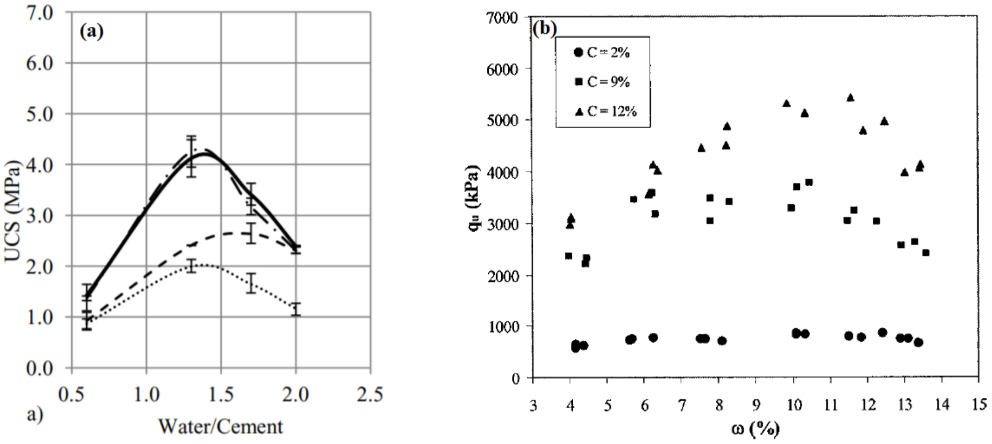

Figure 7 – Effect of porosity on soil-cement mixtures (a) 10% of cement (b) various cement contents (RIBEIRO *et al.*, 2016; CONSOLI *et al.*, 2007)

Considering the same amount of cement, the water content influences the bonds geometry and dispersion within the matrix of the soil which, ultimately, impacts on the mechanical response of the soil-cement specimens (RIBEIRO *et al.*, 2016; CARDOSO *et al.*, 2017). Generally, when the availability of water is small, the bonds are concentrated at the grains contact. For higher moisture contents (up to a certain limit), however, the bonds disperse over the grains surface, forming a more homogeneous structure.

2.2.4 Curing Period

The kinetics of the cement hydration changes over the time and the outcomes of the particular reactions that comprehend the hydration processes are formed (and modified) at distinct moments (TAYLOR, 1997). Moreover, the overall processes are highly dependent upon the cement's type. Yet, according to Odler (2004), the mechanism of hydration can be roughly divided in four stages:

1) Pre-induction period (first minutes): occurs immediately upon the cement contact with water and is characterized by the dissolution of the ionic species into the liquid phase and formation of a hydrated paste;
2) Induction (first few hours): the hydration of all the clinker minerals progresses very slow and C-S-H starts to be formed;
3) Acceleration stage (3 – 12 hours after mixing): the reaction rate accelerates again and the formation of cementing products is increased;
4) Post-acceleration phase: the hydration rates gradually slow down. If enough water is available, the hydration progress until all the original cement contents are consumed. An ageing of the cementing products also takes place with modifications in the C-S-H structure.

Figure 8 graphically summarizes the progress of hydration of an ordinary Portland cement. The rates of consumption (Fig. 8a) of the original constituents and, as well, of formation of the cementing products (Fig. 8b) are promptly noticed.

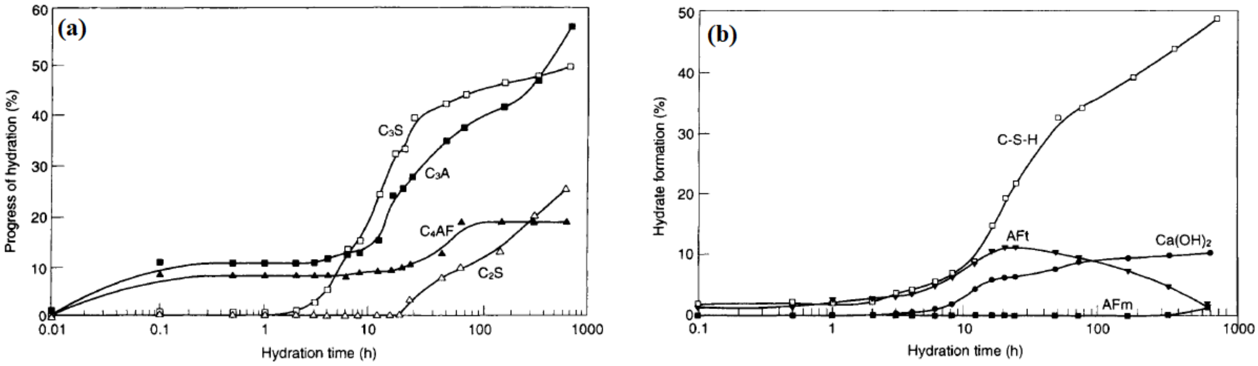

Figure 8 – Hydration kinetics of an ordinary Portland cement (a) progress of consumption (b) hydration formation

(ODLER, 2004)

Naturally, for soil-cement mixtures, it is expected a direct proportionality between strength and curing period. This was demonstrated by Clare and Pollard (1951) in the results depicted in Figure 9. However, strength gains are not infinitely and there is a tendency to reduction in the strength increment rate as the curing time progresses because no cement hydration products can be further formed. Yao *et al.*, (2019) modelled this trend for a variety of cemented-soil using a hyperbolic model, as shown in Figure 10.

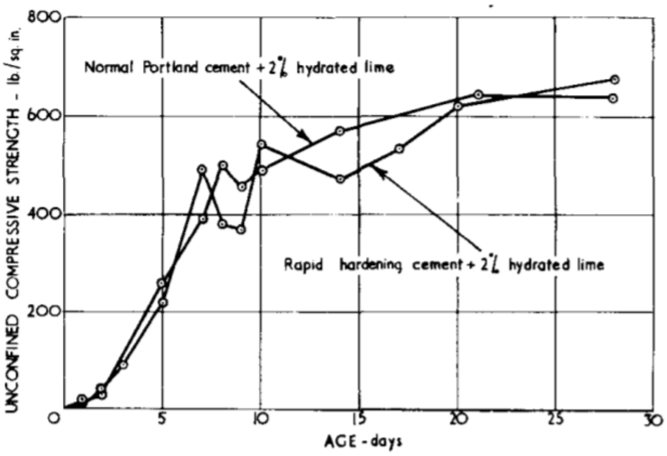

Figure 9 – Unconfined compression strength as a function of the curing period for sand-cement-lime mixtures

(CLARE & POLLARD, 1951)

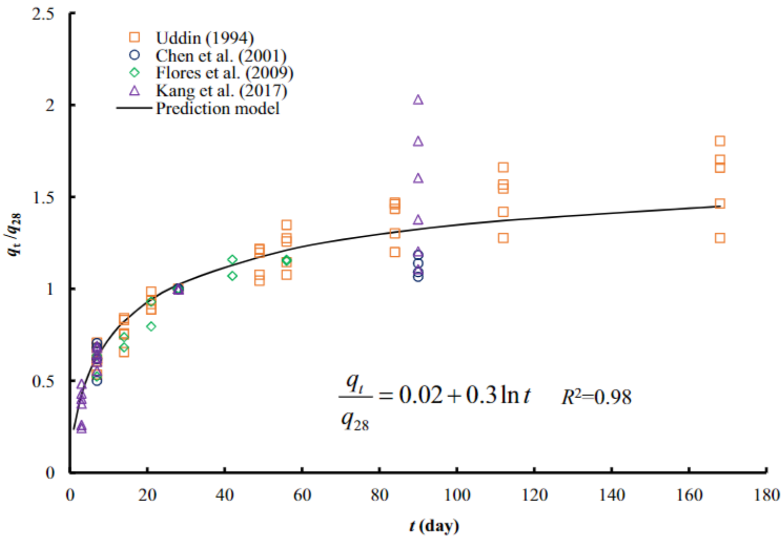

Figure 10 – Rate of strength development as a function of the curing period for cement-soil mixes (YAO *et al.*, 2019)

2.2.5 Curing Temperature

The hydration of Portland cement is an exothermic process and the surrounding temperature affects the total heat evolved during this process, as exemplified in Figure 11 in which calorimetry curves of cement pastes are displayed as a function of ambient temperature (BERGSTRÖM, 1953; ESCALANTE-GARCIA & SHARP, 2000). That being so, up to certain limits, higher curing temperatures contribute to accelerate the kinetics of cement hydration. Thus, the mechanical response of soil-cement mixtures is naturally affected by changes in the curing temperature, which is exemplified in Figures 12a and 12b (CLARE & POLLARD, 1954; SATO, 2006; HO *et al.*, 2020; ZHANG, *et al.*, 2014; ZHANG, *et al.*, 2021).

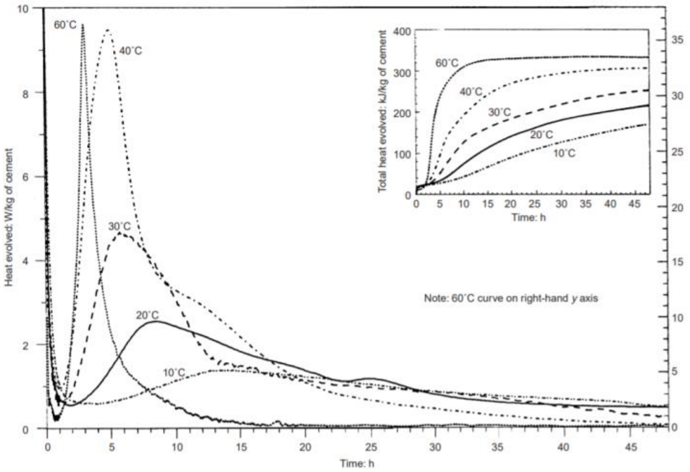

Figure 11 – Heat evolved during Portland cement hydration as a function of the temperature (ESCALANTE-GARCIA; SHARP, 2000)

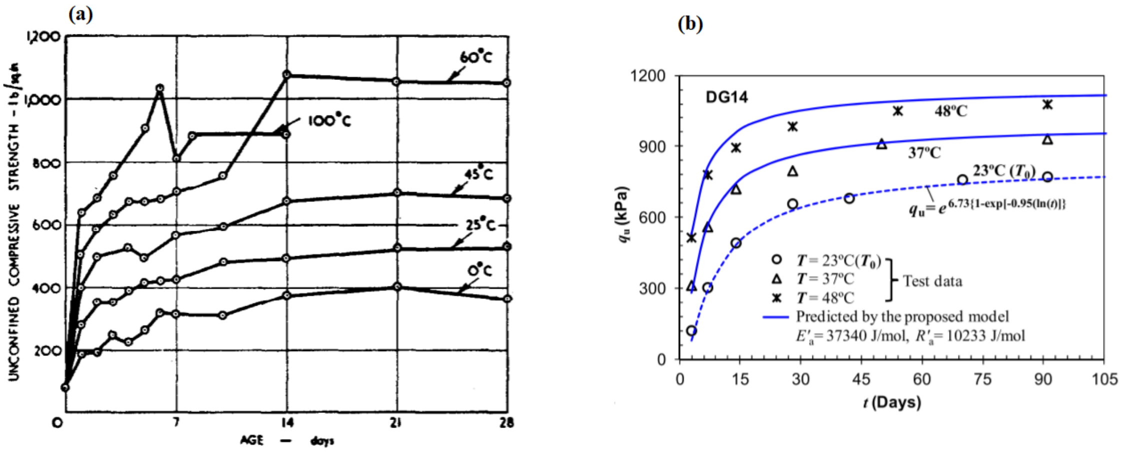

Figure 12 – Unconfined compressive strength of soil-cement mixes as a function of curing time and temperature (a) silty soil (b) clayey soil

(CLARE & POLLARD, 1954; ZHANG *et al*., 2014)

2.3 STRUCTURED SOILS AND CEMENTED SOILS

In structured soils, part of the strength and stiffness arise from the interparticle bonding, enabling the structured material to exist at states which are not possible for the non-structured or reconstituted soil to endure (CUCCOVILLO & COOP, 1999; FEARON & COOP, 2000). The bonding exerts a noteworthy influence on the stress-strain behavior of the material and have been recognized amongst a variety of geomaterials such as soft clays, stiff clays, granular soils and residual soils (LEROUEIL & VAUGHAN, 1990). When naturally occurring, the interparticle bonding may arise from the deposition or precipitation of a cementing agent at particles contacts (e.g. carbonates and hydroxides), from recrystallization of minerals during weathering of rocks, from interparticle attractive forces in clayey soils, among other complex processes (FERNANDEZ & SANTAMARINA, 2001). Nonetheless, from a mechanical perspective, artificially structured materials, such as cemented soils, soft rocks and as- like bonded materials are located in an intermediate category of materials which behavior lies between the classical soil mechanics and the rock mechanics.

For granular materials, the structure arises as a combination between the bonding existing amongst the particles and the soil’s fabric, reflecting the interaction between cementation and particle´s arrangement. (CUCCOVILLO & COOP, 1999; LADE & TRADS, 2014). The bonding existing in the soil prevents the relative movement between the individual grains before the breakage of this bonded structure starts to occur. Thus, generally, the cementing matrix implies in an augment of stiffness and peak strength which are coupled with a more dilatative response and post-peak brittleness in comparison to the unstructured (or untreated) soil (COOP & ATKINSON, 1994; LADE & TRADS, 2014; LADE & OVERTON, 1989). Even so, the role of the cementation along the shearing phase depends upon the effective state of stress prior to this stage. In brief, the response of the cemented material resembles the natural (uncemented) soil's behavior if the bonds are broken during the consolidation phase.

2.3.1 Unconfined Compressive Strength and Split Tensile Strength of Cemented Soils

The existence of a bonded structure in artificially cemented soils gives rise to a "true cohesion", namely, a strength component which exists in the absence of confinement stresses (i.e., $p' = 0$). Thus, either unconfined compressive strength and split tensile strength tests are useful to evaluate the effect of the amount of cement and, as well, of the dry density for compacted soil-cement mixtures for low confinement levels, for example (PCA, 1995; LIU *et al.*, 2008). As already mentioned, the unconfined strength of soil-cement specimens is primarily controlled by the degree of cementation and the by compactness of the medium (SCHNAID *et al*., 2001; CONSOLI et al., 2007a LADE & TRADS, 2014). Moreover, the quotient between the tensile strength and the compressive strength lies in the range of 9% to 18% for cemented soils (e.g. CLOUGH *et al.*, 1981; CONSOLI, *et al.*, 2010; DIAMBRA *et al.*, 2018; BALDOVINO *et al.*, 2020).

2.3.2 Isotropic Compression of Cemented Soils

The behavior of structured soils, either artificially or naturally cemented, under isotropic compression has been thoroughly studied by Leroueil and Vaughan (1990), Coop and Atkinson (1993); Cuccovillo and Coop (1999), Coop and Wilson (2003), Rotta *et al*. (2003), Prietto (2004), Consoli *et al.* (2002, 2006, 2007b), Rios *et al.* (2012), Marques (2016), among others. The bonds enable the soil to exist in states which are impossible for the de-structured (non-cemented) soil. Namely, the former can reach states outside of the intrinsic normal compression line (NCL) defined by the non-cemented soil, as shown in Figure 13 (LEROUEIL & VAUGHAN, 1990; CUCCOVILLO & COOP, 1999). The bonds enlarge the elastic zone of the material and make the initial stress-strain behavior stiffer in comparison to the natural soil. As a reason, the structured material tends to present a brittle response and an abruptness yield point, marked by the commencement of the bond's degradation (ROTTA *et al.*, 2003). Afterwards, the yielded cemented-soil may directs towards to the NCL.

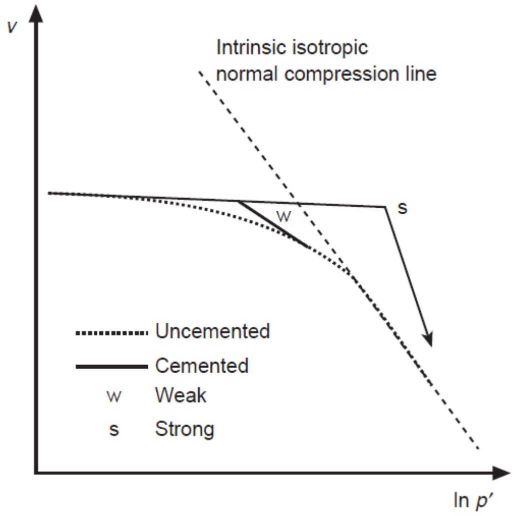

Figure 13 – Influence of cementation during isotropic compression

(CUCCOVILLO & COOP, 1999)

For an artificially cemented silty-sand cured under stress, Rotta *et al*. (2003) have shown that the primary yield point was dependent upon the curing stress, the curing void ratio and the cement content. Post yield compression lines were defined according to the cement contents, yet they appear to converge to the intrinsic compression line for greater confinements (Figure 14).

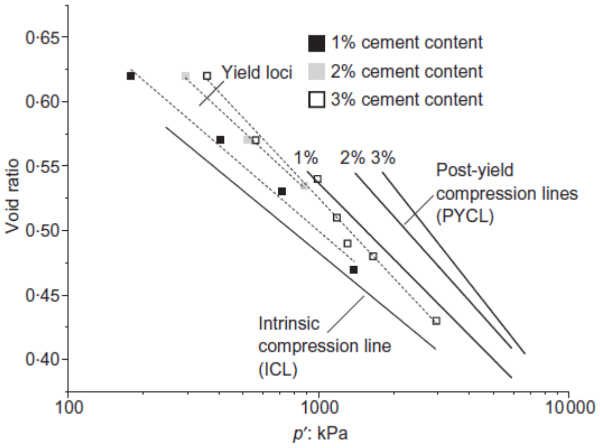

Figure 14 – Post-yield behavior according to cement content

(ROTTA *et al*., 2003)

2.3.3 Triaxial Compression of Cemented Soils

During shearing under drained conditions, Coop and Atkinson (1993) and Cuccovillo and Coop (1999) have identified three modes of behavior for cemented carbonate sands which depended upon the initial state of the sample relative to the yield curve of the cement bonds. A schematic diagram is shown in Figure 15a. At low confining pressures (1), relative to the yield of the bonds, the stress-strain response was nearly elastic up to a well-defined yield point, followed by a strain-softening in the direction of the critical state line. At intermediate levels of confinement (2), the yield occurred prior to critical state and the failure was primarily frictional. The bonds have only contributed to enhance the initial stiffness of the material. For higher pressures (3), the bonds have already yielded during consolidation and the behavior was entirely frictional. That is, the response was not influenced by the cementing agent in this case (3).

In this regard, Lade and Trads (2014) have differentiated the shearing behavior between strongly cemented soil and weakly cemented soil by including two stress-strains responses at intermediate confinement levels for weakly cemented soil specimens (Figure 15b). Both exhibits a slightly pronounced peak, yet the one with highest deviatoric stress (2) starts to be sheared inside the cement's yield surface. Nonetheless, differences between the idealized behavior of strongly and weakly cemented soil primarily rely on the size of the cement yield surface.

(a) **Strongly cemented soil**

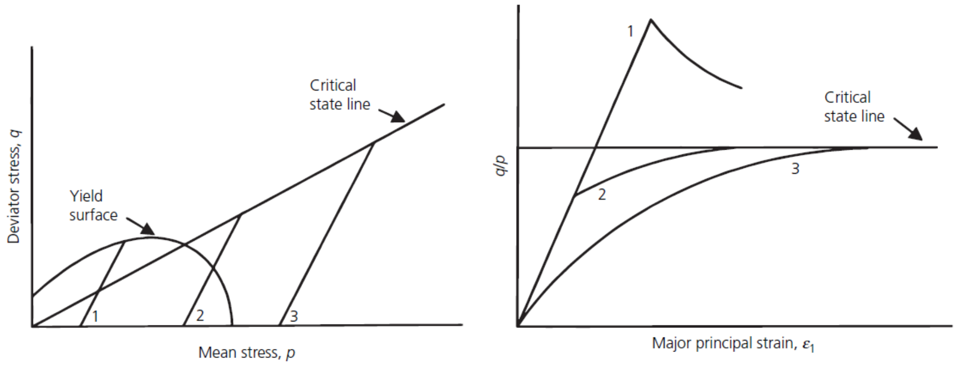

(b) **Weakly cemented soil**

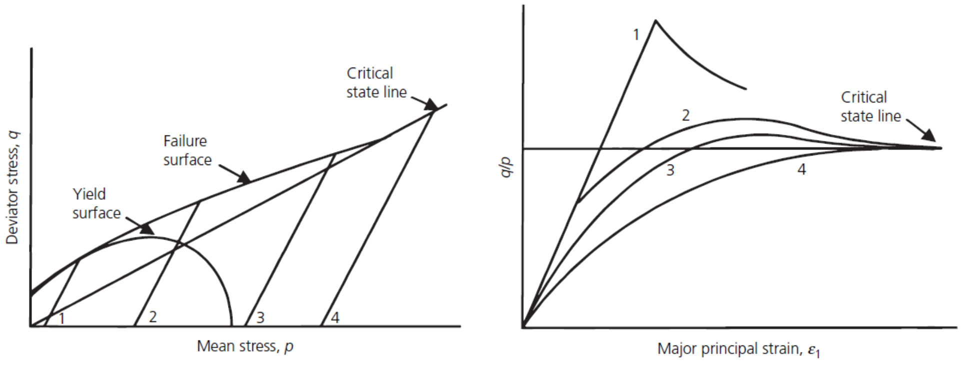

Figure 15 – Effect of mean stress on the response of strongly and weakly cemented soils

(CUCCOVILLO & COOP, 1999; LADE, P. V. & TRADS, 2014)

Roughly, the cement matrix controls the material's behavior up to the bond's yield, as the cohesive parcel is mobilized first (LADE & TRADS, 2014). Thereafter, the friction component starts to act. Yet, if the bond's yield surface is reached prior to the shearing phase, the material response is controlled by its frictional component and the effects of the initial amount of cement on the effective stress parameters is negligible (ROTTA *et al.*, 2003; YUN & SANTAMARINA, 2005). Moreover, once the bonds are broken, the soil does not unavoidably returns to the behavior of the uncemented soil, as lumps of cemented material may act as larger particles and or the cement induced modification in the soil's fabrics may not be fully erased during the shearing (CLOUGH *et al.*, 1981; LADE & TRADS, 2014).

Along shearing, the volume change behavior depends primarily on the effective confining pressure and on the porosity of the material (CLOUGH *et al.*, 1981; LADE & OVERTON, 1989). Consequently, contraction occurs at high levels of confinement and/or elevated porosities and dilation takes place for the opposite conditions. Prior to the bond's yield, the volumetric strains are meant to be elastic and contractive (LADE & TRADS, 2014). Afterwards, plastic dilative volume changes may occur. Those trends are readily noticed in Figures 16 and 17. In the first, the stress-strain responses of a silty-sand is depicted aside with the same silty-sand, but with the addition of 5% of cement. The latter shows the comparison between the triaxial response of a cement and an uncemented sand.

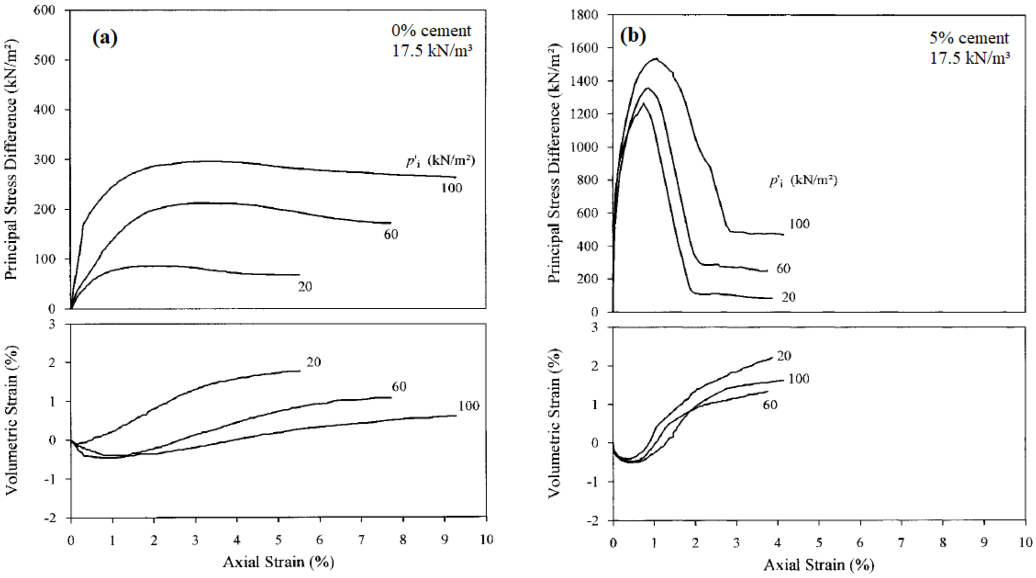

Figure 16 – Stress-strain and volume change response of a silty sand and a cemented silty-sand

(SCHNAID *et al.*, 2001)

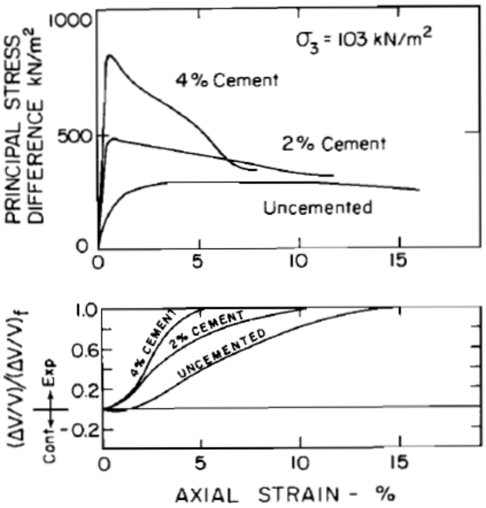

Figure 17 – Stress-strain and volume change response of cemented and uncemented sand

(CLOUGH *et al.*, 1981)

2.3.4 Durability

Amongst several interpretations, durability can be defined as the capacity of a material to retain its integrity when exposed to destructive weathering conditions (DEMPSEY & THOMPSON, 1968). A criterion to measure this characteristic in compacted soil-cement mixtures is the accumulated loss of mass (ALM) due to wetting-drying-brushing cycles, following the ASTM D559 standard (ASTM, 2015), and/or freezing-thawing-brushing cycles, observing the ASTM D560 standard (ASTM, 2016). Through the outcomes of the durability tests, it is possible, for example, to separately assess the effects of the dry unit weight and the amount of cement on the ALM per cycle of the test. Several studies have already been conducted to assess the durability of a variety of geomaterials amended with Portland cement, and the results can be presented as exemplified in Figure 18 (e.g. ZHANG & TAO, 2008; SHIHATA & BAGHDADI, 2001; CONSOLI *et al.*, 2017, 2018a, 2018b; SUDDEEPONG *et al.*, 2018)

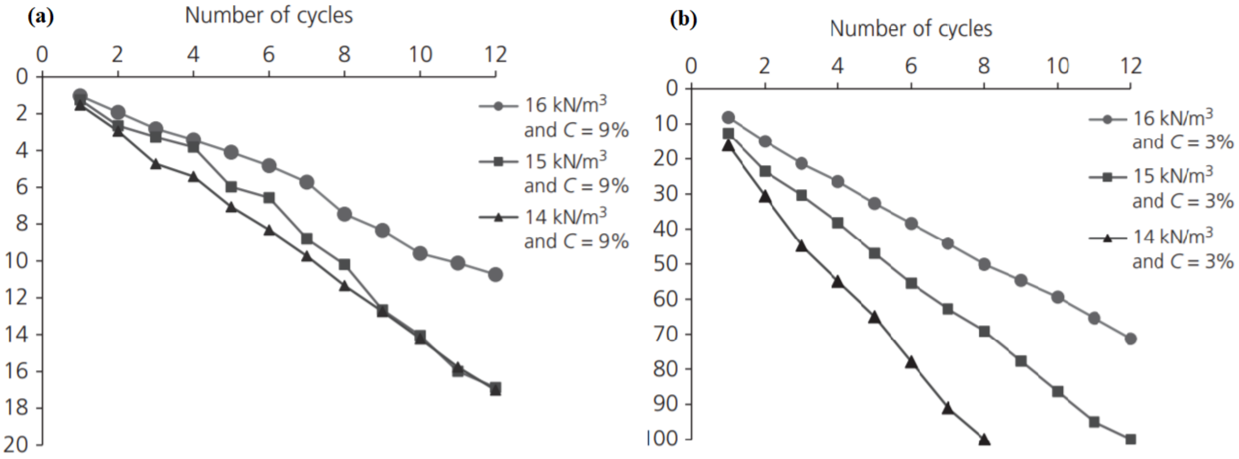

Figure 18 – Typical outcomes of a durability test in sand-cement mixtures: (a) 9% of cement (b) 3% of cement (CONSOLI *et al*., 2017a)

2.3.5 Stiffness of Cemented Soils

According to Clayton (2011), the stiffness of a body is the resistance of that body to deformation under applied effort and results from (i) the shape of the body, (ii) the boundary conditions and (iii) the inherent stiffness properties of its constituent materials. The stress-strain behavior of soils is notably known to be non-linear which implies in the stiffness variation as the straining progress (ATKINSON, 2000; MITCHELL; SOGA, 2005). Figure 19a presents elementary stiffness and strength parameters for a soil specimen submitted to a triaxial test (constant σ'_3 path), with insight to the Young's modulus: initial (E_0), tangent (E_t) and secant (E_s). At very small strains, there is a region in which the stiffness is roughly constant ($E_t = E_s = E_0$). Following, there is a zone of small strains in which rapid decrements of stiffness occur as the straining progress. Finally, at the region of large strains, E_s is virtually constant and E_t is zero. The same is valid for structured and/or cemented soils in which the onset of bonds degradation changes the dynamics of the stiffness variation.

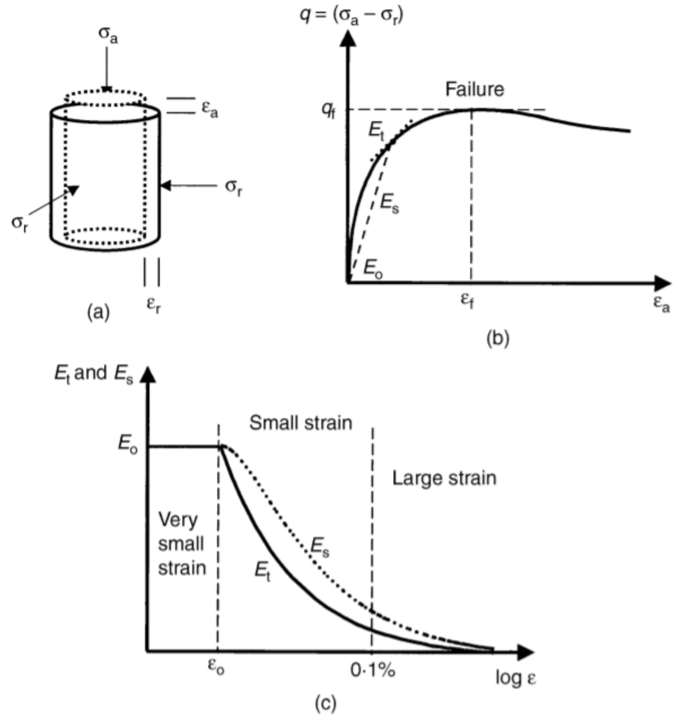

Figure 19 - Stiffness variation in triaxial test

(ATKINSON, 2000)

At the region of very small strains, the stiffness can be assessed by means of dynamic methods or using local gauges, when laboratory tests are considered (MITCHELL & SOGA, 2005). Considering linear elastic conditions, the initial shear modulus (G_0) can be given by the product between the material's bulk density (ρ) and the square of the velocity of a shear wave (V_S) passing through it. Such velocity may be assessed, for example, using pair of bender elements, resonant column test and ultrasonic pulse velocity test (CASCANTE & SANTAMARINA, 1996; FERNANDEZ & SANTAMARINA, 2001; RINALDI & SANTAMARINA, 2008; BORTOLOTTO, 2017).

At this region of very small strains, particle deformation is the prevailing deformation mechanism in geomaterials. Thus, the stiffness is fundamentally affected by the void ratio, interparticle contact dynamics and inherent material properties (CASCANTE & SANTAMARINA, 1996; CLAYTON, 2011). As a reason, the existence of a cementing agent around interparticle contacts will ultimately changes the load-induced stress distribution mechanism around these contacts (YUN & SANTAMARINA, 2005). From a micromechanical viewpoint, the Hertzian contact theory can give important insights relative to the small-strain stiffness of granular materials, cemented or not (FERNANDEZ & SANTAMARINA, 2001). In this regard, the small-strain stiffness of the granular skeleton (E_{skel}) is

$$E_{skel} = \frac{r_c}{R} \cdot \frac{G_g}{\left(1 - \upsilon_g\right)} \qquad (1)$$

In which:
r_c = radius of the contact area
R = particle radius
G_g = shear modulus of the mineral particle
υ_g = Poisson’s ratio of the mineral particle

From the relationship 1, it is prompt noticeable the great influence of the contact area between the soil’s grain in the small-strain stiffness of the material. The cementation implies the augment of the contact area between the material’s particles. Thus, the r_c value increases and, consequently, E_{skel} enhances. Moreover, the increment in the cement content causes an increase in the yield stress, postponing the onset of the bond’s degradation and enlarging the cementation controlled region (RINALDI & SANTAMARINA, 2008). Figure 20 schematically shows this mechanism by comparing the interparticle contact area of an uncemented material and a cemented material. As well, it presents the effect of cementation on the shear wave velocity (V_s). Naturally, as the strain enlarges owing to the loading process, the contact area initially increases. Following, the bonds begin to degrade and the stress state influence begins to prevail (FERNANDEZ & SANTAMARINA, 2001).

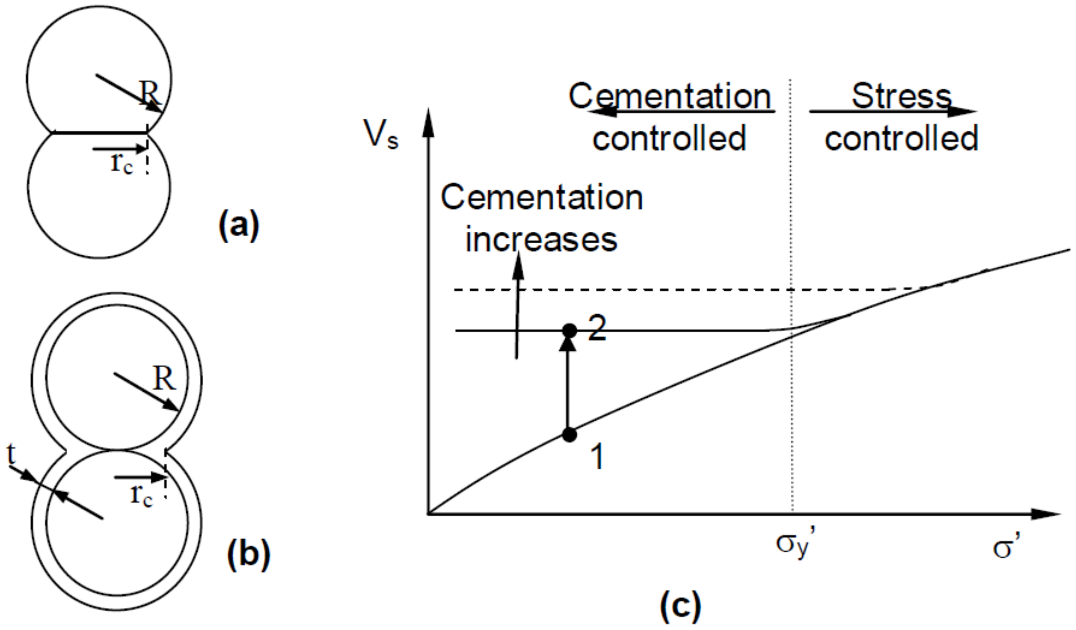

Figure 20 – Contact area (a) uncemented particle (b) cemented particle (c) shear wave velocity

(RINALDI & SANTAMARINA., 2008)

As the debonding takes place, the cemented-material response cannot be taken as linear elastic, or even nonlinear elastic (Fig. 19). From this point beyond, an elastoplastic path takes place and the stiffness degradation exhibits a nonlinear format that resembles a hyperbole (ATKINSON, 2000; SHARMA & FAHEY, 2003).

2.3.6 Degradation of the Bonded Structure in Cemented Soils

As already mentioned, the bonding structure may exert a major influence on the mechanical response of structured soils. Even so, the definition of yield for structured soils is an intricate theme, as various interpretations of the term "yield criterion" coexist (MALANDRAKI & TOLL, 1996). The classical denotation of Theory of Plasticity states the yield as a condition that sets the limit of elasticity and beginning of plastic deformation under any possible combination of stresses (YU, 2006). That is, it delimits the region of recoverable deformation (elastic zone) and irrecoverable/permanent deformation (plastic zone). For a one-dimensional loading, the yield criterion would be graphically defined by a point, whereas for two-dimensional and three-dimensional stress-states this would be, respectively, a curve and a surface.

The fully understanding of the behavior of structured materials relies on the knowledge of the onset (and progression) of bonds degradation. Namely, the determination of the point at which this occurs on stress-strain curves. Some authors (e.g. LEROUEIL & VAUGHAN, 1990; COOP & ATKINSON, 1993; COOP & WILLSON, 2003; ROTTA *et al.*, 2003; CARRETTA *et al.*, 2021) have defined the yield point as a stress state at which the material presents a discontinuity in the stress-strain response, as depicted in Figure 21. This approach gives rise to the possibility for more than one yield point, that is, distinct points relative to different phases of the bond's degradation along shearing. In this context, Vaughan *et al.* (1988) defined two yield points for a structured residual soil. The first representing the beginning of bonds failure and the second denoting an equilibrium between the decreasing bond strength and the increasing bond stress. This second yield point may be defined as the point of maximum curvature on a log-log scale plot of the stress-strain curve, yet it does not coincide with the complete destruction of the bonds, which occurs at larger strains. (BRESSANI 1990; MACCARINI, 1987).

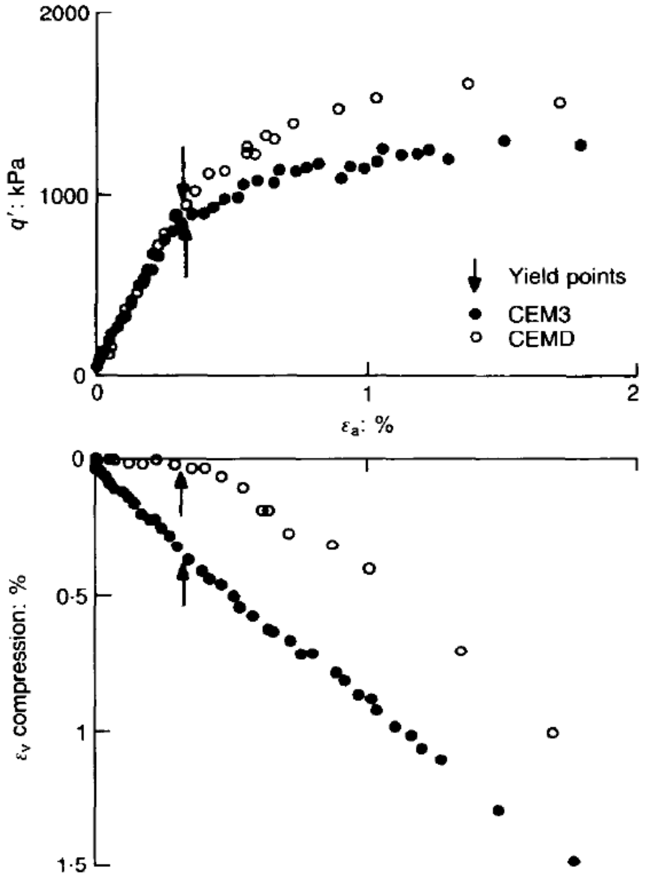

Figure 21 – Identification of yield points for cemented-soil samples

(COOP & ATKINSON, 1993)

An alternative approach is the definition of the yield points based on changes in stiffness of the material along the strain progression, as exemplified in Figure 22. Malandraki and Toll (1996) have pointed out that this approach is more accurate in addressing the yield, since it tends to clearly show the points at which major losses in stiffness initiate. In this regard, Jardine (1992) has suggested three yield conditions which act as boundaries separating three distinct zones (I, II and III) in the triaxial stress space (Figure 22a). Y1 represents the limit of the linear elastic response, Y2 delimits the recoverable (elastic) behavior zone and Y3 states the complete destruction of the material's bonded structure. Zones I and II are kinematic and moveable according to the stress path, whereas zone III is static and independent of the stress history.

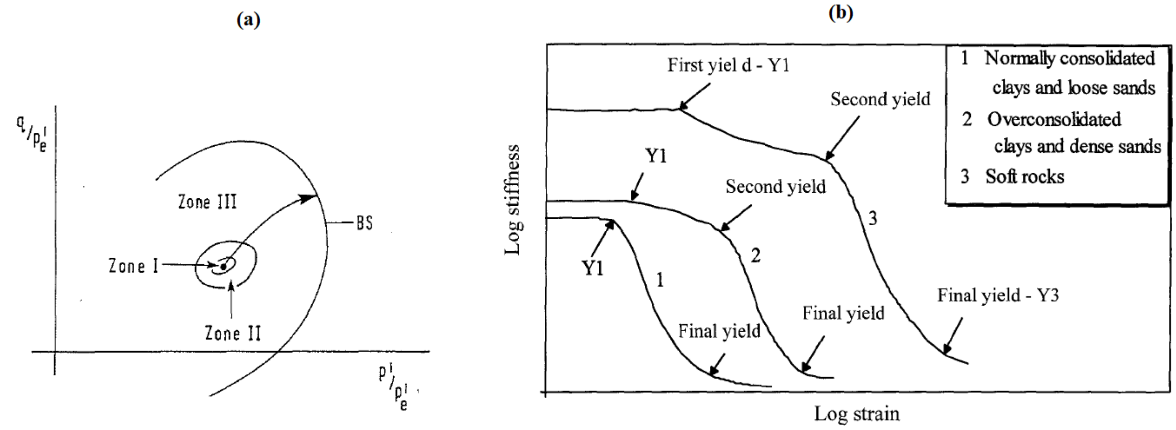

Figure 22 – Identification of multiple yield points for structured materials

(JARDINE, 1992; MALANDRAKI & TOLL, 1996)

Similarly, Malandraki and Toll (1996, 2000) have defined three yield points for bonded soils. The first is denoted by a first loss in stiffness, and suggests the onset of bond's degradation, being equivalent to the Y1 point. A second point is called "bond's yield" and is marked by a major loss in tangential stiffness, occurring between the first yield and the third ("final yield"). This third yield is analogous to the Y3 point, and represents a condition of fully bonds degradation, being of the order of magnitude as for the de-structured material. Figure 5 exemplify this approach by presenting the normalized tangential stiffness, as a function of the axial strain, for triaxial tests carried out on artificially cemented soil samples. Two different stress paths were studied at the same mean effective stress of 35 kPa: lowering a constant p' (test cp'(35)) and constant σ'_3 (test cσ'_3(35)). The results of the uncemented material for a constant $\sigma'_3 = 35$ kPa test, molded at the same void ratio, are also shown.

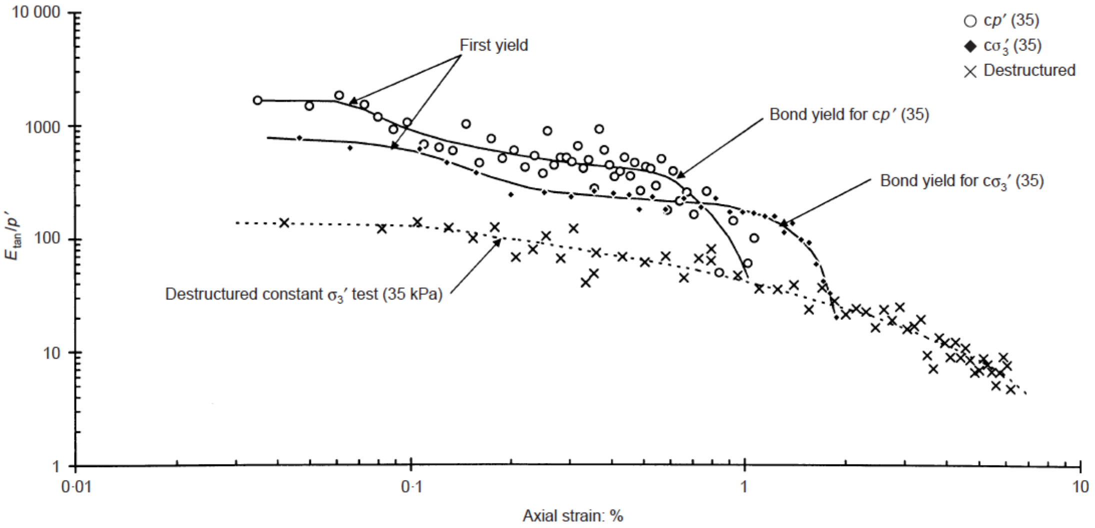

Figure 23 – Bond yield for different stress paths

(MALANDRAKI & TOLL, 2000)

According to Malandraki and Toll (1996, 2000), four distinct zones of behavior can be identified from the relative position of the failure surface and the second yield surface, as shown in Figure 24. In the first zone (1), the material's behavior at failure is entirely controlled by the bonds and the failure surface coincides with the second yield surface (bonds yield surface). In the second zone (2), the soil's response at failure is only partially governed by the bonds and the bond yield is reached before the failure. Nonetheless, the material still presents a higher maximum strength ratio (*q/p´)* than that of the de-structured soil owing to the post-yield influence of the cement matrix, such as more pronounced rates of dilation as a result of greater particle interlocking and delayed dilation (LADE & OVERTON, 1989, FERNANDEZ & SANTAMARINA, 2001; YUN & SANTAMARINA, 2005; LADE & TRADS, 2014). As the mean effective stress increases (↑*p´*), this post yield influence diminishes. In the third sector (3), the soil's response is independent of the bonding, which degrades in the beginning of the shearing. In the fourth zone, the behavior is analogous to that observed in the third zone, though the cementing matrix yielding (second yield) occurs during the isotropic compression (i.e. in the consolidation phase). In the third and fourth zones, the failure surface of the structured material coincides with that of the de-structured soil.

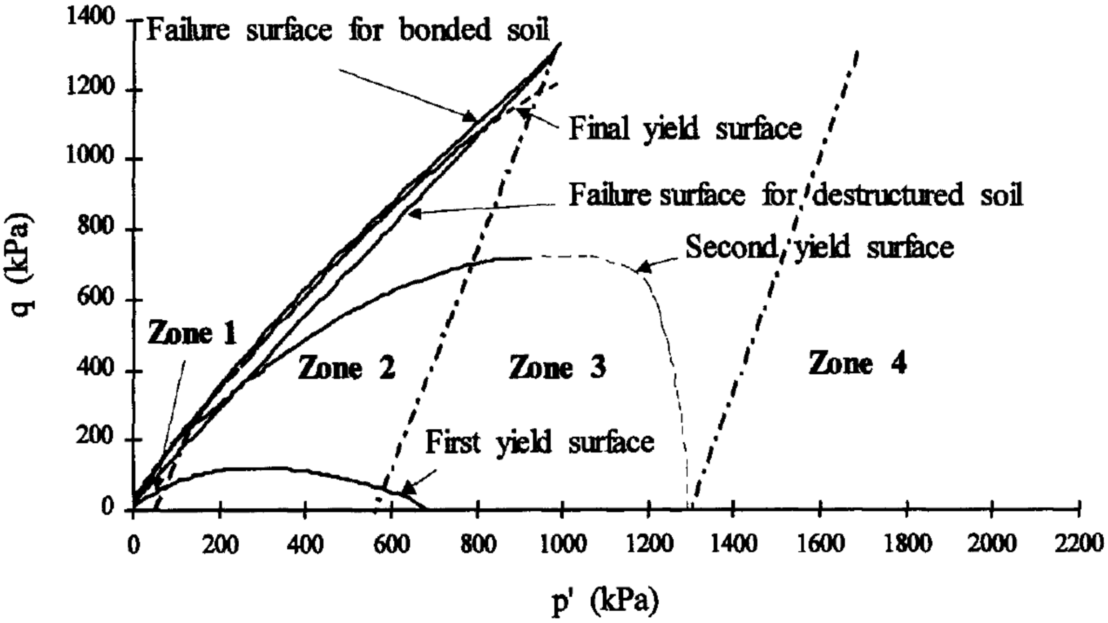

Figure 24 – Four zones of behavior for a structured soil

(MALANDRAKI & TOLL, 1996)

2.3.7 Stress-dilatancy Behavior for Cemented Soils

At drained conditions, granular materials experience volume changes under the action of shear stress (FEDA, 1982). That is, they exhibit dilatancy which is generally defined as the tendency of granular materials to change volume upon shearing (BEEN & JEFFERIES, 2016). A general overview regarding the dilatant behavior of particulate materials, including soils, was presented by Reynolds (1885), Rowe (1962), Wroth and Basset (1965), Bishop (1966), Rowe and Parkin (1969), De Josselin De Jong (1976), Bolton (1986), Muhunthan and Olcott (2002), Collins and Muhunthan (2003), among others.

Irrespective of its initial state, the continuous shearing of a granular material will ultimately reach a reference state, usually called critical state, in which the material is at constant void ratio and has no propensity to change from this condition (BEEN & JEFFERIES, 2016). That is, it continues to distort without any changes of shear stress or normal stress or void ratio, as shown in Figure 25 (ATKINSON, 2007). Such state is expressed in terms of the constant volume friction angle (ϕ'_{cv}) and the critical shear stress ratio (M). Nonetheless, the initial state (void ratio and mean effective stress) affects the stress-strain response and volume change behavior of the material up the critical state. As a reason, a loose material’s behavior is different from a dense material’s response. In the first, the strength can be fully expressed by means of the ϕ'_{cv} as no peak strength is expected and the behavior is fully contractive, whereas in the latter the strength is not entirely dependent upon the frictional component ϕ'_{cv} and a peak strength, associated to a component resultant from the dilation, is await.

For a purely frictional material, the volume changes during shearing are associated to the rearrangement of the particles. Thus, in a highly compacted soil, the interlocking between the particles implies the dilatative trend to enable shearing, as much more energy is required for particle breakage. This is schematically illustrated through a sawtooth model of dilatancy (Figure 25d), in which the angle of dilation (ψ) is the angle made by the teeth to the horizontal. Consequently, the peak friction angle (ϕ'_m) is given by:

$$\phi'_m = \phi'_{cv} + \psi \tag{2}$$

In which:

ψ = angle of dilation

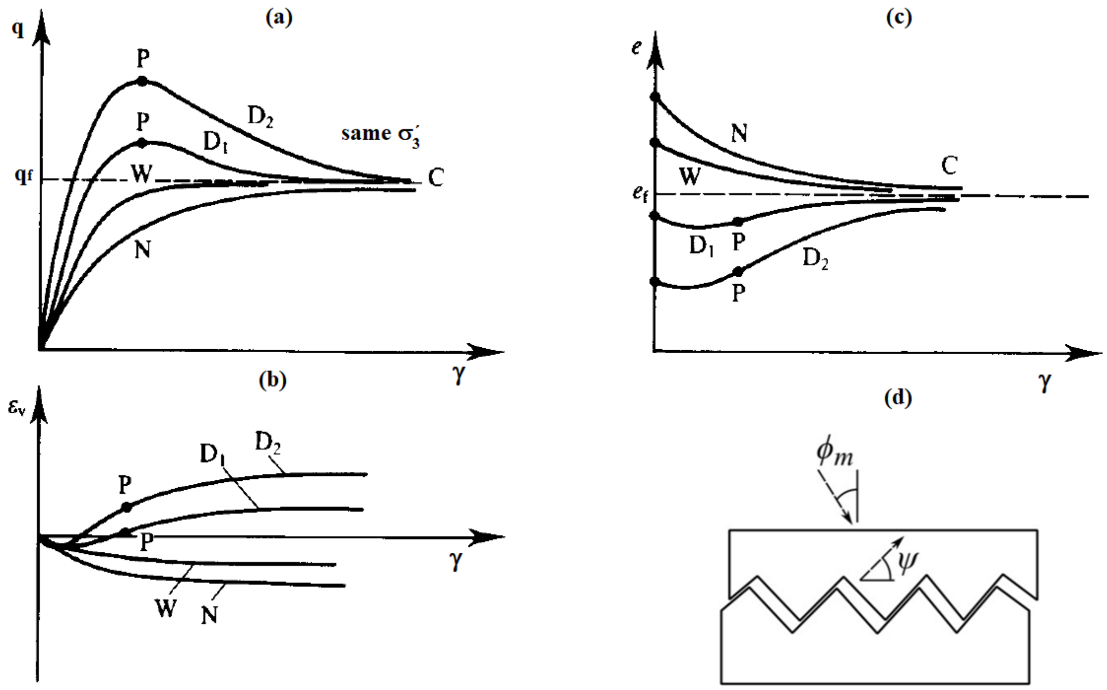

Figure 25 – Typical shearing behavior of a purely frictional material (a) stress-strain response (b) volume change behavior (c) void ratio change (d) sawtooth model for dilatancy

(after ATKINSON, 2007; KULYAKHTIN & HØYLAND, 2015)

In terms of energy, the total energy supplied per unit volume of soil (δU) is partially stored within the sample (elastic deformation) and partially dissipated (δE) through plastic straining. Hence, relationship 3 is valid for axis-symmetry conditions of loading (ROSCOE & SCHOFIELD 1963; CUCCOVILLO & COOP, 1999; PRIETTO, 2004).

$$\delta E = p' \delta \varepsilon_p^p + q \delta \varepsilon_s^p \tag{3}$$

In which:
q= deviatoric stress
p' = mean effective stress
$\delta \varepsilon_p{}^p$ = increment of plastic volumetric strain
$\delta \varepsilon_q{}^p$ = increment of plastic shear strain

If it is supposed that friction is the only mechanism responsible for energy dissipation, the first term of equation (3) can be neglected. In addition, as the ratio q/p' at the critical state is a constant denoted as M, being an intrinsic property of the material, the sum between the friction and dilatancy components must be constant. Therefore, relationship (3) can be rewritten as:

$$M = \frac{q}{p'} + \frac{\delta \varepsilon_p^p}{\delta \varepsilon_s^p} = \frac{q}{p'} + \frac{\delta \varepsilon_v^p}{\delta \varepsilon_q^p} \tag{4}$$

The behavior of cemented soils is not entirely frictional, yet the stress-dilatancy analysis for shearing of cemented materials can give valuable insights regarding the overall response of cemented materials (e.g. CUCCOVILO & COOP, 1999; LO & WARDANI, 2002; COOP & WILSON, 2003; PRIETTO, 2004; DALLA ROSA, 2006; CRUZ, 2008; MARQUES, 2016). As already discussed, up to the onset of bonds breakage, the stress-strain behavior is completely controlled by the bonds and the response is fully elastic. As the cement yields, the material starts to dilate and the dilatancy rates may be much higher in comparison to the uncemented soil owing to the delay in dilation caused by the presence of the interlocked fabric due to the cement bonds. That is, this initial impediment of dilation is later compensated by a faster dilation rate which contributes to enhance the peak strength of the structured material (CUCCOVILLO & COOP, 1999).

Initially, part of the energy is spent in disrupting the structure of the cemented soil (ΔW_{struc}) and, later on, the frictional dissipation commences. Consequently, according to Cuccovillo and Coop (1999), a new term must be added to equation 5 in order to maintain its balance as follows:

$$M = \frac{q}{p'} + \frac{\delta\varepsilon_p^p}{\delta\varepsilon_q^p} - \frac{\Delta W_{struc}}{p'\delta\varepsilon_q^p} \qquad (5)$$

In this regard, Prietto (2004) has affirmed:

> Owing to the existence of cementation, the available work to be dissipated by friction is smaller for a period of time. As the bond's degradation intensifies, the dilation progresses and augments even after the decline in the stress ratio. At the end, the work is purely frictional and the material tends to reach $\delta\varepsilon_p^p/\delta\varepsilon_q^p = 0$, namely, the critical state.
>
> […] the points corresponding to the maximum dilation rate, top stress ratio and greatest stress ratio/dilation rate quotient do not coincide. Based on the observed behavior, the last is earliest reached, followed by the peak stress ratio and, right after, the highest dilation rate. Then, the material gradually directs towards the critical state.
>
> At the point relative to the maximum dilation rate, the cohesion between the particles has already been completely eliminated and the material's behavior is, theoretically, fully frictional.

Coop and Wilson (2003) have graphically presented the stress-dilatancy data of shearing for a Castlegate sandstone in terms dilation rate ($\delta\varepsilon_p/\delta\varepsilon_s$) versus stress ratio ($q/p'$), as exhibited in Figure 26. Up to the bond's yield, an almost vertical stress path is detached as the "cemented trend". Once the breakage of the cement bonds occurs, the material starts to dilate at elevated rates up to the peak stress ratio. Right after, the material strains soften and follows a frictional trend. The authors have not made differentiations regarding the elastic and plastic strain components, and expressed the increments in terms of total deformations.

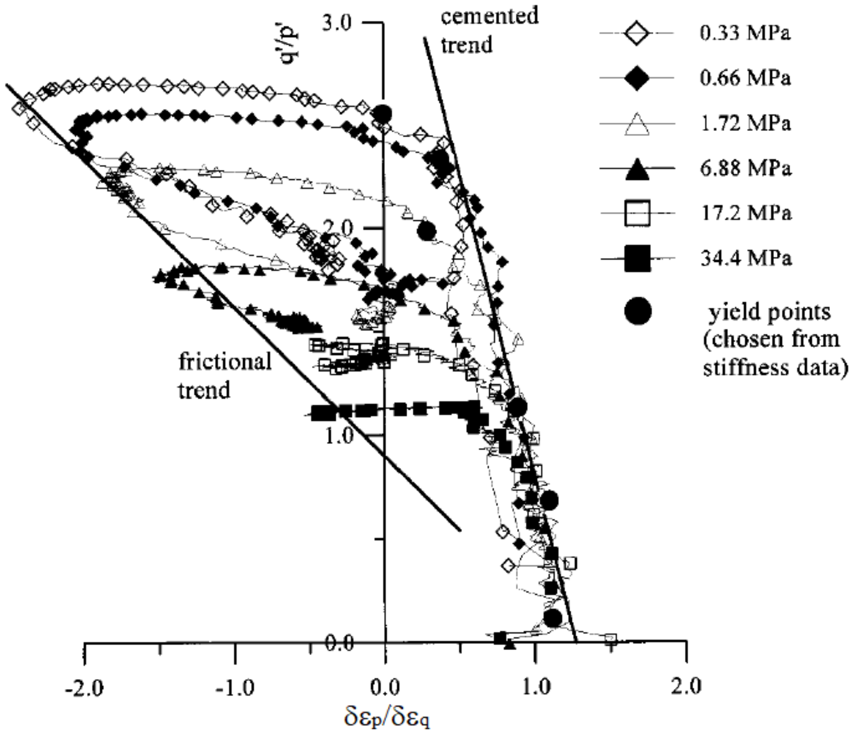

Figure 26 – Stress-dilatancy for shearing of Castlegate sandstone

(COOP &WILSON, 2003)

Similar trends were found by Marques (2016) for triaxial compression tests carried out on artificially cemented sands. The results are summarized in Figure 27.

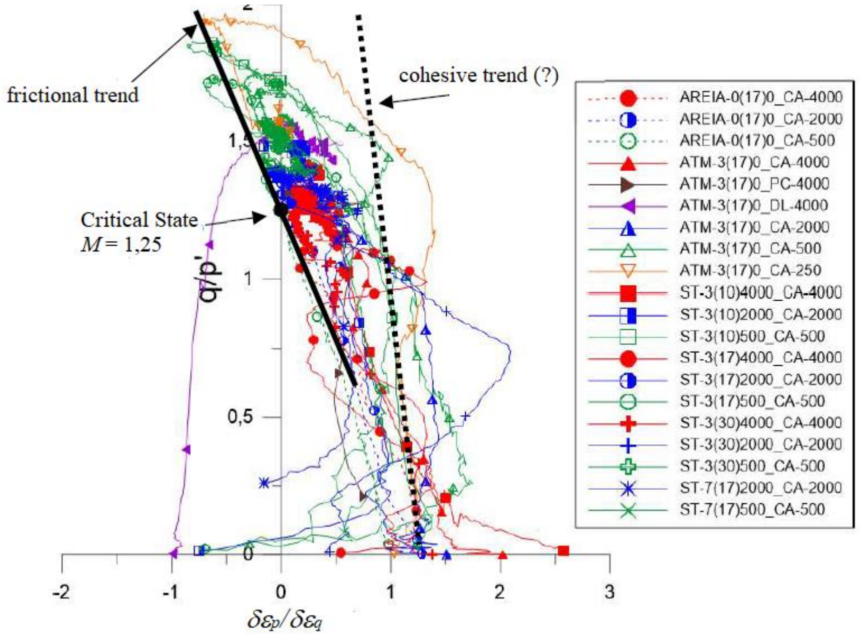

Figure 27 – Stress-dilatancy for shearing of sand-cement mixtures

(MARQUES, 2016)

2.4 THE POROSITY/CEMENT INDEX

The dosage of compacted soil-cement mixtures fundamentally involves the determination of three main aspects, namely: compactness (dry density), amount of cement and water quantity (PCA, 1995). These are dependent upon the soil's nature and on the required application of the technique. The latter will establish the minimum requirements for mechanical characteristics such as strength, stiffness and durability specifications. Thus, the dosage process usually demands numerous laboratory tests in order to fulfill these needs and provides necessary information for the design process. In this regard, ASTM D558M standard (ASTM 2019a) indicates tests for the determination of optimum water content and maximum dry density to be used in soil-cement specimens. Portland Cement Association (PCA, 1995), as well, presents a complete engineering bulletin relative to soil-cement applications. Table 1 exhibits the usual cement contents utilized for pavement applications suggested by Ingles and Metcalf (1972), whereas table 2 presents the same but proposed by PCA (1995). In both, the cement is expressed in relation to the mass of dry soil.

Table 1 – Amount of cement as a function of the type of soil for pavement applications

Soil Type	Cement Content (%)
Fine crushed rock	0.5 – 2
Well graded sandy clay gravels	2 – 4
Well graded sand	2 – 4
Poorly graded sand	4 – 6
Sandy clay	4 – 6
Silty clay	6 – 8
Heavy clay	8 – 12
Very heavy clay	12 – 15
Organic Soils	10 – 15

(INGLES & METCALF, 1972)

Table 2 – Amount of cement according to AASHTO soil group for pavement applications

AASHTO soil group	**Cement content (%)**
A-1-a	3 – 5
A-1-b	5 – 8
A-2-4	5 – 9
A-2-5	5 – 9
A-2-6	5 – 9
A-2-7	5 – 9
A-3	7 – 11
A-4	7 – 12
A-5	8 – 13
A-6	9 – 15
A-7	10 – 16

(PCA, 1995)

Larnach (1960) has assessed the strength of compacted sand-clay-cement mixtures, varying the molding moisture content and the dry unit weight within each adopted cement content (5.3%, 11.1% and 17.7%). The author related the unconfined compressive strength of the mixtures, cured along 7 days, to the ratio between the absolute volume of voids and absolute volume of cement (V_v/V_c) and obtained a relationship as expressed in Figure 28.

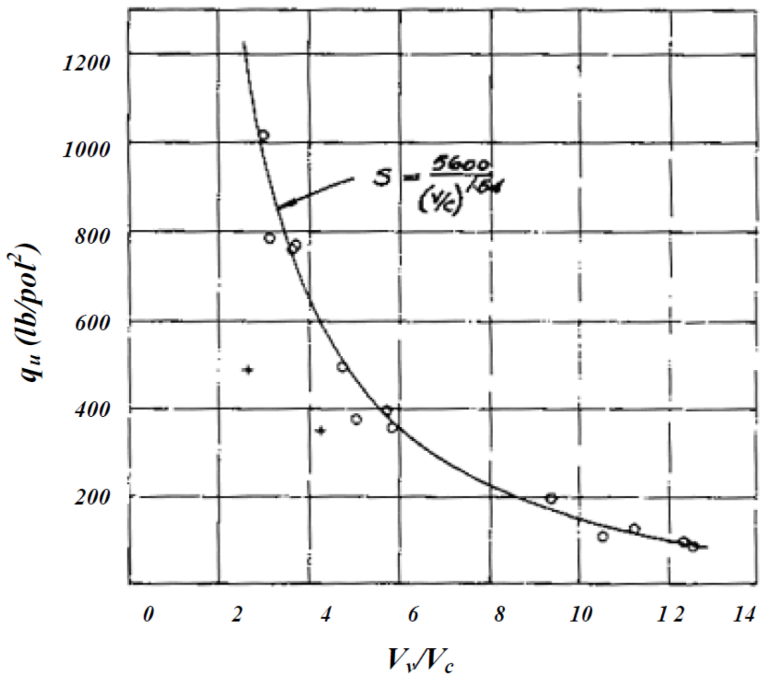

Figure 28 - Unconfined compressive strength of soil-cement mixtures versus *Vv/Vc* ratio

(LARNACH, 1960)

Considering the formerly proposed relationship by Larnach (1960) and highlighting, amongst other parameters, the importance of the dry unit weight (γ_d) and the cement content (C) on the strength of compacted soil-cement mixtures, Foppa (2005) has proposed a rational dosage method for soil-cement mixtures. The role of the compactness was expressed by means of the porosity (η), whereas the influence of the cementation was given by the volumetric cement content (C_{iv}). Therefore, the author has empirically found that the unconfined compressive strength (q_u) of compacted soil-cemented specimens could be related to the quotient η/C_{iv} through the use of an adjustment exponent (k), yielding the following power-type empirical relationship:

$$q_u = B \cdot \left[\frac{\eta}{(C_{iv})^k}\right]^b \tag{6}$$

In which:

B = multiplying scalar

η = porosity expressed as a percentage of the volumes of void over the total volume of the specimen (V_v/V_T)

C_{iv} = volumetric cement content expressed as the percentage of cement divided by the total volume of the specimen (V_c/V_T)

k = adjustment coefficient

b = power coefficient

The relationship 6 is graphically expressed in Figure 29. Theoretically, once this is established for a particular soil, a required strength (q_r) can be obtained for a unique $\eta/(C_{iv})^k$ value. Which, in turn, may be attained for different combinations of porosity values and amounts of cement.

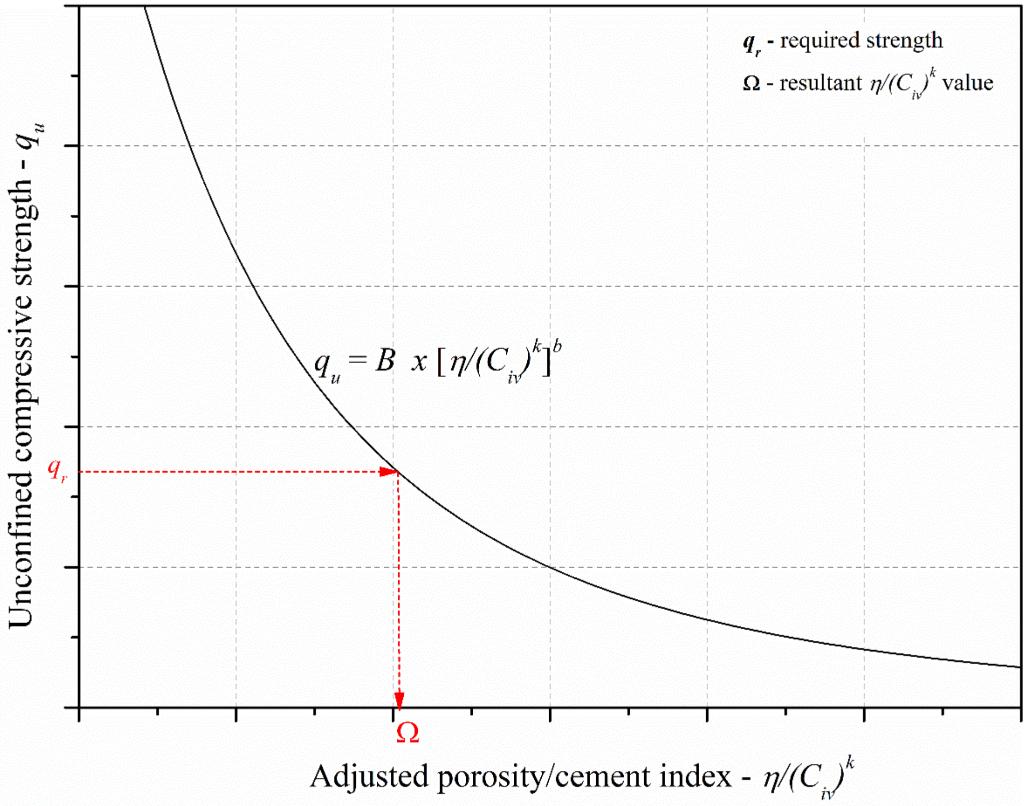

Figure 29 – Unconfined compressive strength of soil-cement mixtures versus adjusted

The adjustment coefficient k, applied to the volumetric cement content, enables the agreement between the relative effects of the porosity and the volumetric cement content on a given soil. A k equals to one ($k = 1$) indicates that either the porosity and the amount of cement exert equivalent influence regarding the strength of a particular soil mixed with cement. A positive k value, however less than one ($k < 1$), denotes a greater effect of the compactness relative to the strength of cemented-soil mixtures. The opposite is valid if k is greater than one ($k > 1$), namely, this would indicate a more prominent impact of the cement content. As a reason, the adjustment exponent k seems to be highly influenced by the nature of the soil itself as complex interactions occur owing to peculiarities related to the soil's fabric, mineralogy and grain size distribution

(CROFT, 1967; MITCHELL & SOGA, 2005). The scalar *B*, in turn, appears to be mostly affected by the curing conditions that encompass time and temperature. Table 3 summarizes the obtained parameters of relationship (2) for a variety of soils-cement mixtures, cured along 7 days at 23°C.

Table 3 – Relationship (6) parameters

Author	**Soil type**	**C (%)**	**η (%)**	**Equation parameters**		
				B (x 10^7)	b	k
Foppa (2005)	Clayey sand	1 – 12	25 – 35	6.37	-3.40	0.28
Cruz (2008)	Fine sand	1 – 12	40.5 – 44	0.003	-1.35	1.0
Floss (2012)	Sandy gravel	1 – 9	26.7 – 32.3	0.0125	-2.10	0.85
Floss (2012)	Gravelly sand	2 – 7	36.5 – 45.1	0.00878	-1.50	0.85
Floss (2012)	Fine sand	1 – 9	44.7 – 50.8	392	-4.26	0.23
Floss (2012)	Uniform sand	2 – 7	57 – 63.2	309	-7.98	010
Moreira *et al.* (2019)	Silty-sand+5%TL	3 – 9	44 – 52	0.00795	-1.35	1.0
Khajeh *et al.* (2019)*	Poor graded sand	2 – 8	36 – 39.5	0.000188	-1.52	1.0
Corte (2020)	Uniform graded sand	1.7 – 6.8	42 – 48.5	0.0043	-1.40	1.0
Baldovino *et al.* (2020)	Silty-sand	3 – 9	35 – 48	0.068	-2.00	0.45

(after FOPPA, 2016; CORTE 2020)

In addition to the unconfined compressive strength of soil-cement mixtures, the $\eta/(C_{iv})^k$ ratio was correlated to other mechanical properties such as initial shear modulus (G_0) and accumulated loss of mass (ALM) observed in durability tests. Table 4 presents examples of the literature relative to the correlation of the porosity/cement ratio with a few mechanical properties of a variety of soil-Portland cement mixtures.

Table 4 – Porosity/cement index related works

Property/Test Method	Reference
Unconfined Strength Tests	Foppa (2005, 2016), Consoli *et al*. 2007, 2009a, 2009b, 2009c, 2011a, 2011b, 2012a, 2013, 2016, 2016b, 2016c, 2018b, 2019, 2020; Stracke *et al*. (2012), Rios *et al*. 2012, 2013, Rios and Viana da Fonseca 2013, Festugato *et al*. 2017, 2021, Marques (2016), Mola-Abasi *et al*. 2017, de Paula *et al*. 2019, Henzinger and Schömig 2019, Khajeh *et al*. (2019), Baldovino *et al*. (2020a), Corte (2020)
Initial Shear Modulus (G_0)	Cruz (2008), Fonini (2012), Hoch (2017), Bortolotto (2017), Consoli *et al*. (2017d), Tomasi (2018), Corte (2020)
Accumulated Loss of Mass (ALM)	Consoli *et al*. (2017a, 2017b, 2018), Hoch (2017), Baldovino *et al*. (2020b)

2.4.1 Theoretical Derivation for Unconfined Compressive Strength Correlations

A theoretical derivation of relationship 7 was presented by Diambra *et al*. (2017) in order to establish a proper connection between the material properties and the governing coefficients of relationship 6. The authors have theoretically demonstrated that the coefficients k and b are dependent on the soil matrix and can be related to the parameter a as $k = 1/a$ and $b = -a$. The parameter a governs the dependence of soil strength on its density. The multiplying parameter B is affected by the combined properties of the soil matrix and the cement phase, and is highly influenced by the curing conditions as this governs the cement phase development. The relationship 6 can, thus, be presented as:

$$q_u = B \cdot \left[\frac{\eta}{(C_{iv})^{1/a}}\right]^{-a} \tag{7}$$

Diambra *et al.* (2017) have assumed the artificially cemented soil as an isotropic composite material in which the failure is determined by superimposing the strength contributions of either the cement and the soil phases. Moreover, it is supposed strain compatibility between these two phases and, as well, it is presumed a simultaneous failure in both. The strength of the cement phase was described by the Drucker-Prager failure criterion, whereas the resistance of the soil matrix was represented by relating the mean stress ratio (q_m/p_m) to a state parameter in terms of the material's porosity (current porosity/porosity at the critical state). Roughly, the proposed model relies on the following parameters:

M: critical state strength ratio of the soil;
η_{cs}: critical state porosity, which is taken as a constant for each soil;
a: parameter governing the dependence of soil strength on its density;
σ_c^c: cement phase compressive strength at a specified curing period;
β: uniaxial compression and extension cement strength ratio;
K_c: cement stress ratio.

The following relationship thus results from the aforementioned assumptions:

$$q_u = \frac{6\mu_c \sigma_c^c}{K_c(1-\beta)+3(\beta+1)}\left[\frac{K_c - M\left(\frac{\eta_{cs}}{\eta}\right)^a}{3 - M\left(\frac{\eta_{cs}}{\eta}\right)^a}\right] \tag{8}$$

Where:
$\mu_c = C_{iv}/100$

Relationship 8 does not resemble the empirical formula stated in relationship 6 as it is not a linear function of the peak strength of the soil. Yet, the following approximation can be introduced:

$$\frac{K_c - M^*}{3 - M^*} \cong M^*(-0.6 + 0.45K_c) \tag{9}$$

If relationship 9 is introduced in (8), and with further manipulation, a full conformity between the theoretical and the empirical approaches can be reached as shown in relationship 10. Through this approach, it is clear that the coefficients k and b from (6) rely on the soil matrix properties. Moreover, the scalar parameter B is the first term in the left sided equation and is either influenced by the soil and cement phase properties.

$$\frac{6M\sigma_c^c(-0.6+0.45K_c)\eta_{cs}^a}{100[K_c(1-\beta)+3(\beta+1)]}\cdot\left[\frac{\eta}{(C_{iv})^{1/a}}\right]^{-a} = B\cdot\left[\frac{\eta}{(C_{iv})^{1/a}}\right]^{-a} \tag{10}$$

2.4.2 Theoretical Derivation for Initial Shear Modulus Correlations

Based on previous power-type correlations between the small strain stiffness (G_0) and the adjusted porosity/cement index for soil-cement specimens (equation 6), Diambra *et al*. (2019) have attempted to give a theoretical justification for the existence of such relationship. Thus, the meaning of the terms composing the equations were discussed and explained through the parallelism of relationship (11) to formerly proposed approaches.

$$\frac{G_0}{p_r} = C\cdot\left[\frac{\eta}{(C_{iv})^b}\right]^d \tag{11}$$

Where:
p_r = reference pressure (1 MPa)

Based mainly on Hardin (1978) and Viggiani and Atkinson (1995) works, Trhlíková *et al.* (2012) have proposed an equation considering the effect of cementation and, as well, the existing mean effective stress (p') for cemented/structured soils. Hence, the following relationship was suggested:

$$\frac{G_0}{p_r} = A\left(\frac{p'}{p_r}\right)^n\left(\frac{p_e^*}{p'}\right)^m\left(\frac{S}{S_f}\right)^l \tag{12}$$

Where:
A, *n*, *m* and *l* = model constants
p_e^* = Horslev equivalent pressure
S = measure of structure of cemented/structured soil
S_f = measure of structure for uncemented/unstructured soil

In this context, Diambra *et al.* (2019) have indicated that the degree of structure/cementation of the material (S/S_f) can be represented by the quotient between the Horselv equivalent pressure of the cemented material and the Horselv equivalent pressure of the uncemented material (p'_e/p^*_e). Moreover, based on previous results (e.g. DOS SANTOS *et al.*, 2010; RIOS *et al.*, 2012), the authors have assumed that the Normal compression line (NCL) of the cemented and uncemented soils are parallel (same λ inclination) to each other, being the shifting (different T values) dependent upon the cement content. This is summarized in Figure 30, below.

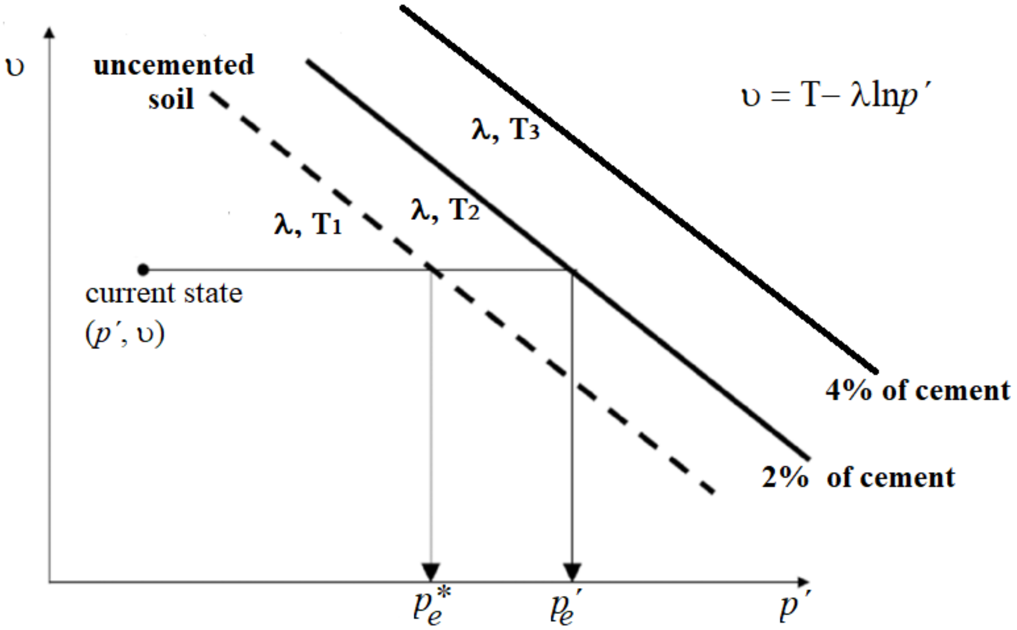

Figure 30 – Unconfined compressive strength of soil-cement mixtures versus adjusted porosity/cement ratio

(after DIAMBRA *et al.*, 2019)

Considering that the initial stiffness does not depend on the confining pressure at low levels of stress or unconfined stress conditions ($p' = p_r$) and adopting the approach proposed by Diambra et *al.* (2019) to account for the structure effects, equation 12 can be rewritten as:

$$\frac{G_0}{p_r} = A\left(\frac{p_e'}{p_r'}\right)^m \left(\frac{p_e'}{p_e^*}\right)^q \qquad (13)$$

Where:

p_e' = mean pressure for a given specific volume in the cemented soil

Relationship 13 still does not resemble the power-type equation 11. Yet, at unconfined compression condition, p_e^* depends solely on the specimen's porosity (η). Thus, p_e^* can be related to the porosity by means of two fitting parameters (*f* and *D*) as follows:

$$p_e^* = D\eta^{-f} \tag{14}$$

In the light of a linear trend in the ʋ-lnp' plane (NCL) and considering the parallelism between the lines of the cemented and uncemented soils, the quotient $p_e^{'}/p_e^*$, for a fixed cement content, can be expressed by:

$$\frac{p_e^{'}}{p_e^*} = \frac{e^{(T_c-\upsilon)\lambda}}{e^{(T-\upsilon)\lambda}} \tag{15}$$

Where:
T_c = relative to the cemented soil
T = relative to the uncemented soil

By plotting the $p_e^{'}/p_e^*$ ratio as a function of the volumetric cement content (C_{iv}) for a particular cemented soil, a linear trend of the following form can be adjusted:

$$\frac{p_e^{'}}{p_e^*} = 1 + HC_{iv} \tag{16}$$

Where:
H = inclination of the adjusted line

If equations 14 and 15 are introduced into equation 13, the following relationship is derived:

$$\frac{G_0}{p_r} = AD^m \left[\frac{\eta}{(HC_{iv} + 1)^{q/(fm)}} \right]^{-fm} \tag{17}$$

In order to equation 17 reflect the power-type relationship expressed by equation 11, Diambra *et al.* (2019) have proposed that the following approximation can be performed for low volumetric cement contents ranging between 1 and 4:

$$HC_{iv} + 1 \approx LC_{iv} \tag{18}$$

As a reason, equation 19 is yielded:

$$\frac{G_0}{p_r} = AD^m L^q \left[\frac{\eta}{(C_{iv})^{q/(fm)}} \right]^{-fm} \tag{19}$$

Consequently, a full parallelism is achieved between relationships 11 and 19. The adjustment parameters of the first (*A*, *D*, *L*, *m*, *f* and *q*) are dependent upon material characteristics and are related to the parameters of the former equation (*C*, *d* and *b*) as follows:

$$\mathrm{C} = \mathrm{A}D^m L^q \tag{20}$$

$$\mathrm{b} = \frac{q}{fm} \tag{21}$$

$$d = -fm \tag{22}$$

To apply this approach (relationship 19) for a given cemented soil, isotropic compression tests, performed either in the natural soil and in soil-cement mixtures containing distinct amounts of cement, are needed. These outcomes enable the determination of p_e^* and, as a reason, of the D and f parameters. The H and L coefficients are obtained through the relationship of the $p_e^{'}/p_e^*$ ratio to the volumetric cement content (C_{iv}). Moreover, a few results of initial shear modulus (G_0), measured at unconfined conditions, are required for the obtainment of the parameters A, m and q. These may be graphically obtained via an iterative process that involves plotting relationship 13 and attempting to input different values for the coefficient m, being A and q the results of a power-type fitting equation with the greatest coefficient of determination for a given m value.

3. RESEARCH PROGRAM

This session presents the experimental program carried out to investigate the mechanical response and the microstructure of the BRS-cement mixtures. Considering the stiffness, unconfined compression strength tests and durability tests, the testing setup was planned intending to enable a statistical evaluation of the results. That is, to check for possible equivalence of performance of specimens molded at the same $\eta/(C_{iv})^{0.28}$ index value but having different dosages.

3.1 INITIAL SHEAR MODULUS, UNCONFINED COMPRESSION AND SPLIT TENSILE TESTS

The adopted approach was proposed in order to assess the mechanical behavior of BRS-cement mixtures molded with 7 distinct values of the $\eta/(C_{iv})^{0.28}$ index. Within each porosity/cement ratio value, at least three distinct dosages were assembled by varying the cement content (C) and the dry unit weight (γ_d), but maintaining the $\eta/(C_{iv})^{0.28}$ index value constant. A total of 26 different dosages were established as summarized in Table 5. The main curing period was set as 7 days. Yet, additional strength tests were performed after 28 and 90 days. The molding moisture content was defined at 10%, irrespective of the adopted mix design. Considering the 7 days curing period, five specimens were molded within each mix design (i.e., quintuplicates). For other the times of curing, three samples were used (i.e., triplicates).

Table 5 – Dosage characteristics for the strength and initial shear modulus tests

$\eta/(C_{iv})^{0.28}$	Mix Design	γ_d (kN/m³)	C (%)
45	1	16.59	1.00
	2	15.61	1.50
	3	14.87	2.00
40	4	17.53	1.00
	5	16.65	1.50
	6	14.96	3.00
35	7	18.55	1.00
	8	17.11	2.00
	9	15.50	4.00
	10	14.96	5.00
30	11	18.31	2.00
	12	17.45	3.00
	13	16.87	4.00
	14	15.96	6.00
25	15	18.85	3.00
	16	17.88	5.00
	17	17.21	7.00
	18	16.94	8.00
22.5	19	18.67	5.00
	20	18.34	6.00
	21	18.05	7.00
	22	17.81	8.00
20	23	19.04	6.50
	24	18.70	8.00
	25	18.49	9.00
	26	18.32	10.00

3.2 DURABILITY TESTS

Durability tests through wetting-drying-brushing cycles were carried out in order to evaluate the performance of the BRS-cement mixtures under harsh environmental conditions. The same strategy previously embraced for the strength tests was adopted herein, yet only two dosages within each $\eta/(C_{iv})^{0.28}$ index value were assessed due to the enormous amount of time and material needed in the conduction of this test. In addition, the dosages corresponding to the $\eta/(C_{iv})^{0.28}$ index values of 40 and 22.5 were withdraw from the analysis. The chosen mix designs corresponded to the extremes inside each $\eta/(C_{iv})^{0.28}$, that is, the most porous with higher amount of cement (↑η and ↑C) and the least porous with smaller amount of cement (↓η and ↓C). Four specimens were molded for each mix design, three to be actually tested and one for moisture control during the cycles. The curing period was, as well, 7 days. Table 6 summarizes the tested dosages.

Table 6 – Dosage characteristics for the durability tests

$\eta/(C_{iv})^{0.28}$	Mix Design	γ_d (kN/m³)	C (%)
45	1	16.59	1.00
	3	14.87	2.00
35	7	18.55	1.00
	10	14.96	5.00
30	11	18.31	2.00
	14	15.96	6.00
25	15	18.85	3.00
	18	16.94	8.00
20	23	19.04	6.50
	26	18.32	10.00

3.3 TRIAXIAL TESTS

Aiming to assess the effect of the $\eta/(C_{iv})^{0.28}$ index on the stress-strain response and on the volume change behavior of the BRS-cement mixtures, isotropically consolidated drained triaxial tests were conducted. The same strategy formerly presented for the durability tests was employed for triaxial testing, that is, two dosages were tested within each adjusted porosity/cement index. Yet, no replication was done considering the same dosage and the same confining presure. The curing period was established as 7 days. An effective confining pressure (σ'_3) of 35 kPa was adopted for all the tests conducted herein, whereas confining pressures of 70 and 140 kPa were used for all the dosages molded for the $\eta/(C_{iv})^{0.28}$ values of 25, 30 and 35. Moreover, complementary tests were conducted at different confinements for a few dosages, as depicted in table 7.

Table 7 – Triaxial testing program

$\eta/(C_{iv})^{0.28}$	Mix Design	γ_d (kN/m³)	C (%)	σ'_3 (kPa)
45	1	16.59	1.00	35
	3	14.87	2.00	
35	7[a]	18.55	1.00	35, 70 and 140
	10	14.96	5.00	
30	11[a]	18.31	2.00	
	14	15.96	6.00	
25	15	18.85	3.00	
	18[b]	16.94	8.00	
20	23	19.04	6.50	35
	26	18.32	10.00	

a – a complementary test at σ'_3 = 95 kPa was conducted considering this mix design
b – a complementary test at σ'_3 = 300 kPa was conducted considering this mix design

Additionally, three triaxial tests were carried out on the natural soil, using disturbed soil samples molded at the respective dry unit weight values: 19.0 kN/m³ (e = 0.39); 17.5 kN/m³ (e = 0.51) and 16.0 kN/m³ (e = 0.66). The employed effective confining pressure was 35 kPa. To sum up, a total of 27 triaxial tests were carried out for the present research. Besides, the magnitude of the confining pressures was chosen in order to guarantee the intactness of the cement bonds during the consolidation phase. It was intended that the bonds would only yield owing to the shearing process (e.g., cases 1 and 2 of Figure 15). In this regard, the unconfined compressive strength (q_u) of the cemented specimen can be a rough estimate of the order of magnitude of the bond's degradation in the consolidation phase (e.g., ROTTA *et al*., 2003). As a reason, none specimen was consolidated beyond its q_u value, for example.

3.4 SCANNING ELECTRON MICROSCOPE TESTS

In order to account for differences in the fabrics of the BRS-cement specimens molded with the same $\eta/(C_{iv})^{0.28}$ index, but using different dosages, scanning electron microscopy (SEM) were conducted. The SEM tests were performed for every $\eta/(C_{iv})^{0.28}$ values, considering the two most extreme dosages (i.e., ↑η and ↑C and ↓η and ↓C). Table 8 summarizes the mix designs used for the SEM tests.

Table 8 – Dosage characteristics for the SEM tests

$\eta/(C_{iv})^{0.28}$	Mix Design	γ_d (kN/m³)	C (%)
45	1	16.59	1.00
	3	14.87	2.00
40	4	17.53	1.00
	6	14.96	3.00
35	7	18.55	1.00
	10	14.96	5.00
30	11	18.31	2.00
	14	15.96	6.00
25	15	18.85	3.00
	18	16.94	8.00
22.5	19	18.67	5.00
	22	17.81	8.00
20	23	19.04	6.50
	26	18.32	10.00

3.5 MERCURY INTRUSION POROSIMETRY TESTS

Intending to characterize the pore size distribution (PSD) of the BRS-cement specimens molded with the same $\eta/(C_{iv})^{0.28}$ index, but using different dosages, mercury intrusion porosimetry (MIP) tests were carried out. Owing to the elevated costs of such test, it was only performed for the $\eta/(C_{iv})^{0.28}$ values of 35, 30 and 25, considering the two most extreme dosages (i.e., $\uparrow\eta$ and $\uparrow$C and $\downarrow\eta$ and $\downarrow$C). Table 9 summarizes the dosages used for the MIP tests.

Table 9 – Dosage characteristics for the MIP tests

$\eta/(C_{iv})^{0.28}$	Mix Design	γ_d (kN/m³)	C (%)
35	7	18.55	1.00
	10	14.96	5.00
30	11	18.31	2.00
	14	15.96	6.00
25	15	18.85	3.00
	18	16.94	8.00

4 MATERIALS AND METHODS

This chapter presents the characterization of the materials employed herein and, as well, describes the procedures relative to samples preparation, tests and equipment.

4.1 MATERIALS

Three materials were employed in the present research as follows: a residual soil in an unstructured state known as Botucatu Residual Soil (BRS), high early strength Portland cement and distilled water. Each one of these are separately characterized below.

4.1.1 Botucatu Residual Soil

The soil used herein is known as Botucatu Residual Soil (BRS) and has been thoroughly used in geotechnical researches along the past three decades (e.g. NUÑEZ, 1991; PRIETTO, 1996, 2004; HEINECK, 1998; ROTTA, 2000, 2005; MARTINS, 2001; CRUZ, 2004; 2008; FOPPA, 2005, WINTER 2018, DE PAULA, 2020). The BRS derives from the Botucatu sandstone which is a sedimentary rock of eolian origin formed by a superposition of paleodunes with a stratification of cross-bedding type (MARTINS *et al*., 2005). The BRS preserves the original sandstone fabric over a substantial depth (horizon C of tens of meters) and may be called a rock from a geological perspective. Nonetheless, it presents a very low strength and it is easily manually excavated which enables its classification as a soil from a geotechnical viewpoint. Particularly, the BRS has been chosen for the present study owing to its workability and, primarily, due to its capability to exists under a wide range of void ratios. As a reason, it is possible to achieve several dosages within a fixed $\eta/(C_{iv})^{0.28}$ index value.

The soil was collected in a disturbed and de-structured state by manual excavation from a slope in the locality of Vila Scharlau, municipality of São Leopoldo – RS (Figure 31).

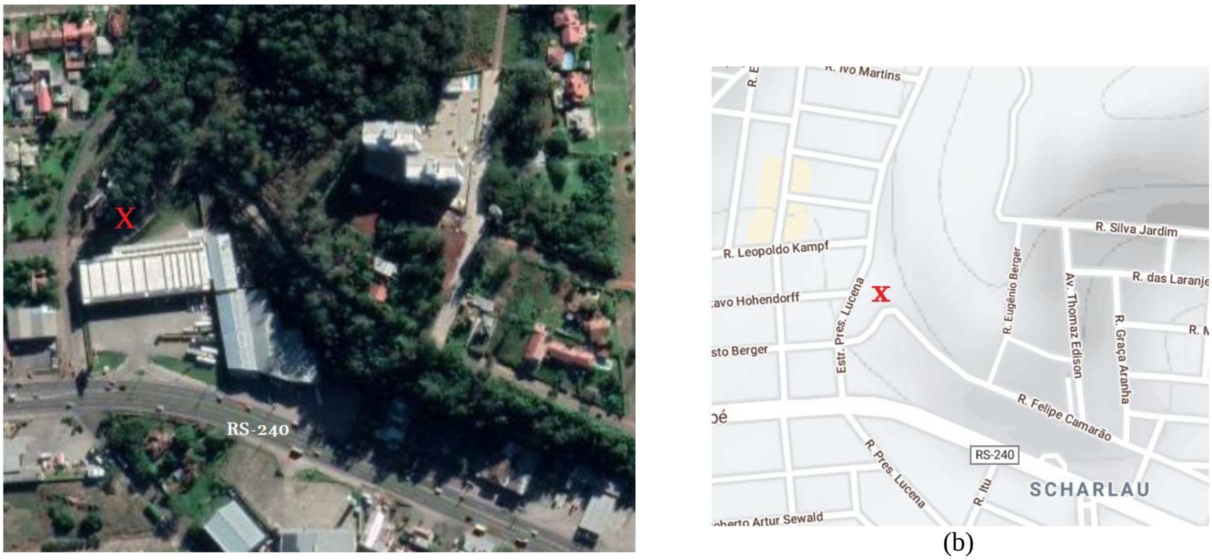

(a) (b)

Figure 31 - Soil collection site (a) satellite image (b) terrain map

Figure 32 presents the grain size distribution of the BRS used in the present work altogether with the granulometry of BRSs used in other researches, but collected at the same (or nearby to) Scharlau site. It is possible to attest a great similarity regarding the grain size distribution of those soils. Table 10 summarizes the main characteristics of the BRS utilized herein. According to Unified Soil Classification System – ASTM D2487 (ASTM, 2017), Botucatu Residual Soil is a clayey sand (SC).

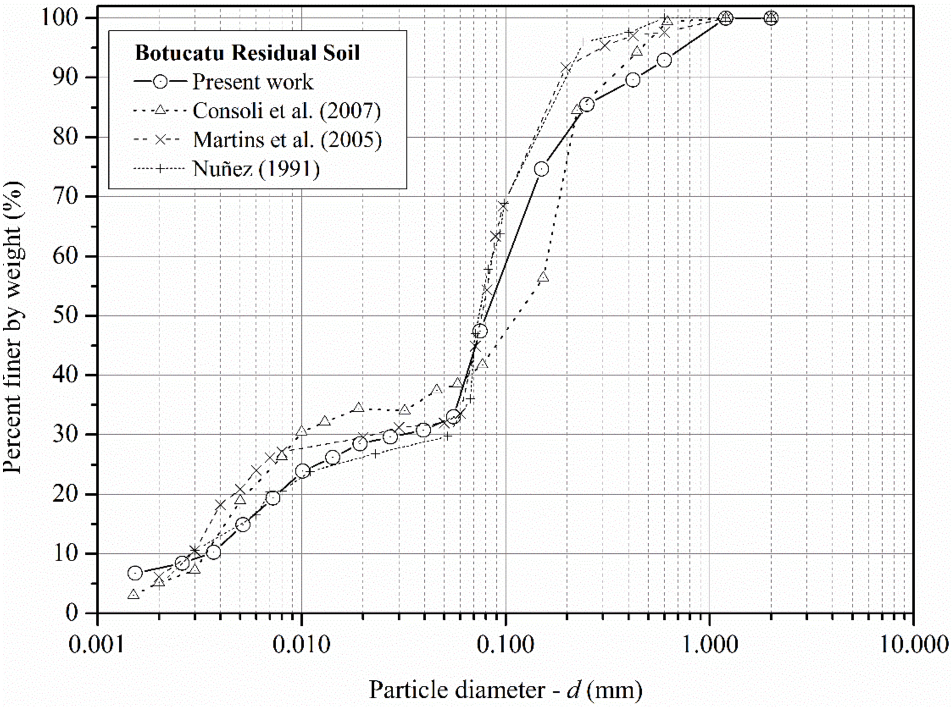

Figure 32 – Grain size distribution of the Botucatu Residual Soil

Table 10 – Main characteristics of the Botucatu residual soil

Physical properties	Botucatu Residual Soil	Test method
Liquid limit (%)	22	NBR 6459
Plastic limit (%)	13	NBR 7180
Plastic index (%)	9	-
Specific gravity	2.65	NBR 6457
Coarse Sand (2.00 mm < d < 4.75 mm) (%)	0	NBR 7181
Medium Sand (0.425 mm < d < 2.00 mm) (%)	10.4	
Fine Sand (0.075 mm < d < 0.425 mm) (%)	42.2	
Silt (0.002 < d < 0.075 mm) (%)	40.7	
Clay (d < 0.002 mm) (%)	6.7	
Effective diameter (D_{10}) (mm)	0.0035	
Uniformity Coefficient (C_u)	28.57	
pH	5.10	ASTM D4972

The compaction characteristics of the soil were obtained through Proctor compaction tests using the standard and modified efforts. The recommendations of NBR 7182 (ABNT 2020) were followed. The results are depicted in Figure 33.

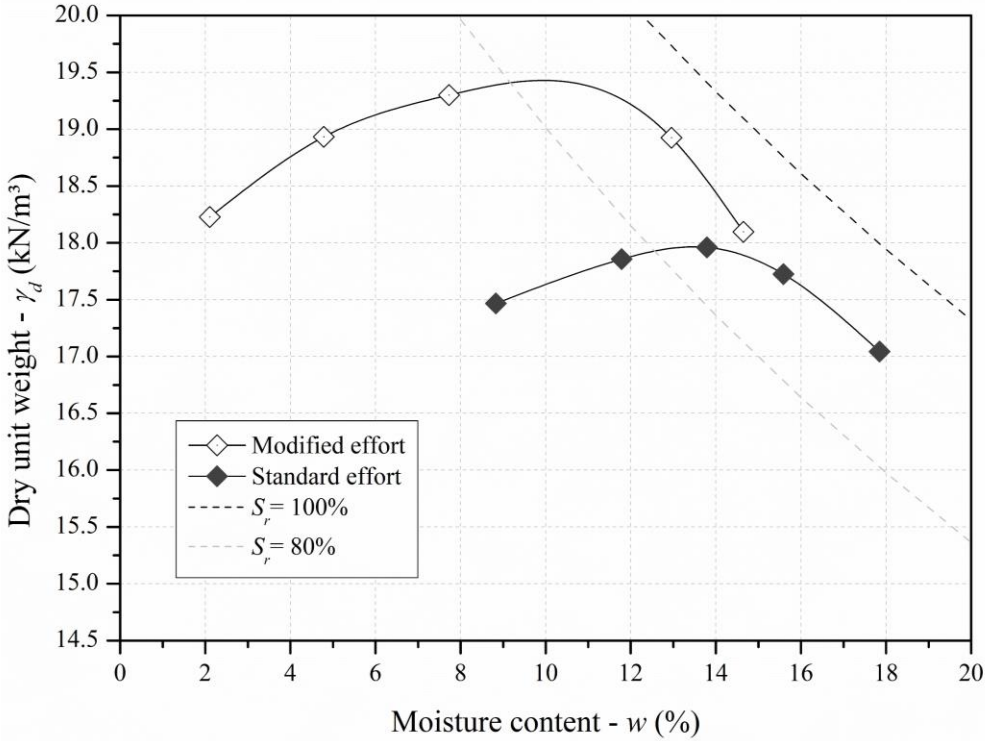

Figure 33 – Compaction curves of the Botucatu Residual Soil

The sand and silt portions of the BRS are mainly composed by quartz grains, whereas the clay fraction is constituted by kaolinite, hematite, illite and quartz (NUÑEZ, 1991). The undisturbed

BRS consists of dentritic quartz grains linked by kaolinite particles clusters which are reinforced by an iron oxide coating (MARTINS *et al*., 2005). These bridge-like clusters form a cement material in the intact/undisturbed soil and confer it a structure (see item 2.3), as can be seen in the Scanning Electron Microscope (SEM) micrograph displayed in Figure 34. On the other hand, the fabrics of the remolded BRS are substantially different since the structure is lost and the clay particles became randomly distributed, covering the surface of most of the quartz grains. In other words, the fabrics of the remolded BRS is made up of quartz grains embedded into a clay matrix that is mainly composed by kaolinite. This is noticeable on the SEM micrographs taken on remolded BRS samples (*e* = 0.60) and shown in Figure 35. In this regard, Fig. 35c and Fig. 35d show in detail the staking of kaolinite particles, which is a typical form of aggregation of this mineral (e.g., IVANIĆ *et al*., 2015; URAL, 2020).

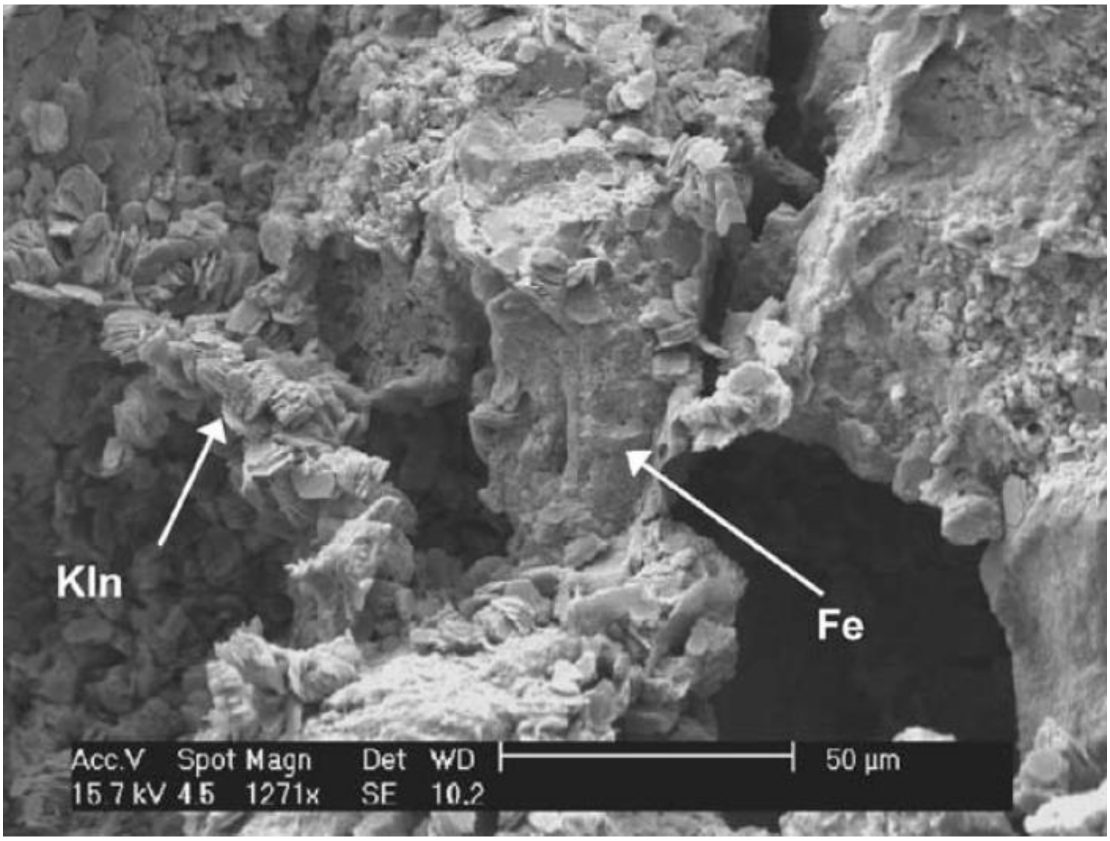

Figure 34 – Intact BRS sample SEM micrograph (*e* = 0.70)

(MARTINS et al., 2005)

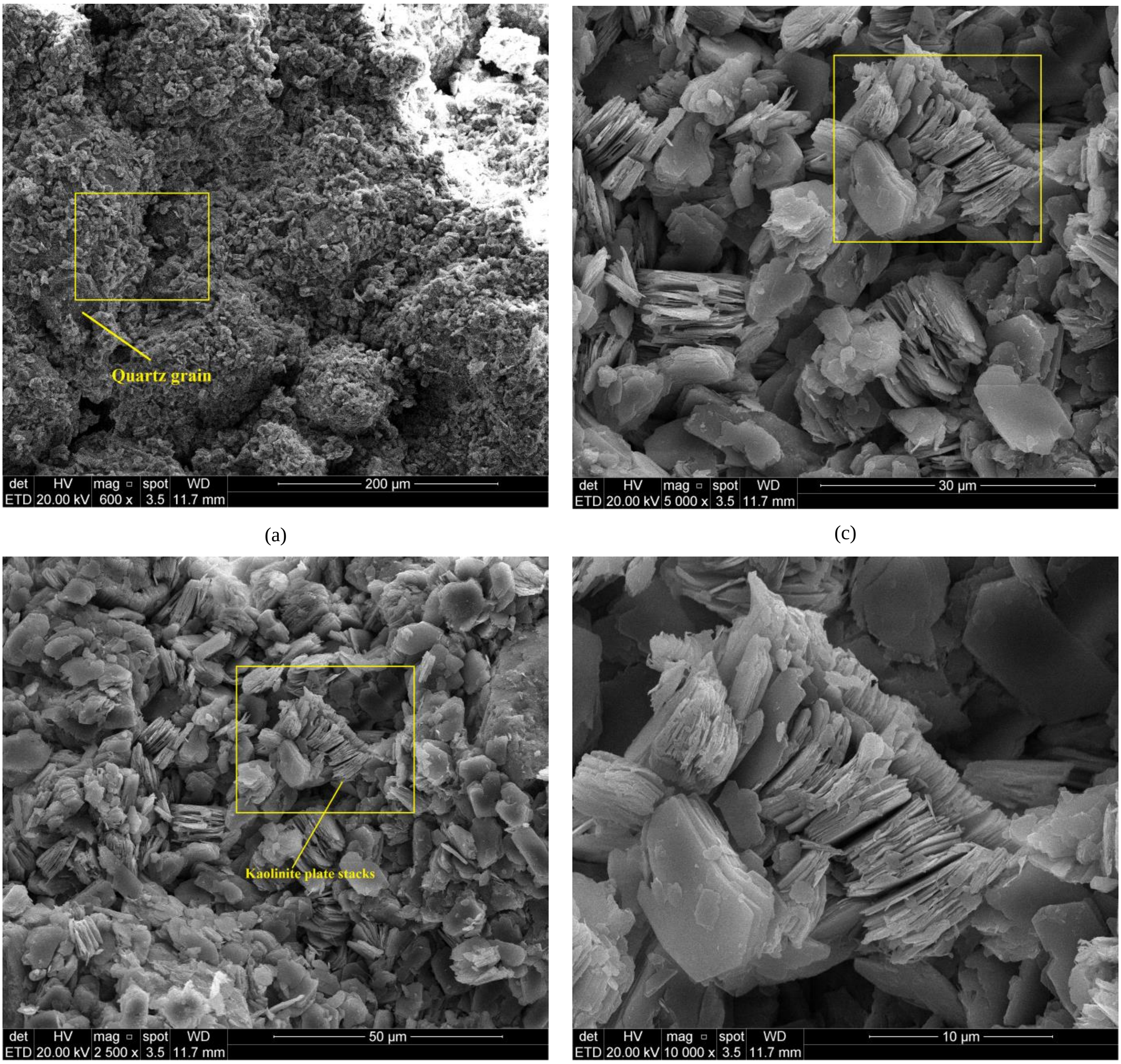

(a) (c)

(b) (d)

Figure 35 – SEM micrographs of remolded BRS sample, magnification of (a) 600x (b) 2500x (c) 5000x (d) 10000x

4.1.2 Cement

The cementing agent used herein was a high early strength Portland cement known as CP V – ARI. It is classified as type III according to ASTM C150 (ASTM, 2020). It possesses an elevated rate of strength gain at initial period of curing, reaching up to 80% of its top strength at only 7 days. The specific gravity of the cement is 3.15.

4.1.3 Water

Distilled water was used for the specimen’s preparation, irrespective of the test method. In the triaxial test, distilled water was used either in the confinement of the test sample and on the percolation process. For the durability test, tap water was used in during the immersion period.

4.2 METHODS

4.2.1 Mixtures Design Setting

Based on Foppa (2005), Consoli *et al.* (2007), Diambra *et al.* (2017), among others, it is well established that the internal adjustment exponent k (see relationship 6) is 0.28 for modelling the mechanical response of compacted BRS-cement mixtures. Therefore, the definition of the dosage characteristics initiated by the selection of seven $\eta/(C_{iv})^{0.28}$ values considering the range previously presented by Consoli *et al.* (2007) and, as well, observing the established ranges for dry unit weight values and amounts of cement defined herein. Due to molding limitations, it was assumed that the dry unit weight (γ_d) could vary between 14.80 kN/m³ and 19.10 kN/m³. The molding moisture content (w) was set as 10%, regardless of the γ_d value, as formerly done by Consoli *et al.* (2007). The amount of cement could assume values between 1% and 10% (relative to the mass of dry soil). Such cement contents are usual for soil stabilization purposes as earlier discussed (see item 2.4). Ergo, each dosage was calculated using the following equation:

$$\frac{\eta}{(C_{iv})^{0.28}} = \frac{{V_v}/{V_T}}{\left({V_c}/{V_T}\right)^{0.28}} = \frac{100 \cdot \left[1 - \frac{\gamma_d}{\gamma_s \cdot \left(1 + {C}/{100}\right)} + \frac{\gamma_d \cdot \left({C}/{100}\right)}{\left(1 + {C}/{100}\right) \cdot \gamma_c}\right]}{\left[100 \cdot \frac{(C/100) \cdot \gamma_d}{\left(1 + {C}/{100}\right)}\right]^{0.28}} \qquad (23)$$

In which:

V_v = volume of voids

V_c = volume of cement

V_T = total volume of the specimen

γ_d = dry unit weight
C = amount of cement, expressed in percentage and calculated relative to the dry mass of soil
γ_c = unit weight of cement grains
γ_s = unit weight of soil grains

Within a defined $\eta/(C_{iv})^{0.28}$ value (45, 40, 35, 30, 25, 22.5 or 20), each dosage was obtained by an iterative process. The cement contents could assume the following values: 1%, 1.50%, 2.0%, 3.0%, 4.0%, 5.0%, 5.0%, 6.0%, 6.5%, 7.0%, 8.0%, 9.0% and 10%. The dry unit weight, in turn, could vary between any value ranging from 14.80 kN/m³ to 19.10 kN/m³. A graphical representation of these dosages (and the $\eta/(C_{iv})^{0.28}$ values) can be obtained using a contour plot relating the amount of cement (C) and the dry unit weight (γ_d) as depicted in Figure 36. Basically, the $\eta/(C_{iv})^{0.28}$ values are delimited within zones which size change as C and γ_d changes.

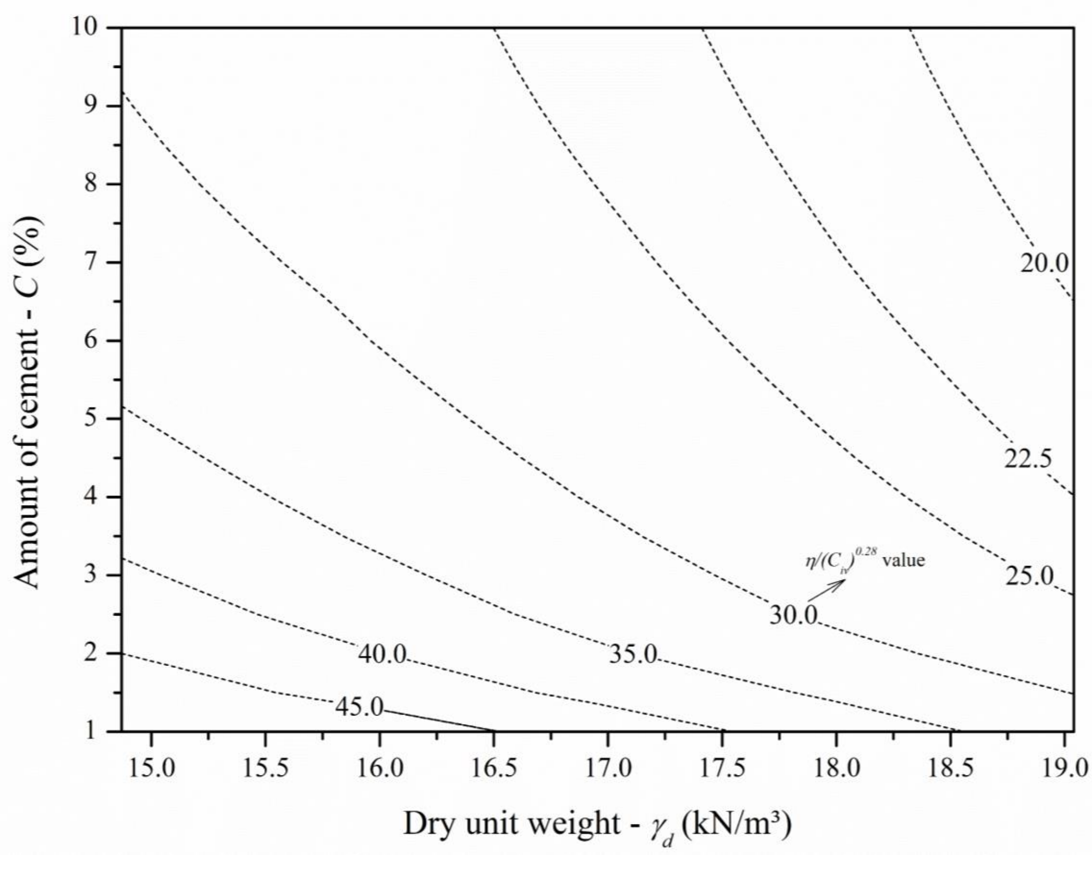

Figure 36 – Dosage setting contour plot

4.2.2 Specimens Preparation

Cylindrical specimens were individually molded for the tests following the undercompaction method proposed by Ladd (1978) using cylindrical split molds. For the unconfined compression tests, split tensile tests, initial shear modulus tests and triaxial tests, the specimens were 50 mm in diameter and 100 mm in height. For the durability tests, the samples were 100 mm in diameter and 120 mm in height. Once the dry materials (cement and soil) were weighed, they were mixed until a visual uniformity was acquired. Following, the correct amount of distilled water was added and the mixing continued until the formation of a homogeneous mass. Then, the specimen was statically compacted in three layers inside the mold to its target dry unit weight, being the top of the first and second layer slightly scarified in order to guarantee adherence. Next, the specimen was removed from the mold, weighed, measured and sealed in a plastic bag to be cured along the defined period in a humid room at 23 ± 2°C with relative moisture of about 95%. Each specimen was considered adequate for testing if the attained dry unit weight was within ± 1% of the target value and the moisture content ranged within ± 0.5% of the design value.

4.2.3 Unconfined Compression and Split Tensile Strength Tests

The unconfined compression tests (UCS) were carried out on an automatic loading press at a displacement rate of 1.14 mm per minute (Fig. 37a). A load cell with 10 kN of capacity and 0.005 kN of resolution was used to register the resultant load during the test. At the penultimate day of curing, each specimen was removed from the plastic bag and submerged in a water tank for 24 hours at 23 ± 2°C intending to minimize possible suction effects. Every test specimen was removed from the tank and superficially dried with an absorbent cloth promptly before the strength test. Within each mix design, as an acceptance criterion, it was established that the individual strength of the replicate specimens should not deviate by more than 15% of the mean strength. The unconfined compressive strength (q_u) is given by:

$$q_u = \frac{P}{A} \tag{24}$$

Where:

P = maximum load registered during the test
A = transversal area o the cylindrical specimen

The split tensile strength test (STS) procedures are identical to those described for the unconfined compression tests. The only difference relies on the position of the soil-cement specimen on the equipment that is positioned horizontally, being the load applied along its height (Figure 37b). A load cell with 5 kN of capacity and 0.005 kN of resolution was used for the STS tests. The split tensile strength (q_t) can, thus, be calculated by:

$$q_t = \frac{2P}{\pi D h} \tag{25}$$

Where:
P = maximum load registered during the test
D = diameter of the cylindrical specimen
h = height of the cylindrical specimen

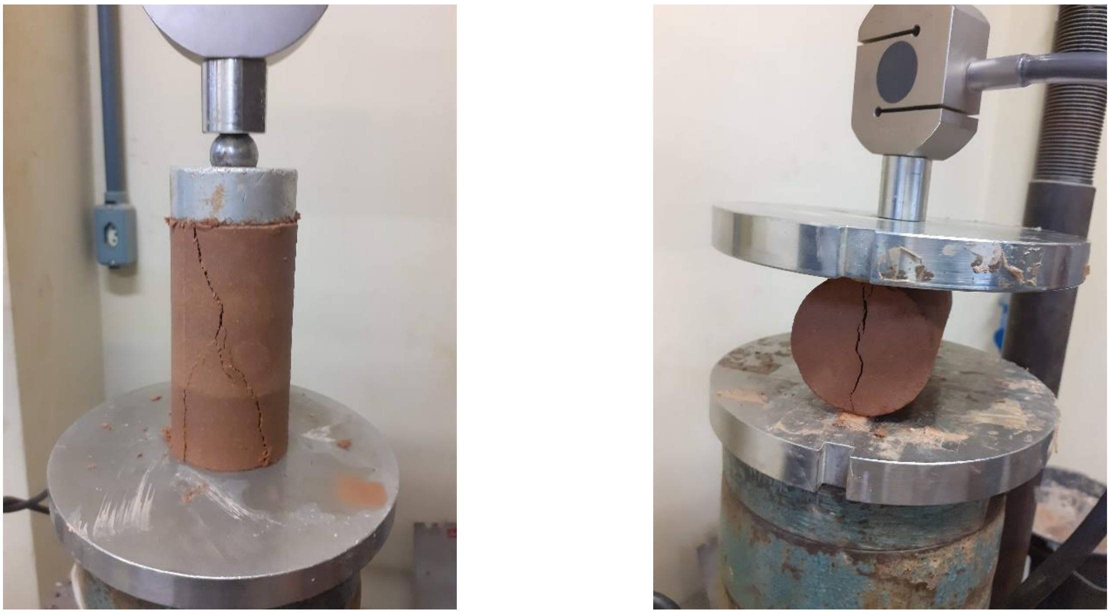
(a) (b)
Figure 37 – Unconfined strength tests (a) compressive strength (b) split tensile strength

4.2.4 Initial Shear Modulus

As already mentioned, the initial shear modulus (G_0) of an ideal elastic isotropic medium can be obtained by measuring the velocity of a shear wave (V_s) passing through it (ASTM, 2019c). Therefore, the following relationship is valid:

$$G_0 = \rho \cdot V_s^2 \tag{26}$$

Where:

ρ = bulk density of the tested specimen

Herein, an ultrasonic pulse device was used to measure the travel time (t_s) of a shear wave through the BRS-cement cylindrical specimens. This wave was emitted at a frequency of 150 kHz using special transducers that were coupled to the test samples by means of a special shear gel. Prior to the t_s assessment, the travel time of a compressive wave (t_p), emitted at a frequency of 54 kHz, was also measured. Figure 38 exhibits a typical outcome of the ultrasonic pulse velocity test using the Pundit Lab+ ® software. As this test is non-destructive, it was carried out on the same specimens that were submitted to the unconfined compressive strength tests, right after the specimens were taken out of the water tank.

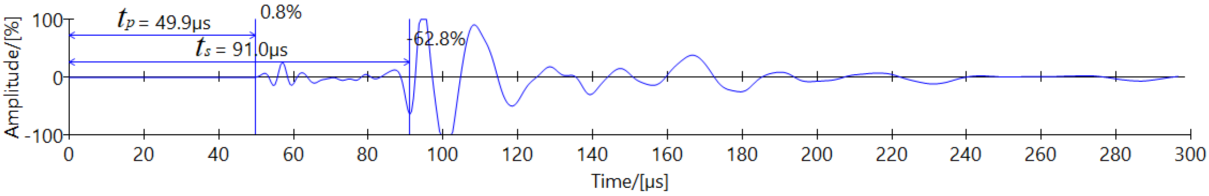

Figure 38 – Typical signal using software Pundit Lab+ ®

4.2.5 Measurement of Suction Using Filter Paper

The immersion of the compacted BRS-cement specimens along 24 hours in water does not guarantee the full saturation. Therefore, it was essential to evaluate the suction and its relative magnitude to the unconfined compressive strength of the samples. Consequently, the matric suction was measured using the contact filter paper technique. Basically, the filter paper comes to equilibrium with the soil after a certain period of time, as it absorbs the water from the soil specimen. At the equilibrium condition, the suction value of the filter paper and the soil will be the same and the moisture content of the filter paper (w_f) can be measured by gravimetric means. Thus, by using a calibration curve for the correct paper filter type, w_f can be converted into matric suction.

For the present research, within each $\eta/(C_{iv})^{0.28}$ value, some dosages were selected for the matric suction measurement (S_m). After the unconfined compressive strength tests, the BRS-cement specimen was manually broken and a piece was selected. Its internal surface was regularized and three small slices of Whatman n. 42 filter paper were put in direct contact with this surface. Right after, this piece containing the filter paper slices was tightly enveloped using a transparent PVC film (Figure 39). Then, this enwrapped piece of BRS-cement was kept in a styrofoam box along 7 days at controlled temperature of 23°C. Once this period was finished, each filter paper slice was carefully weighed using a high precision analytical balance and forwarded to be dried during 2 days in an oven regulated at 60°C. Finally, the slices were, once again, weighed which permitted the determination of the moisture content of each filter paper (w_f). The calibrations equations presented by Chandler *et al.* (1992) and Marinho (1995) were used as follows:

$$\text{If } w_f > 47\%: \quad S_m(kPa) = 10^{(6.05 - 2.48 \log w_f)} \tag{27}$$

$$\text{If } w_f \leq 47\%: \quad S_m(kPa) = 10^{(4.84 - 0.0622 \log w_f)} \tag{28}$$

Figure 39 – Enwrapped piece of BRS-cement with three filter paper slices

4.2.6 Durability Tests

The durability tests were performed in accordance to the procedures stated by ASTM D559 (ASTM, 2015). Such normative states the methods to evaluate the loss of mass of cylindrical soil-cement specimens throughout 12 wetting-drying-brushing cycles which emulates harsh environmental conditions. Four specimens were molded for each tested dosage, one for moisture assessment during the cycles and three for the loss of mass control, totalizing 40 specimens. In other words, one specimen was only submitted to the wetting-drying process and was not brushed, whereas the other three were exposed to the three steps of the test. The durability cycle initiated once the 7 days curing period was finished, by submerging the specimens in water during 5 h at 23°C ± 2°C. Next, the samples were dried in a stove at 71°C ± 2°C for 42 h and, afterwards, brushed with a wire brush using a force of 15 N (18 to 20 brushings in the lateral surface to cover it twice and 4 brushings in the top and bottom surfaces). The loss of mass owing to the brushing process was accounted. Each cycle took 48 hours and the durability test was composed by 12 cycles, that is, around one month of testing. The accumulated loss of mass (*ALM*), expressed in percentage, is defined as the cumulative loss of dry mass due to the brushing process per cycle over the initial dry mass of the test specimen (e.g., SALDANHA *et al.*, 2017).

4.2.7 Triaxial Tests

Isotropically consolidated drained triaxial tests were conducted herein aiming to assess the stress-strain behavior and the volume change response of a variety of BRS-cement samples. A few tests were also carried out on the disturbed soil, without cement addition. The minimum effective confining pressure (σ'_3) adopted at the present study was equal to 35 kPa. At this confinement level, the bonds would not be broken, controlling the behavior of the mixtures up to a certain stress level. Confining pressures of 70 kPa, 140 kPa and 300 kPa were also used in some specimens and, as well, the bonds have not been damaged during the consolidation phase in these pressures (see table 7). Recommendations stated by standard ASTM D7181 (ASTM, 2020), Head (1998) and Lade (2014) were followed throughout the triaxial tests.

In essence, the triaxial tests comprehended 3 stages: (i) saturation, (ii) consolidation and (iii) shearing. The saturation process consisted of three substeps: CO_2 percolation during 30 minutes, followed by distilled water percolation up to a volume equal to twice of the estimated volume of voids of the sample (or along 24 hours) and, finally, applications of increments of backpressure until a *B* value greater than 0.94 was achieved (SKEMPTON, 1954). In all of these three substages, the mean effective stress (*p*´) was maintained constant and equal to 20 kPa. The minimum final backpressure value was equal to 400 kPa.

Once the saturation was terminated, the consolidation could initiate. For the lowest confining pressure, it was performed through a single increment of 15 kPa in the confinement level, whereas two increments of 25 kPa were used for the intermediate confinement, four increments of 30 kPa were employed for 140 kPa confining pressure and eight increments of 35 kPa were adopted for σ'_3 = 300 kPa. Each increment in the confinement was maintained until the pore pressure stabilized at the original value, namely, the value prior to the commencement of the saturation stage. The shearing was conducted at a constant σ'_3 stress path under a strain-controlled rate equal to 2 mm per hour. Such rate was found adequate as the excess of pore-pressure generated during the shearing could be easily controlled. The shearing always started at the seventh day of curing for the cemented specimens.

Figure 40 presents a general overview of the triaxial test setup. The confining pressure and the backpresure were independently monitored using Ashcroft ® electronic pressure transducers. Either were applied through an oil/water interface system. The load was registered by a 10 kN load cell with 0.01 kN of resolution. The axial external displacements were measured using a potentiometric linear ruler with 0.01 mm of resolution. Internally, as shown in Figure 41, two hall effect sensors were used to evaluate the axial displacements and one was employed in the measurement of the radial displacements (CLAYTON & KHATRUSH, 1986). The volumetric variation was monitored through the flow of water in/out of the specimen along the shearing using bellofram type volumetric transducer of Imperial College design (Figure 40).

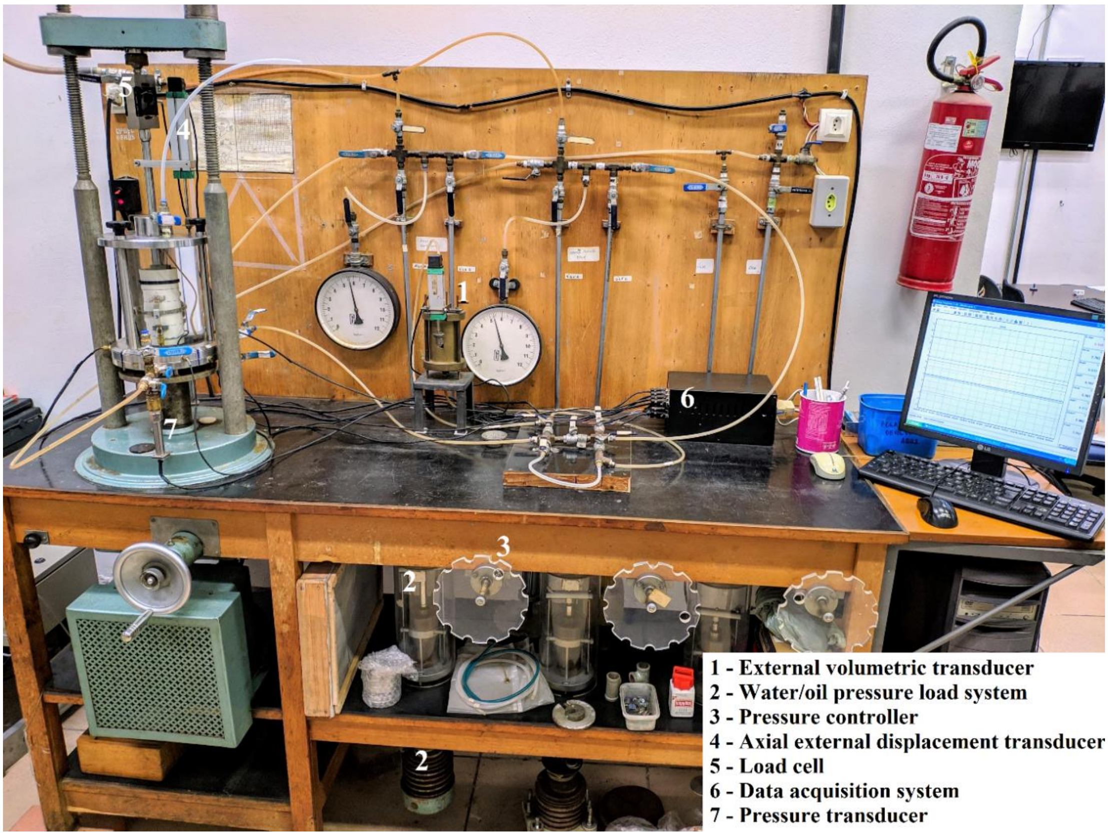

Figure 40 – General overview of the triaxial equipment

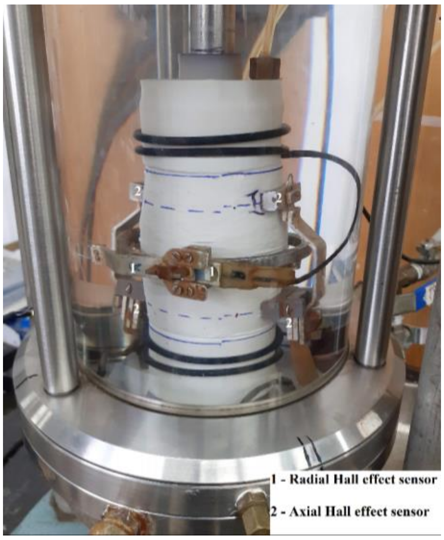

Figure 41 – Detail of the test specimen during the test with highlight to the internal displacement transducers

The cross-section area correction followed the recommendations presented by La Rochelle *et al.* (1986). For most of the specimens, it was assumed a barreling failure combined with a shear plane failure mechanism for the BRS-cement specimens. Up to the peak deviatoric stress (q_{max}), solely the bulging was considered in the correction. Right after, a shear plane starts to form and a combination of either bulging and shear plane failure was assumed. Once the test was finished, the cross-section area of the majority of the samples resembled an ellipse. Ergo, it was possible to measure the d_a and d_b dimensions of the tested sample (e.g., LA ROCHELLE *et al*., 1986).

4.2.8 Scanning Electron Microscope Tests

The scanning electron microscope (SEM) tests were carried out using a JEOL JSM-6610LV scanning electron microscope coupled to a Bruker Nano X-ray energy dispersive spectrometer Flash Detector 5030. The tests were performed on small intact samples (Figure 42) of the compacted BRS-cement mixtures which were coated with carbon right before the SEM tests in order to improve the imaging of the samples as a conductive layer was created. These small samples were retrieved from larger cubic specimens (around 1 cm of edge) which, in turn, were obtained by cutting cylindrical samples (5 cm of diameter and 3.33 cm in heigh) that were molded following the procedures described on item 4.2.2. Once the curing period of 7 days was finished, these small cubes were submerged in acetone in order to cease the cement hydration reactions through the replacement of the bound/pore water existing in the samples by acetone (e.g., TREZZA, 2007; SARAYIA, 2010; ZHANG & SCHERER, 2021). A volume ratio of around 1:100 (cubic specimen:acetone) was used and the cubic samples were kept completely submerged for 5 days in small glass recipients. After this period was finished, the specimens were retrieved from the acetone, superficially dried and wrapped in a plastic film. According to Collier *et al*. (2008), the usage of an organic solvent for hydration stoppage is the method which incurs in least damage to the material’s pore structure when compared to freeze drying or oven drying, for example. Thus, it tends to preserve the fabrics.

Figure 42 – BRS-cement specimens ready for SEM test

4.2.9 Mercury Intrusion Porosimetry Tests

The mercury intrusion porosimetry (MIP) tests were carried at the Laboratório de Caracterização Tecnológica (LCT) of Universidade Federal de São Paulo (USP) out using a specific equipment named Autopore IV developed by Micrometrics®. The main goal of this tests consists on determining the pore-size distribution (PSD) of the tested specimens. For this, cubic samples having edges of approximately 2 cm were used. These specimens were obtained by cutting larger cylindrical samples (5 cm of diameter and 3.33 cm in heigh) which were molded following the procedures described on item 4.2.1. Once the curing period of 7 days was accomplished, the cubic samples were dried in acetone using the procedures previously described on item 4.2.7. Thereafter, they were ready to be tested.

In essence, the MIP test employs a pressurized chamber to force the mercury intrusion into the voids of a porous sample (GIESCHE, 2006). Once the pressure is applied, mercury fills larger pores first. As pressure increases, the filling progressively proceeds to pores having a smaller size. Through the Washburn equation it is possible to estimate the pore diameter (d_p), since it relates the applied pressure to the physical properties of the non-wetting liquid (mercury in this case). Hence, considering cylindric pores, the following relationship can be used:

$$d_p = \frac{-4\sigma \cos\theta}{P} \tag{29}$$

Where:
σ = surface tension of the liquid (σ_{Hg} = 0.485 N/m)
θ = contact angle of the intruder liquid ($\theta_{Hg} = 130°$)
P = applied pressure

Throughout the test, both the volume of intruded mercury into the sample and the pressure increments are monitored, which enable the establishment of proper relationships to assess the pore-size distribution (PSD) of the tested specimen. In the present research, the maximum applied pressure was around 412 MPa. Moreover, despite not being so common to characterize the PSD of cemented materials, as mercury may not reach the smaller pores without breaking the way through them (DIAMOND, 2000), MIP tests have been carried out to characterize the PSD of a variety of soil-cement samples as it is possible to detect the contrast between macro and mesopores (e.g., ABELL *et al*., 1999; HORPIBULSUK *et al*., 2010; CARDOSO 2016, 2017; YU *et al*., 2019).

5. RESULTS

The results regarding the tests which were carried out are exhibited and discussed below. Each subitem of the chapter comprehends the results of each type of test.

5.1 INITIAL SHEAR MODULUS

Ultrasonic pulse velocity tests were carried out for the 26 different dosages previously displayed in Table 5. Five specimens were tested within each dosage when the curing period of 7 days was considered, totalizing 130 samples. As this is a non-destructive test, the same specimens which were going to be tested for unconfined compression, after the curing period of 7 days was accomplished, were used. In brief, the G_0 was correlated to the $\eta/(C_{iv})^{0.28}$ index, then the results within each adjusted/porosity cement value were individually analyzed and, finally, the theoretical approach, proposed by Diambra *et al.* (2019), was used in order to justify the adjustment parameters of the power-type relationship.

5.1.1 Initial Shear Modulus versus $\eta/(C_{iv})^{0.28}$

An inverse trend between the initial shear modulus and the $\eta/(C_{iv})^{0.28}$ index was attained. Namely, higher stiffness values were observed for the lowest values of the adjusted porosity/cement index owing to the more compacted and/or cemented structure. Relationship 30 was obtained as a result of the G_0 and $\eta/(C_{iv})^{0.28}$ correlation, yielding a coefficient of determination equal to 98%. Figure 43 summarizes the stiffness outcomes, containing the results of the tests, the fitting equation 30, and 95% prediction bands that encloses the area that it is expected to comprehend 95% of the experimental data points (including present and future results).

$$G_0(MPa) = 29.00\ \times 10^5\ \cdot \left[\frac{\eta}{(C_{iv})^{0.28}}\right]^{-2.30} \tag{30}$$

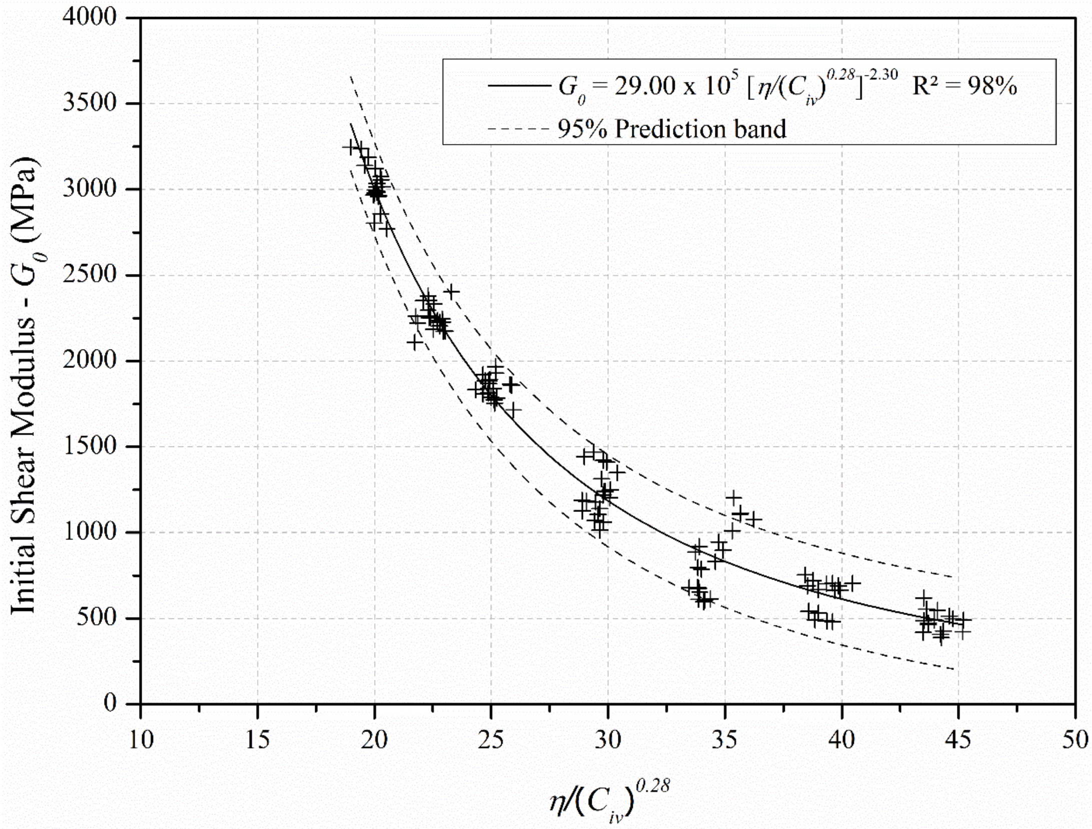

Figure 43 – Initial shear strength results versus $\eta/(C_{iv})^{0.28}$

5.1.1.1 Individual Analysis

Irrespective of the adopted mix design, the adjusted porosity/cement index seems to control the small strain stiffness of the BRS-cement specimens, as can be noticed through the great coefficient of determination ($R^2 = 98\%$) and the quite low scatter of the data points in relation to the adjusted equation. In general, all the results lie within the 95% prediction band. Nonetheless, an individual analysis of the data was carried out within all the studied $\eta/(C_{iv})^{0.28}$ index values (Figures 44 to 50). For each mix design, the specimen's initial shear modulus is indicated by a "x" and the average of these values is represented by a square. In addition, a 95% confidence interval (CI) is plotted for each dosage around its mean G_0 value. The CI was calculated using the pooled standard deviation (σ_{pl}) that is the weighted average of the obtained standard deviations within each dosage for a single $\eta/(C_{iv})^{0.28}$ index value. Roughly, the confidence interval represents a long-run frequency of confidence intervals that contain the true value of the average G_0 within each dosage. That is, in a 95% confidence interval 19 out of 20 tests would generate an interval containing the true mean initial shear modulus value.

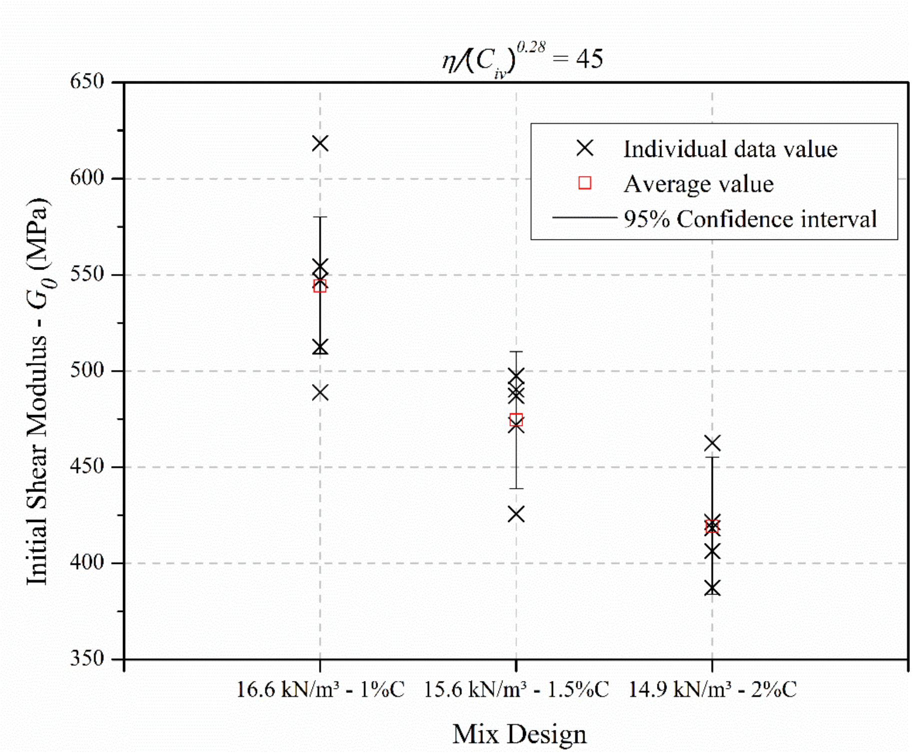

Figure 44 – Individual G_0 results for $\eta/(C_{iv})^{0.28} = 45$

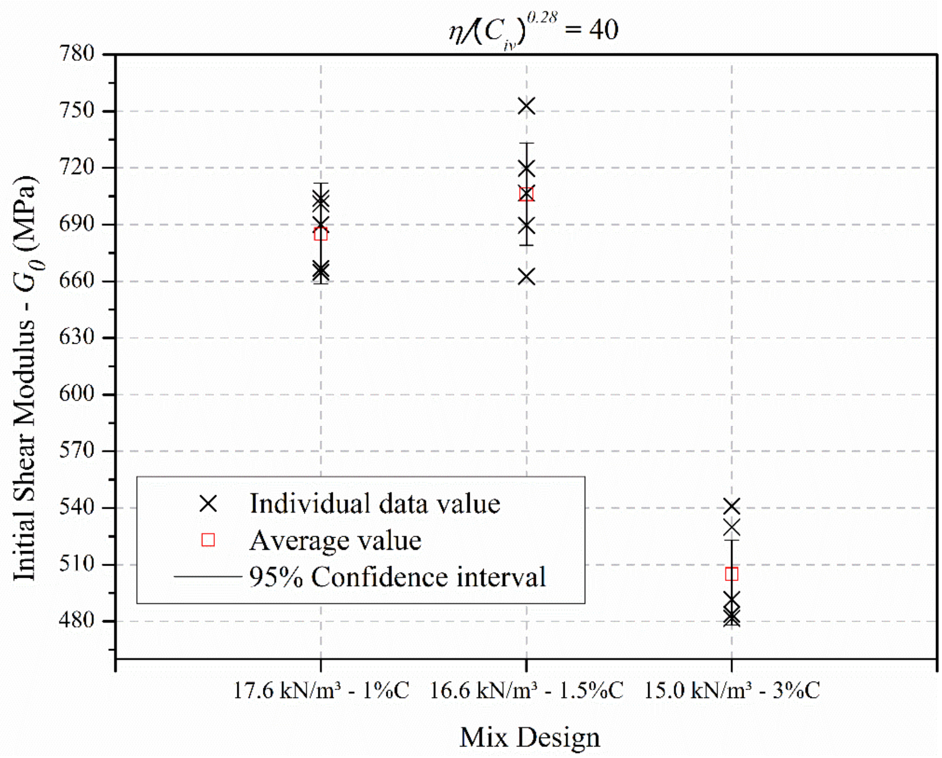

Figure 45 – Individual G_0 results for $\eta/(C_{iv})^{0.28} = 40$

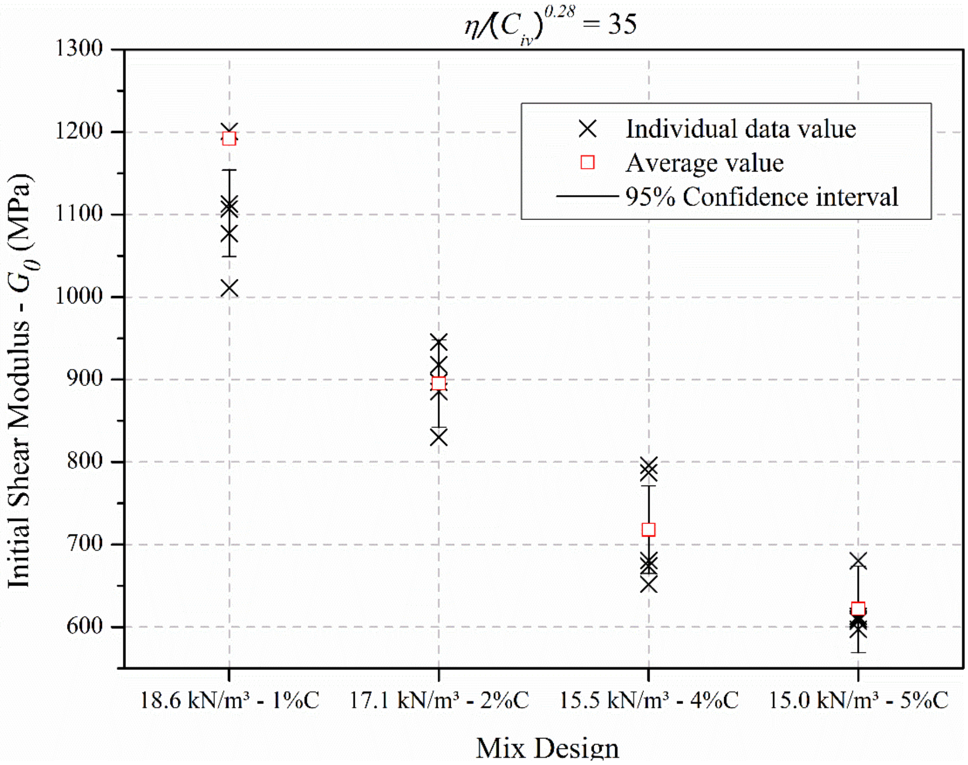

Figure 46 – Individual G_0 results for $\eta/(C_{iv})^{0.28} = 35$

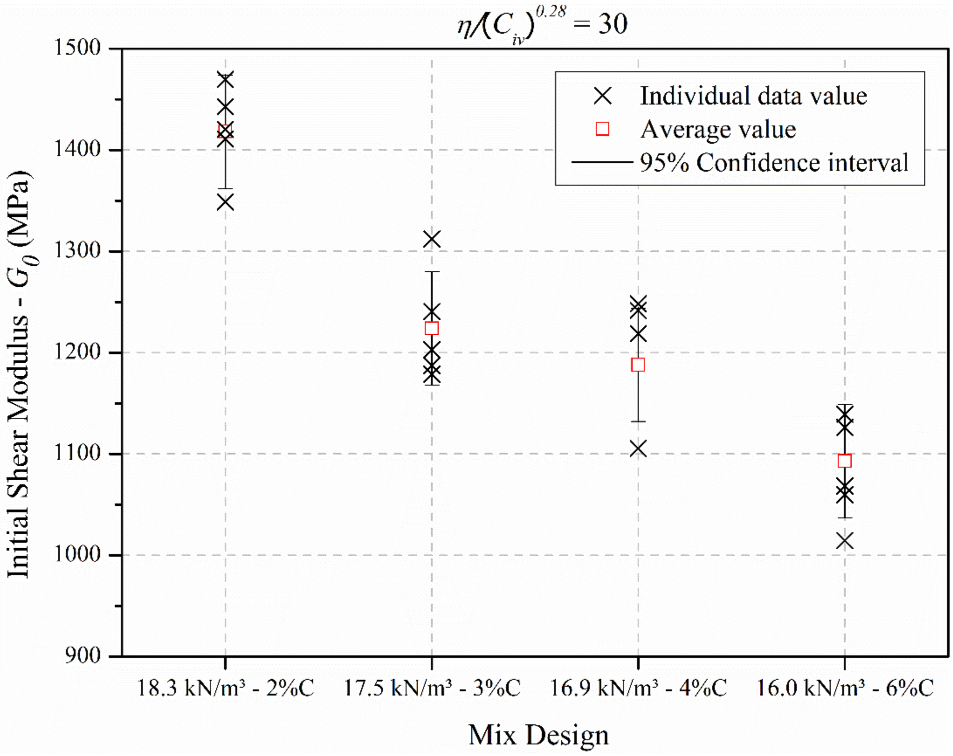

Figure 47 – Individual G_0 results for $\eta/(C_{iv})^{0.28} = 30$

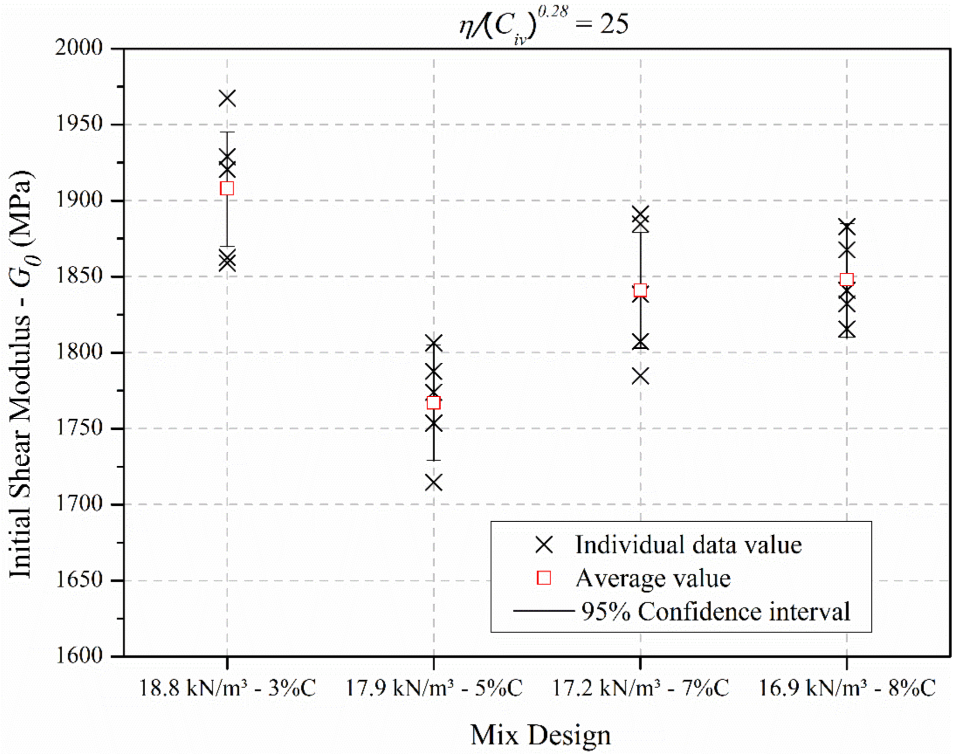

Figure 48 – Individual G_0 results for $\eta/(C_{iv})^{0.28} = 25$

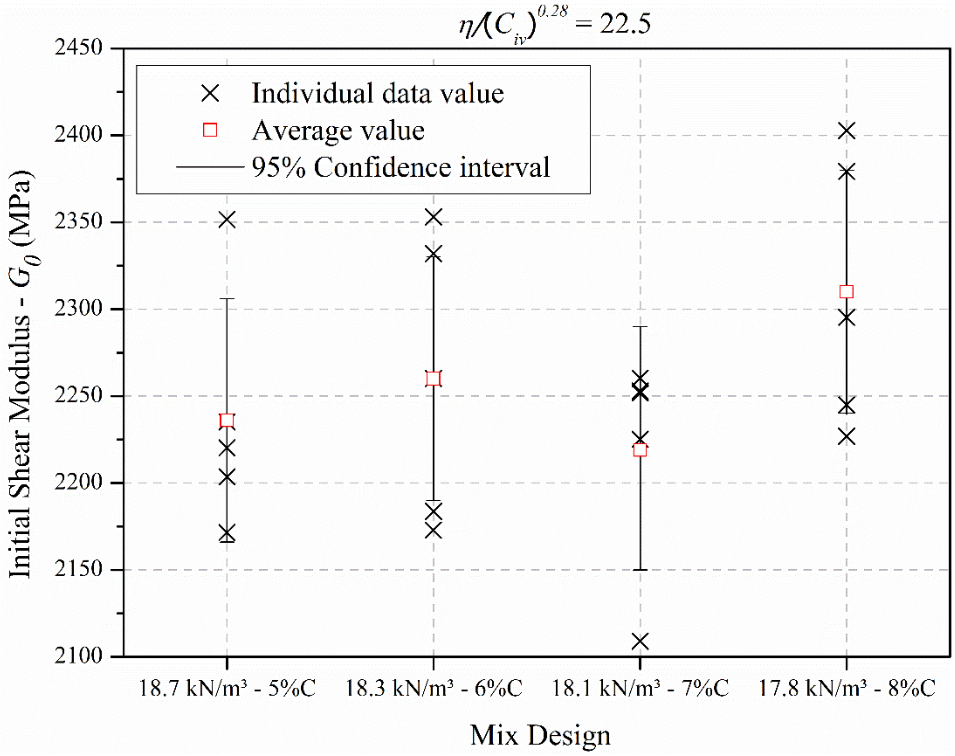

Figure 49 – Individual G_0 results for $\eta/(C_{iv})^{0.28} = 22.5$

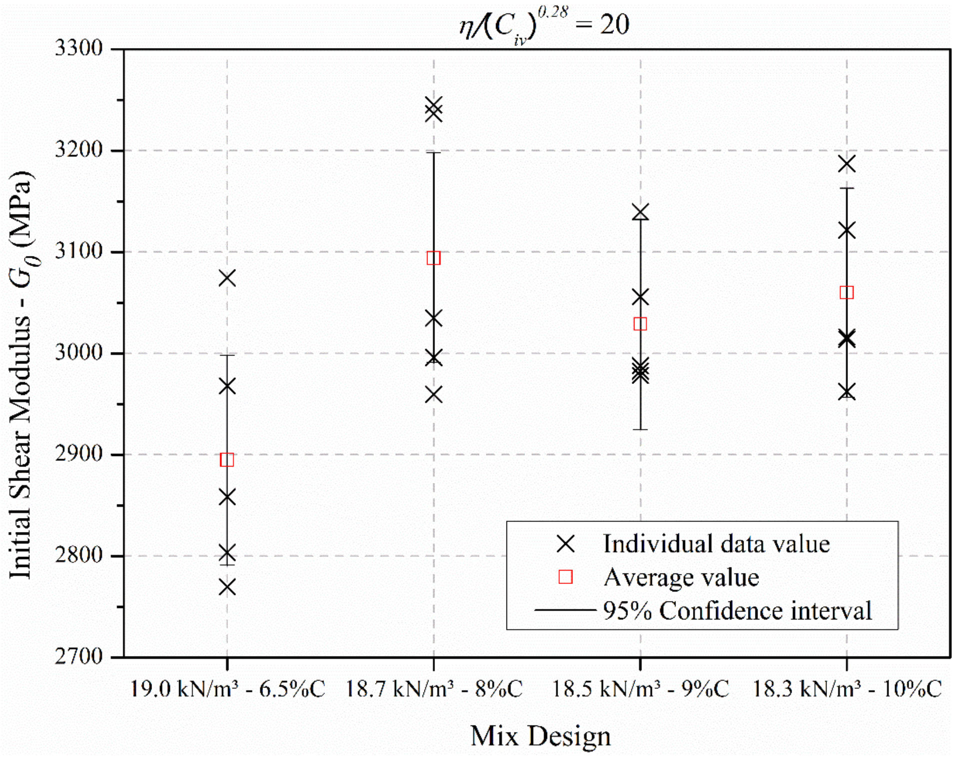

Figure 50 – Individual G_0 results for $\eta/(C_{iv})^{0.28} = 20$

Essentially, within each $\eta/(C_{iv})^{0.28}$ value, small differences were detectable between the average small strain stiffness of each tested dosage. These distinctions were more pronounced amongst the dosages when the $\eta/(C_{iv})^{0.28}$ value was equal to 35. Nonetheless, these divergences have not prevented a proper correlation between G_0 and the adjusted porosity/cement index, irrespective of the adopted mix design. As a reason, it appears that the contact area between the particles is of similar order of magnitude for the same adjusted porosity/cement ratio value (see section 2.3.5). That is, for these cases, the augment in the contact area owing to the higher degree of cementation ($\uparrow C$ and $\uparrow \eta$ specimen) has had a similar effect than the enlargement in the contact area due to the greater degree of interlocking for the lesser porous specimens containing a small amount of cement. Thus, the initial shear modulus maintains a similar order of magnitude within each porosity/cement index value, regardless of the dosage. Otherwise, the scatter of the data would be much greater around the fitted curve previously presented in Figure 43.

5.1.1.2 Statistical Analysis

A one-way analysis of variance (ANOVA) would be sufficient to determine the existence of any statistically significant differences between the means of the dosages for each $\eta/(C_{iv})^{0.28}$ value (BOX & HUNTER, 2005; MONTGOMERY, 2013). That is, a p-value greater than the adopted level significance would point out differences amongst the means of each mix design. Nonetheless, such approach would not indicate where these differences occur. Hence, multiple comparison tests (MCT) were carried out within each adjusted porosity/cement index value using the Tukey´s method to simultaneously test for differences of means between each mixture. Basically, this MCT method pairwise compare the differences of means between the groups to determine whether these differences are statistically significant or not. For this, a statistic test that measures the size of the differences in relation to the variation existing in the sample, the T-value, is used. This consists on the quotient between the pair's differences in means and the standard error of the difference, which is an estimate of the standard deviation of the normal distribution of the mean's differences (McHUGH, 2011, LEE & LEE, 2018). Thus, if the T-value exceeds a critical point, obtained using a studentized range distribution, the compared means are said to be significantly different at that adopted level (i.e., the null hypothesis is rejected).

The results of the MCT are summarized in Table 12, and the dosages that share the same reference letter (within each $\eta/(C_{iv})^{0.28}$ value) are statistically equal with relation to their initial shear modulus values. In general, at least two mix designs were statistically equivalent when considering each $\eta/(C_{iv})^{0.28}$ value and, despite small eventual statistical differences, the correlation between the stiffness and the $\eta/(C_{iv})^{0.28}$ index has worked. To exemplify, there is no statistical difference on using dosages n. 4 (17.53 kN/m³ - 1%C) and n. 5 (16.65 kN/m³ - 2%C) when G_0 is considered, whereas dosage n. 6 (14.96 kN/m³ - 3%C) differs from those two. As a reason, the choice between dosages n. 4 and n. 5, for practical purposes, would rely on aspects such as financial and/or technical reasons, for example.

Table 11 – Summary of G_0 results

$\eta/(C_{iv})^{0.28}$	Mix Design	γ_d (kN/m³)	C (%)	Average G_0 (MPa)	MCT
45	1	16.59	1.00	544	A
	2	15.61	1.50	474	B
	3	14.87	2.00	419	B
40	4	17.53	1.00	685	A
	5	16.65	1.50	706	A
	6	14.96	3.00	505	B
35	7	18.55	1.00	1101	A
	8	17.11	2.00	895	B
	9	15.50	4.00	717	C
	10	14.96	5.00	622	C
30	11	18.31	2.00	1418	A
	12	17.45	3.00	1188	B
	13	16.87	4.00	1071	B
	14	15.96	6.00	1093	B
25	15	18.85	3.00	1908	A
	16	17.88	5.00	1767	B
	17	17.21	7.00	1841	A
	18	16.94	8.00	1848	A
22.5	19	18.67	5.00	2236	A
	20	18.34	6.00	2261	A
	21	18.05	7.00	2219	A
	22	17.81	8.00	2310	A
20	23	19.04	6.50	2895	B
	24	18.70	8.00	3094	A
	25	18.49	9.00	3028	A, B
	26	18.32	10.00	3060	A, B

By plotting the statistical equal dosages as a function of the $\eta/(C_{iv})^{0.28}$ index (Figure 51) a negligible difference occurs. That is, the scalar of equation (30) is altered from 29.00 x 10^5 to 29.50 x 10^5 and the scatter around the power-type relationship was slightly reduced as the dosages n. 1, 6, 7, 8, 11, 16, and 23 were withdrawn from this analysis. This corroborates the assumption that the adjusted porosity/cement index is adequate to model the G_0 of the compacted BRS-cement specimens, irrespective of the adopted mix design.

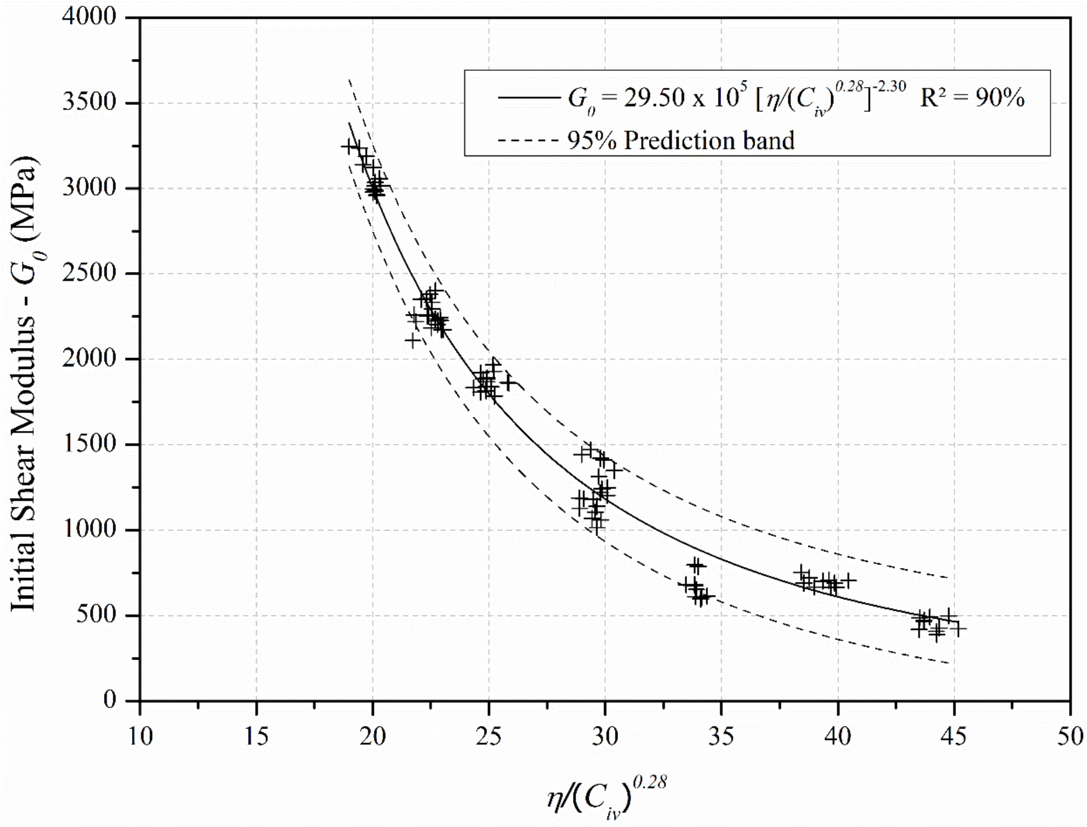

Figure 51 – G_0 results for the specimens cured along 7 days related to the porosity/cement parameter for statistically equal dosages within the same index value

5.1.2 Theoretical Approach for the Initial Shear Modulus

The theoretical derivation proposed by Diambra *et al.* (2019) was applied to the BRS-cement mixtures attempting to verify if the measured small strain stiffness values fit the conceptual equation derived from this procedure. Therefore, it was assumed that the BRS presents a single NCL and the addition of cement simply implies the offset of such line in the υ-lnp' space. The isotropic compression tests used to calibrate the model are exhibited in Figure 59 and have been carried out by Rotta *et al.* (2003). These were conducted out in either remolded BRS sample (initial void ratio of around 0.65) and in BRS-cement specimens containing 1%, 2% and 3% of Portland cement. The lines shown in Figure 59, relative to the cemented specimens, are what the authors have called “post-yield compression lines”. The λ value was equal to -0.067 for all the tested specimens, whereas the T values were dependent upon the cement content and are displayed in Figure 52. In order to calibrate the model, the initial shear modulus results of dosages number 2, 11 and 15 were used. The intercept value (T) for the specimen number 2, which contains 1.5% of cement, was obtained via interpolation and was equal to 2.004. Once the values of specific volume (υ) of each tested specimen was known, equation 16 can be used to calculate p_e^*, $p_e^{'}$ and, thus, the ratio $p_e^{'}/p_e^*$. Thereafter, the procedures described on item 2.4.2 were followed, yielding the parameters summarized in Table 12.

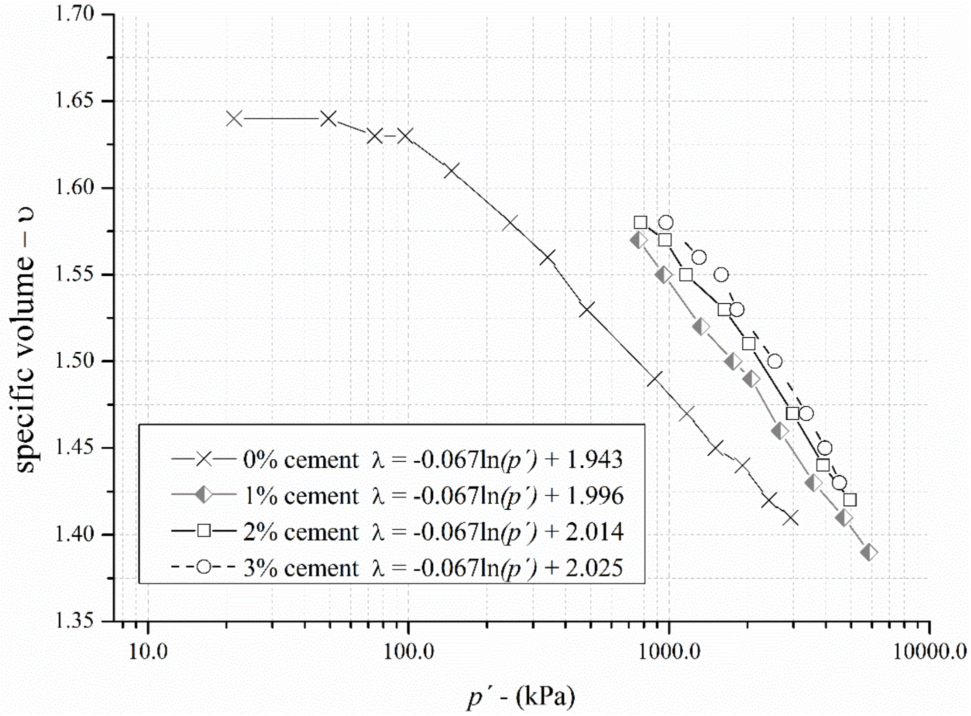

Figure 52 - Isotropic compression tests

(after ROTTA *et al.* 2003)

Table 12 – Parameters for the theoretical approach relative to the initial shear modulus

Parameter	**Value**
m	0.29
q	0.81
A	71407
D	3 x 10^{19}
f	10.95
L	2.375
C	64.03 x 10^{6}
d	-3.17
b	0.25

By applying the *b*, *d* and *C* values to equation 19, the following relationship is derived:

$$G_0(\text{MPa}) = 58.36\ x\ 10^5 \cdot \left[\frac{\eta}{(C_{iv})^{0.25}}\right]^{-2.51} \tag{31}$$

The obtained b, d and C values using the approach proposed by Diambra *et al.* (2019) are in consonance to the empirical adjustment power-type relationship 11, derived from the correlation between the measured stiffness values and the $\eta/(C_{iv})^{0.28}$ index. In fact, the b value equals to 0.25 is very close to the adopted 0.28 value, which sort of explain the great coefficient of determination obtained using equation 30. Moreover, the d equals to -2.51 is, as well, similar to the value obtained in the correlation that resulted in equation 30 (-2.29).

Figure 60 presents the theoretical derived equation 31 and, also, the measured G_0 values following the procedures described in the item 2.4.2. The data points are plotted as a function of the $\eta/(C_{iv})^b$ index, but using a b value equals to 0.25, instead of 0.28, in order to comply with the Diambra *et al.* (2019) procedure. As can be noticed, the measured stiffness values all lie nearby the theoretical derived equation 33, which is corroborated by a coefficient of determination (R^2) of 97%. Thus, concerning the results presented herein, there is a parallelism between the empirical power relationship 19 and the well-established approaches to model the small strain stiffness of cemented soils (e.g., HARDIN, 1978; TRHLÍKOVÁ *et al.*, 2012). The higher differences between the “predicted” and measured values have occurred for the smaller $\eta/(C_{iv})^b$ index values, which may be linked to the fact that the calibration of the model was performed using stiffness data of higher $\eta/(C_{iv})^b$ values. Nonetheless, it is worth mention that such methodology is highly sensible to data used in the calibration process.

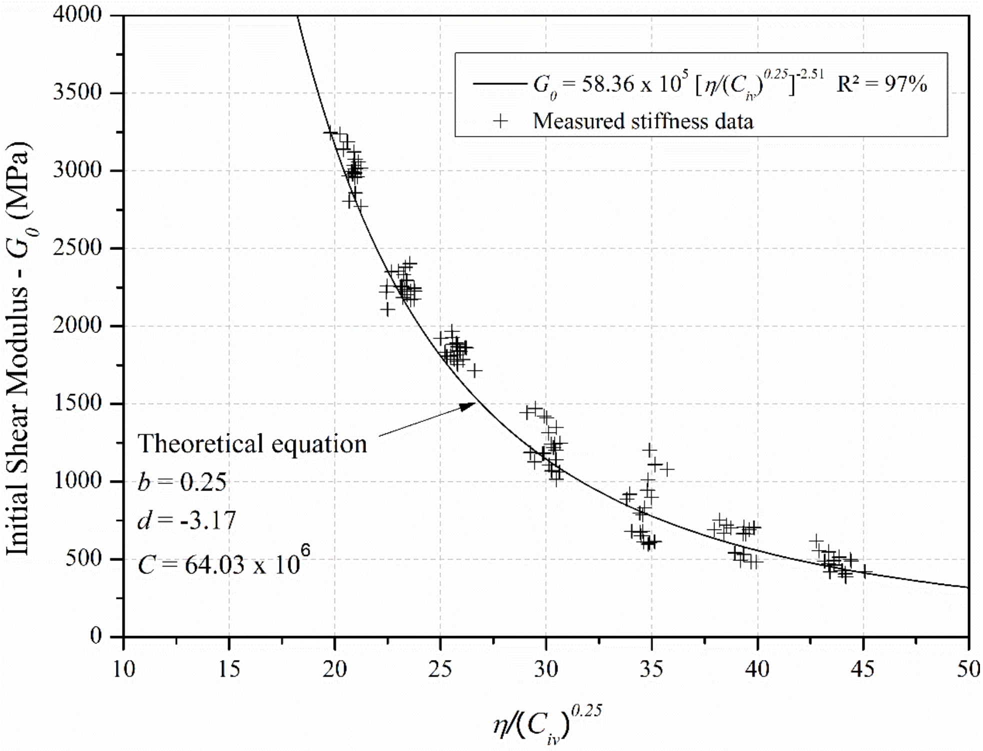

Figure 53 – Measured stiffness data and theoretical equation

5.2 UNCONFINED STRENGTH TESTS

The unconfined strength tests are divided between unconfined compression tests and split tensile tests. Both are presented and discussed in the following pages of this subsection.

5.2.1 Unconfined Compressive Strength Tests

Unconfined compression tests were carried out for the 26 different dosages previously displayed in Table 5. Five specimens were tested within each dosage when the curing period of 7 days was considered, totalizing 130 samples. Additional tests were conducted for samples cured during 28 days and 90 days, using triplicates for each mix design.

Figure 54 presents the unconfined compressive strength (q_u) as a function of the adjusted porosity/cement index for the test specimens cured along 7 days. As previously noticed for the stiffness results, an inverse trend was obtained between the strength and the adjusted porosity/cement index. Namely, as the $\eta/(C_{iv})^{0.28}$ reduces (either by increment of the cement content or reduction of porosity) q_u increases. The relationship obtained when associating the strength data to the $\eta/(C_{iv})^{0.28}$ parameter is in consonance to the general model previously proposed by Diambra *et al.* (2017) which was exemplified in equation 7 (section 2.4.1). Ergo, the following equation was obtained:

$$q_u(kPa) = 10.3 \times 10^7 \cdot \left[\frac{\eta}{(C_{iv})^{0.28}}\right]^{-3.57} \quad (32)$$

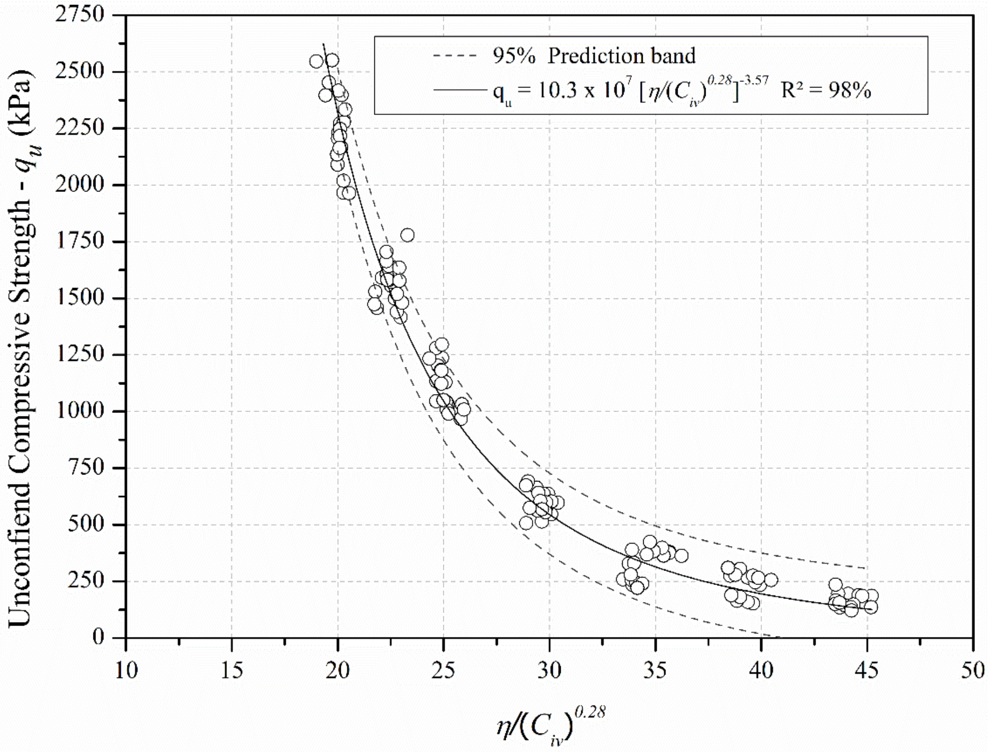

Figure 54 – UCS results for the specimens cured along 7 days related to the porosity/cement index

The attained coefficient of determination (R²) was equal to 98%. A 95% prediction band was also plotted in Figure 54. As a manner of validation of the approach adopted herein, data points presented by Consoli *et al*. (2007a), using the same materials, were plotted in conjunction with results formerly shown in Figure 54. This is represented in Figure 55, where it is observable that most of them lie within the prediction bands and, as well, in the vicinity of the line expressing relationship 32.

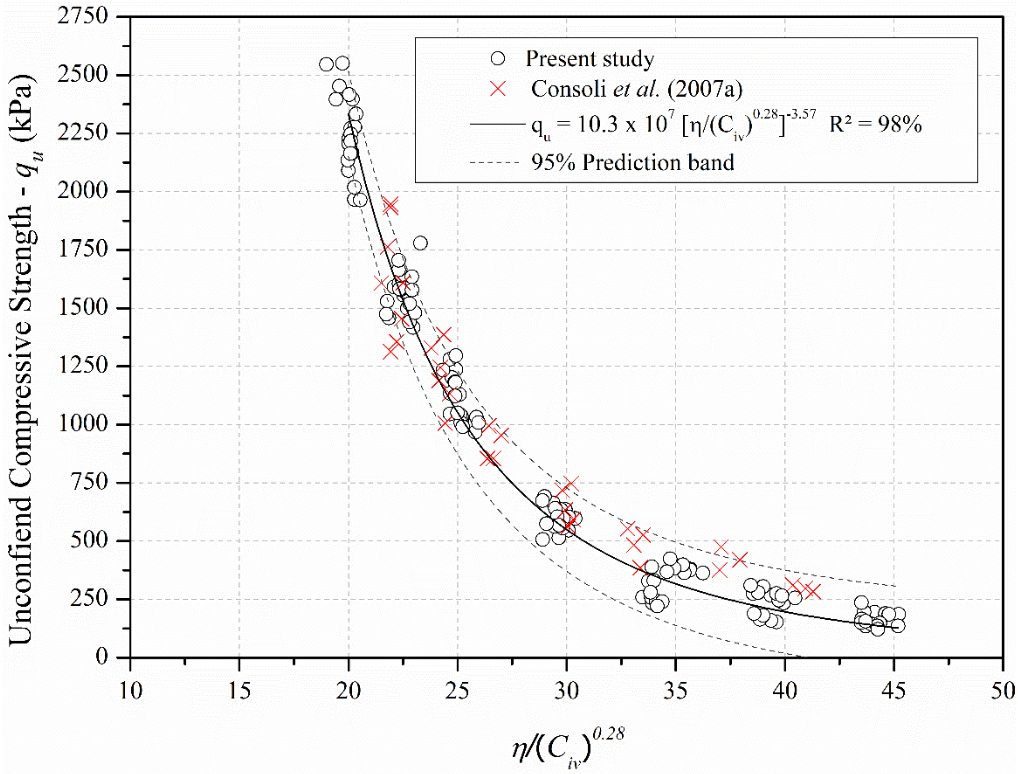

Figure 55 – UCS results for the specimens cured along 7 days related to the porosity/cement index

The strength results relative to all of the curing periods are summarized below, in Figure 56. The curing period has only affected the *B* scalar, maintaining unchanged the other coefficients of relationship 32. The coefficient of determination also has remained unaltered. The scalar *B* has slightly increased around 1.26 times from 7 days to 28 days of curing, whereas it has augmented 1.57 times when comparing the lowest curing period to the highest. The strength rate gain between 7 and 28 days and 28 and 90 days was quite similar. Nonetheless, when considering distinct $\eta/(C_{iv})^{0.28}$ values, it seems that slightly more pronounced increments were attained for higher cement contents. This is expected, as more cement is available to hydrate over a larger period of time.

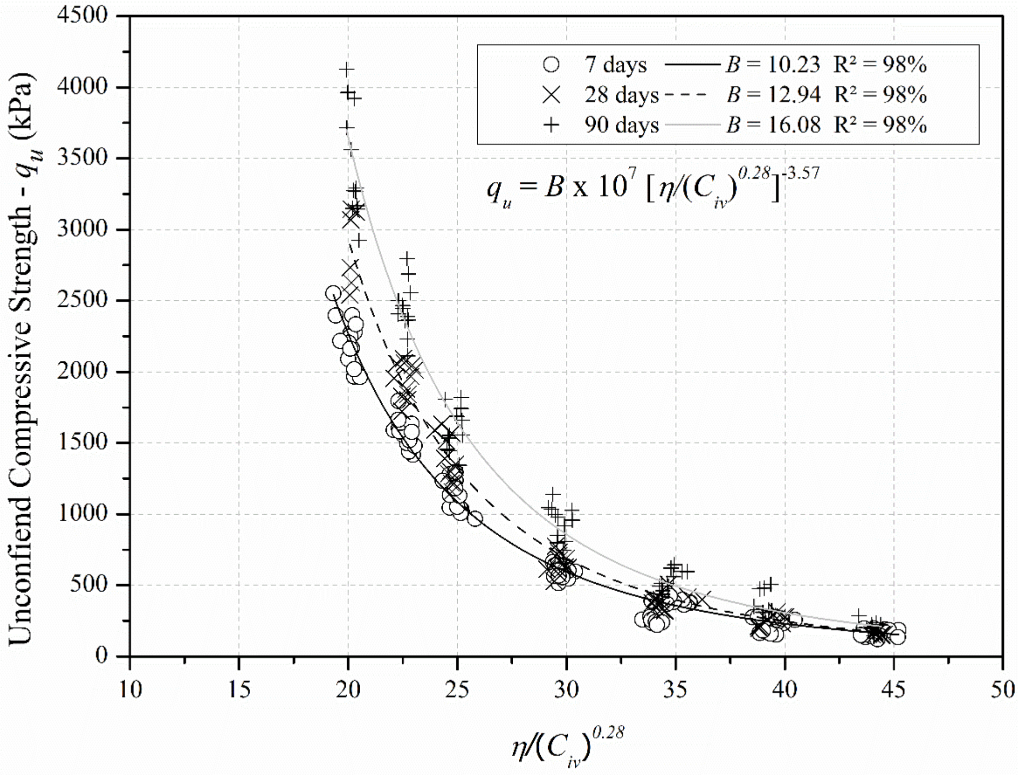

Figure 56 – UCS results for the specimens cured along 7 days related to the porosity/cement index

Essentially, the unconfined compressive strength seems to depends solely on the $\eta/(C_{iv})^{0.28}$ index value for the compacted BRS-cement specimens, regardless of the adopted mix design within this fixed porosity/cement parameter value.

5.2.1.1 Individual Analysis

In order to proper present the unconfined compressive strength results for each mix design, these were individually presented from Figures 57 to 63 following the same approach as formerly presented for the G_0 data. Each figure corresponds to the results of a unique $\eta/(C_{iv})^{0.28}$ index value, in which the individual strength of each tested specimen is plotted as a function of its dosage. Solely the outcomes of the specimens cured along 7 days were considered in this analysis. Therefore, within each mix design, 5 points (discernible as circles) indicate the sample's unconfined compressive strength and one point (identifiable as a triangle) is relative to the average of these five data values. A 95% confidence interval (CI) is also plotted for each dosage around its mean. The CI was determined through the pooled standard deviation (σ_{pl}) that is the weighted average of the obtained standard deviations within each dosage for a single $\eta/(C_{iv})^{0.28}$ index value

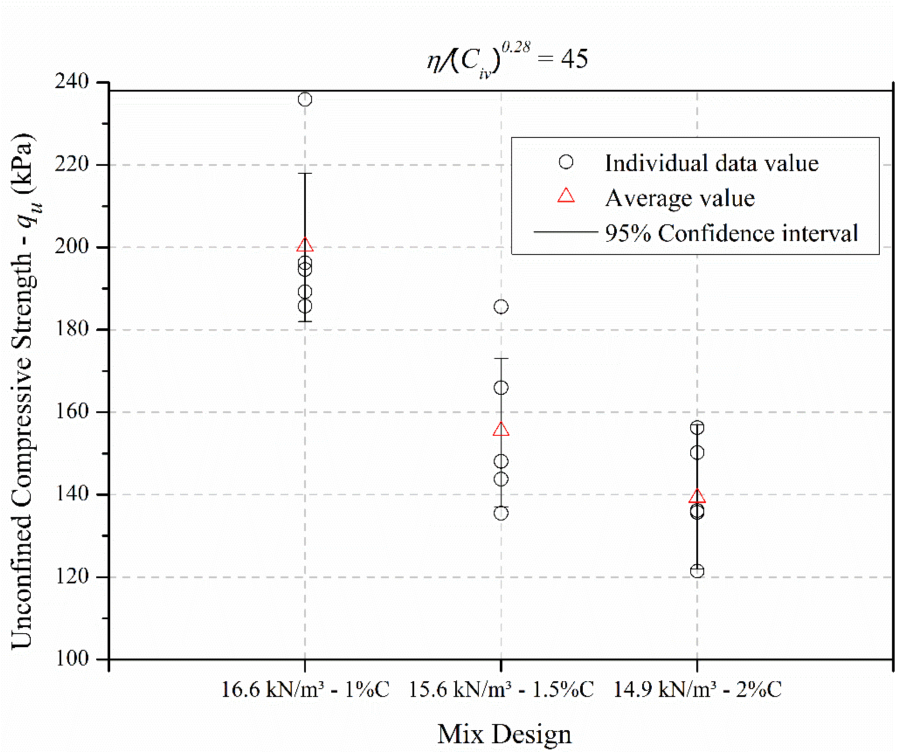

Figure 57 – Individual UCS results for $\eta/(C_{iv})^{0.28} = 45$

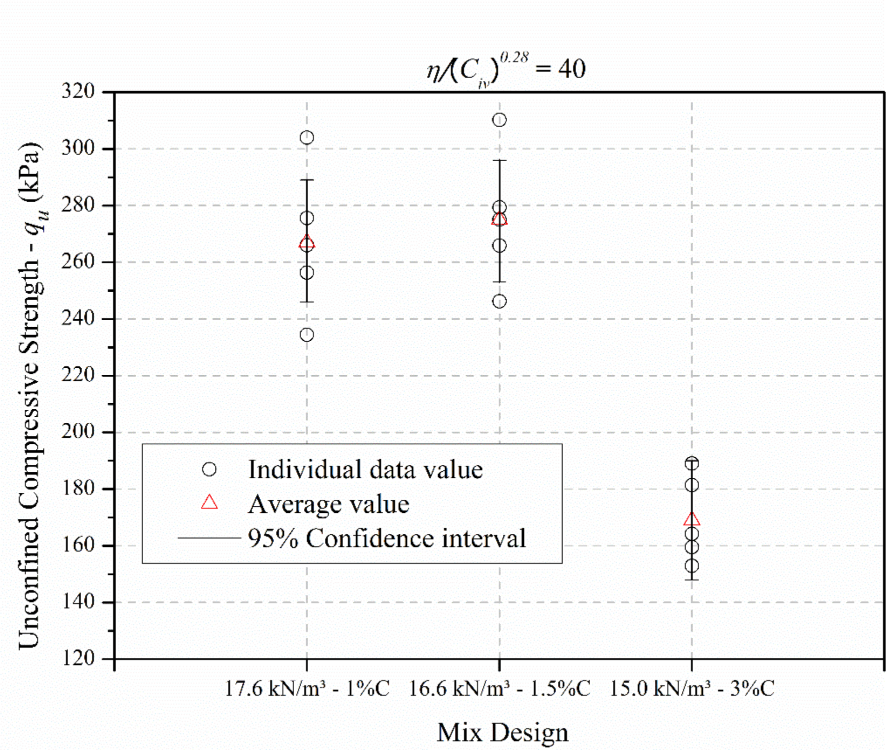

Figure 58 – Individual UCS results for $\eta/(C_{iv})^{0.28} = 40$

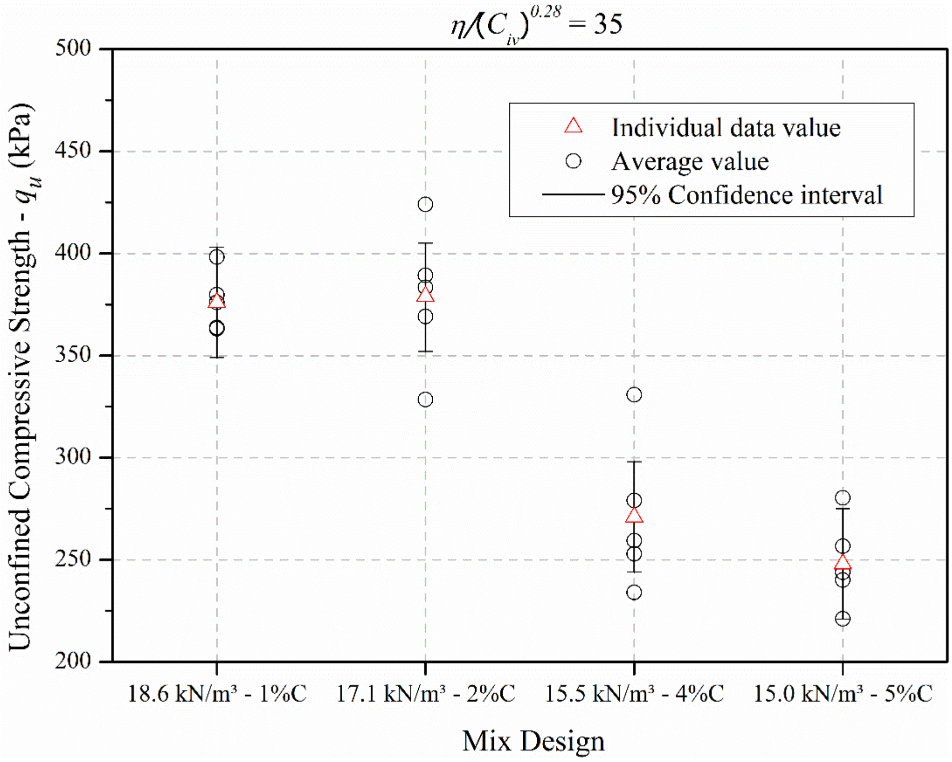

Figure 59 - Individual UCS results for $\eta/(C_{iv})^{0.28} = 35$

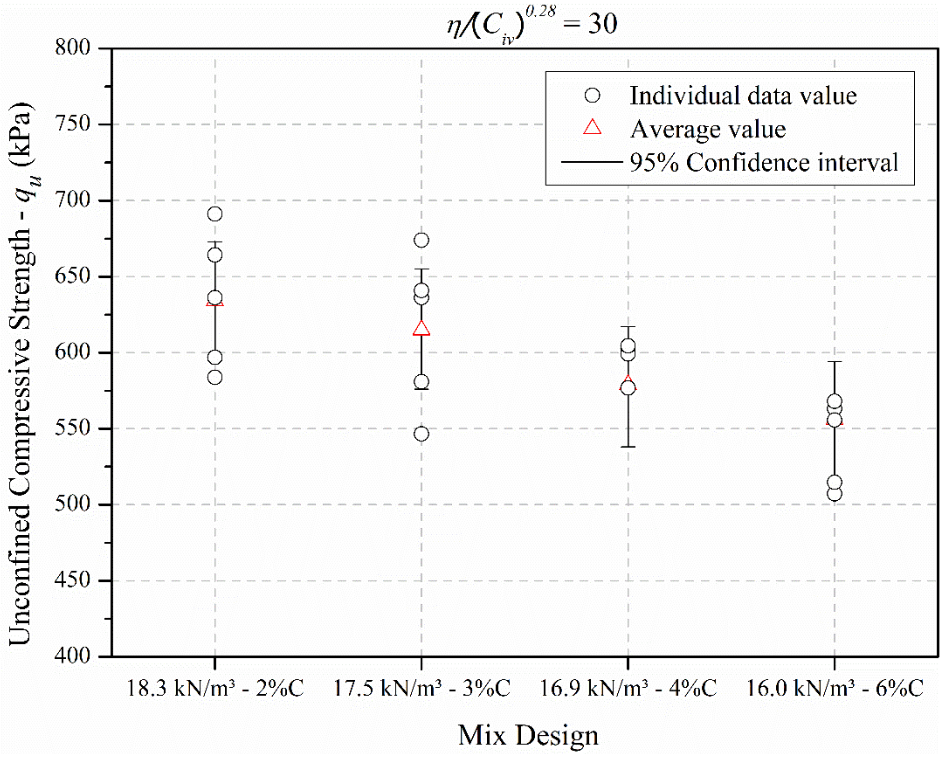

Figure 60 – Individual UCS results for $\eta/(C_{iv})^{0.28} = 30$

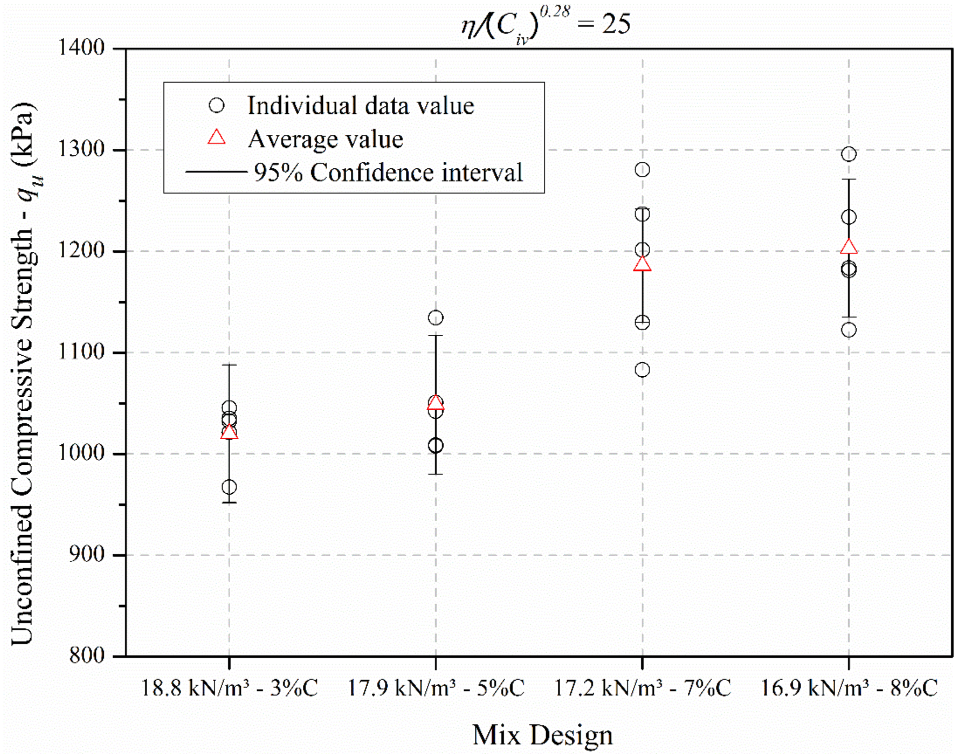

Figure 61 – Individual UCS results for $\eta/(C_{iv})^{0.28} = 25$

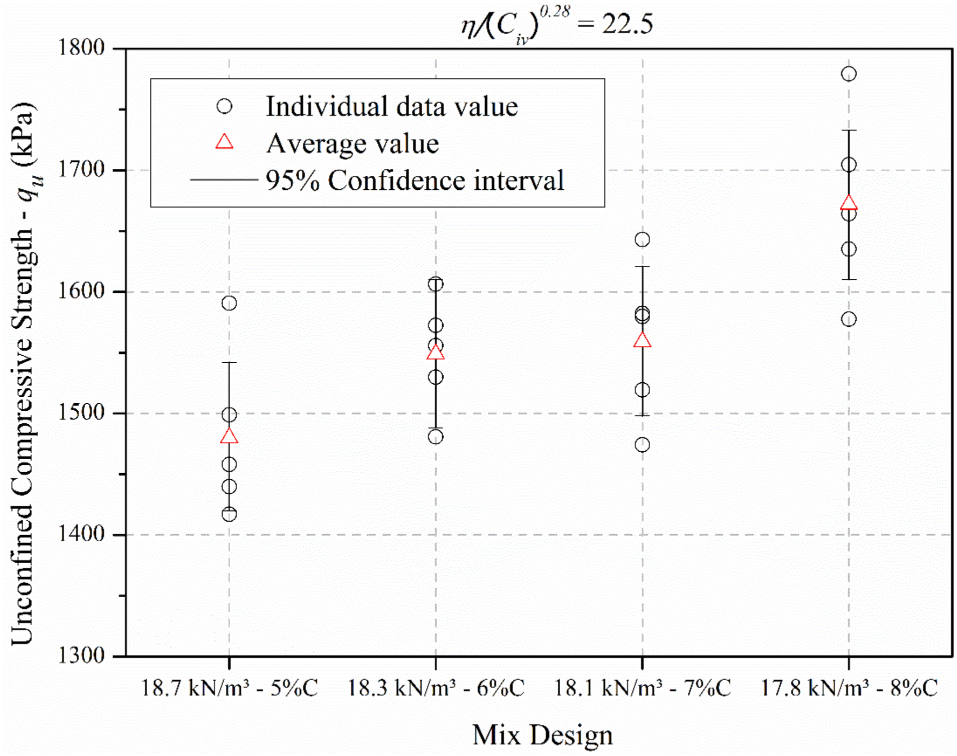

Figure 62 – Individual UCS results for $\eta/(C_{iv})^{0.28} = 22.5$

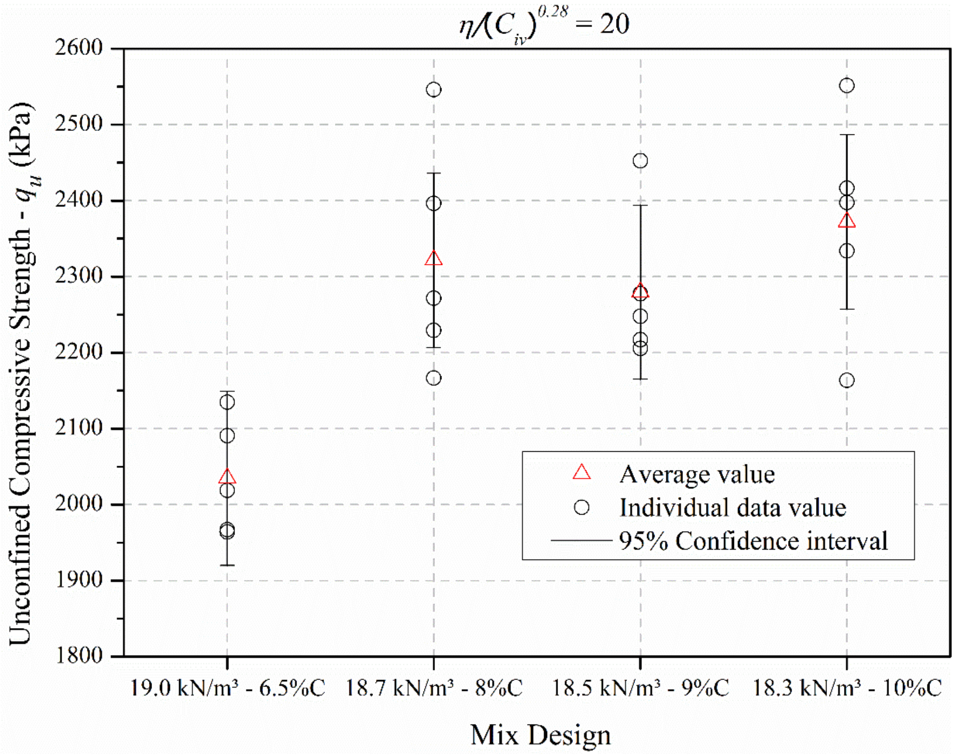

Figure 63 – Individual UCS results for $\eta/(C_{iv})^{0.28} = 20$

In general, within each $\eta/(C_{iv})^{0.28}$ value, no substantial differences were observable between the average strengths of each tested mix design. Namely, it seems that altering the dosage via distinct porosities and cement contents combinations, but maintaining the $\eta/(C_{iv})^{0.28}$ parameter constant, seems to have little effect on the unconfined compressive strength of the tested specimens. Hence, it appears that the strength owing to the loss of interlocking between the soil-cement particles (when the dry unit weight is lowered) is compensated by the increment of the cementing bonding due to the increase in the cement content. As a consequence, the strength maintains a similar order of magnitude within each porosity/cement index value, irrespective of the mix design. Otherwise, it would not be possible to construct the curve presented in Figures 54 and 55, for example. That is, the scatter of the data would be much greater.

5.2.1.2 Statistical Analysis

As earlier presented for the initial shear modulus results, multiple comparisons tests (MCT) were carried out within each $\eta/(C_{iv})^{0.28}$ parameter value aiming to determine if there exist statistically significant differences between the dosages. The results of the MCT are summarized in Table 13, and the dosages that share the same reference letter (within each $\eta/(C_{iv})^{0.28}$ value) are statistically equal with relation to their unconfined compression values. As can be noticed, the trends observed in Table 13 are similar to what was previously noticed for the stiffness (Table 11). That is, the statistical equality amongst the dosages molded having the same $\eta/(C_{iv})^{0.28}$ value is similar when comparing the strength and the stiffness outcomes. In general, at least two mix designs were statistically equivalent when considering each $\eta/(C_{iv})^{0.28}$ value and, despite small eventual statistical differences, the correlation between the stiffness and the $\eta/(C_{iv})^{0.28}$ index has worked.

Table 13 – Multiple comparison test results for the unconfined compression results

$\eta/(C_{iv})^{0.28}$	Mix Design	γ_d (kN/m³)	C (%)	Average q_u (kPa)	MCT	Matric suction (kPa)
45	1	16.59	1.00	200	A	12.07
	2	15.61	1.50	155	B	
	3	14.87	2.00	139	B	6.60
40	4	17.53	1.00	268	A	16.81
	5	16.65	1.50	275	A	-
	6	14.96	3.00	169	B	-
35	7	18.55	1.00	379	A	27.00
	8	17.11	2.00	376	A	-
	9	15.50	4.00	271	B	-
	10	14.96	5.00	248	B	6.87
30	11	18.31	2.00	634	A	25.34
	12	17.45	3.00	615	A, B	-
	13	16.87	4.00	579	A, B	-
	14	15.96	6.00	556	B	11.16
25	15	18.85	3.00	1020	A	40.13
	16	17.88	5.00	1064	A	-
	17	17.21	7.00	1186	B	-
	18	16.94	8.00	1203	B	15.65
22.5	19	18.67	5.00	1481	A	23.43
	20	18.34	6.00	1549	A	-
	21	18.05	7.00	1560	A, B	
	22	17.81	8.00	1672	B	21.52
20	23	19.04	6.50	2035	B	30.16
	24	18.70	8.00	2322	A	-
	25	18.49	9.00	2280	A	-
	26	18.32	10.00	2372	A	34.79

Exemplifying, there is no statistical difference between the unconfined compression results of mix designs No. 4 (17.53 kN/m³ - 1%C) and No. 5 (16.65 kN/m³ - 1.5%C) when $\eta/(C_{iv})^{.28}$ = 40. Yet, the dosage No. 6 (14.96 kN/m³ - 3%C) statistically differs from those two. In general, at least two mix designs were statistically equivalent within each one of the adopted $\eta/(C_{iv})^{0.28}$ values. Anyhow, even when there were observed statistical differences between mix designs that share the same porosity/cement index value, such deviations were small in comparison to the magnitude of the strengths and have not globally affected the approach proposed by relationship 6. In order to demonstrate it, Figure 64 presents the unconfined compressive strength results as a function of the adjusted porosity/cement index containing only the dosages which are statistically equivalent within each $\eta/(C_{iv})^{.0.28}$ value. Therefore, mix designs numbers 1, 6, 9, 10, 14, 17, 18, 19, 20, 21, and 23 were withdrawn from the analysis. Even so, the prediction equation remained practically unaltered, but as expected, with less scatter around the fitted curve and, thus, a greater coefficient of determination ($R^2 = 0.99$).

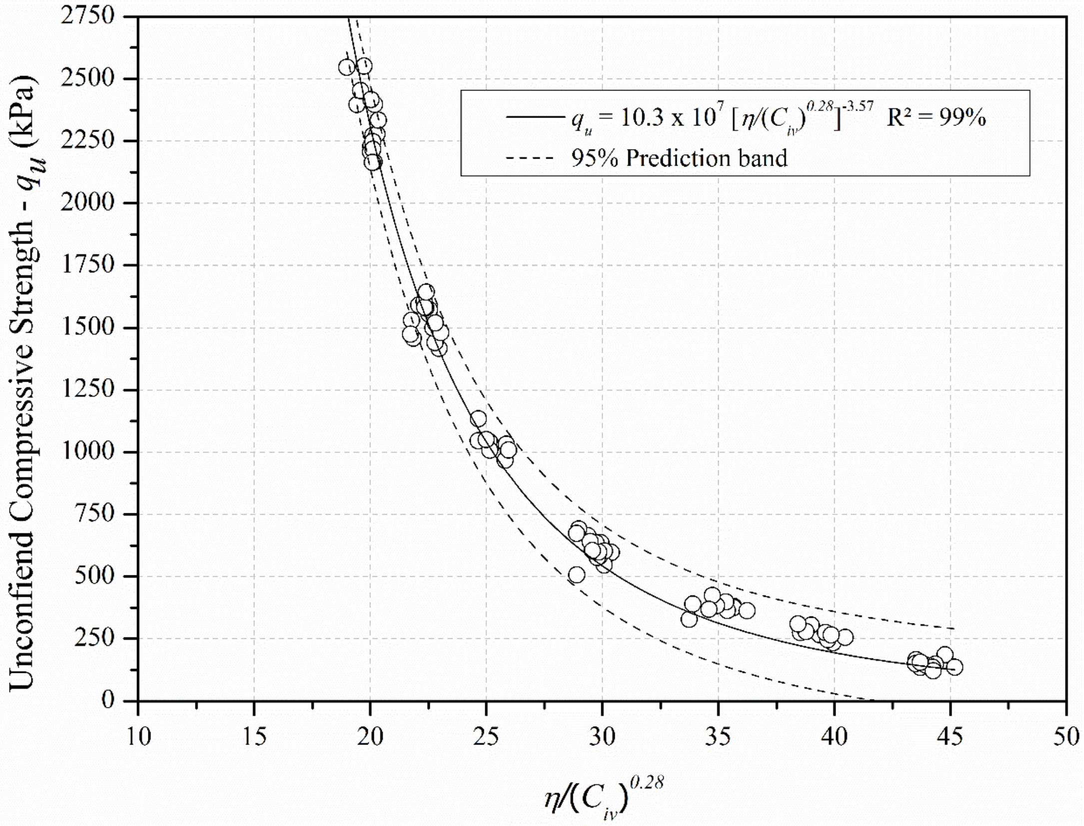

Figure 64 – UCS results for the specimens cured along 7 days related to the porosity/cement parameter for statistically equal dosages within the same index value

5.2.1.3 Matric Suction Results

The last column of the formerly presented Table 13 contains the matric suction values for the two most opposite dosages within each $\eta/(C_{iv})^{0.28}$ index value. Irrespective of the adopted mix design, the magnitude of the matric suction has not represented more than 10% of the unconfined compressive strength of the soil-cement specimens. This indicates that submerging the samples along 24 hours prior to the strength tests is efficient in order to minimize the influence of suction on the unconfined compressive strength of the tested mixtures.

5.2.1.4 Theoretical Model Application

The model previously proposed by Diambra *et al.* (2017) was applied to the present work and compared to the obtained unconfined compressive strength results. As a reason, equation 10 was employed using the parameter values introduced by Diambra *et al.* (2017), that are summarized in Table 14, below. Nonetheless, a controversial aspect of such approach is its dependency on a critical state porosity value (η_{cs}) because the model concerns the unconfined compressive strength of cemented soil specimens that do not reach the critical state and, by definition, are far from achieving such state. Moreover, η_{cs} is dependent upon the mean effective stress and we are dealing with unconfined conditions herein. Hence, a parametric assessment was carried out by varying the η_{cs} value from 24 to 34 intending to assess the effect of such parameter on the adequacy of the model with relation to the experimental data. Hence, the resultant curves were, thus, compared to the experimental strength data. The critical state stress ratio (*M*) was taken as 1.46 (see item 2.3.5). Consequently, the curves depicted in Figure 65 were generated.

Table 14 – Parameters of equation 10

Parameter	**Value**
M	1.46
σ_c	90
β	-6
K_c	4
a	3.5

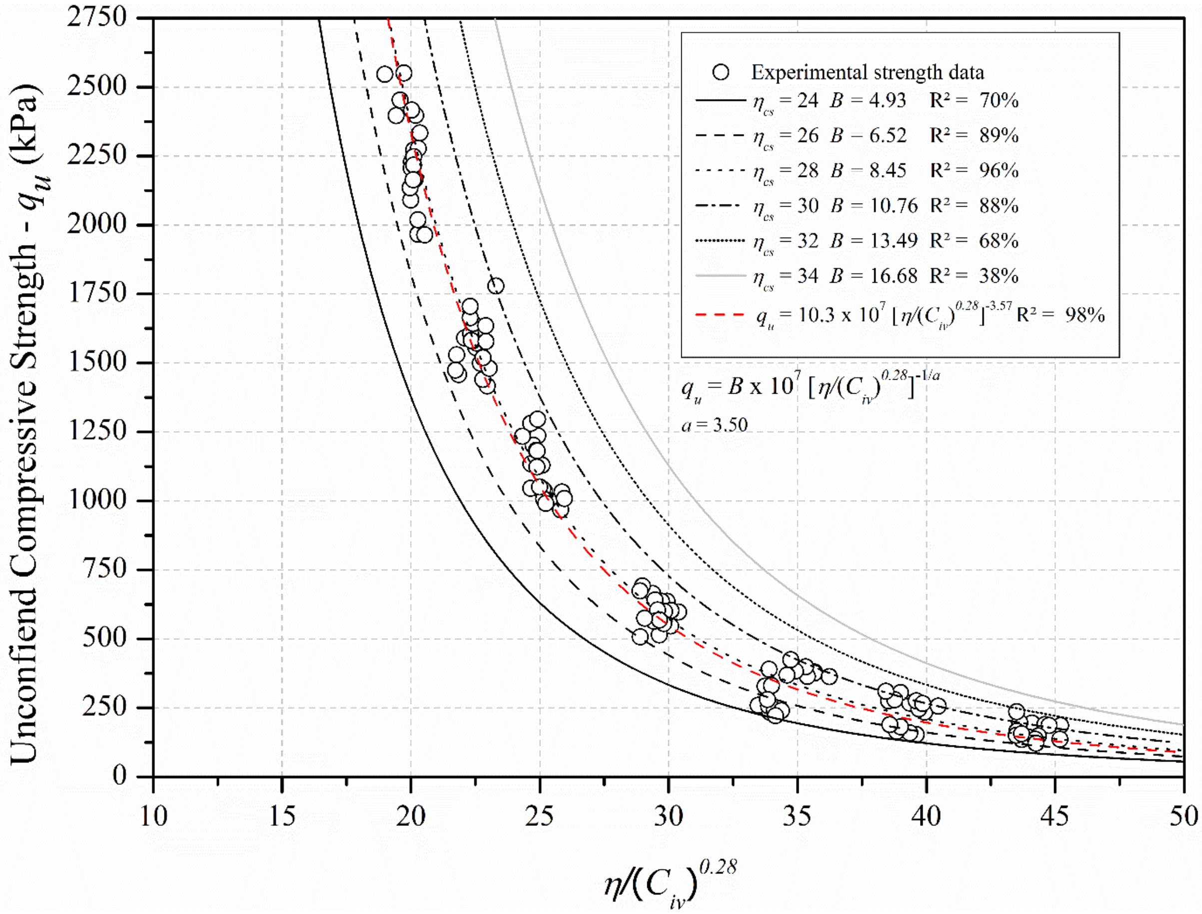

Figure 65 – Measured unconfined compression data versus theoretical equation

As observable, a η_{cs} equals to 28 has yielded the equation that achieved the greatest concordance with the experimental data, resulting in the highest coefficient of determination (R^2) value. Such curve was able to satisfactorily express the unconfined compressive strength as a function of the adjusted porosity/cement index and is similar to the curve resultant from the experimental data (eq. 32) that is represented in red dashes in Fig. 65. Besides, it is clear that η_{cs} values smaller than 26 or greater than 30 have resulted in curves which were not capable to properly model the strength of the studied mixtures. This points out the importance of conducting a parametric analysis when the intention is to use such approach and, as well, it endorses the value of conducting, at least, few experimental points. In brief, the curves represented in Fig. 65 are of the form of eq. 33 which resembles eq. 6. The *B* scalar values are summarized in Table 15.

$$q_u(\text{kPa}) = B \cdot \left[\frac{\eta}{(C_{iv})^{0.28}}\right]^{-3.50} \tag{33}$$

Table 15 – Parameters of the curves depicted in Fig. 65

η_{cs}	B	R² (%)
24	4.93	70
26	6.52	89
28	8.45	96
30	10.76	88
32	13.49	68
34	16.88	38

5.2.1.5 Parallelism with the Stiffness Data

As already mentioned, the stiffness data has presented the same overall tendency as the unconfined compression results. That is, an inverse trend when correlated to the $\eta/(C_{iv})^{0.28}$ index and, likewise, small differences amongst the distinct dosages assembled with the same adjusted porosity/cement value. As a reason, it is clear that a direct proportionality exists between the strength and the stiffness of the studied specimens as portrayed in Figure 66, below. In brief, the stiffer samples tend to be, as well, the ones that present higher strength values. In this regard two linear relationships have resulted when the initial shear modulus data was correlated to the unconfined compressive strength outcomes and seven zones, each corresponding to one $\eta/(C_{iv})^{0.28}$ value, were discernible. The first linear trend passes through the origin whereas the second does not. Physically, the fist interpretation means that a compacted BRS-cement specimen which does not possess unconfined compressive strength would, as well, presents no rigidity at tiny strain values. This is not valid for the second approach, in which the sample would present stiffness, regardless the absence of unconfined compressive strength.

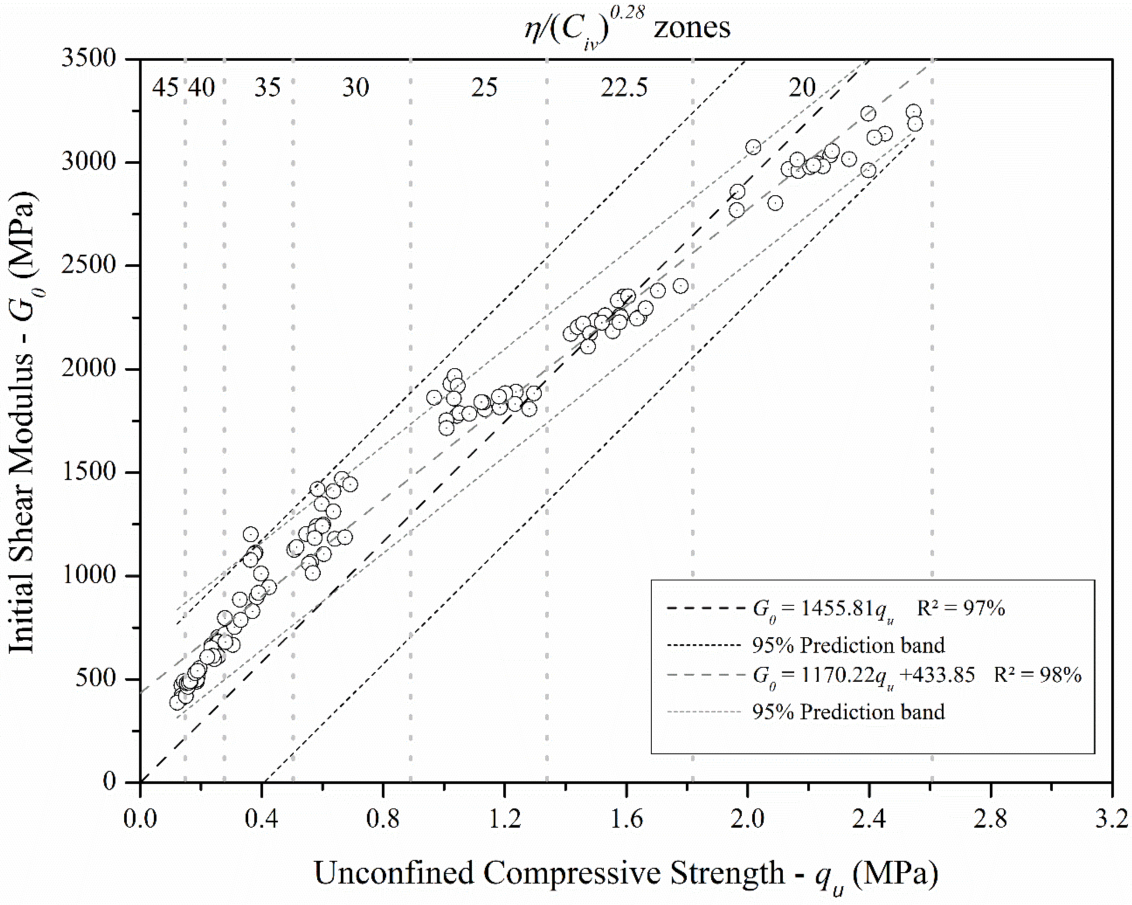

Figure 66 – G_0 and q_u relationships

5.2.2 Split Tensile Strength Tests

Split tensile strength tests (q_t) were performed for the dosages number 1 to 24 (Table 5) for a curing period equal to 7 days. Triplicates were tested within each mix design. As formerly presented for the unconfined compression tests, the q_t results were correlated to the adjusted porosity/cement index and are summarized in Figure 67, below. As expected, an inverse trend between q_t and $\eta/(C_{iv})^{0.28}$ was observed and the following power-type equation was obtained with a coefficient of determination (R²) equal to 94%.

$$q_t(kPa) = 1.40 \times 10^7 \cdot \left[\frac{\eta}{(C_{iv})^{0.28}}\right]^{-3.57} \tag{34}$$

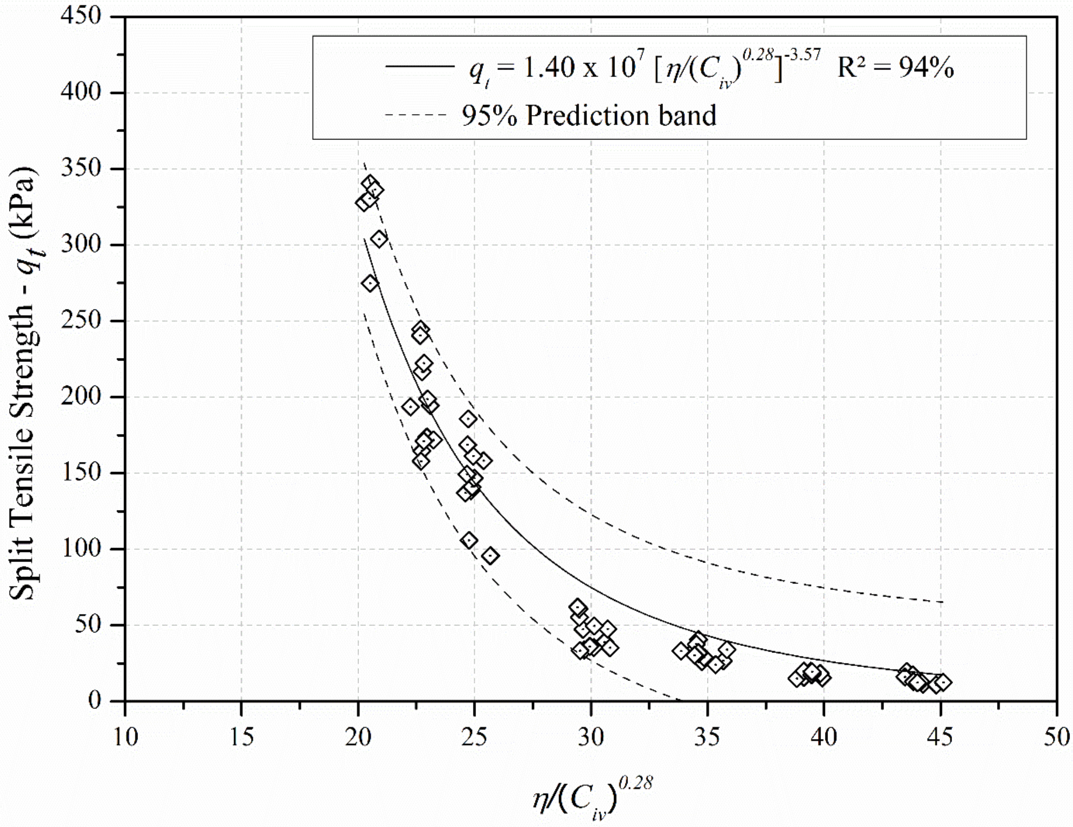

Figure 67 – Split tensile strength test results versus $\eta/(C_{iv})^{0.28}$

Through the quotient between equation 34 and equation 32, the overall split tensile strength/unconfined compressive strength ratio (q_t/q_u) is obtained, being equal to 13.5%. This is in accordance to previous results regarding soil-cement mixtures (e.g. CLOUGH *et al.*, 1981; CONSOLI *et al.*, 2010; DIAMBRA *et al.*, 2018; BALDOVINO *et al.*, 2020a).

5.3 DURABILITY TESTS

The durability tests were carried out using triplicates within each dosage which permitted the conduction of a statistical analysis within each $\eta/(C_{iv})^{0.28}$ value, similar to what was previously demonstrated for the stiffness and strength data. Yet, as only the performance of two different dosages was compared, a one-way analysis of variance (ANOVA) could be performed rather than a multiple comparison test to check for possible statistical equivalence of the means. In addition, the results were correlated to the $\eta/(C_{iv})^{0.28}$ index.

5.3.1 General Overview

Figure 68 summarizes the durability outcomes for all the tested dosages relating the mean accumulated loss of mass ($ALM_{,m}$) to the number of cycles. $ALM_{,m}$ is the mean accumulated loss of mass calculated within a triplicate. From the outcomes depicted in Fig. 68, below, it is visible that specimens assembled with equal $\eta/(C_{iv})^{0.28}$ values have exhibited almost identical mean durability responses. That is, the $ALM_{,m}$ for each cycle of the densest and least cemented specimens (↓η and ↓C) was very close the loss of mass of the most porous and most cemented specimens (↑η and ↑C) considering the same $\eta/(C_{iv})^{0.28}$.

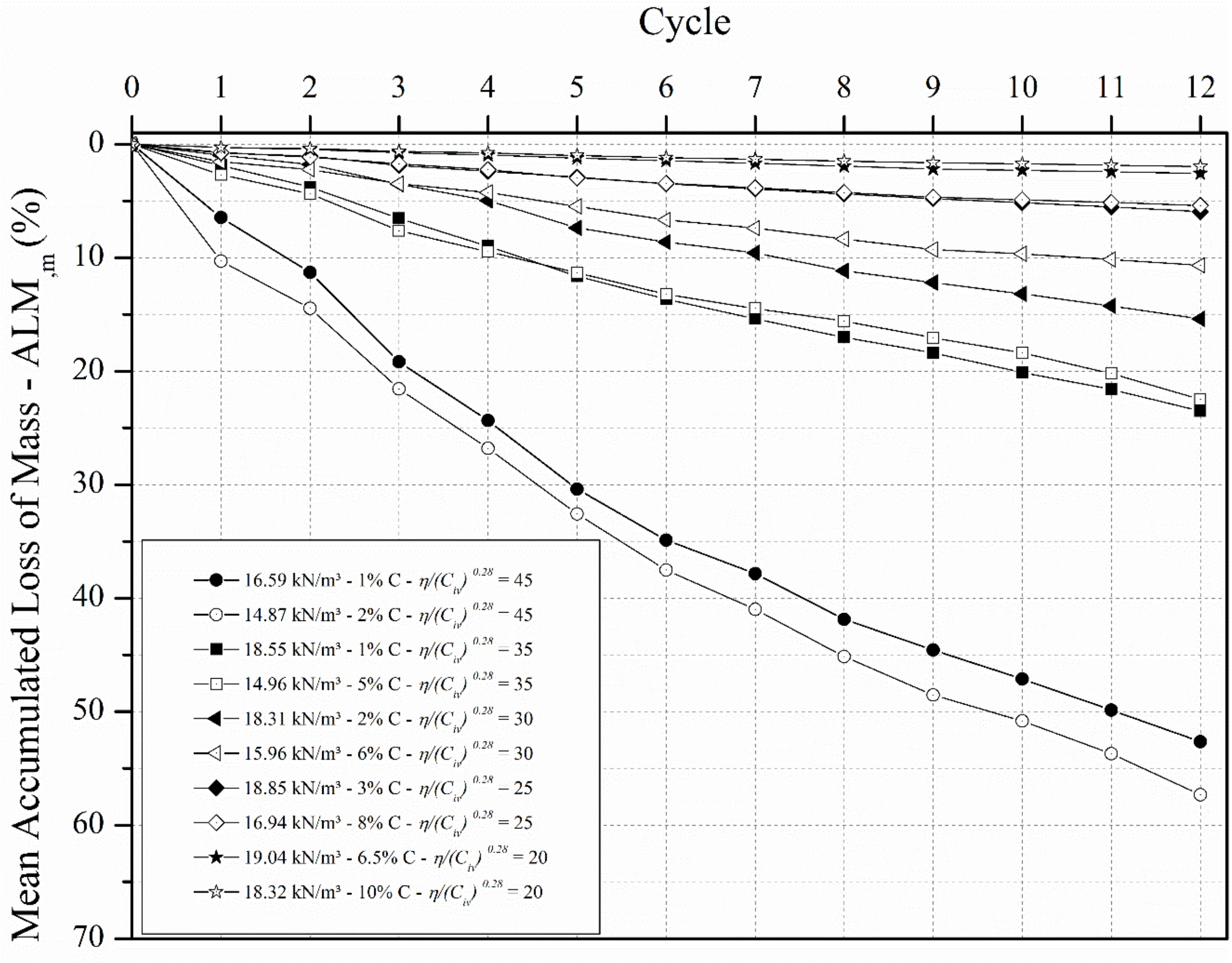

Figure 68 – Mean durability test results

All the results relative to the durability tests are presented from Figures 69 to 78, being each figure relative to the data from a single dosage. Within each graph, the ALM per cycle of each tested specimen, as well as the triplicate's mean ALM per cycle accompanied by a standard error (SE) bar, is shown. This error bar indicates the spread of the data around the mean value and was calculated as the quotient between the standard deviation amid the samples and the square root of the sample size (i.e., n =3).

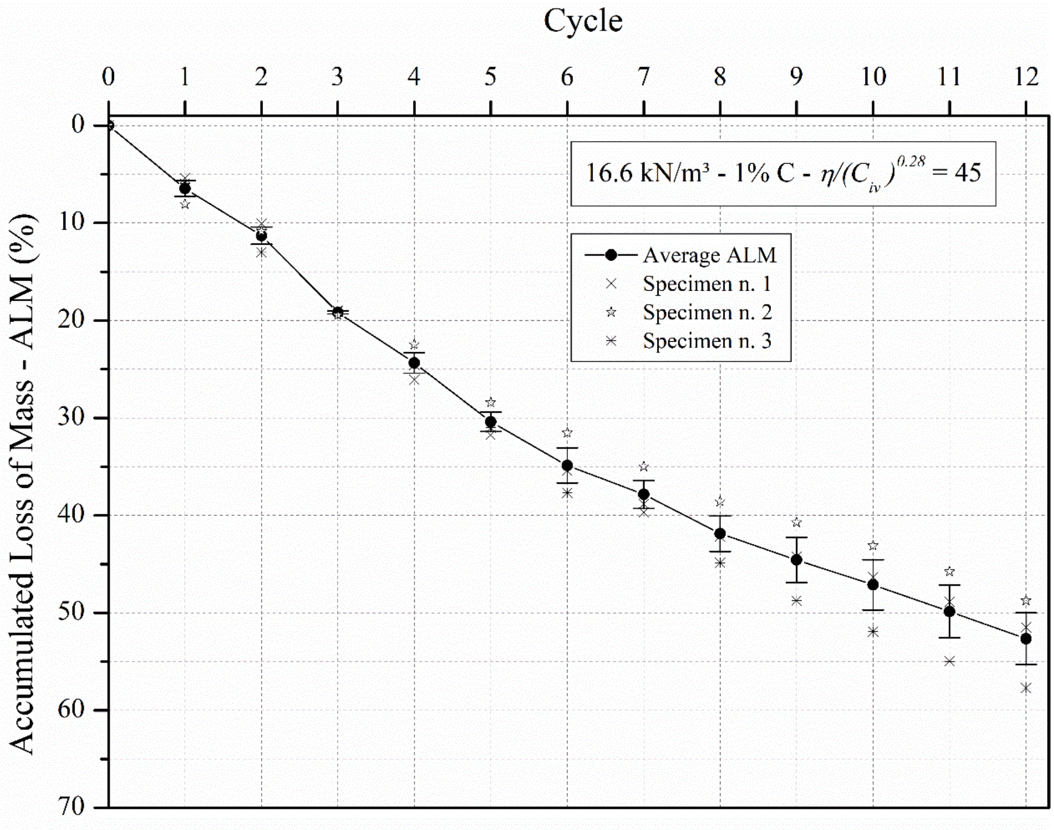

Figure 69 – Durability test results for $\eta/(C_{iv})^{0.28}$ = 45 (least porous sample)

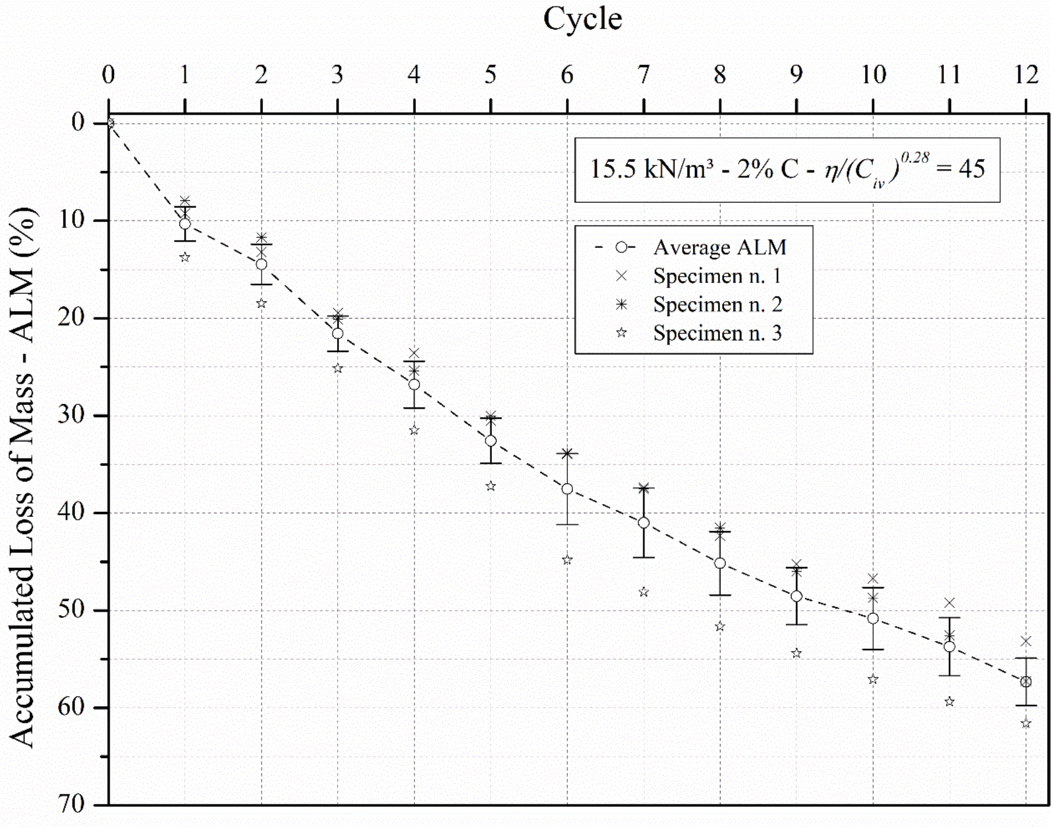

Figure 70 – Durability test results for $\eta/(C_{iv})^{0.28}$ = 45 (most porous sample)

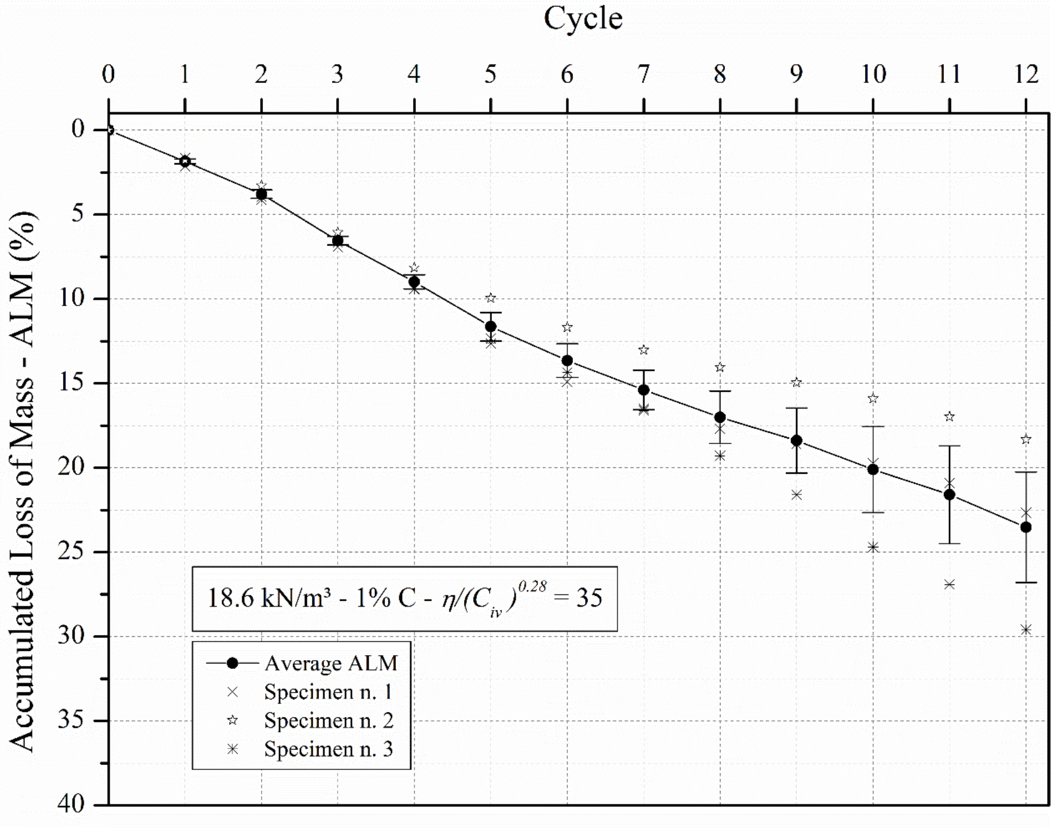

Figure 71 – Durability test results for $\eta/(C_{iv})^{0.28}$ = 35 (least porous sample)

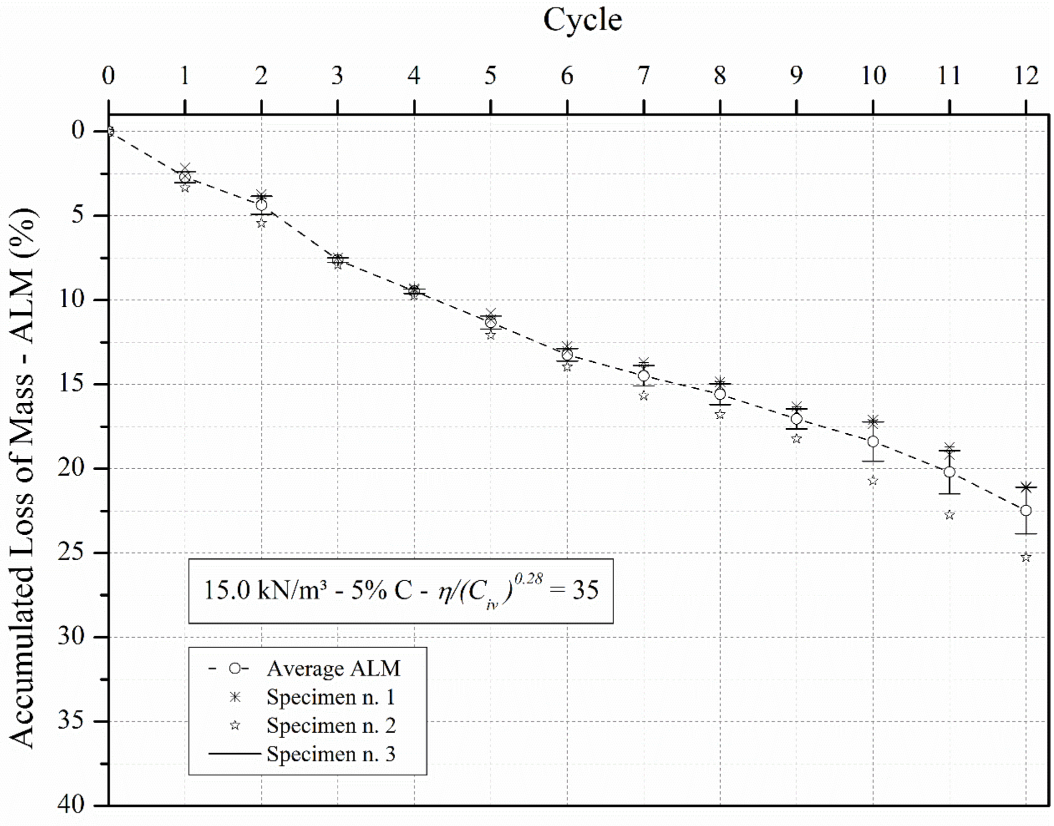

Figure 72 – Durability test results for $\eta/(C_{iv})^{0.28}$ = 35 (most porous sample)

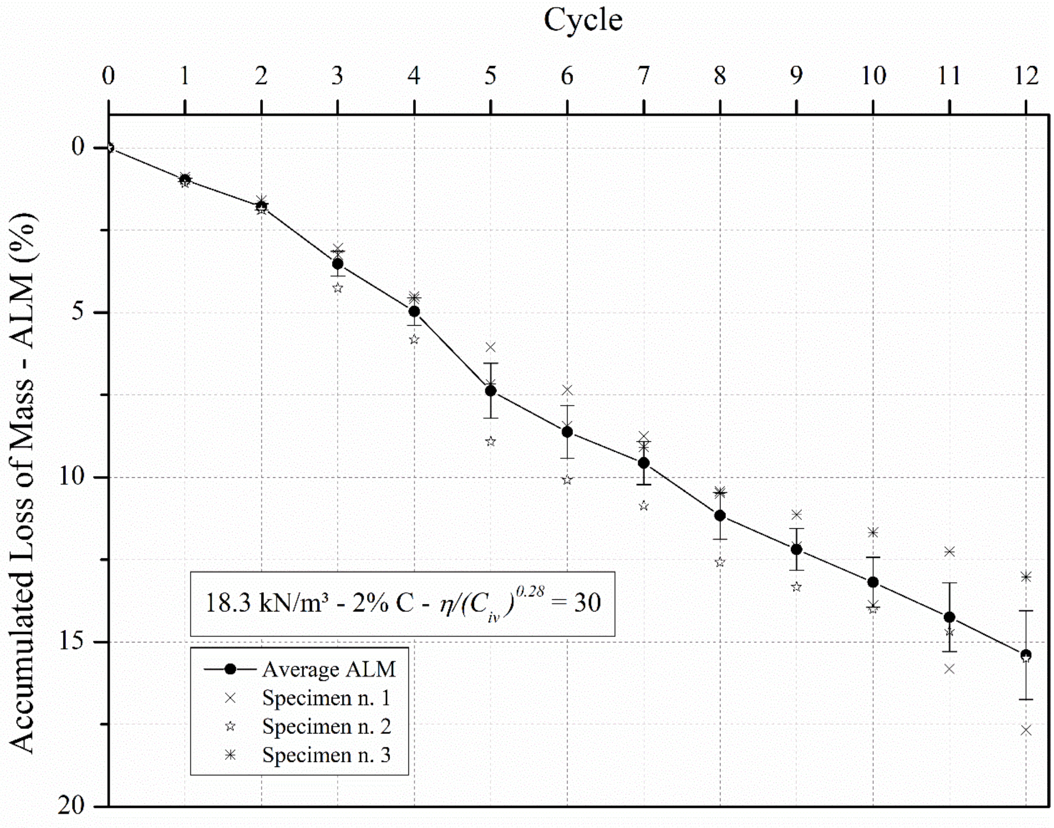

Figure 73 – Durability test results for $\eta/(C_{iv})^{0.28}$ = 30 (least porous sample)

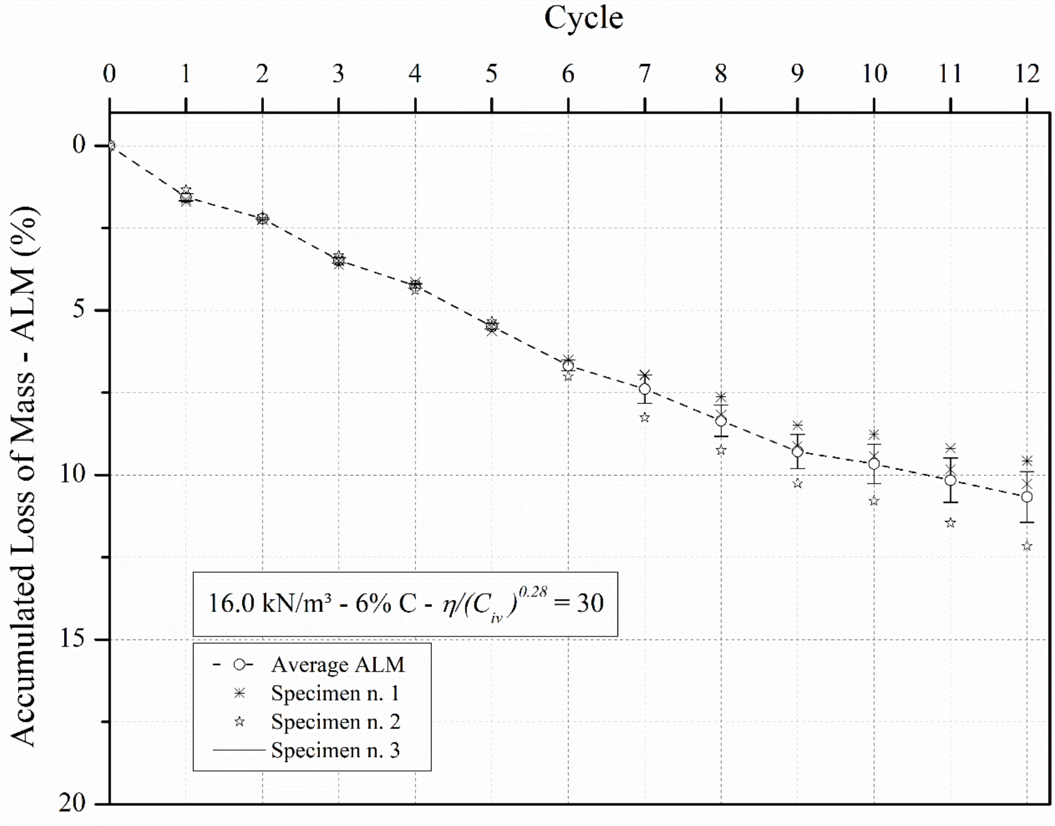

Figure 74 – Durability test results for $\eta/(C_{iv})^{0.28}$ = 30 (most porous sample)

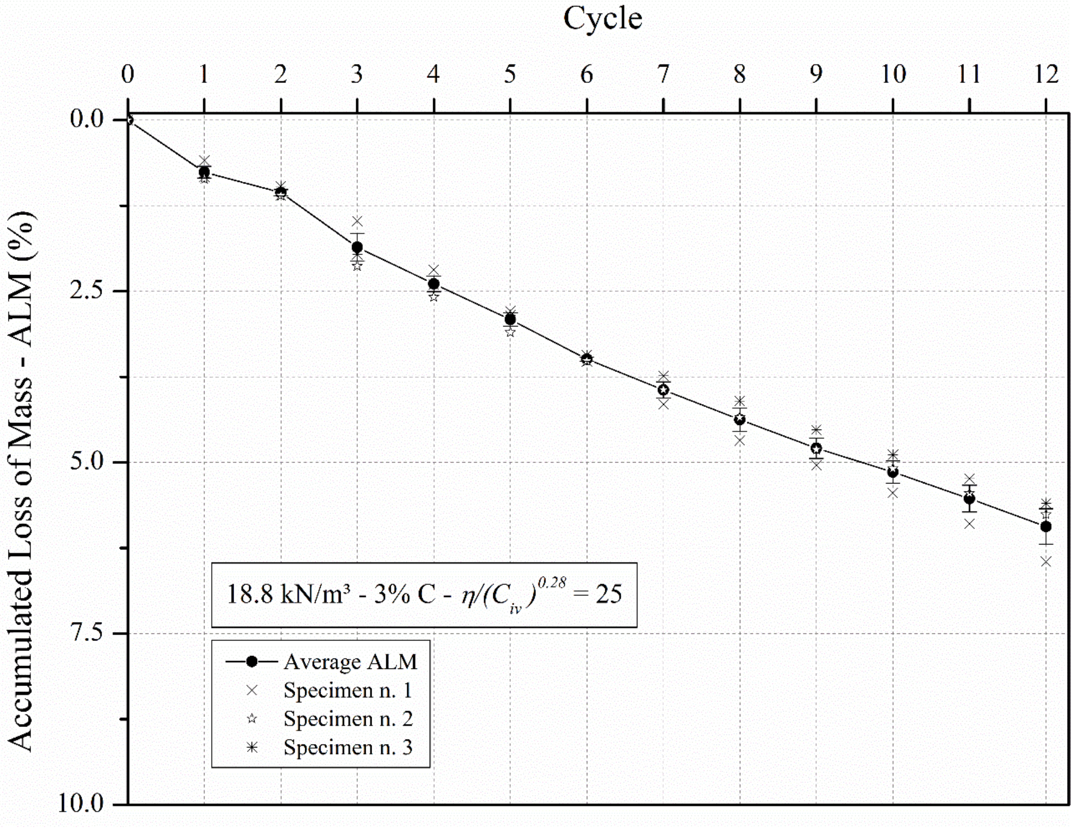

Figure 75 – Durability test results for $\eta/(C_{iv})^{0.28}$ = 25 (least porous sample)

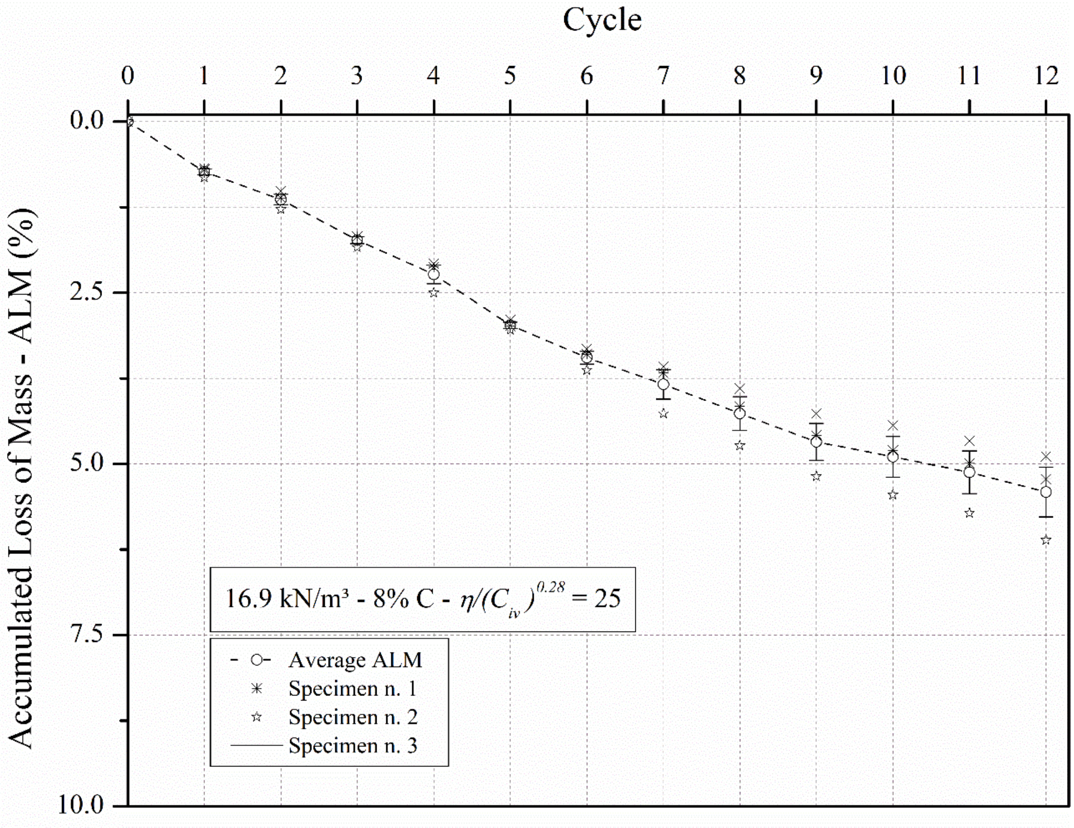

Figure 76 – Durability test results for $\eta/(C_{iv})^{0.28}$ = 25 (most porous sample)

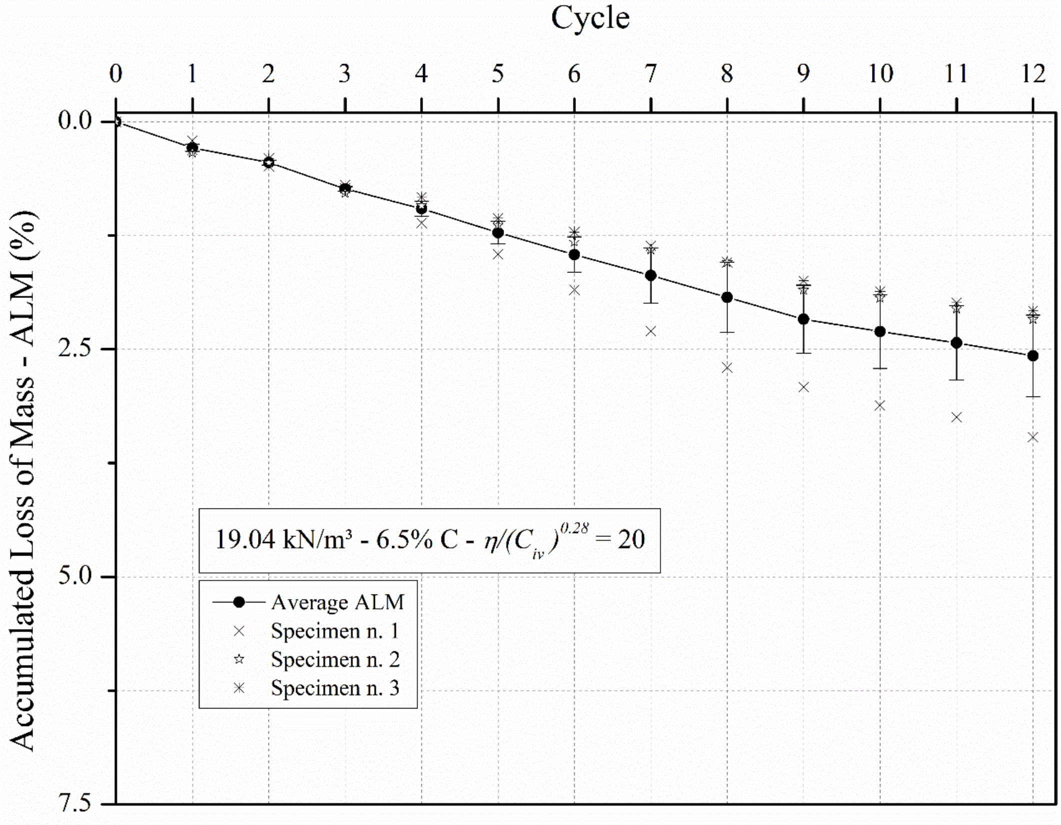

Figure 77 – Durability test results for $\eta/(C_{iv})^{0.28}$ = 20 (least porous sample)

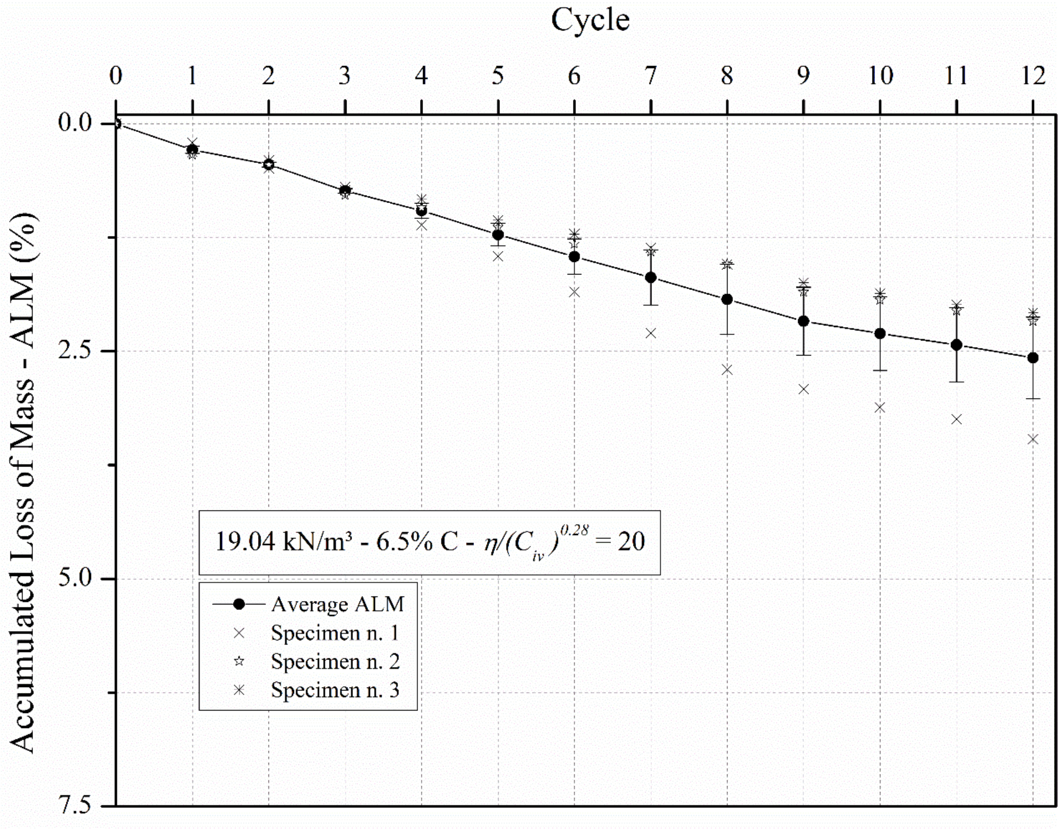

Figure 78 – Durability test results for $\eta/(C_{iv})^{0.28}$ = 20 (most porous sample)

By observing the previously displayed results, it was clear that a similar durability response was attained within each $\eta/(C_{iv})^{0.28}$ value, regardless of the adopted dosage. Hence, it appears that an equivalent performance can be obtained by either the increase in the amount of cement and decrease in the compaction energy or, contrariwise, decrement in the cement content and augment of the compactness, if the $\eta/(C_{iv})^{0.28}$ is kept constant. Namely, a more developed cement phase can compensate the disadvantages related to a more porous structure and vice-versa. Amidst the tested $\eta/(C_{iv})^{0.28}$ values, larger ALM has occurred for greater adjusted porosity/cement index. In other words, a direct proportional relationship appears to exist between the ALM per cycle and the $\eta/(C_{iv})^{0.28}$ index. Moreover, a consistency can be perceived when the ALM within the triplicates of the same dosage is analyzed as the scatter around the mean was low.

5.3.2 Relationship with the Adjusted porosity/cement Index

Fig. 79 displays the accumulated loss of mass results for cycles 1, 3, 6, 9 and 12, relative to all the tested specimens, as a function of the $\eta/(C_{iv})^{0.28}$ index. For each cycle, a power-type relationship of the form (35) was obtained, being the scalar B and the attained coefficients of determination (R²) displayed in Table 16.

$$ALM_{cycle} = B\ x\ 10^{-6}\left[\frac{\eta}{(C_{iv})^{0.28}}\right]^{4.0} \tag{35}$$

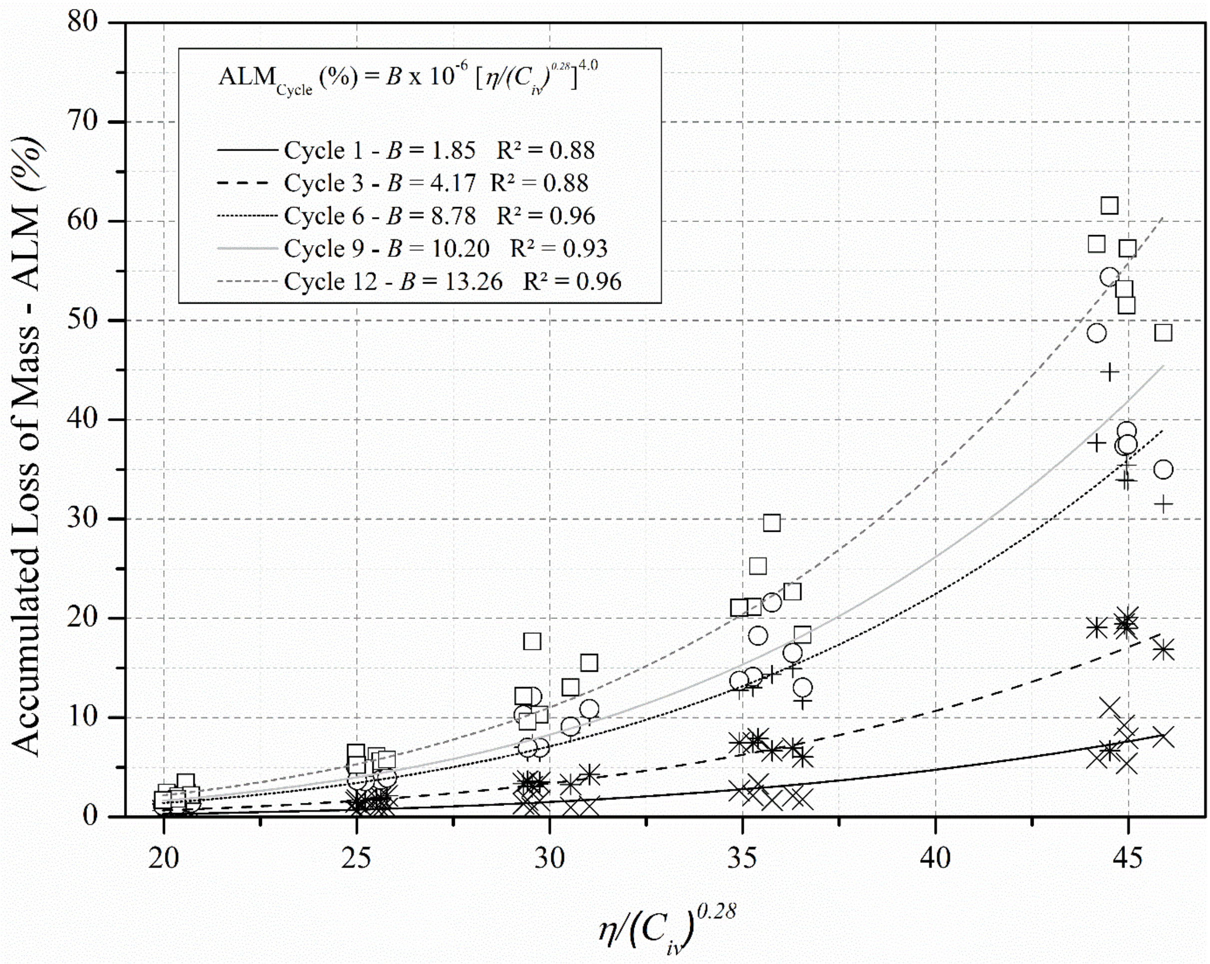

Figure 79 – Durability test results as a function of the $\eta/(C_{iv})^{0.28}$ parameter

Table 16 – Parameters of relationship 35

Cycle	B	Coefficient of determination (R^2)
1	1.85	0.88
3	4.17	0.88
6	8.78	0.96
9	10.20	0.93
12	13.26	0.96

In general, good agreements were obtained between the ALM_{cycle} and the adjusted porosity/cement index as noticeable owing to the great values of the coefficients of determination ($R^2 > 88\%$). Also, a direct proportionality is expressed between the accumulated loss of mass and the $\eta/(C_{iv})^{0.28}$ index by relationship 35. That is, lower ALM values, within each cycle, were observed on the denser and/or more cemented samples (i.e. smaller $\eta/(C_{iv})^{0.28}$ values). Analogous trends have already been reported by Consoli *et al.* (2017b, 2018a, 2018b), Consoli and Tomasi (2018), Baldovino (2020b), among others. Furthermore, the fact that the tests were conducted on specimens molded having different dosages, but the same $\eta/(C_{iv})^{0.28}$ index value, have not negatively contributed to use the approach stated in eq. 35. Otherwise, it would not be possible to express the durability data as a function of the adjusted porosity/cement index with great levels of concordance as observed in Table 16.

Besides, the value of the external exponent (4.20) has resulted from the average between the external exponents resultant from the best fitting within each cycle. These were all close to 4.20. At a first glance, no parallelism can be drawn between this exponent and the one derived by Diambra *et al.* (2017) as the mechanisms of strength mobilization involved in the unconfined compression tests and in the durability are not the same. Nonetheless, the proximity between either exponents (3.57 and 4.20) may be partially explained by the existing relationship between the strength and the durability results, as formerly presented by Consoli *et al.* (2018a, 2019b)

5.3.3 Statistical Analysis

In order to check if there were any statistical differences between the results at the end of the durability test (ALM_{12}) for the different dosages molded using the same $\eta/(C_{iv})^{0.28}$, one-way analysis of variance (ANOVA) tests were carried out. In such test, the hypothesis that all the means are equal (i.e. null hypothesis – H_0) is tested against an alternative hypothesis (i.e. inequality of means – H_1) considering a significance level (α) of 5% (MONTGOMERY, 2013). The ANOVA tests were performed in the statistical software *Minitab* and the results are summarized in the fifth column of Table 16, which exhibits the p-value of the analysis considering each assessed $\eta/(C_{iv})^{0.28}$. The p-value is the probability of obtaining results at least as extreme as the attained outcomes of a hypothesis test if it is assumed that H_0 is correct (GAO, 2020; GIBSON, 2020). In other words, it is the smallest level of significance at which the null hypothesis would be rejected. As a reason, a larger p-value provides stronger evidence in favor of H_0. In spite of $\eta/(C_{iv})^{0.28} = 30$, every dosage molded at the same adjusted porosity/cement index value was statistically equal considering this statistical framework. Namely, enough support against the null hypothesis was only provided for $\eta/(C_{iv})^{0.28} = 30$. Exemplifying, there is no statistical difference between the accumulated loss of mass after 12 cycles when the dosage 1 (16.59 kN/m³ - 1% C) is compared to the mix design 3 (14.87 kN/m³ - 2% C).

This means that there would be no practical difference on the performance of compacted BRS-cement mixtures if a greater compaction energy was used with a smaller cement content or, on the contrary, more cement was used with a lower compactness if $\eta/(C_{iv})^{0.28}$ was kept equal to 45, for example. The same is valid for the other statistically equal dosages. As a reason, it appears that the resistance against the harsh conditions of the durability test is kept practically constant considering the same $\eta/(C_{iv})^{0.28}$. That is, the strength loss due to a least developed cementing bonding is compensated by the increase in the degree of interlocking between the soil-cement particles when the dry unit weight is augmented and the cement content is lowered (for the same $\eta/(C_{iv})^{0.28}$).

Table 17 – Statistical analysis of the durability data

$\eta/(C_{iv})^{0.28}$	Dosage	γ_d (kN/m³)	C (%)	ALM_{12} (%)	p-value	Statistically equivalent
45	1	16.59	1.00	52.64	0.268	Yes
	3	14.87	2.00	57.33		
35	7	18.55	1.00	23.53	0.789	Yes
	10	14.96	5.00	22.48		
30	11	18.31	2.00	15.39	0.038	No
	14	15.96	6.00	10.67		
25	15	18.85	3.00	5.94	0.259	Yes
	18	16.94	8.00	5.41		
20	23	19.04	6.50	2.57	0.299	Yes
	26	18.32	10.00	1.97		

5.3.4 Parallelism with Strength and Stiffness data

An attempt was made to correlate the accumulated loss of mass (ALM) to both the stiffness and strength results in order to check if there exist a coherence amongst these results. Hence, Figure 80 presents the plot of the mean ALM after 12 cycles (ALM_{12}), considering each tested mix design, and the respective mean values of the unconfined compressive strength and initial shear modulus for these dosages. Each data point is, thus, identified according to its respective dosage number (see Table 5). Considering both the q_u and G_0 data, a good agreement and the same inverse power-type relationship trend was obtained when these were correlated to ALM_{12}. In brief, the most resistant specimens against the harsh conditions of the durability tests were, as well, the ones that obtained the highest strength and stiffness results. Moreover, the responses of each one of the five tested $\eta/(C_{iv})^{0.28}$ values are well defined in the graph as the results considering each adjusted porosity/cement index are visibly separated in five groups. This approach enables a rough estimate of the durability response if solely strength and/or stiffness data are measured.

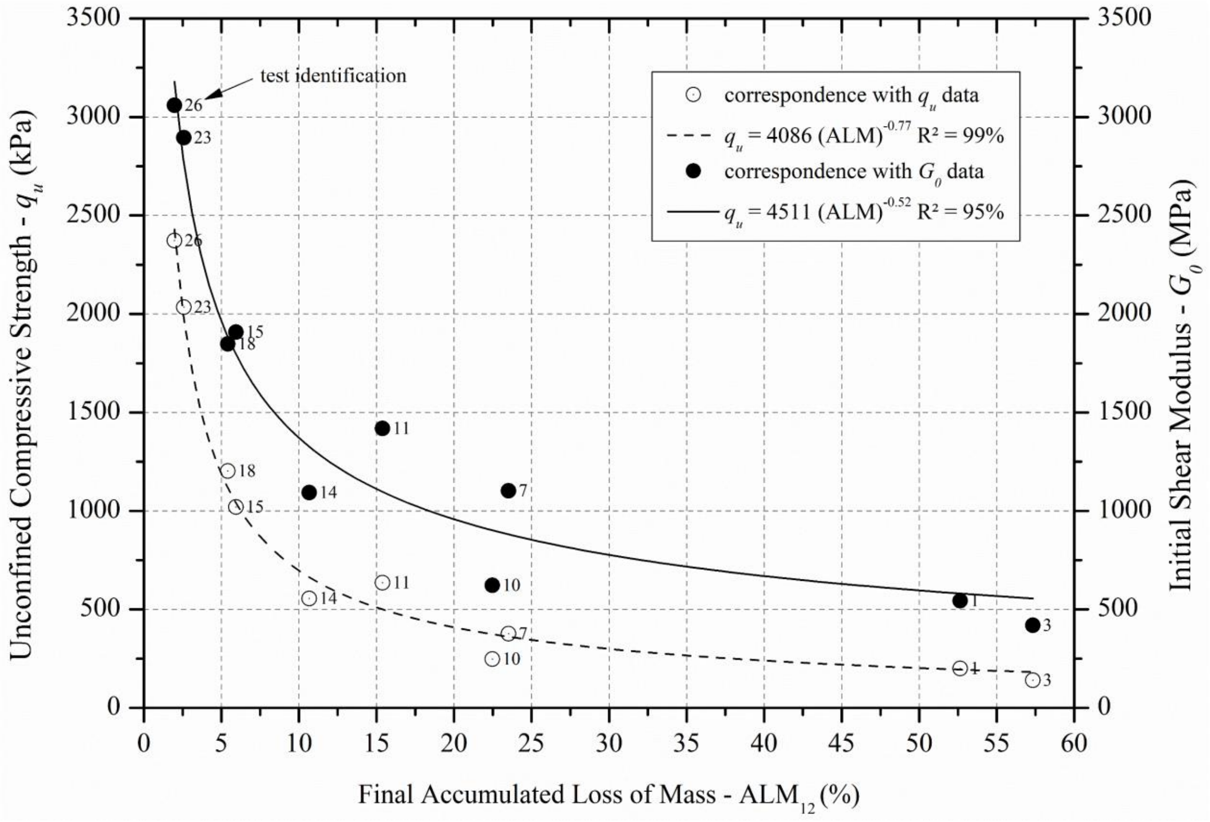

Figure 80 – Accumulated loss of mass related to both strength and stiffness data

5.4 TRIAXIAL TESTS

This chapter presents the results of the triaxial tests for the natural BRS and the compacted BRS-cement specimens. The primary goals of this section can be understood by splitting up the main features addressed herein into:

a) The stress-strain behavior and the volume change behavior of specimens molded using the same $\eta/(C_{iv})^{0.28}$ index value, but having different dosages, at an effective confining pressure of 35 kPa;

b) The mechanical response and the effective strength parameters of samples having the same adjusted porosity/cement index value (35, 30 and 140 kPa), but molded using distinct porosities and amounts of cement;

c) The study of the stiffness degradation aiming to assess the onset of bonds degradation of the tested specimens with parallel to the assessment of the stress-dilatancy paths.

5.4.1 Elementary Definitions

The triaxial tests outcomes relies on fundamental definitions relative to the stress and strains components which, thereafter, are used in the calculation of further material properties. As commonly in the practice of geotechnics, positive strains values are related to compression, whereas negative are associated to expansion. As a reason, the deviatoric stress (q), the mean effective stress (p'), the volumetric strain (ε_v) and the shear strain (ε_s) are defined as follows:

$$q = \sigma'_a - \sigma'_r \tag{36}$$

$$p' = \frac{(\sigma'_a + 2\sigma'_r)}{3} \tag{37}$$

$$\varepsilon_v = \varepsilon_a + 2\varepsilon_r \tag{38}$$

$$\varepsilon_s = \frac{2(\varepsilon_a - \varepsilon_r)}{3} \tag{39}$$

Where:

σ'_a = effective axial stress

σ'_r = effective radial stress

ε_a = axial strain

ε_r = radial strain

The peak effective strength parameters (i.e. cohesion and friction angle) were obtained by adjusting a straight line to the peak stress points in the s'-t diagram. Thus, s' and t are defined as:

$$s^{\prime} = \frac{(\sigma'_a + \sigma'_r)}{2} \quad (40)$$

$$t = \frac{(\sigma'_a - \sigma'_r)}{2} \quad (41)$$

The secant (E_s) and the tangential stiffness modulus (E_t) were determined as follows:

$$E_s = \frac{q}{\varepsilon_a} \quad (42)$$

$$E_t = \frac{\delta_q}{\delta_{\varepsilon_a}} \quad (43)$$

For conventional triaxial compression tests, the critical state friction angle(ϕ'_{cs}) can be given by:

$$sin\,\phi'_{\mathrm{cs}} = \frac{3M}{(M+6)} \quad (44)$$

Where:
$M = q/p'$ stress ratio at the critical state

5.4.2 Stress-Strain Response for the Botucatu Residual Soil

The triaxial test results of the natural Botucatu residual soil (BRS), molded at three distinct dry densities, are presented in Figure 81, below. An effective confining pressure of 35 kPa was used. A defined peak deviatoric stress was observed only for the densest specimen, followed by a strain softening response after the peak stress was achieved. Afterwards, the stress of all the samples converged to, approximately, the same value. With relation to the volume change behavior, the most porous sample presented a fully contractive response, whereas the other two exhibited an initial contraction followed by dilation. Yet, the rate of volume change observed for the intermediate density was negligible, indicating that, at that particular initial state of stress ($p´= 35$ kPa), the intermediary molding void ratio must lie nearby the critical state line of the soil considering this initial specific volume. This is clearly noticed in the stress-dilatancy response of the BRS plotted in Figure 82, in which the dilatancy rate of this test specimen was irrisory. In brief, those results show a typical behavior of a frictional material in which the degree of interlocking plays a major role regarding the strength of the material. Namely, the strength follows the relationship 4 (item 2.3.7), being the peak deviatoric stress, observed in the densest specimen, a result of the dilation.

Furthermore, the critical stress ratio (M) was found to be around 1.46, corresponding to a critical state friction angle ($\phi_{cs}´$) of 35.95°. Prietto (2004) has found a similar M value for the same soil, equal to 1.50. In this regard, the stress ratio versus axial strain results is plotted in Fig. 83, altogether with the outcomes arising from other researches. It is noticeable that the $q/p´$ directs towards the same range of values (i.e. varying from 1.40 to 1.50).

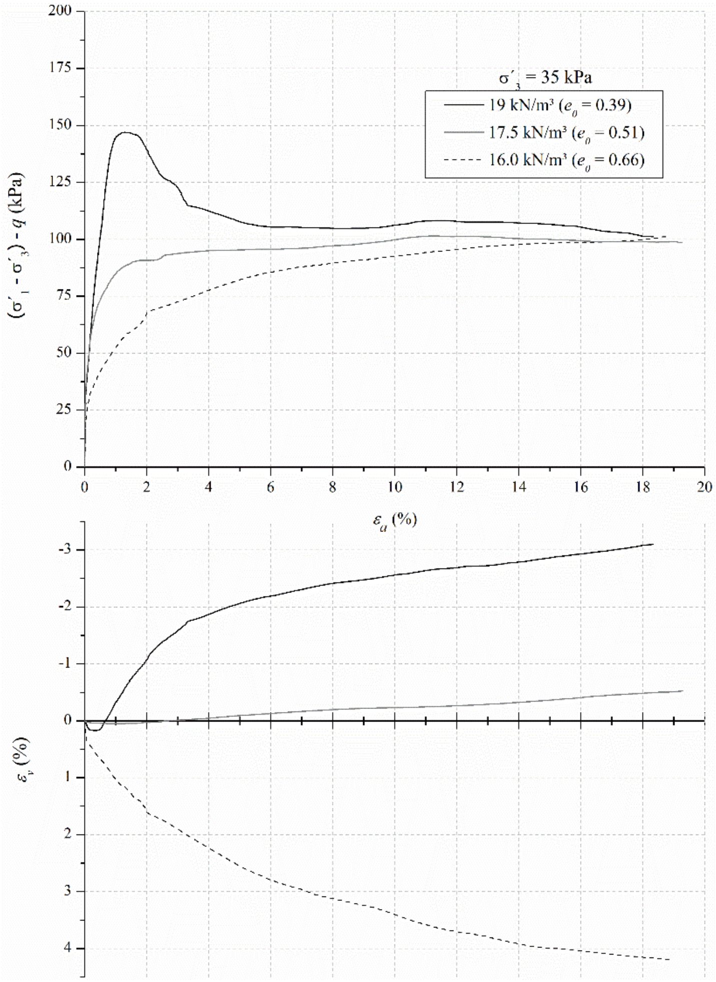

Figure 81 – Stress-strain response and volume change behavior of the BRS

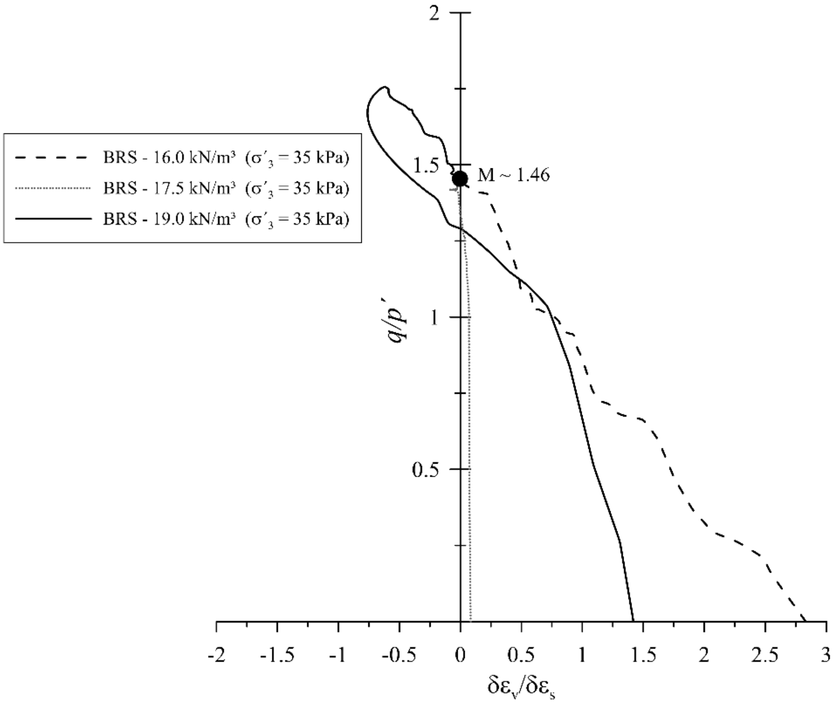

Figure 82 – Stress-dilatancy response of the BRS

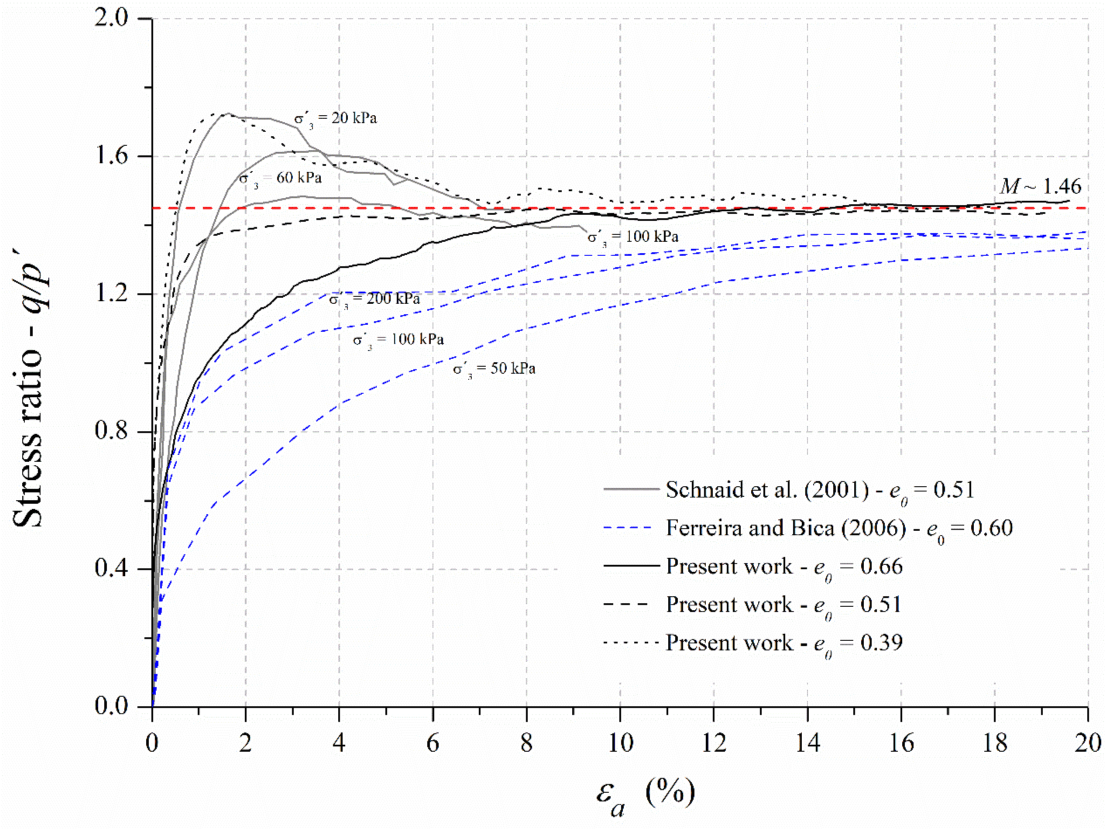

Figure 83 – Stress ratio versus axial strain for BRS

5.4.3 Stress-Strain Response as a Function of the $\eta/(C_{iv})^{0.28}$ Index

The stress-strain (q x ε_a) response and the volume change behavior (ε_v x ε_a) of the triaxial tests conducted on the BRS-cement specimens, under an effective confining pressure of 35 kPa, are presented throughout Figures 84 to 88. Each figure contains the outcomes of the two distinct dosages molded using the same $\eta/(C_{iv})^{0.28}$ index value and, as well, a photo of the BRS-cement specimens taken after the test was accomplished.

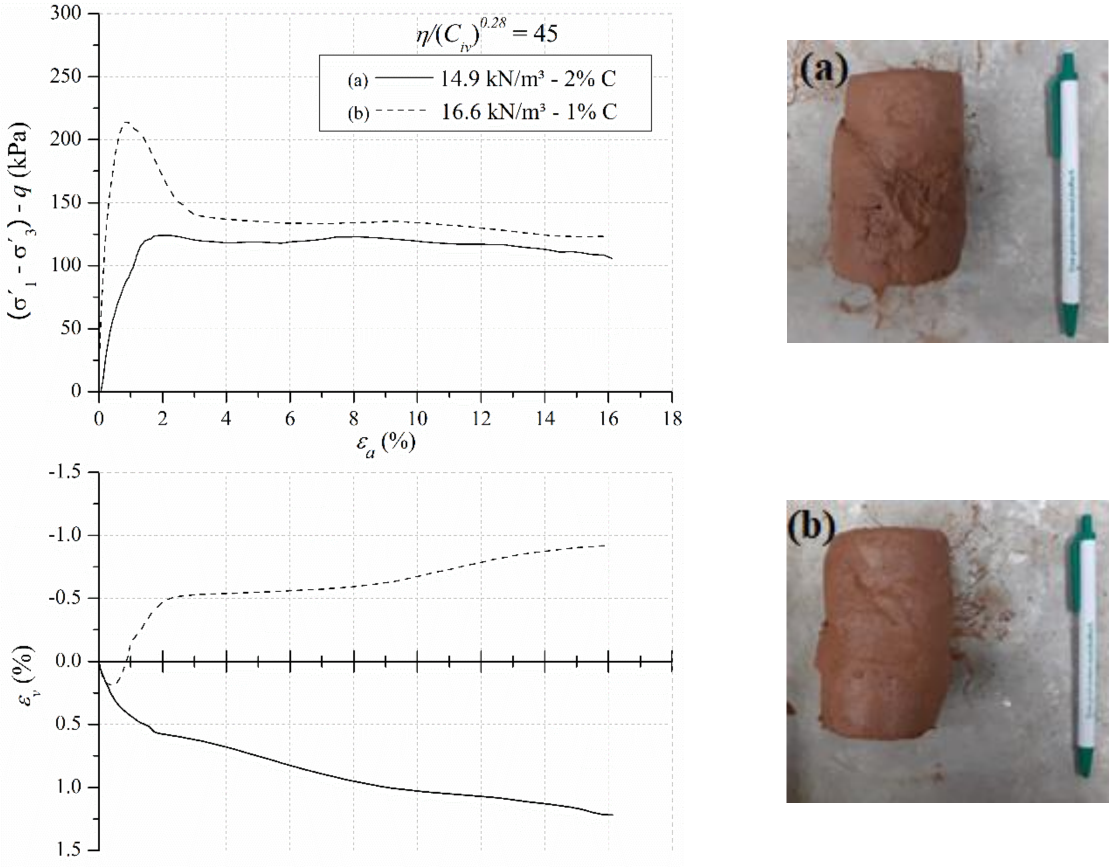

Figure 84 – Stress-strain response and volume change behavior for $\eta/(C_{iv})^{0.28} = 45$

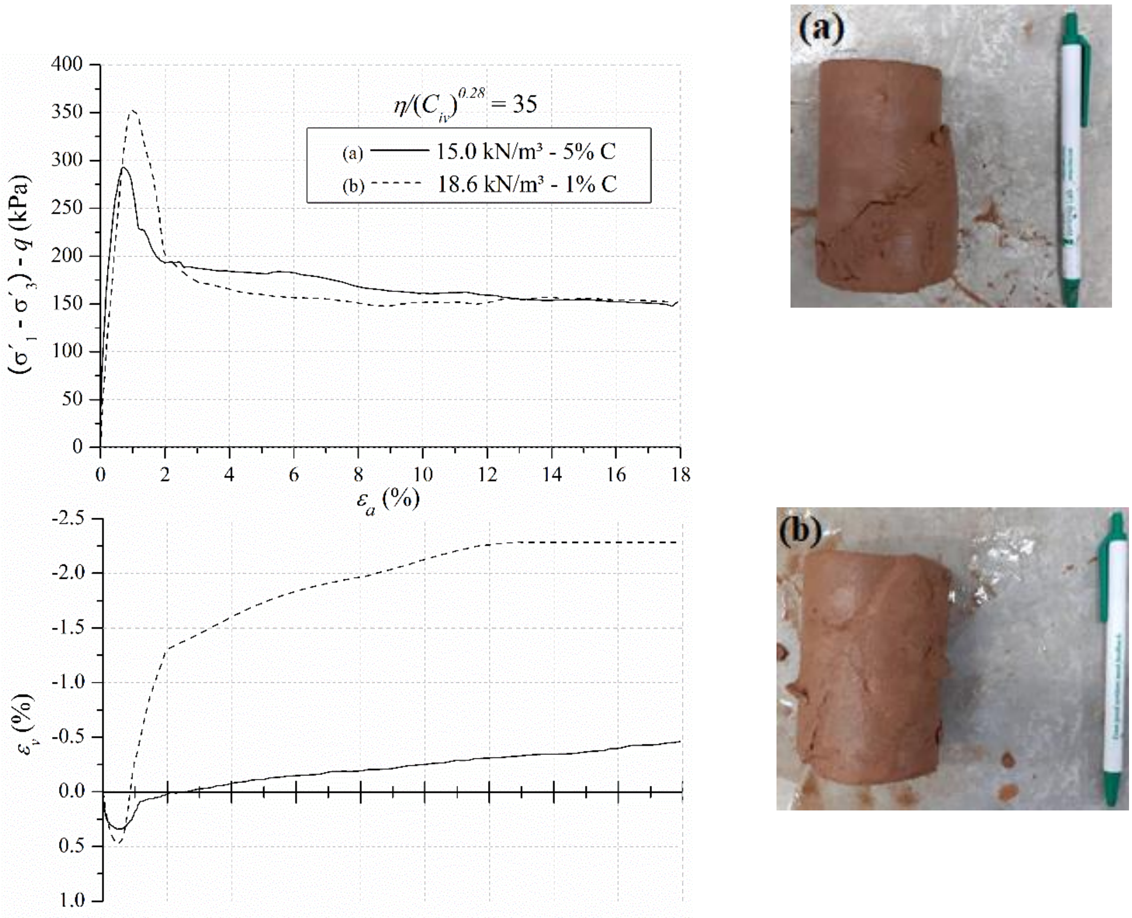

Figure 85 – Stress-strain response and volume change behavior for $\eta/(C_{iv})^{0.28} = 35$

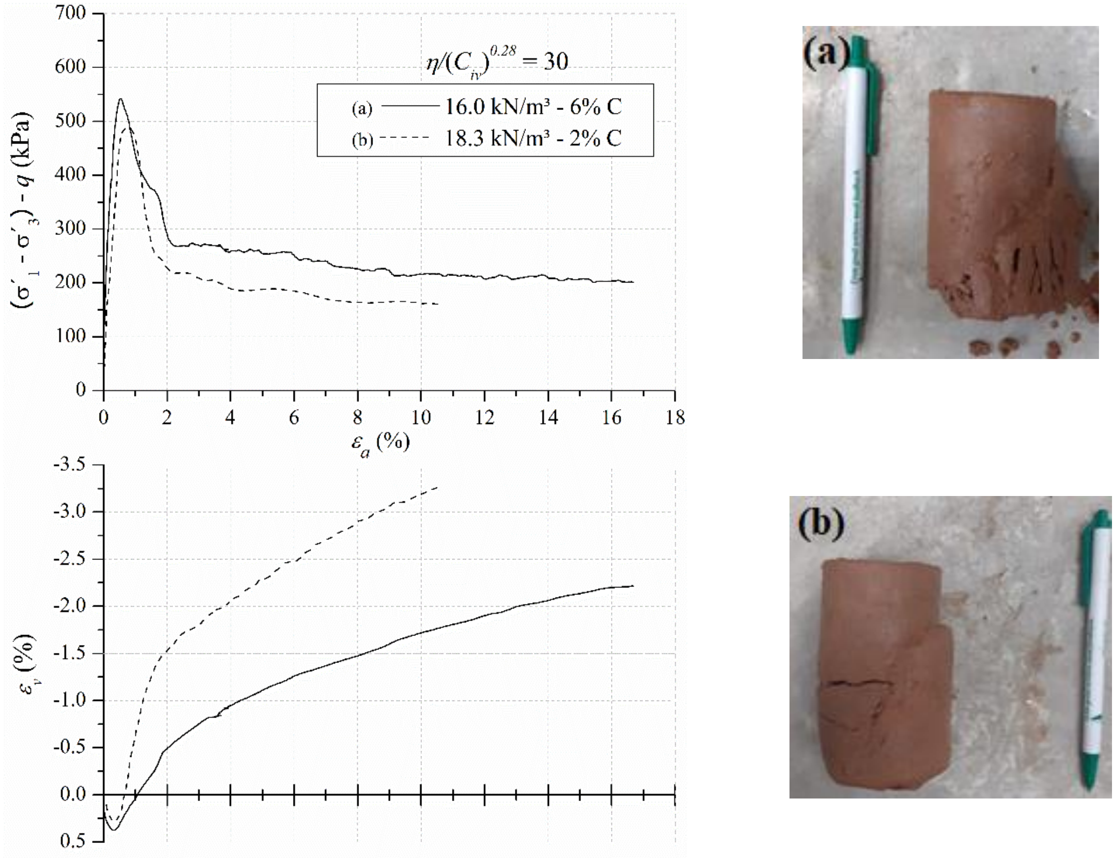

Figure 86 – Stress-strain response and volume change behavior for $\eta/(C_{iv})^{0.28} = 30$

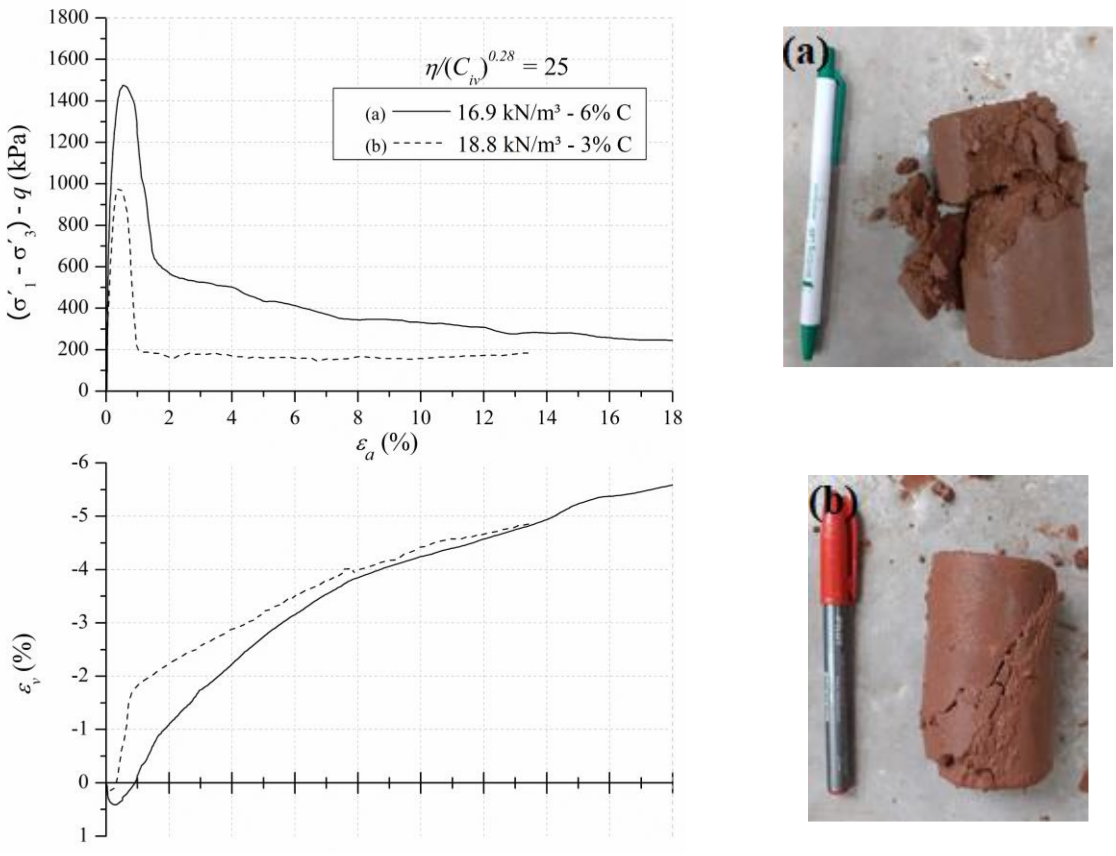

Figure 87 – Stress-strain response and volume change behavior for $\eta/(C_{iv})^{0.28} = 25$

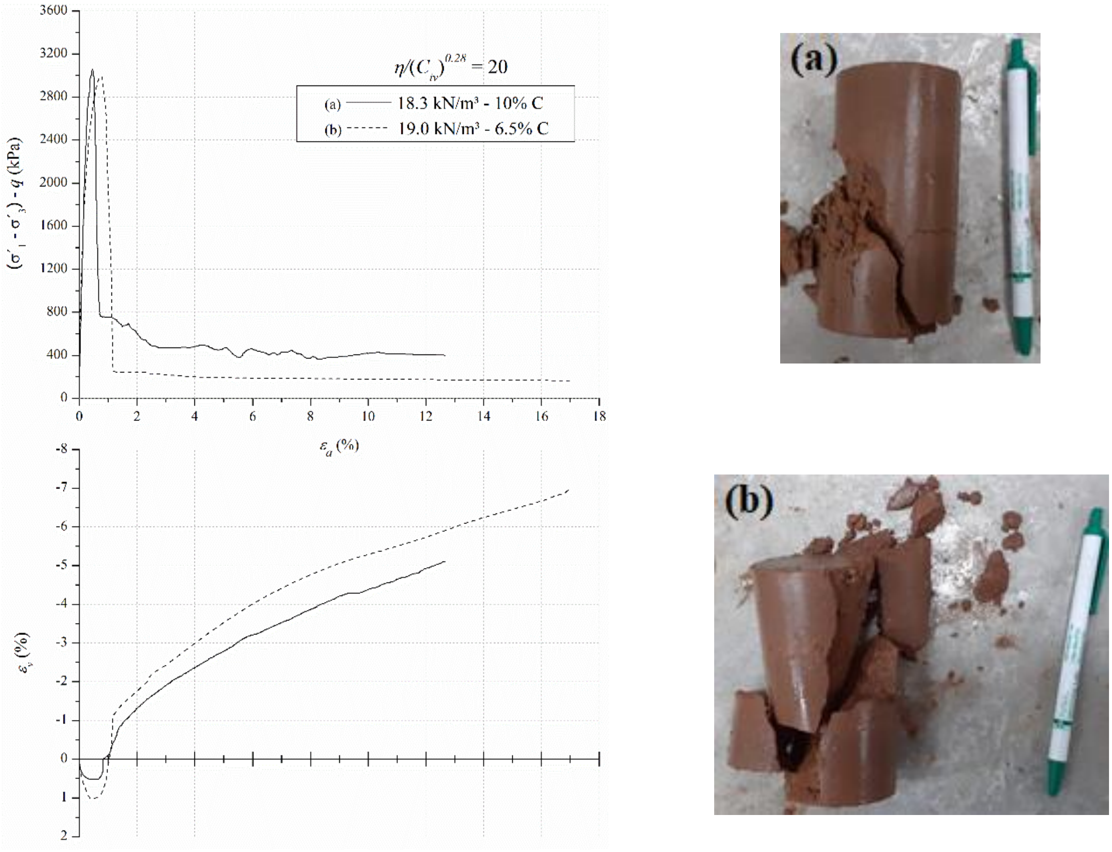

Figure 88 – Stress-strain response and volume change behavior for $\eta/(C_{iv})^{0.28} = 20$

In general, excluding the 14.9 kN/m³ - 2%C dosage, the overall stress-strain behavior of the compacted BRS-cement specimens was typical of a cemented soil. That is, initially stiff and remarkably brittle at failure, presenting a well-defined peak strength (q_{max}). This was accompanied by a preliminary compressive response which turned into a prominent dilatant trend that commenced prior to the peak strength achievement. Naturally, this brittle response was more evidence amongst the densest and most cemented samples (i.e., lower $\eta/(C_{iv})^{0.28}$ values). These contrast with the compressive or slightly dilatative behavior presented by the BRS soil (see Figs. 81 and 82), indicating that even a small amount of cement is sufficient to alter the dynamics of the volume change behavior of compacted soil-cement samples for low confinement levels. Even though the distinct test specimens, molded having the same $\eta/(C_{iv})^{0.28}$, have presented similar strength values, their volume change behavior have quantitatively differed. Generally, the least porous specimen presented a greater rate of volumetric variation when expanding (i.e., higher dilatancy rate). Further aspects regarding this theme are discussed in the next section.

In addition, every test specimen presented a shear band that usually started to become visible after the peak stress was achieved, which typically occur in the shearing of soil-cement specimens (LADE & TRADS, 2014). Hence, the global volumetric variation, measured through the flow of water out/into the specimen, does not necessarily represent the local volumetric variation due to strain localization within the shear band that modifies the drainage condition of the sample (MOONEY & VIGGIANI, 1998; SALVATORE *et al.*, 2017; IMSEEH *el al.* 2020).

As previously observed for the unconfined compression test results, within the same adjusted porosity/cement index values, the maximum deviatoric stress (q_{max}) of the specimens having distinct dosages is similar. When $\eta/(C_{iv})^{0.28}$ = 45, the q_{max} was around 212 kPa for the least cemented specimen (16.6 kN/m³ - 1% C) and reached approximately 125 kPa for the most cemented sample (14.9 kN/m³ - 2% C). For $\eta/(C_{iv})^{0.28}$ = 35, the most compacted mixture (18.6 kN/m³ - 1%C) presented a top strength of about 350 kPa, whereas the least compacted (15.0 kN/m³ - 5%C) exhibited a maximum deviatoric stress close to 300 kPa. For $\eta/(C_{iv})^{0.28}$ = 30, the least porous test specimen (18.3 kN/m³ - 2%C) achieved a top strength of 492 kPa, while the least porous attained nearly 550 kPa. For $\eta/(C_{iv})^{0.28}$ = 25, the maximum strength was observed amongst the most cemented material (16.9 kN/m³ - 6%C), being around 1455 kPa, whereas the least cemented (18.8 kN/m³ - 3%C) achieved a q_{max} of approximately 1000 kPa. For the lowest value of the $\eta/(C_{iv})^{0.28}$ index, the top deviatoric stress was around 3050 kPa for the most cemented sample (18.3 kN/m³ - 10%C) and close to 3005 kPa for the least cemented one (19.0 kN/m³ - 6.5%C).

The maximum deviatoric stress of each tested specimen is plotted as a function of the $\eta/(C_{iv})^{0.28}$ index in Figure 89, below. In addition, the average unconfined compressive strength results, for these respective mix designs, are also plotted on the same graph. For the four highest adjusted porosity/cement ratio values (45, 35, 30 and 25) a fair agreement between the unconfined compression strength and the top deviatoric stress is observed. That is, within each dosage, q_u and q_{max} are really close and the triaxial test conditions (full saturation, low confinement pressure and slower loading rate) seem to have had small effects on the top strength. The same has been attested by Schnaid *et al.* (2001) for the same material (BRS-cement) in specimens presenting an unconfined compressive strength up to 1200 kPa. On the contrary, for the highest $\eta/(C_{iv})^{0.28}$ index value, the differences between the strengths attained in the triaxial tests were, at least, 19% higher when compared to the average unconfined compression test results. Apart from regular experimental scatter, this may have occurred owing to the more pronounced loading rate effect on more compacted and cemented samples.

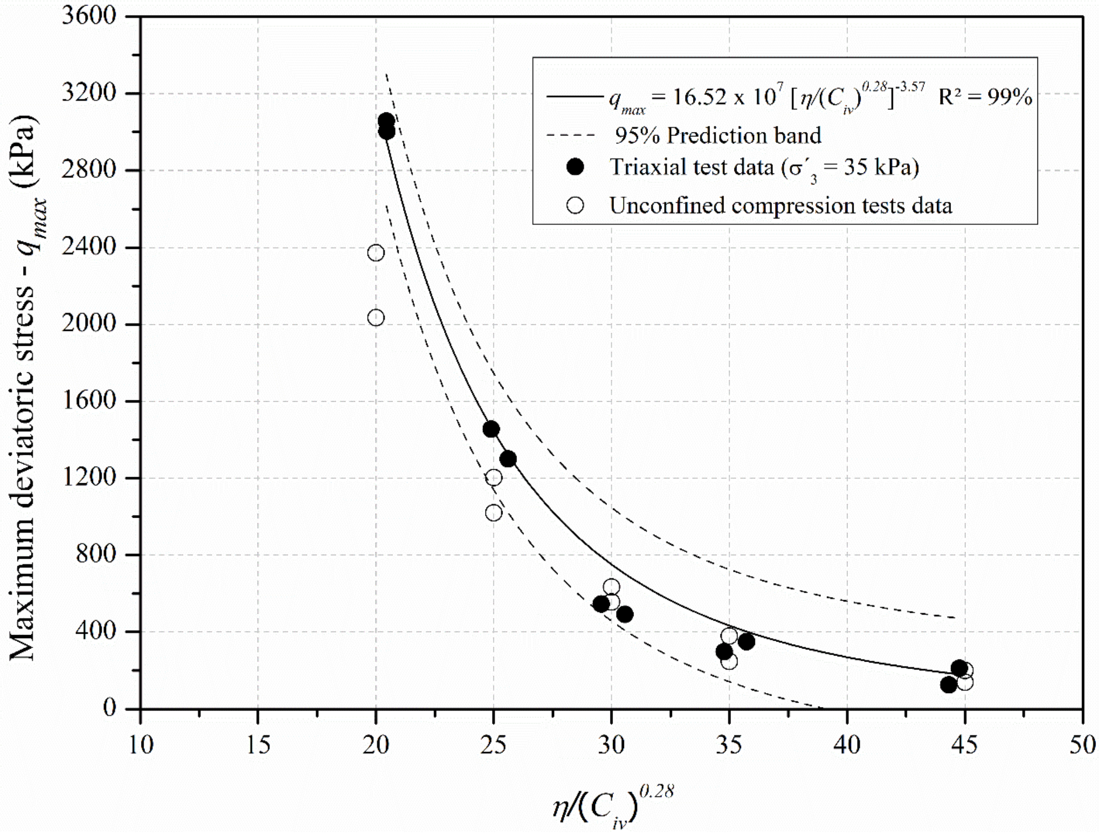

Figure 89 – Maximum deviatoric stress as a function of the $\eta/(C_{iv})^{0.28}$ index

The correlation between the top deviatoric stress (q_{max}) and the adjusted porosity/cement index resulted in an equation of the form of relationship 6, with a *B* value equal to 14.52 x 10^7. It is slightly higher than the one obtained for the unconfined compressive strength results (equation 31) owing to the greater order of magnitude of the strength obtained for the smaller values of the $\eta/(C_{iv})^{0.28}$ parameter. Nonetheless, a great coefficient of determination (R² = 98%) was obtained.

The stiffness degradation throughout the triaxial tests is represented by the secant modulus (E_{sec}) of each tested specimen plotted as a function of the vertical displacement (ε_a) along Figures 90 to 94. Each graph contains the results relative to the same adjusted porosity/cement index value. Within each chart, the position of the peak deviatoric stress, when occurred, is indicated by a lined arrow for the least cemented specimen and by a dashed arrow for the most cemented one. Considering all the test results, up to the peak stress, E_{sec} was generally higher for lower $\eta/(C_{iv})^{0.28}$ values, as occurred for the strength values. Yet, a definite pattern has not occurred within each adjusted porosity/cement index value. Namely, for $\eta/(C_{iv})^{0.28} = 45$, the most compacted specimen presented initially higher stiffness values, whereas for $\eta/(C_{iv})^{0.28}$ values equal to 35 and 30, the most cemented samples were initially stiffer. When considering the two lowest adopted $\eta/(C_{iv})^{0.28}$, the stiffness values up to the peak strength were quite similar. More details regarding the stiffness data can be found on Appendix B.

A full parallelism between these stiffness results and the initial shear modulus presented on section 5.2.1 cannot be fully drawn. The latter is linked to strains at a smaller level ($\varepsilon_s < 0.001\%$), which could not be properly addressed in the present research (ATKINSON, 2000; CLAYTON, 2011). Besides, the test conditions were not the same since the initial shear modulus was measured using an ultrasonic pulse velocity device at unconfined conditions.

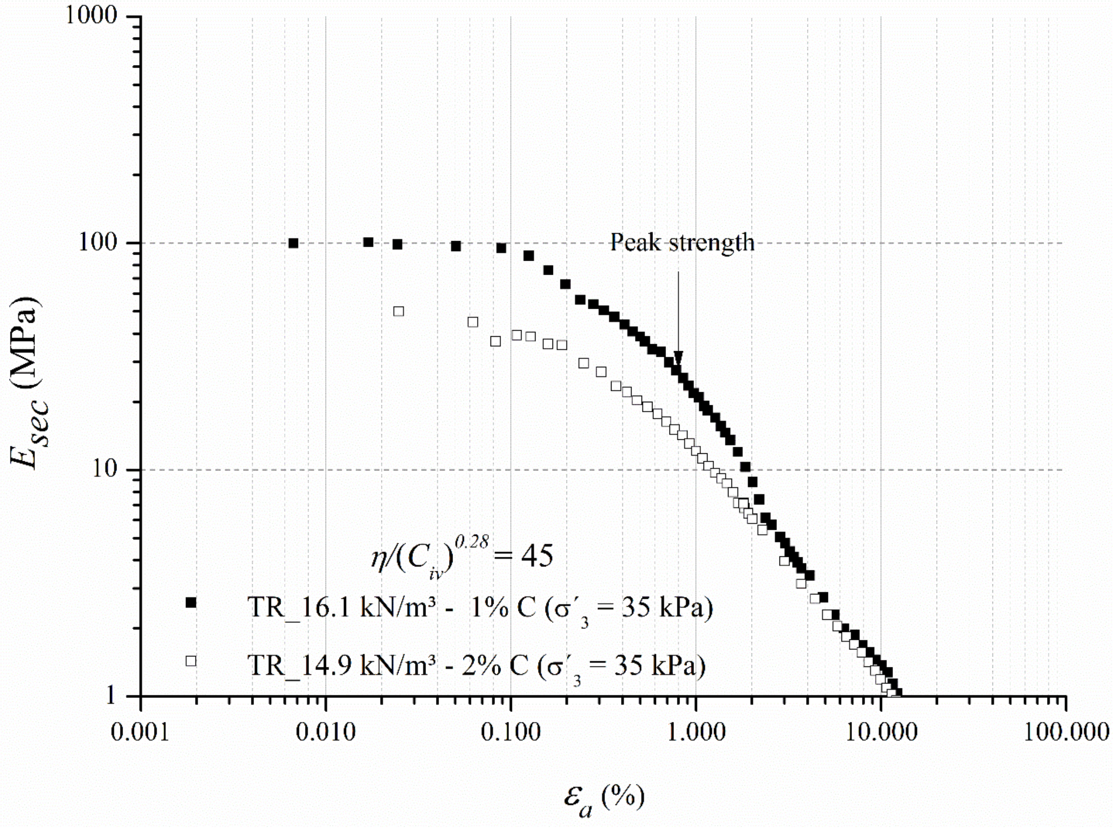

Figure 90 – Stiffness degradation for $\eta/(C_{iv})^{0.28} = 45$

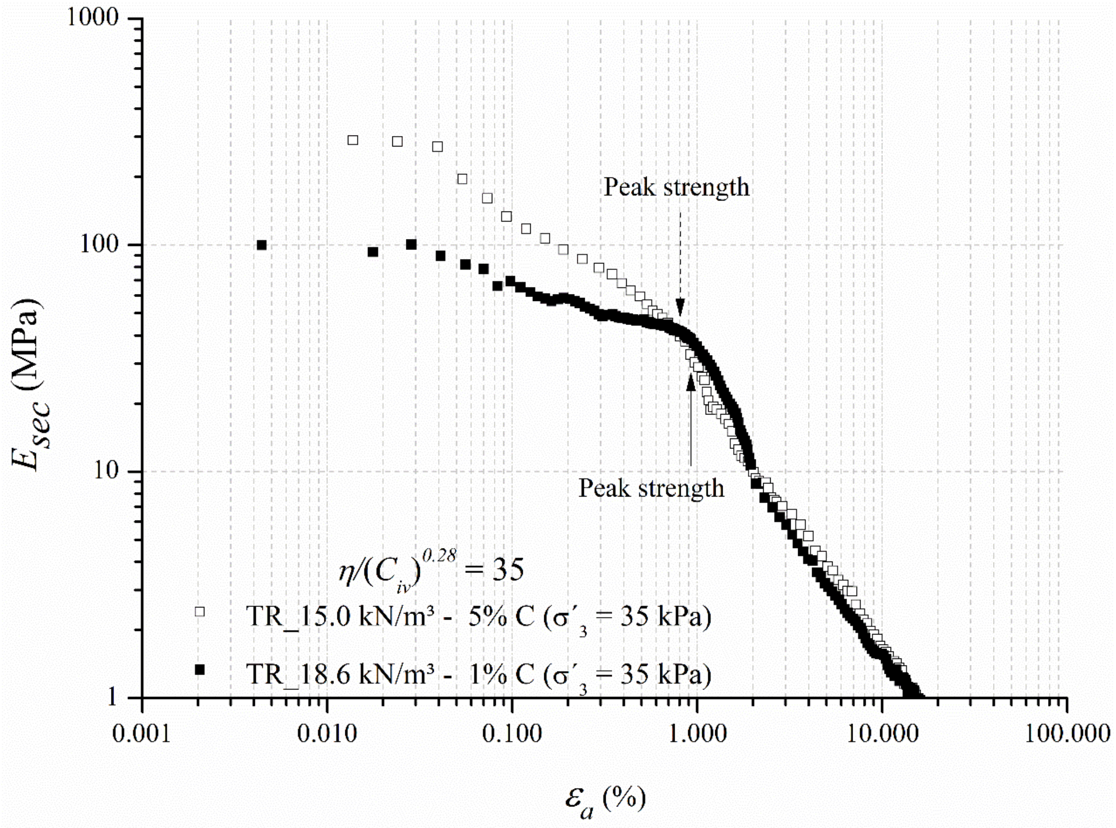

Figure 91 – Stiffness degradation for $\eta/(C_{iv})^{0.28} = 35$

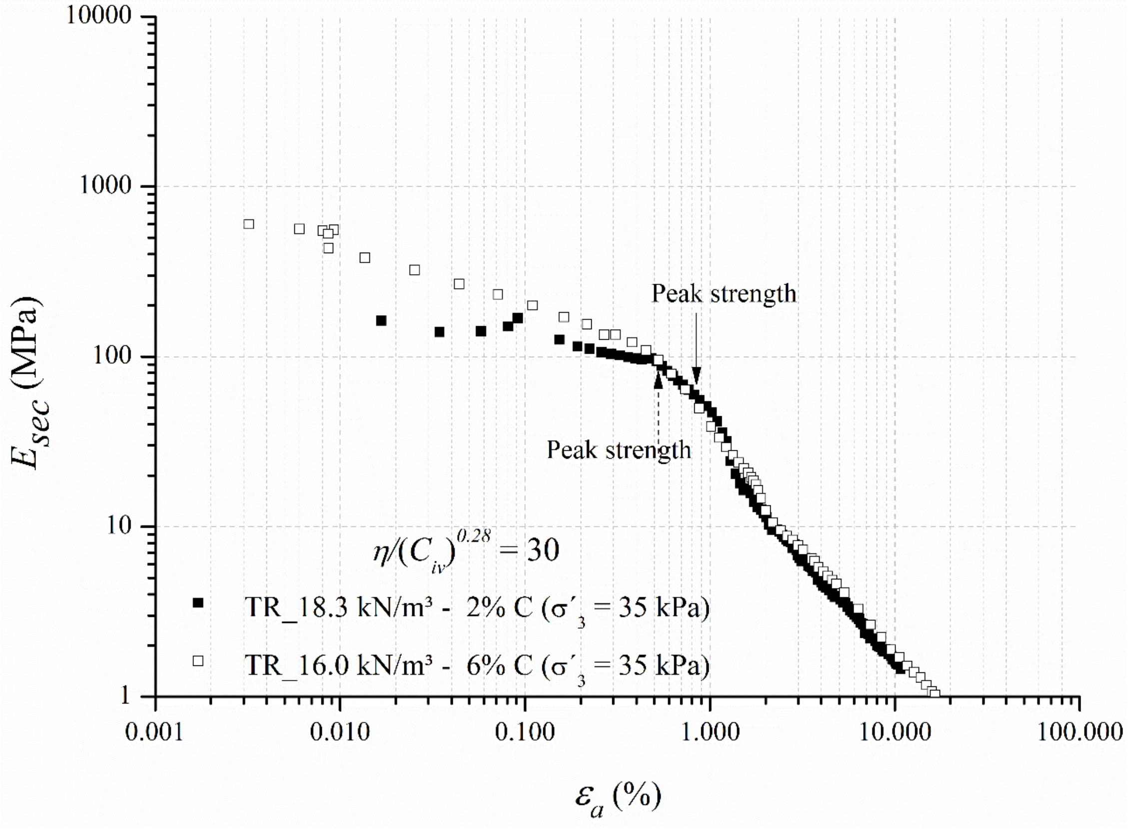

Figure 92 – Stiffness degradation for $\eta/(C_{iv})^{0.28} = 30$

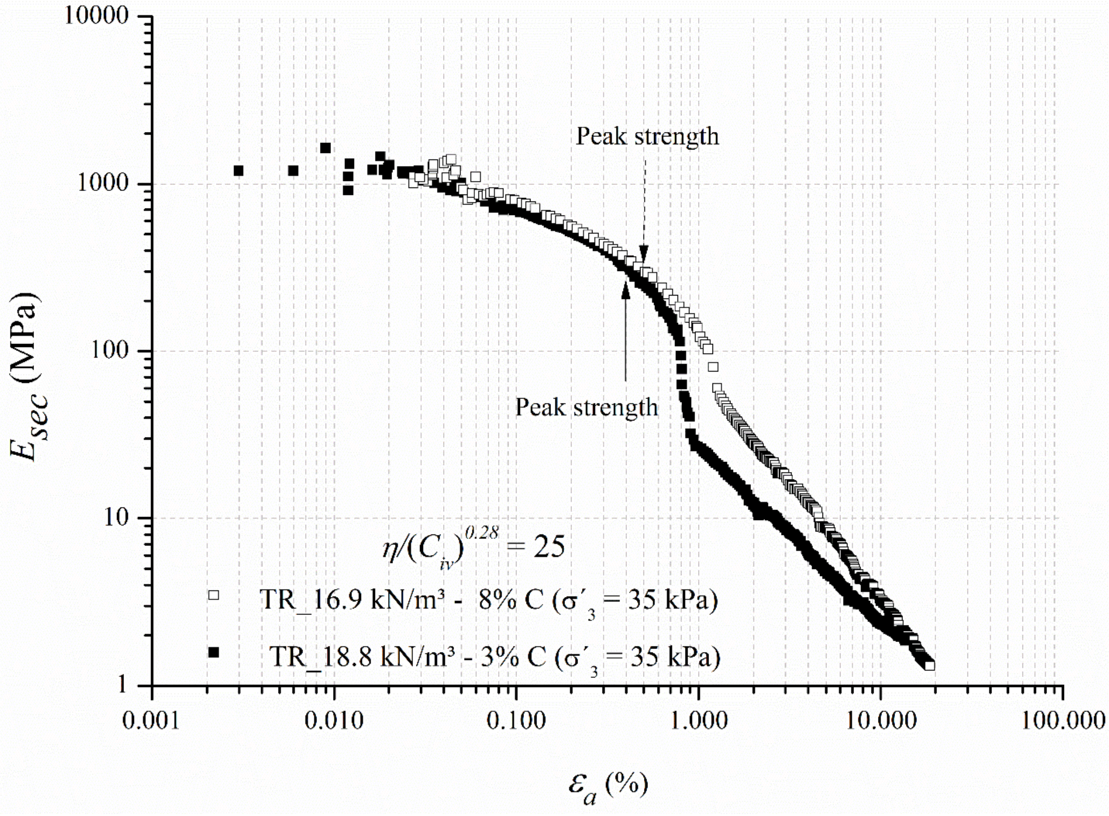

Figure 93 – Stiffness degradation for $\eta/(C_{iv})^{0.28} = 25$

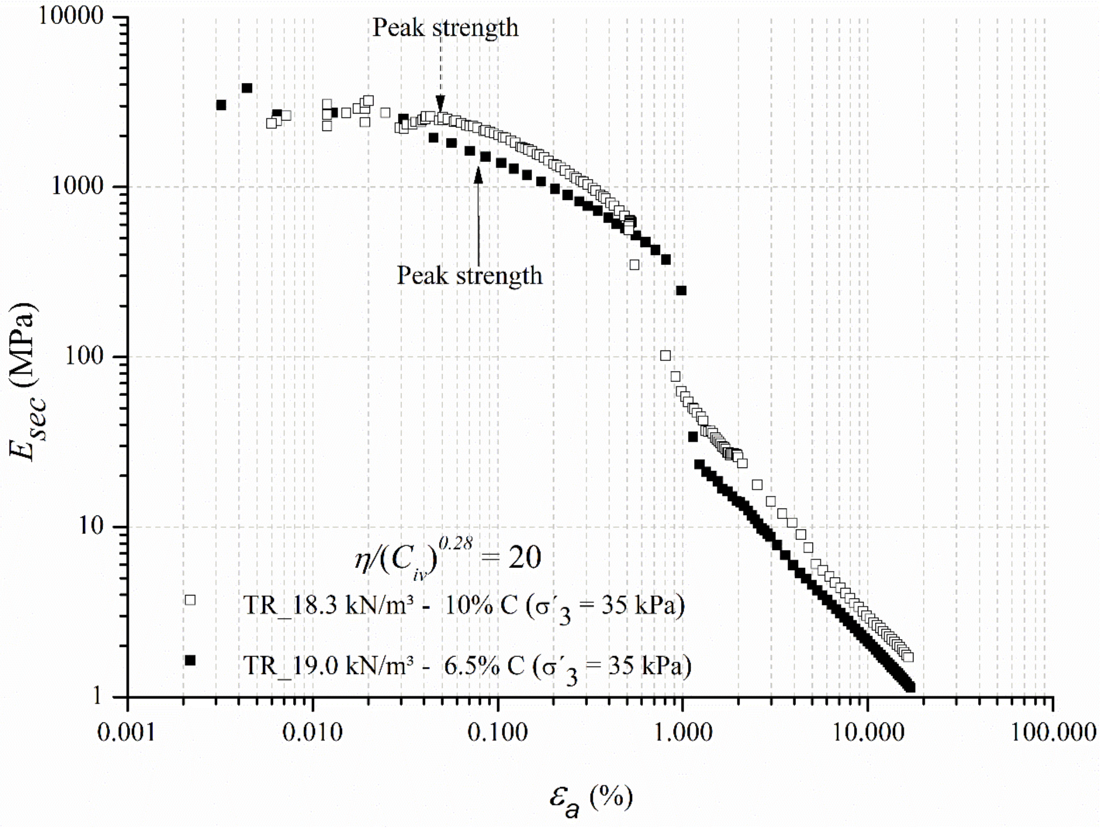

Figure 94 – Stiffness degradation for $\eta/(C_{iv})^{0.28} = 20$

5.4.4 Effective Stress Parameters as a function of the $\eta/(C_{iv})^{0.28}$ Index

As formerly done in the previous section, figures 95, 97 and 99 present the triaxial tests outcomes for the BRS-cement specimens molded using $\eta/(C_{iv})^{0.28}$ values of 35, 30, and 25, whereas figures 96, 98 and 100 depict the cemented BRS specimens after the triaxial tests. Effective confining pressures of 35, 70 and 140 kPa were used considering all the data presented in this section. Moreover, additional tests were carried out at using confinements of 95 kPa and 300 kPa for some specimens. The first was used for the densest specimens having a $\eta/(C_{iv})^{0.28}$ of 35 and 30, whereas the latter (i.e. 300 kPa) was employed for the 16.9 kN/m³ - 8%C sample ($\eta/(C_{iv})^{0.28}$ = 25).

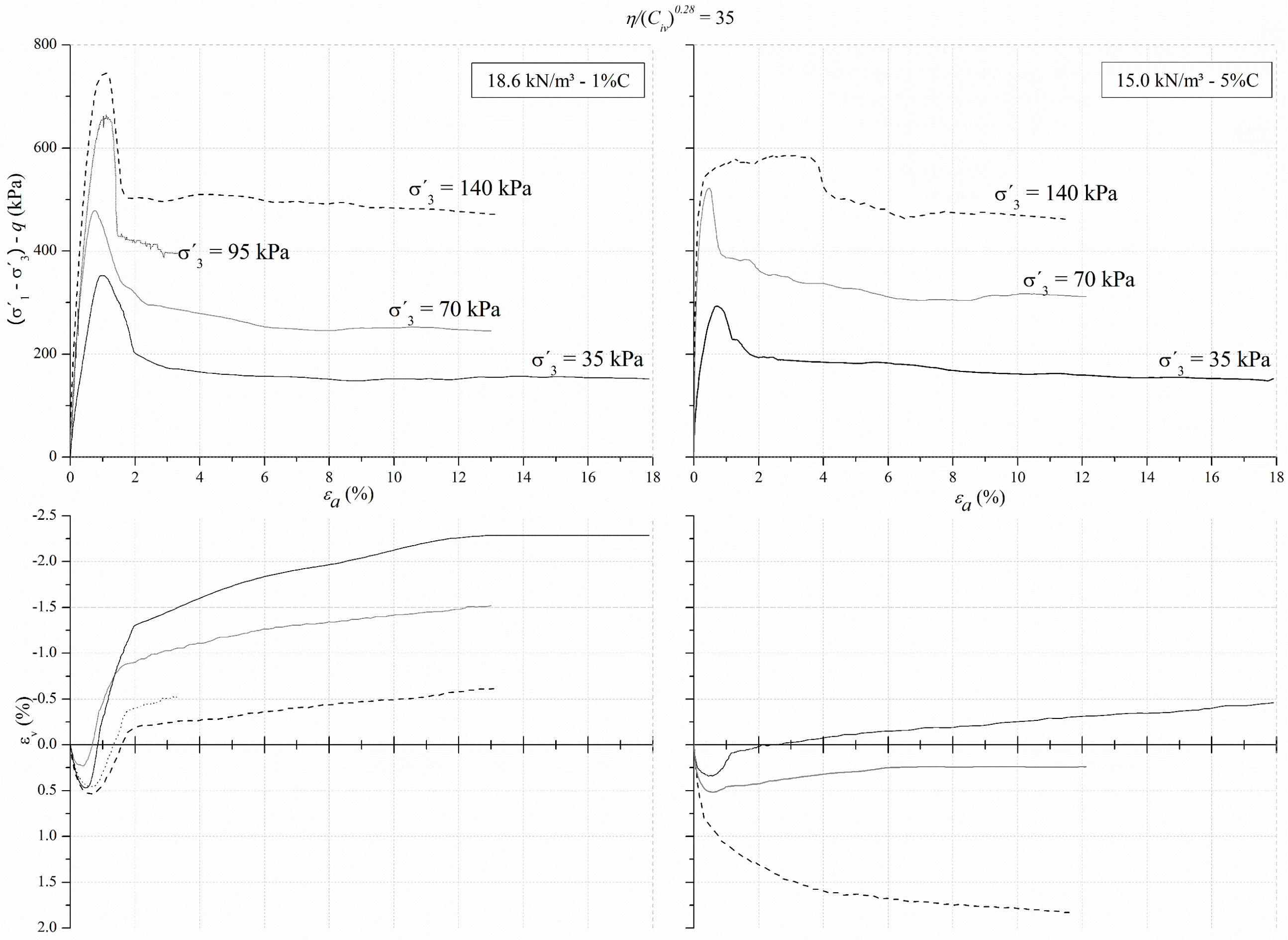

Figure 95 – Stress-strain response and volume change behavior for $\eta/(C_{iv})^{0.28}$ = 35

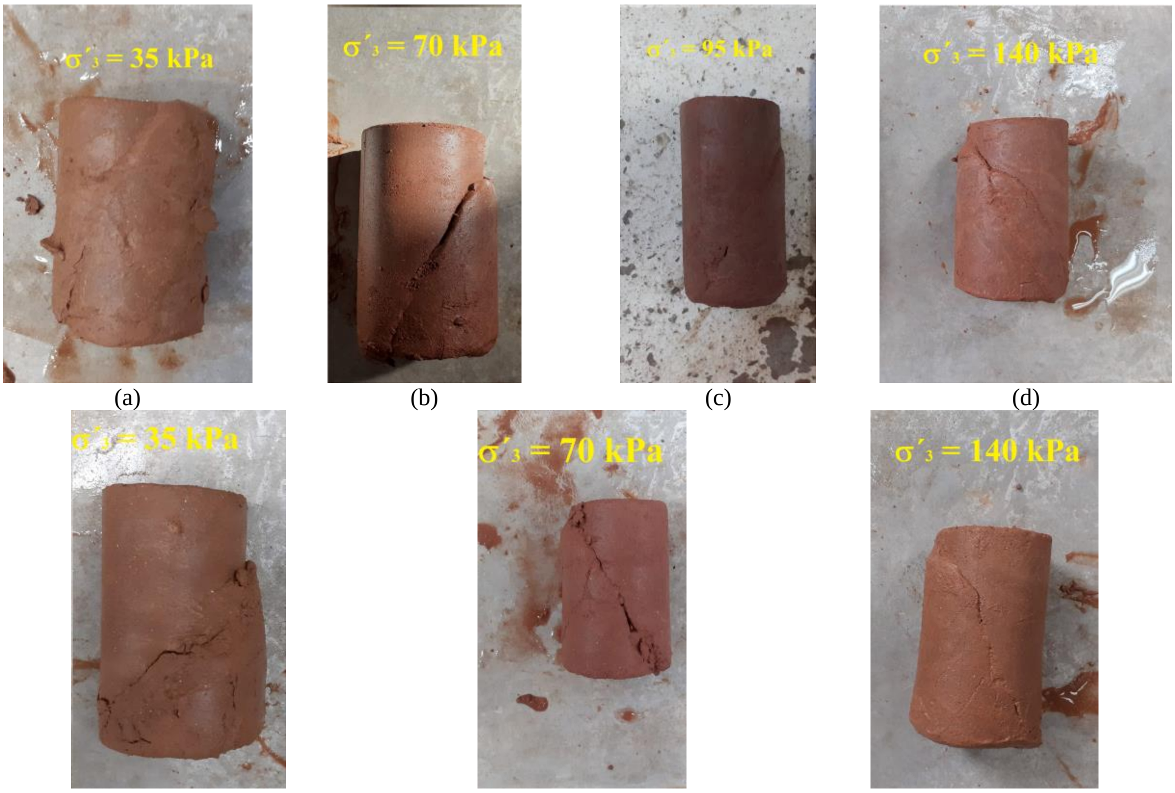

(a) (b) (c) (d)

(e) (f) (g)

Figure 96 - BRS-cement specimens after the triaxial tests for $\eta/(C_{iv})^{0.28}$ = 35 (a) to (d) 18.8 kN/m³ - 1% C (e) to (g) 15.0 kN/m³ - 5% C

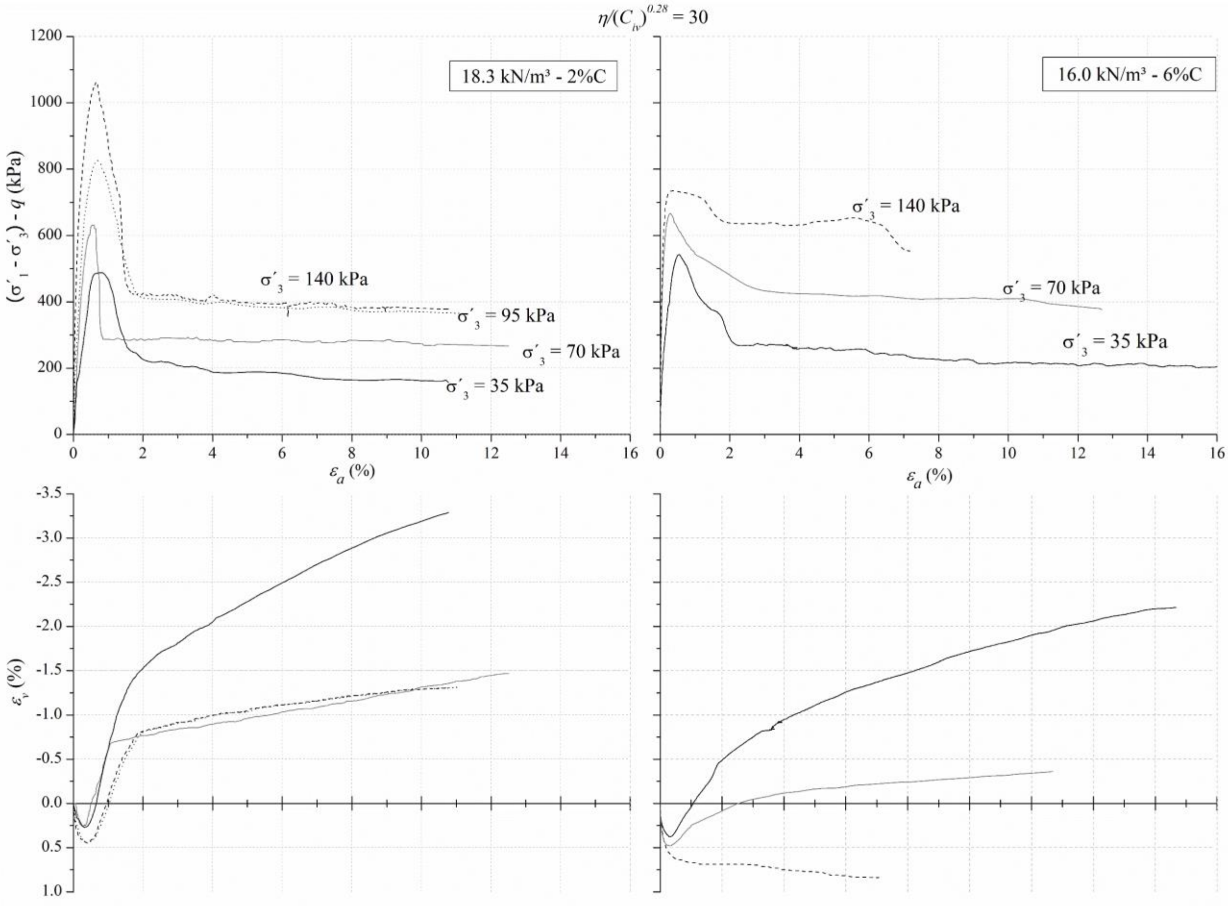

Figure 97 – Stress-strain response and volume change behavior for $\eta/(C_{iv})^{0.28}$ = 30

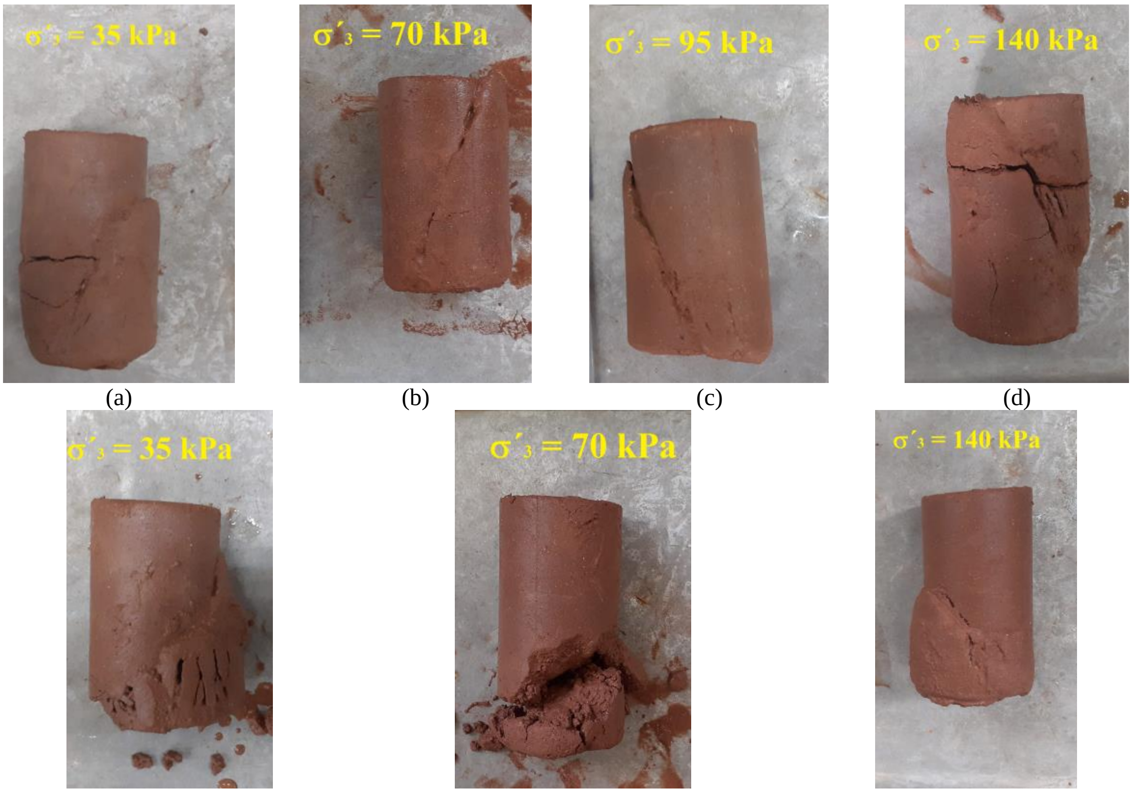

(a) (b) (c) (d)

(e) (f) (g)

Figure 98 - BRS-cement specimens after the triaxial tests for $\eta/(C_{iv})^{0.28} = 30$ (a) to (d) 18.3 kN/m^3 - 2% C (e) to (g) 16.0 kN/m^3 - 6% C

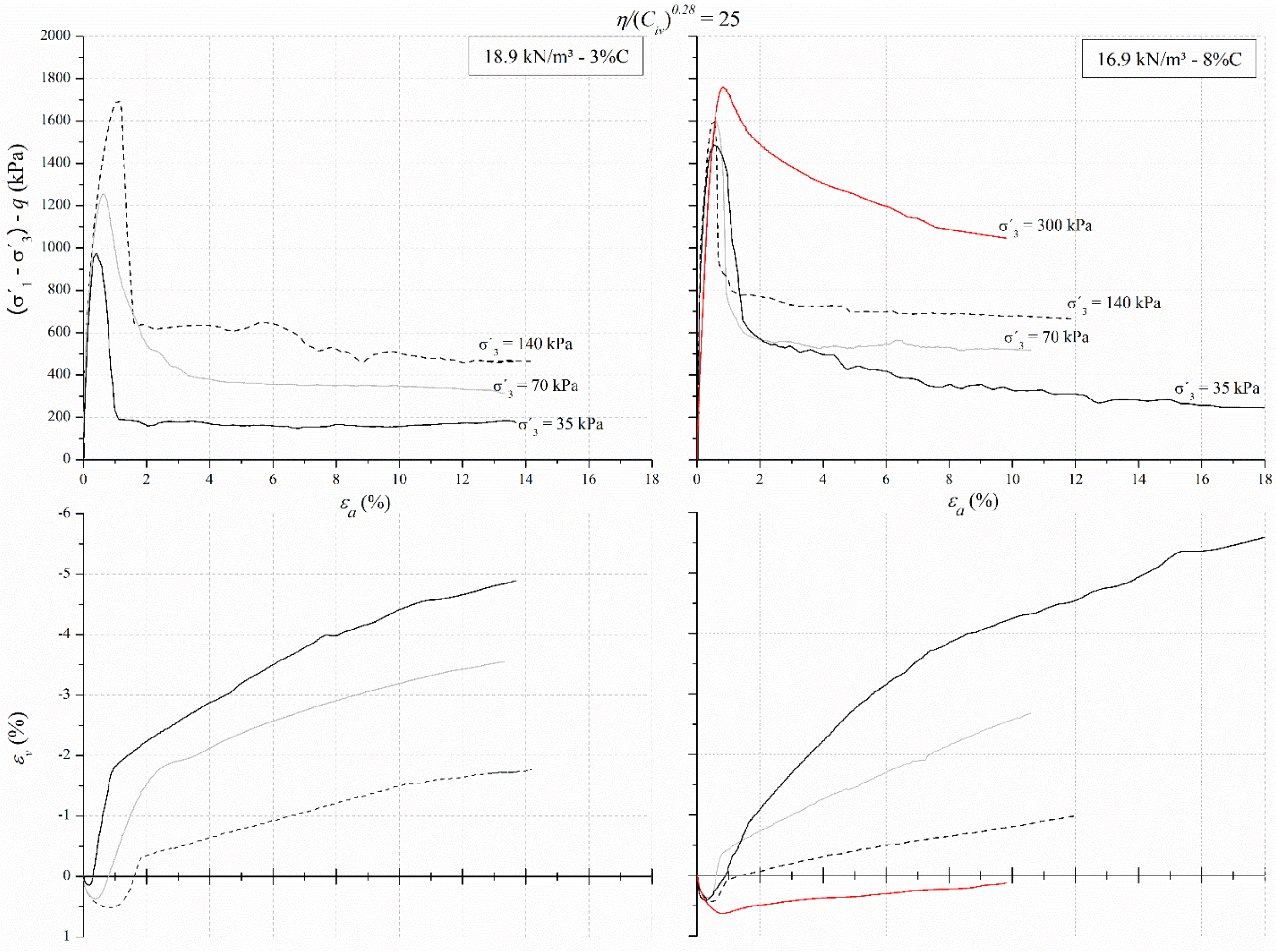

Figure 99 – Stress-strain response and volume change behavior for $\eta/(C_{iv})^{0.28} = 25$

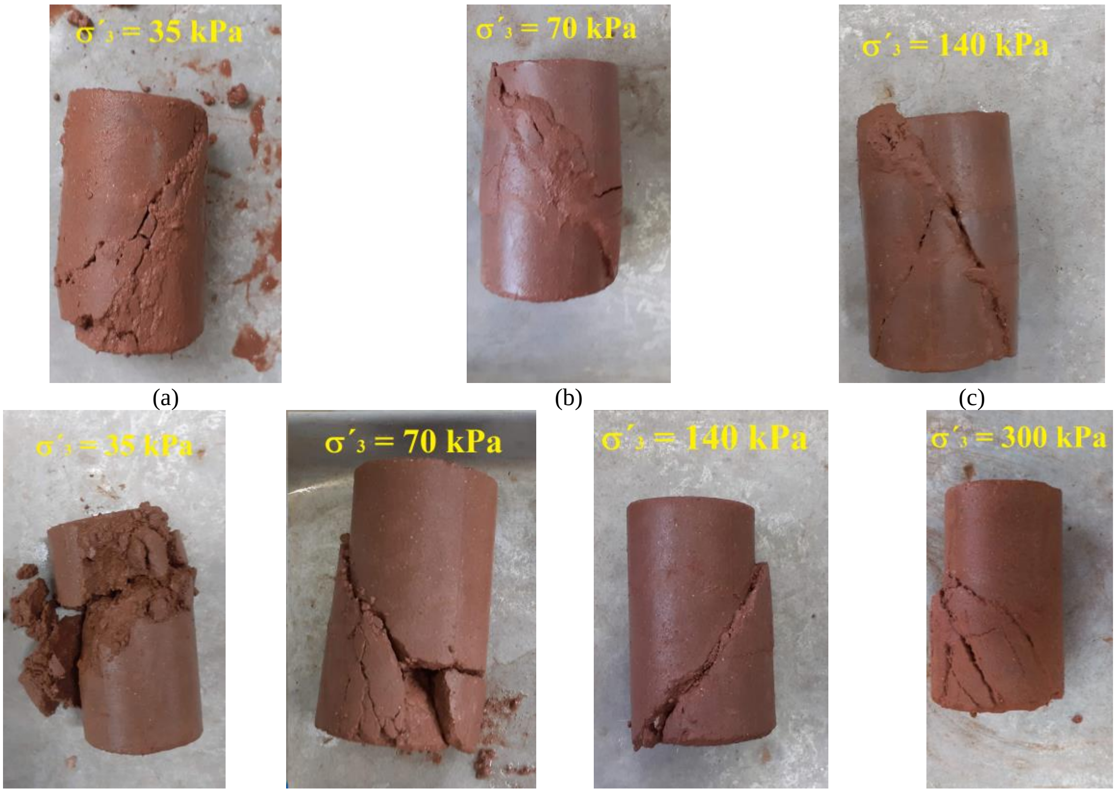

(a) (b) (c)

(d) (e) (f) (g)

Figure 100 - BRS-cement specimens after the triaxial tests for $\eta/(C_{iv})^{0.28}$ = 25 (a) to (c) 18.9 kN/m³ - 3% C (d) to (g) 16.9 kN/m³ - 8% C

Considering the two highest $\eta/(C_{iv})^{0.28}$ (i.e. 35 and 30), the top strength values of the specimens molded with distinct dosages were similar for the two lowest confining pressures (35 kPa and 70 kPa). For the higher confinement value (σ'_3 = 140 kPa), the denser specimen presented a substantially higher strength, and a well-defined peak, when the two adjusted porosity/cement index values are considered. For $\eta/(C_{iv})^{0.28}$ = 35 and σ'_3 = 140 kPa, the densest specimen (18.6 kN/m³ - 1%C) has exhibited a q_{max} of around 820 kPa, while the loosest sample (15.0 kN/m³ - 5%C) has achieved a top deviatoric stress of nearly 590 kPa, without a definite peak strength. The same trend has occurred for the tests conducted at σ'_3 = 140 kPa for the $\eta/(C_{iv})^{0.28}$ index value equal to 30, in which the top strength of the least cemented sample (18.3 kN/m³ - 2%C) was around 1000 kPa, whereas it was close to 710 kPa for the most cemented one (16.0 kN/m³ - 6%C).

With respect to the $\eta/(C_{iv})^{0.28}$ = 25 specimens, the top strength was proportional to the confinement level for the least cemented samples (18.9 kN/m³ - 3%C) as previously observed for the densest samples at the two other adjusted porosity/cement index values. In contrast, the confining pressure seems to have had negligible effect on the strength of the most cemented specimens (16.9 kN/m³ - 8%C). This indicates that the elevated amount of cement has contributed to the creation of a cement phase which was marginally sensible to the confinements varying from 35 kPa to 140 kPa, even though substantial dilation has taken place on these samples. Such trend is evidenced by the effective stress parameters summarized in Table 18. Nonetheless, the test carried out under a σ'_3 = 300 kPa presented a slightly higher peak-strength, accompanied by a somewhat dilatant trend. When comparing the top strength of the 18.9 kN/m³ - 3%C and 16.9 kN/m³ - 8%C specimens, it is clear that higher strengths were obtained for the most cemented samples which were practically insensitive to the confinement.

In general, once the bonds were broken, the highest effective confinement level has diminished and/or inhibited the dilation of the three most porous samples to occur. This was remarkably noticeable amongst the 16.0 kN/m³ - 6%C ($\eta/(C_{iv})^{0.28}$ = 30) and 15.0 kN/m³ - 5%C ($\eta/(C_{iv})^{0.28}$ = 35) samples which volume change responses were substantially altered by the augment in the confinement level. For the 16.9 kN/m³ - 8%C sample ($\eta/(C_{iv})^{0.28}$ = 25) this has taken place at a higher level of confinement (σ'_3 = 300 kPa) due to the greater quantity of cement combined with a denser medium. This probably explains the differences observed in the stress-strain response when compared to least porous samples molded at the same adjusted porosity/cement index.

In contrast, the greater degree of interlocking presented by the three densest samples induced the expansion after the breakage of the bonds. Thus, the dilation parcel must have contributed to the greater differences observed in the top strengths of the pairs within the same $\eta/(C_{iv})^{0.28}$ value. In a certain manner, Figure 101 summarizes these tendencies in the s'- t diagram thorough the adjustment of straight lines as failure envelopes. The highly cohesive character of the 16.9 kN/m³ - 8%C specimens is corroborated by a diminutive friction angle and an elevated cohesive intercept. The resultant peak effective friction angle (ϕ'_{peak}) and effective cohesive intercept (c') are summarized in Table 18, below. Clearly, within each of these three $\eta/(C_{iv})^{0.28}$ values, the strength of the least cemented specimen is dominated by friction, whereas in the most cemented one it is controlled by bonds. The tests conducted at a $\sigma'3$ = 95 kPa corroborate this frictional trend amongst the densest specimens molded at $\eta/(C_{iv})^{0.28}$ of 35 and 30.

Table 18 – Effective stress parameters

$\eta/(C_{iv})^{0.28}$	Mix design	ϕ_{peak}'(°)	c'(kPa)
35	18.6 kN/m³ - 1%C	41.0	48
35	15.0 kN/m³ - 5%C	36.5	58
30	18.3 kN/m³ - 2%C	45.7	62
30	16.0 kN/m³ - 6%C	30.1	139
25	18.9 kN/m³ - 3%C	51.0	129
25	16.9 kN/m³ - 8%C	12.9	542

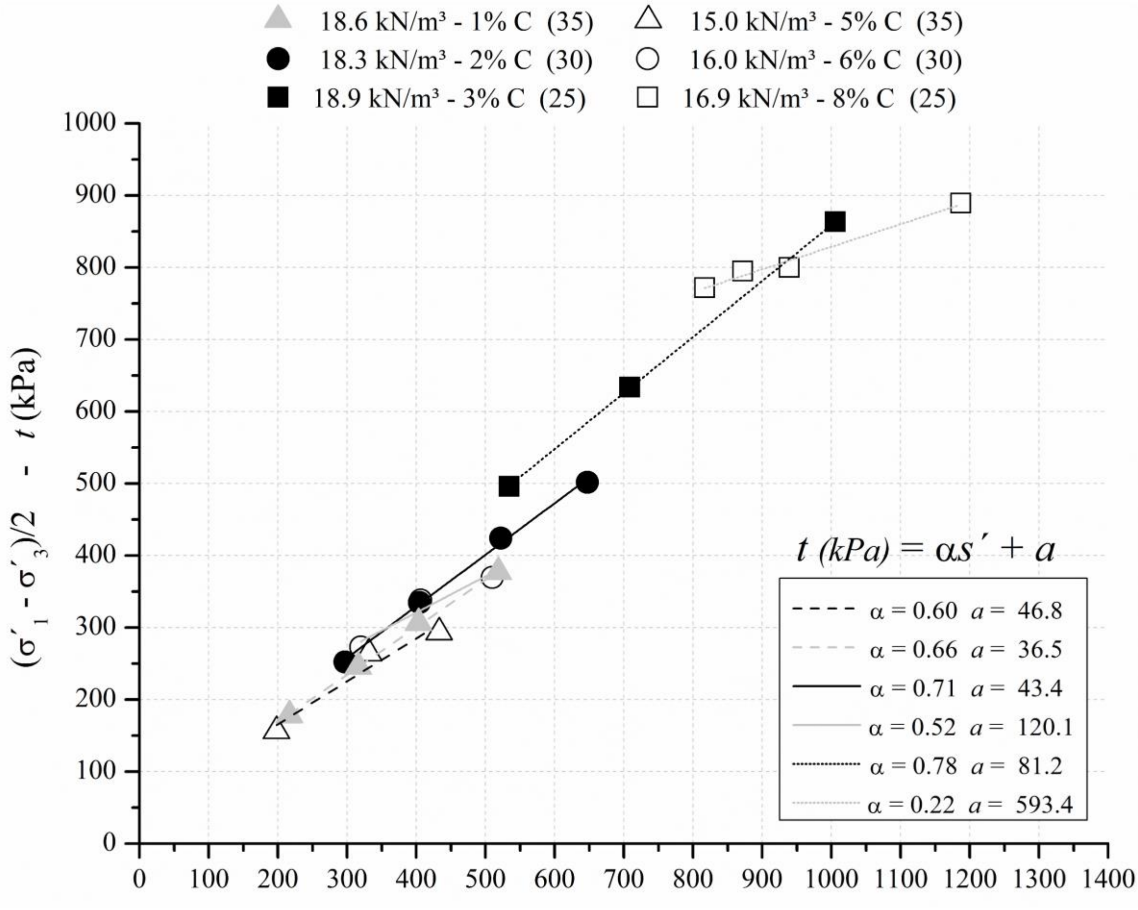

Figure 101 – Failure envelopes in the s' versus t plane for $\eta/(C_{iv})^{0.28}$ values of 25, 30, and 35

5.4.5 Parallel with Unconfined Compressive Strength Data

An attempt was made intending to correlate the unconfined compression data, presented in item 5.2.1, to the top deviatoric stress (q_{max}) obtained in the triaxial tests. As a reason, following Schnaid *et al*. (2001), a general expression relating q_{max} either to the effective confining pressure (or mean effective stress at the beginning of the shearing – p'_i) and to the unconfined compression (q_u) was proposed as follows:

$$q_{max} = k_1 p'_i + k_2 C \tag{45}$$

The first term refers to the purely frictional strength contribution, whereas the latter corresponds to the cohesive parcel in which k_2 indicates the rate of alteration in q_{max} induced by the cementation and C is a measure of the cementation level. C can be replaced by the unconfined compressive strength (q_u), resulting in relationship 46. As a reason, the top deviatoric stress ($q_{max,est}$) can be estimated with solely the effective confining pressure and the $\eta/(C_{iv})^{0.28}$ index value. In this regard, the coefficients of (45) were obtained by a parametric analysis that intended to diminish the mean relative error (MRE) which measures the relative difference between the observed (q_{max}) and estimated ($q_{max,est}$) top strength values. Naturally, eq. (46) is valid within the boundaries of the present study which include limited levels of confinement and certain amounts of cement.

$$q_{max,est} = 1.7p'_i + 10.3\ x\ 10^7 \left[\frac{\eta}{(C_{iv})^{0.28}}\right]^{-3.57} \tag{46}$$

Figure 102 presents the graph which plots the obtained top deviatoric stresses (q_{max}) measured in the triaxial tests altogether with the estimated values using relationship 46. A great agreement between the experimental and the estimated data was obtained as indicated by the coefficient of determination equals to 98%. Moreover, all the data lie within the 95% prediction bands and the MRE, considering the data from this study, was 18.8%. The outcomes presented by Schnaid *et al*. (2001), which comprehended the same BRS mixed with cement and cured along 7 days, were also plotted in Fig. 102 and have exhibited a great concordance with the approach used herein, presenting a MRE of 12.7%. Eq. 46 was used, as well, to determine $q_{max,est}$ of these data. Table 19 presents the triaxial test data for a clearly identification of the points plotted in Figure 102.

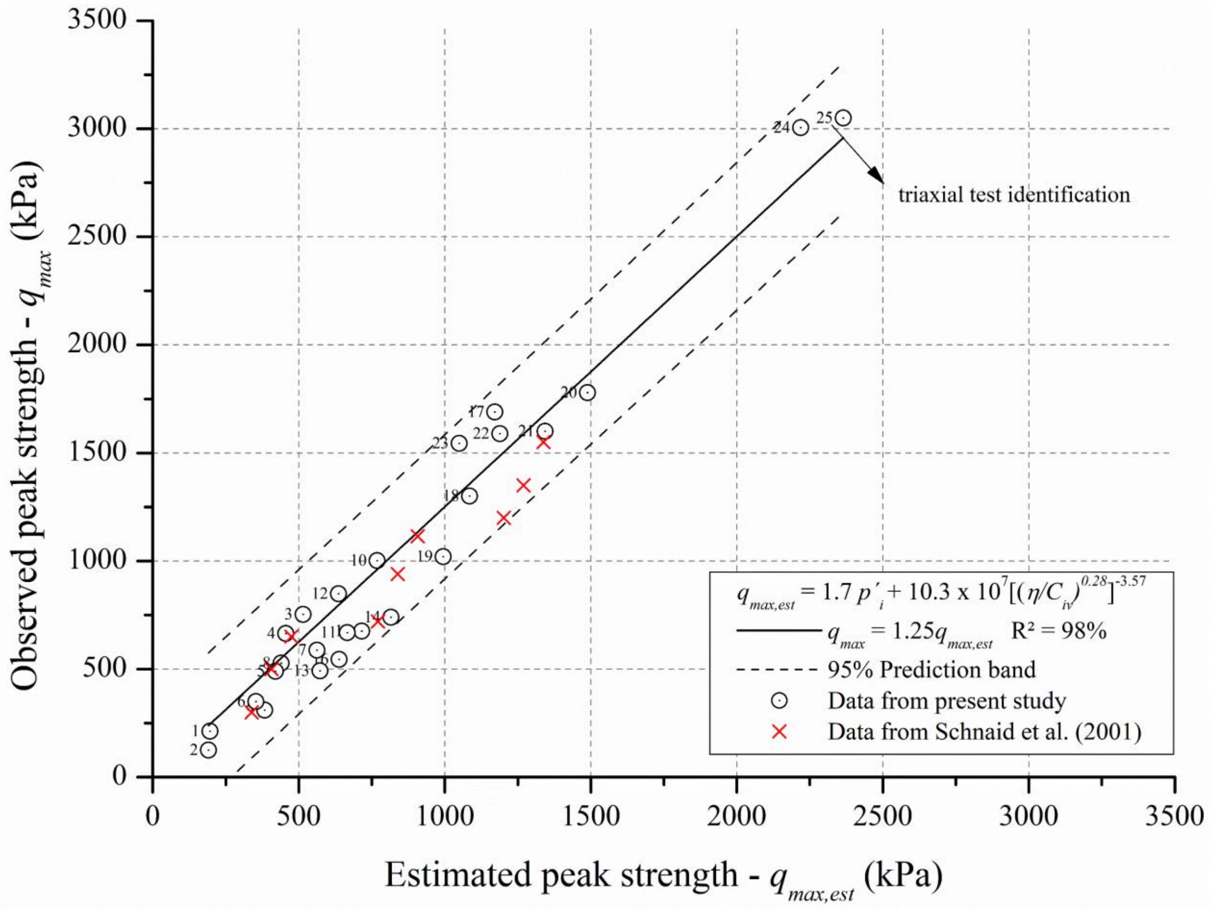

Figure 102 – Top deviatoric stress estimation

Table 19 – Summary of triaxial test data

$\eta/(C_{iv})^{0.28}$	Mix Design	Triaxial test identification	γ_d (kN/m³)	C (%)	p'_i (kPa)
45	1	1	16.59	1.00	35
	3	2	14.87	2.00	35
35	7	3	18.55	1.00	35
	7	4	18.55	1.00	70
	7	5	18.55	1.00	95
	7	6	18.55	1.00	140
	10	7	14.96	5.00	35
	10	8	14.96	5.00	70
	10	9	14.96	5.00	140
30	11	10	18.31	2.00	35
	11	11	18.31	2.00	70
	11	12	18.31	2.00	95
	11	13	18.31	6.00	140
	10	14	15.96	6.00	35
	10	15	15.96	6.00	70
	14	16	15.96	6.00	140
25	15	17	18.85	3.00	35
	15	18	18.85	3.00	70
	15	19	18.85	3.00	140
	18	20	16.94	8.00	35
	18	21	16.94	8.00	70
	18	22	16.94	8.00	140
	18	23	16.94	8.00	300
20	23	24	19.04	6.50	35
	26	25	18.32	10.00	35

5.4.6 Bonds Degradation Analysis

The bonds degradation throughout the triaxial tests was assessed by plotting the tangential stiffness (E_{tan}) as a function of the axial strain (ε_a), both in a logarithm scale, as suggested by Malandraki and Toll (1996). Further details regarding this method can be encountered on item 2.3.6. Within each graph, two yield points were detached as follows:

P_1: is marked by a slightly change in the stiffness of the material, denoting the onset of the bond's degradation;

P_2: is distinguishable owing to an abruptness alteration in the stiffness of the specimen, indicating the complete (or almost complete) degradation of the bonded structure. Beyond this point, the structure can be considered completely degraded and E_{tan} directs towards zero;

Consequently, Figures 103 to 112 presents the E_{tan} versus ε_a graphs for the samples molded having $\eta/(C_{iv})^{0.28}$ values of 35, 30 and 25. Each figure contains the results relative to the same adjusted porosity/cement index for tests conducted under the same effective confining pressure.

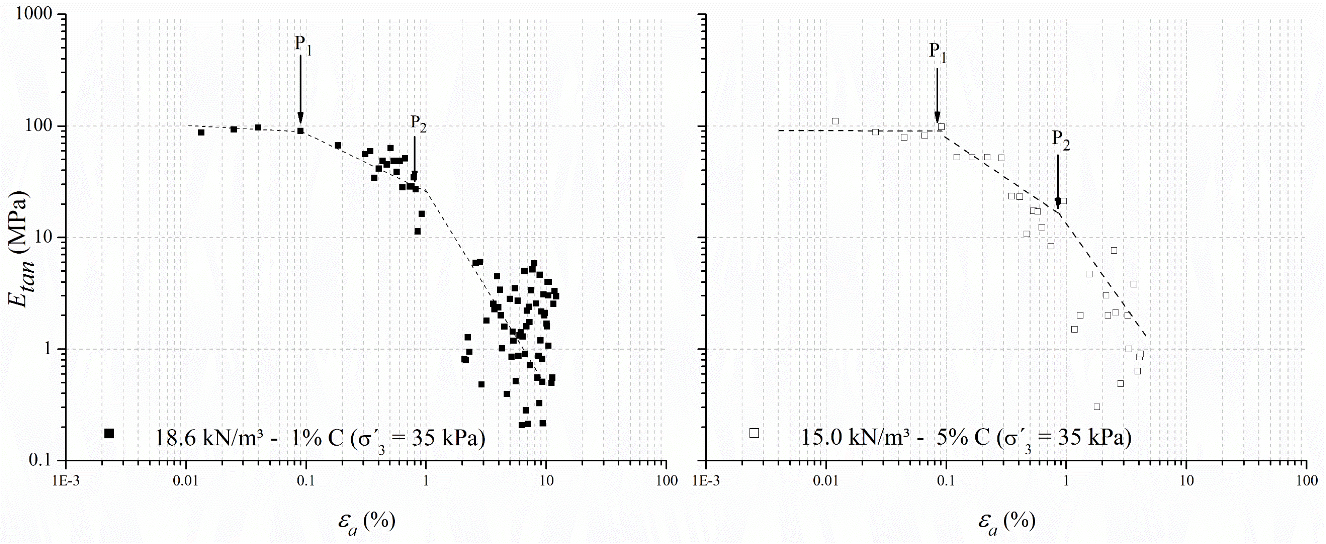

Figure 103 – Yield points for $\eta/(C_{iv})^{0.28}$ = 35 and σ´3 = 35 kPa

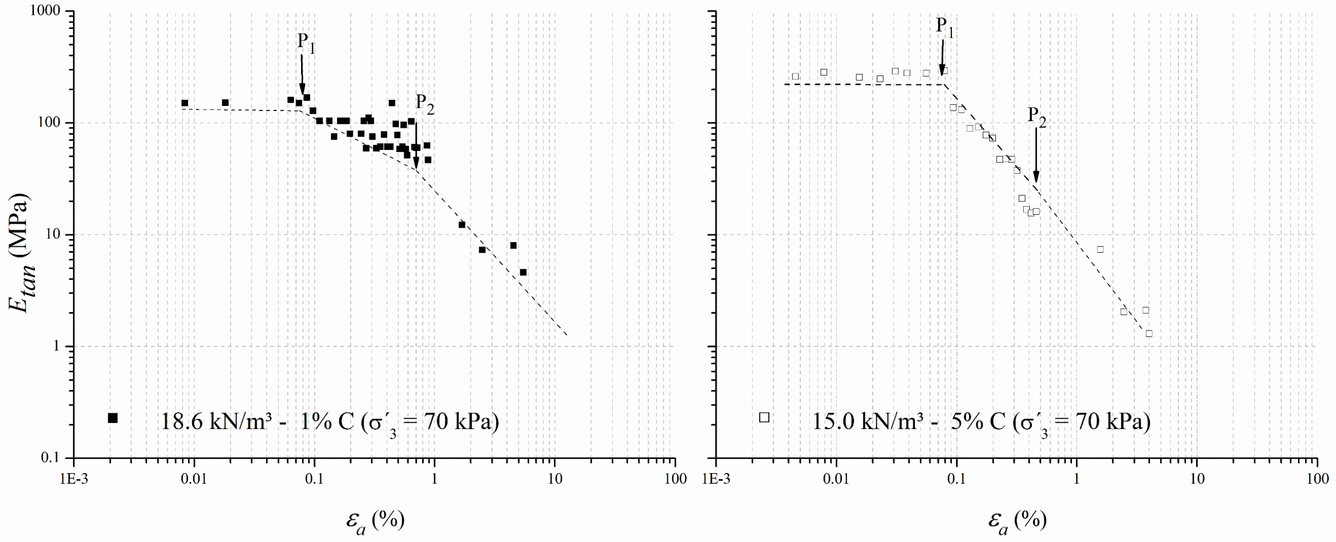

Figure 104 – Yield points for $\eta/(C_{iv})^{0.28}$ = 35 and σ´3 = 70 kPa

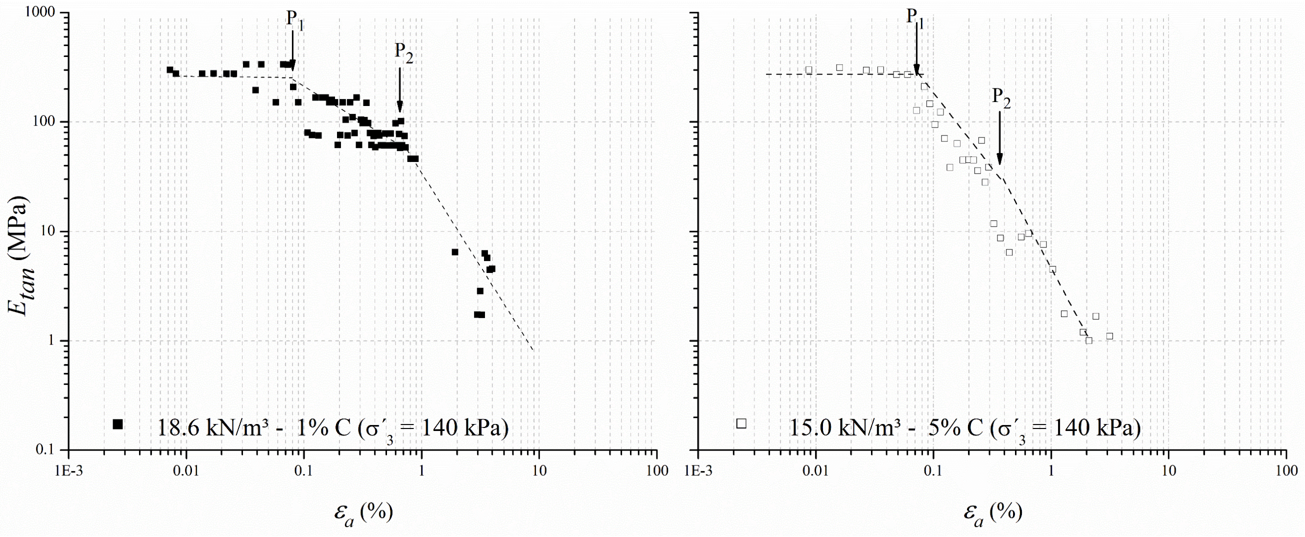

Figure 105 – Yield points for $\eta/(C_{iv})^{0.28}$ = 35 and σ´3 = 140 kPa

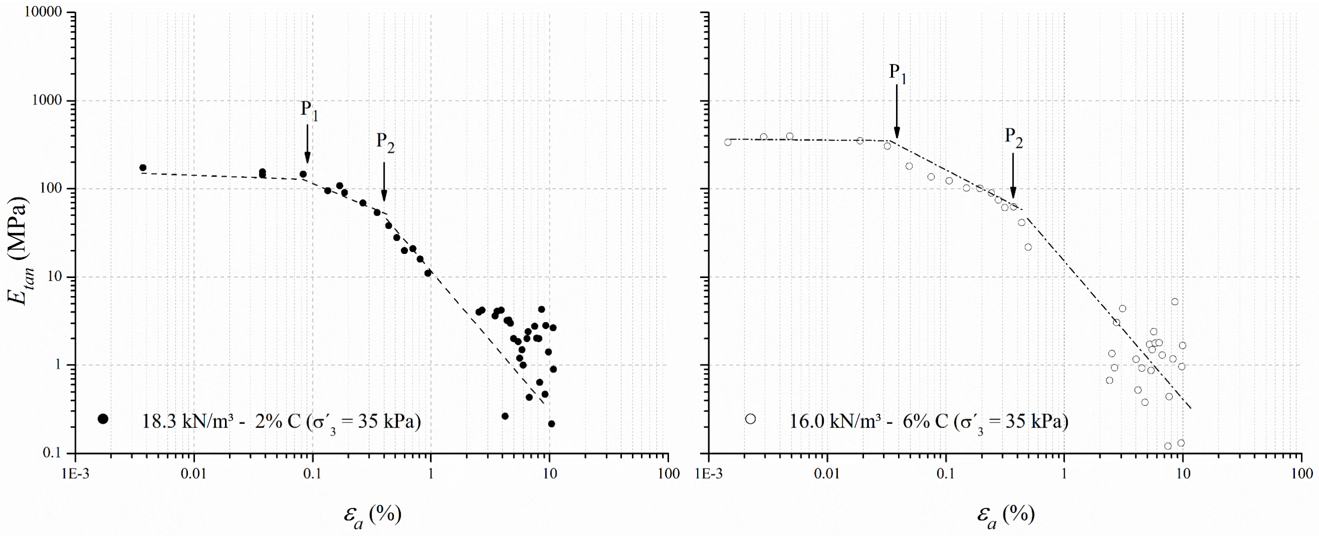

Figure 106 – Yield points for $\eta/(C_{iv})^{0.28}$ = 30 and σ´3 = 35 kPa

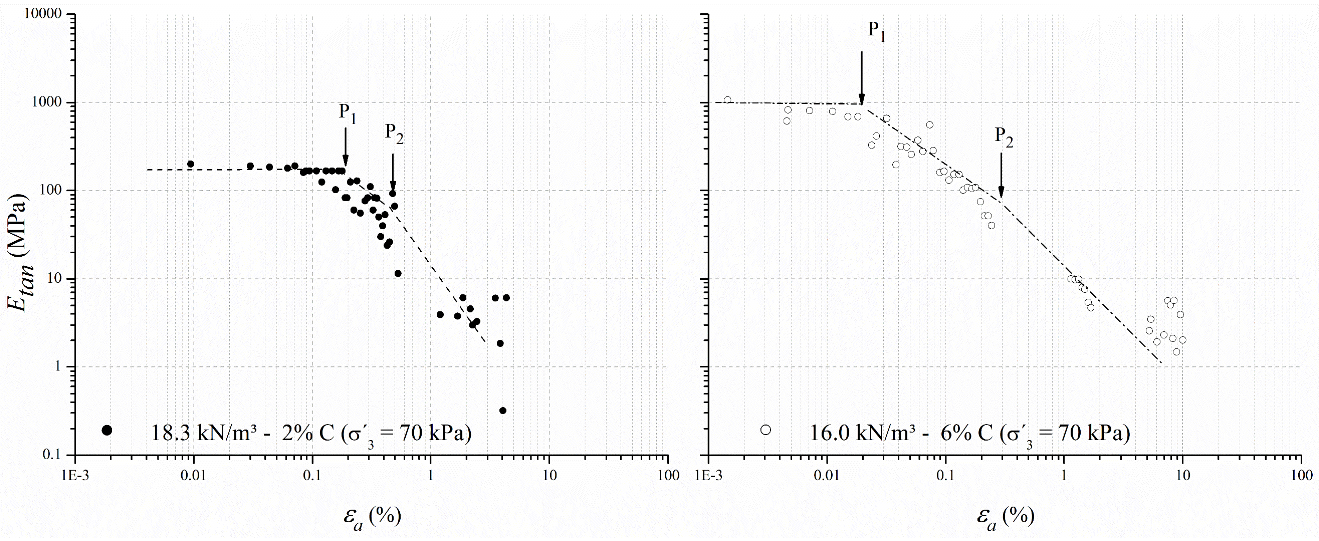

Figure 107 – Yield points for $\eta/(C_{iv})^{0.28}$ = 30 and σ´3 = 70 kPa

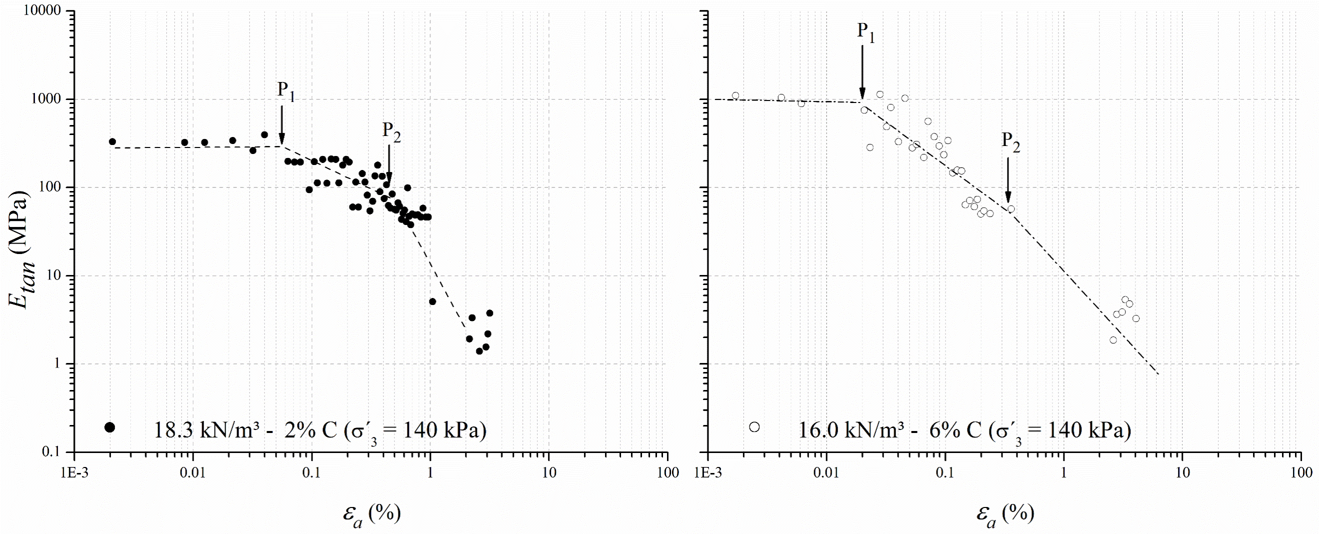

Figure 108 – Yield points for $\eta/(C_{iv})^{0.28}$ = 30 and σ´$_3$ = 140 kPa

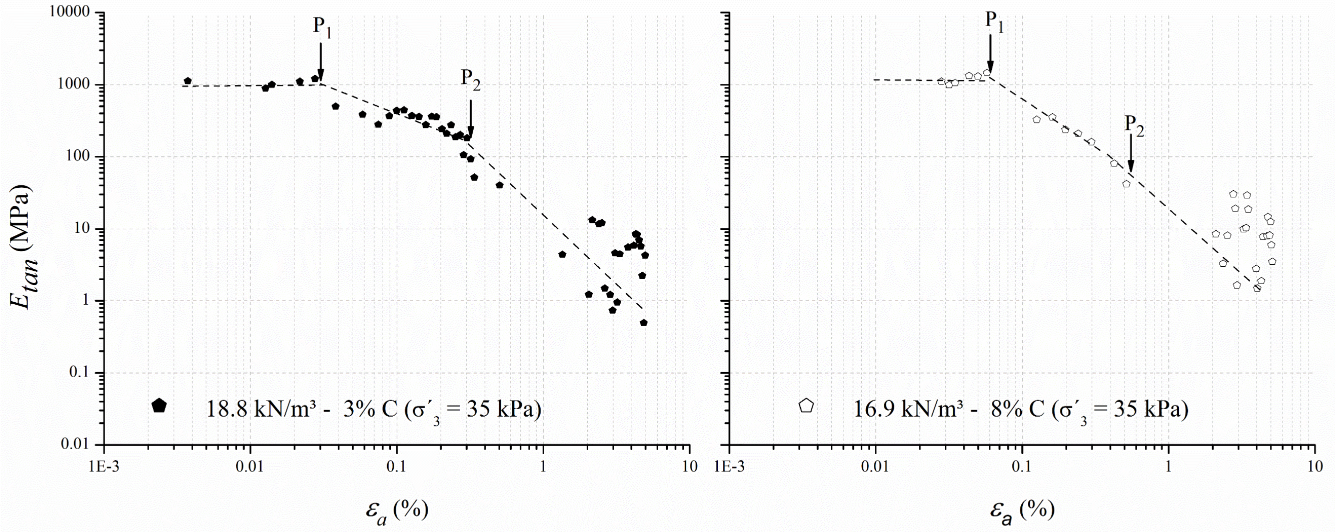

Figure 109 – Yield points for $\eta/(C_{iv})^{0.28}$ = 25 and σ´$_3$ = 35 kPa

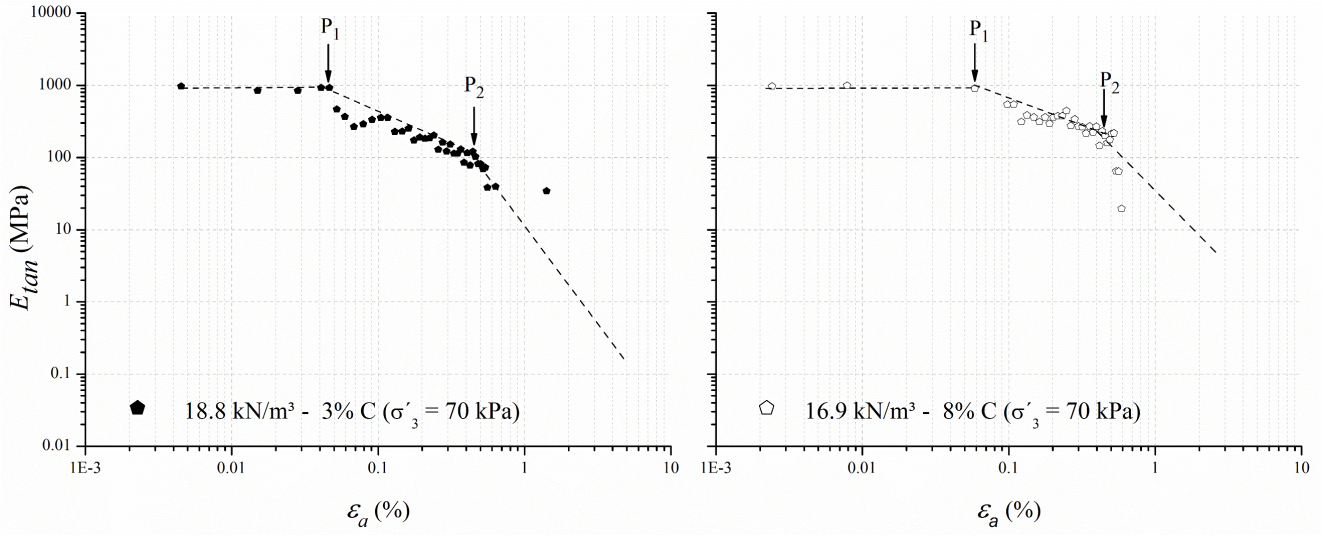

Figure 110 – Yield points for $\eta/(C_{iv})^{0.28}$ = 25 and σ´$_3$ = 70 kPa

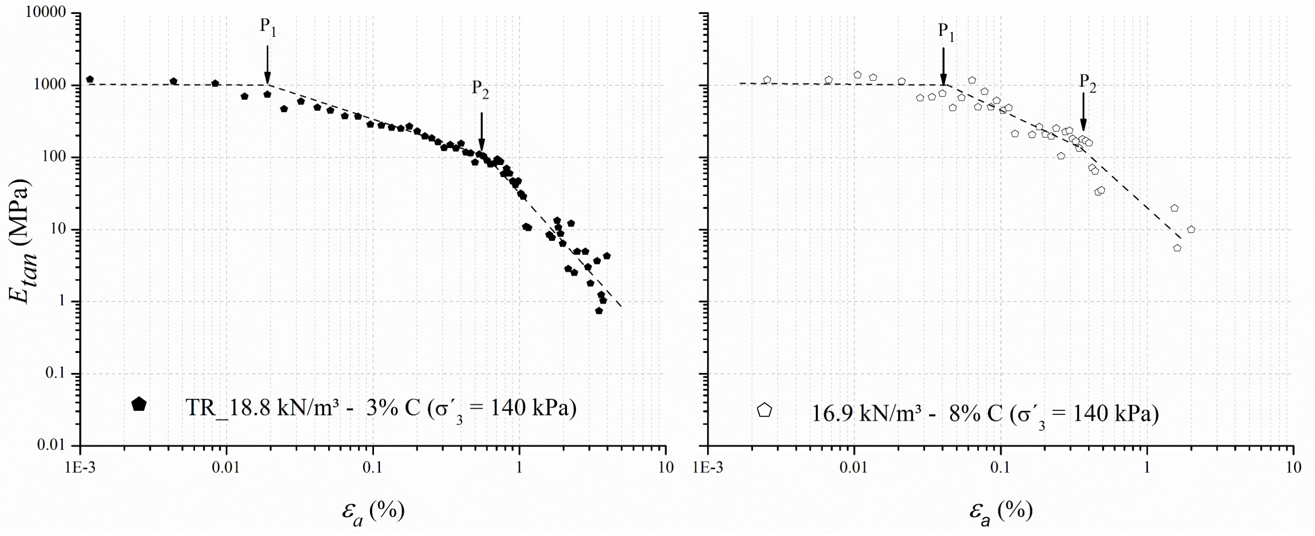

Figure 111 – Yield points for $\eta/(C_{iv})^{0.28}$ = 25 and σ´$_3$ = 140 kPa

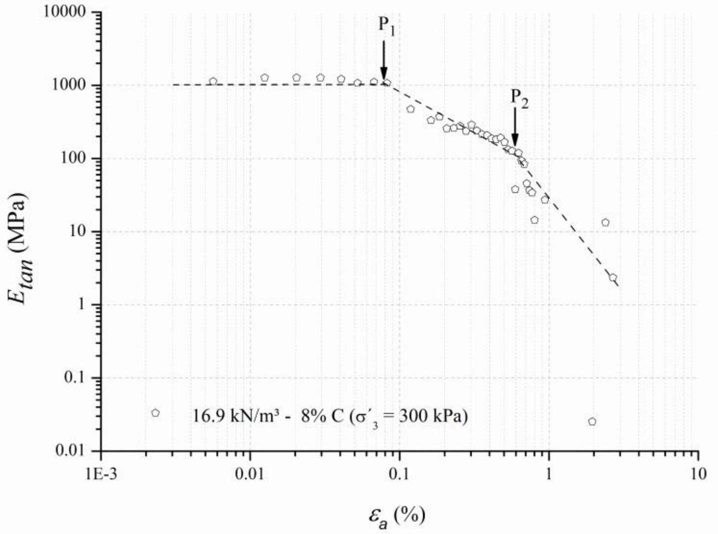

Figure 112 – Yield points for $\eta/(C_{iv})^{0.28}$ = 25 and σ´$_3$ = 300 kPa

Regardless of the adopted adjusted/porosity/cement index value, the commencement of the bond's degradation (P_1) seems to have occurred at relatively small axial strain values. That is, the cemented structure has remained unaltered for a diminutive period throughout the triaxial tests. Once the yield of the bonds has started, a substantial loss in the tangential stiffness (beyond point P_1) has taken place up to a point in which a further greater loss was observed (beyond point P_2). In between yield points P_1 and P_2, the structure was still contributing to the strength and the stiffness of the material. Yet, beyond point P_2, the bonds have been fully degraded. In general, within the same $\eta/(C_{iv})^{0.28}$, the most cemented specimen was slightly stiffer at the beginning of the tests, especially when considering the $\eta/(C_{iv})^{0.28}$ = 30. This trend has been previously reported considering the secant modulus.

Considering the most cemented specimens within each $\eta/(C_{iv})^{0.28}$ index value, the bonds yield (denoted by P_2) has practically coincided to the top strength of the samples irrespective of the adopted confining pressure. In other words, the cementation has controlled the response up to the peak state of stress, being the second yield surface coincident to the failure surface as can be noticed in Figures 113, 114 and 115. In contrast, this has not occurred for the least cemented specimens when the highest effective confining pressure was employed. That is, the cemented structure seems to have fully degraded prior to the peak strength and the second yield surface did not agree to the failure surface. The first yield surface, represented in Figures 113, 114 and 115, is relative to the point P_1.

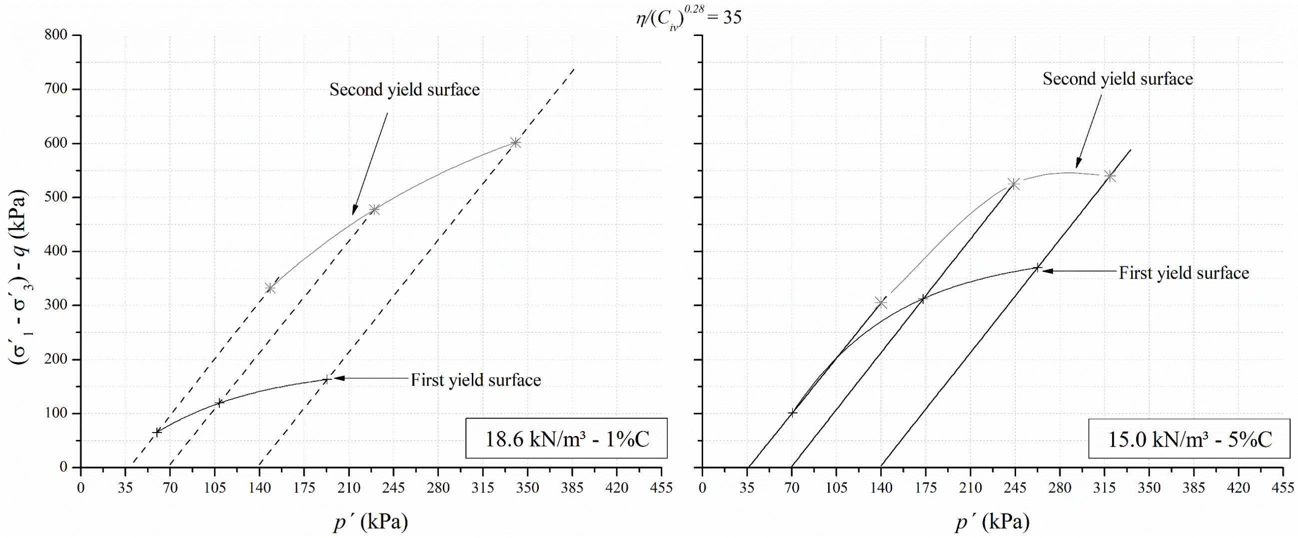

Figure 113 – Stress paths and yield surfaces for $\eta/(C_{iv})^{0.28} = 35$

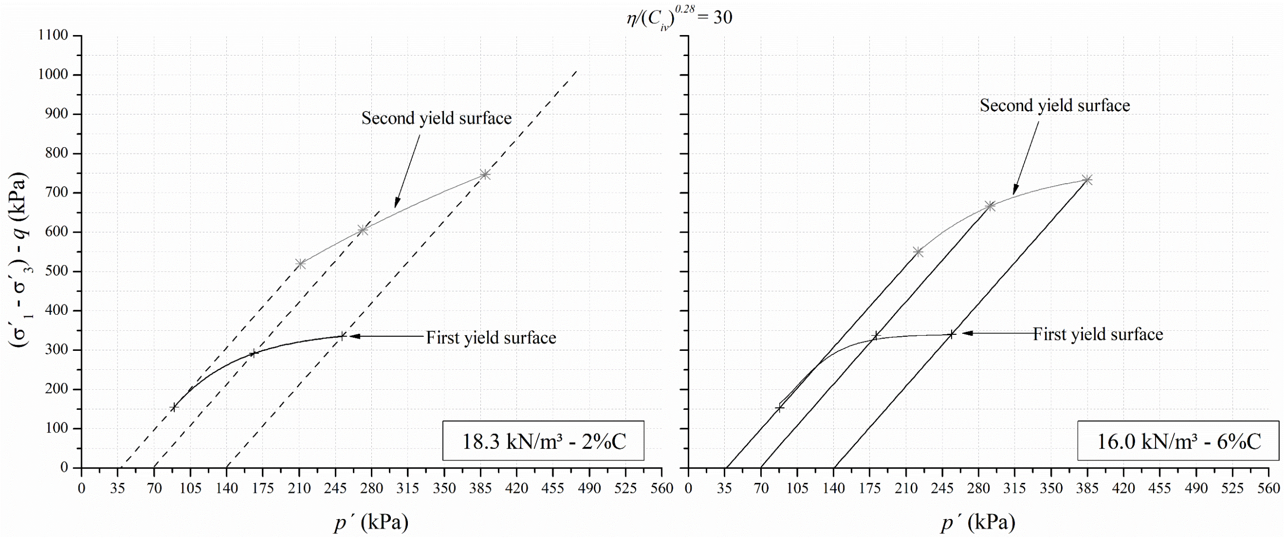

Figure 114 – Stress paths and yield surfaces for $\eta/(C_{iv})^{0.28} = 30$

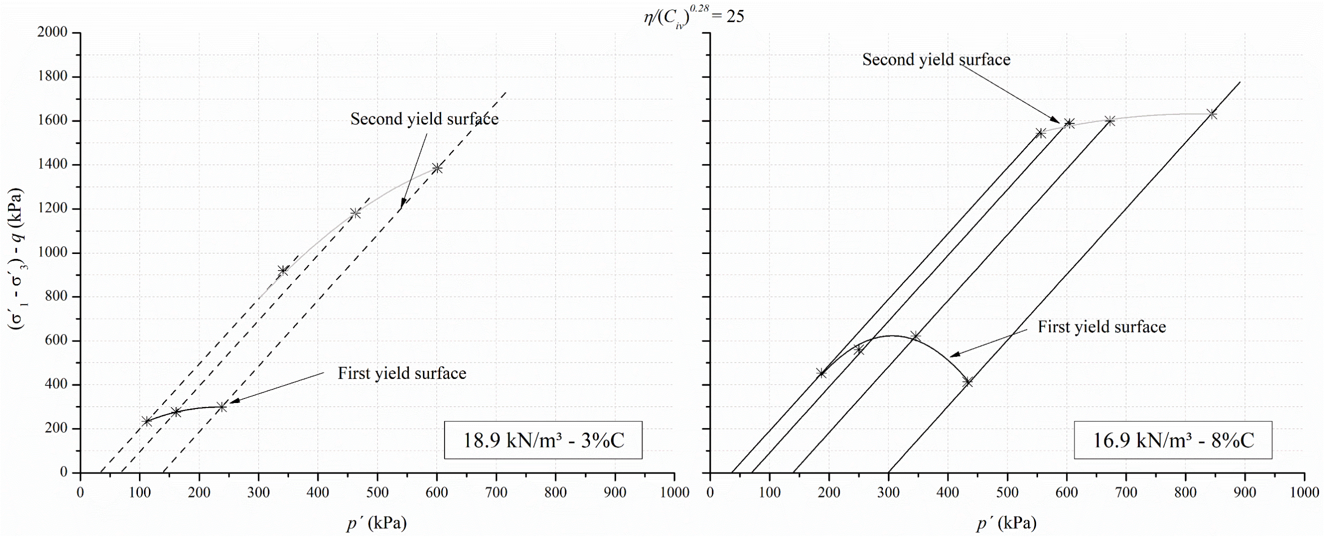

Figure 115 – Stress paths and yield surfaces for $\eta/(C_{iv})^{0.28} = 25$

5.4.7 Stress-Dilatancy Response

Figure 116 summarizes the stress-dilatancy response of all the triaxial tests which have been conducted herein. As formerly done by Prietto (2004), no distinction was done relative to the elastic strain increments and plastic strains increments. In general, a typical cohesive trend is observed when the specimens were compressing, which was denoted by a vertical trend in the $q/p´$ x $\delta\varepsilon_v/\delta\varepsilon_s$ plane. It is clear that this has not happened to the natural (uncemented BRS) as shown in the same graph. The bonds degradation is marked by a shift of this tendency in which the line directs towards the left, indicating the commencement of the dilation. Since the bonds initially suppress the dilatant trend of the material, the dilation rates of the cemented material were higher than that of the natural soil molded at a similar dry unit weight. As a reason, the peak strength of the cemented specimens has resulted as a combined effect of cementation, friction and augmented dilation rate. Once the peak stress ratio was achieved, a strain-softening behavior has been observed and the material followed a purely frictional trend with a substantial decrement in the dilation ration and, as well, in the stress ratio. Similar tendencies have been reported by Coop and Wilson (2003), Prietto (2004), Cruz (2008), Consoli *et al*. (2012b) Marques (2016), Leon (2018), among others. Within the same dosage, the increment in the confining pressure has led to decrement of the dilation rate.

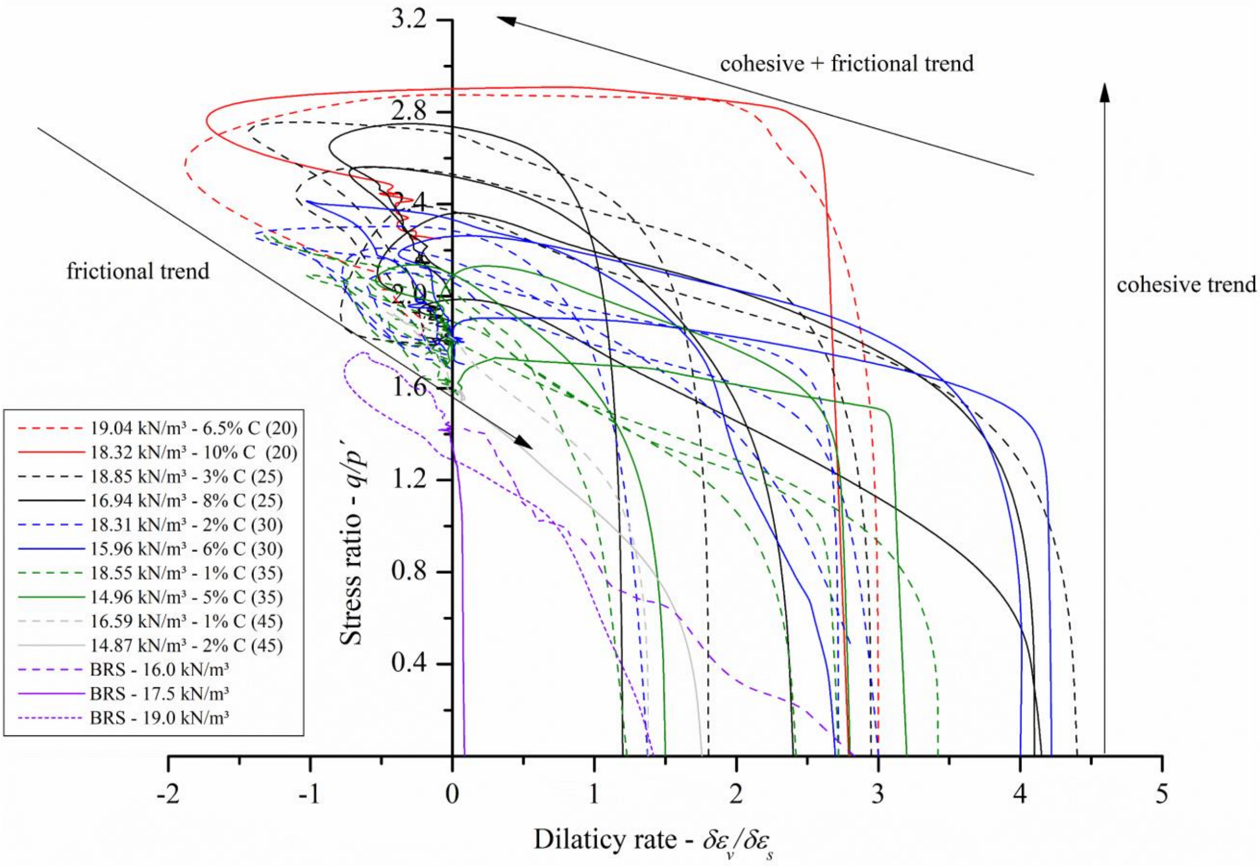

Figure 116 – Stress-dilatancy response for all the triaxial tests

Considering the lowest confinement level, within the same $\eta/(C_{iv})^{0.28}$, the densest and least cemented specimen ($\downarrow\eta$ and $\downarrow C$) has always presented a higher dilation rate in comparison to the loosest and most cemented one ($\uparrow\eta$ and $\uparrow C$). Such trend is expected as either have presented similar top deviatoric stresses. Thus, considering the same adjusted porosity/cement index, the parcel of strength related to bonds in the most porous specimen is, in a certain manner, compensated by the degree of interlocking and the higher dilation rate observed in the least porous sample. The same is valid for the samples which were tested under a confinement of 70 kPa.

Moreover, it is obvious that an interaction occurs between the cement and the dry unit weight, influencing the interlocking between the material's particles and, thus, the dilating response as the addition of cement probably alters the fabrics of the soil. At an effective confining pressure of 35 kPa, the strength, which is fully related to friction of the soil (i.e. dilation rate equals to zero), was around 100 kPa (Figure 81). The addition of cement to the natural soil has implied changes in the strength mechanism mobilization. For example, the specimen 16 kN/m³ - 6%C (mix design n. 14) has presented a peak strength of around 530 kPa, whereas the specimen without cement has not exhibited a peak, being the stress, afterwards, constant and close to 100 kPa (Figure 81). A fully contractive response was observed in the latter, whereas an initial contraction followed by dilation has occurred in the first. Therefore, the addition of cement has, besides influencing the strength, altered the volume change response which, in turn, has led to dilation once the deterioration of the cement bonds started. This is depicted in Figure 117, below, in which the stress-strain response of both cemented and uncemented specimens are plotted together. Similar has occurred when the outcomes of the mix design number 23 (19 kN/m³ - 6.5% C) are compared to the response of the natural soil. The volume change dynamics experienced by the cemented soil were very distinct in comparison to the natural soil.

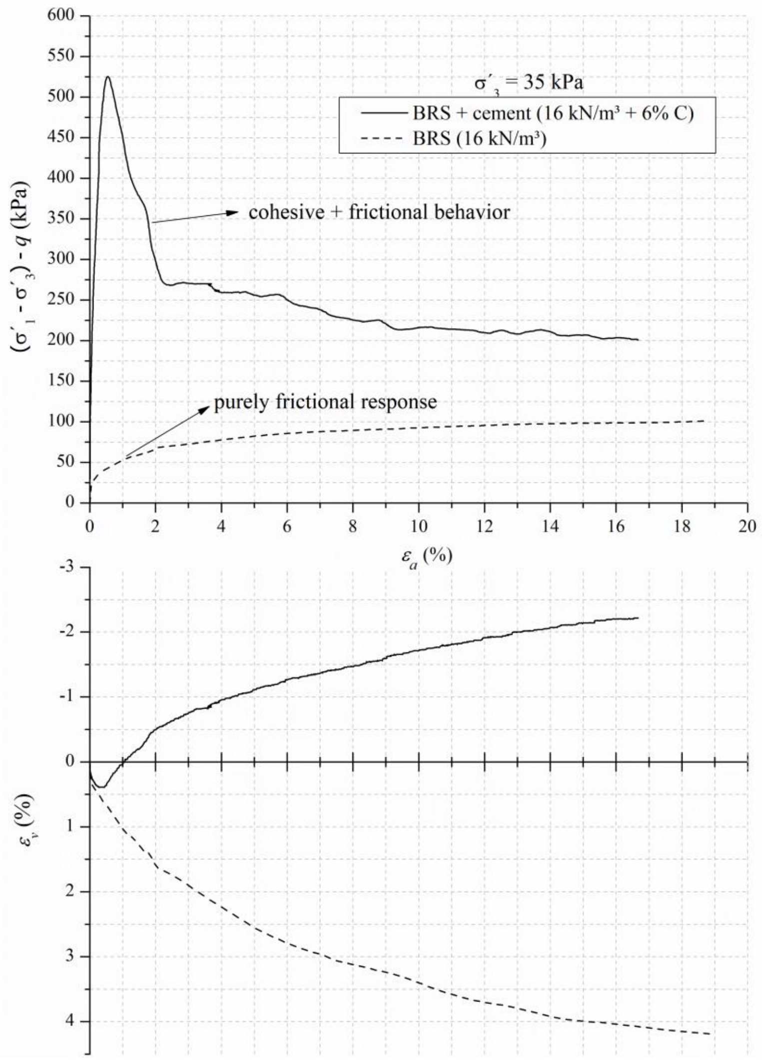

Figure 117 – Effect of cement addition on the stress-strain response of BRS

Figure 118 is an attempt to clearer expose the dilatancy rate data and to correlate it to the adjusted porosity/cement index, thus it graphically presents the minimum dilatancy rate ($\delta\varepsilon_v/\delta\varepsilon_{s,min}$) as function of the $\eta/(C_{iv})^{0.28}$ index value. The data points are, as well, identified according to the level of cementation and to the effective confining pressure used during the shearing. Within each $\eta/(C_{iv})^{0.28}$ index value, and considering the same confinement, the lowest $\delta\varepsilon_v/\delta\varepsilon_{s,min}$ was always observed amongst the denser (i.e. least cemented) specimen, as formerly discussed above. In addition, considering the same dosage, it is promptly noticeable that $\delta\varepsilon_v/\delta\varepsilon_{s,min}$ has decayed due to the increment in the confining pressure, which is expected since the augment in the confinement inhibits the dilation of the specimen to take place (e.g., COOP & WILSON, 2003; MARQUES, 2016). The $\delta\varepsilon_v/\delta\varepsilon_{s,min}$ has decayed, as well, with the diminishing of the $\eta/(C_{iv})^{0.28}$ value, namely, denser and more cemented dosages have dilated more which is in consonance to the higher strength values observed amongst these samples.

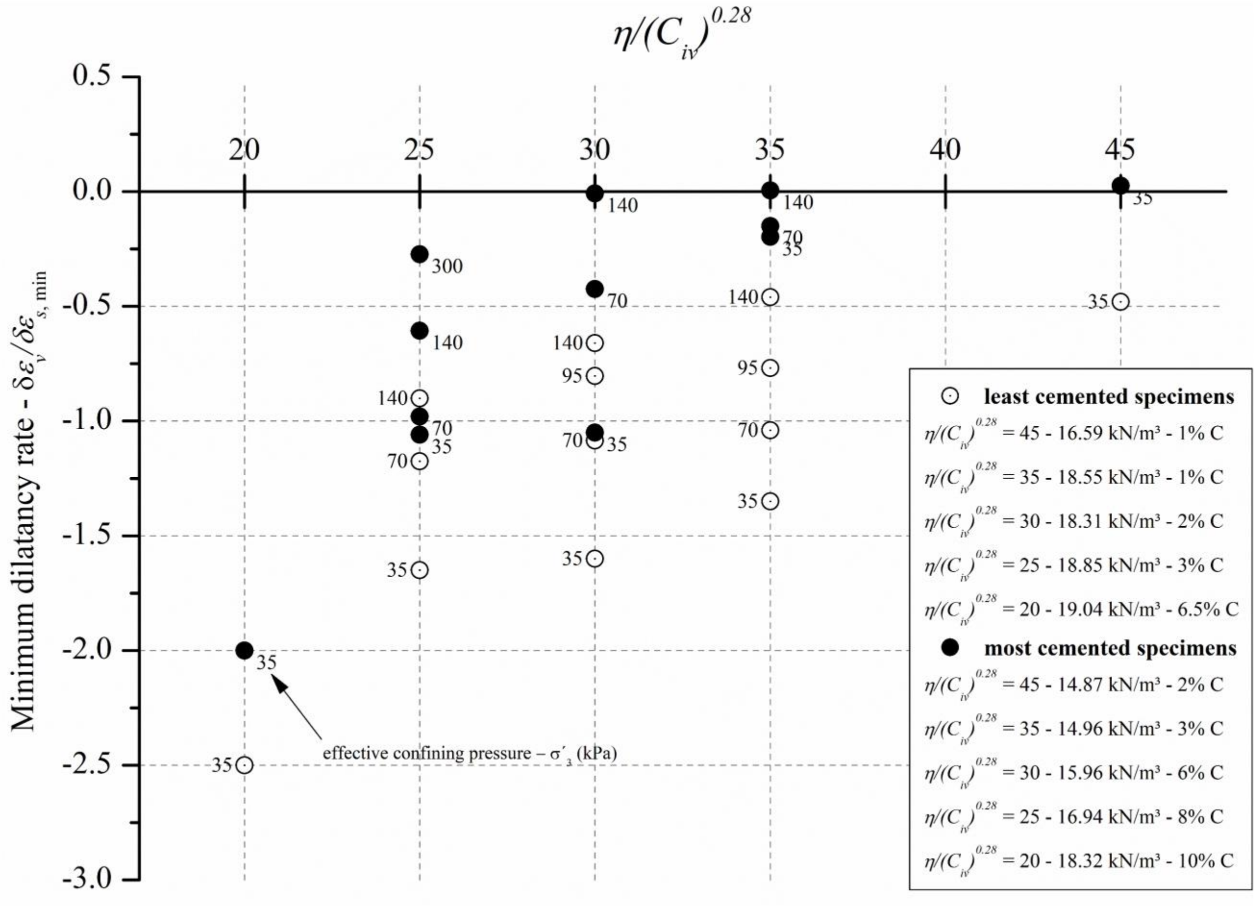

Figure 118 – Minimum dilatancy versus the adjusted porosity/cement index

Figure 119 exhibits a graph in which the top stress ratio (q/p'_{max}) is plotted as a function of the minimum dilatancy rate ($\delta\varepsilon_v/\delta\varepsilon_s{}_{,min}$). Two separated trends were proposed according to the dosage within each $\eta/(C_{iv})^{0.28}$ index value, namely: one tendency for the least cemented specimens (eq. 47) and one for the most cemented samples (eq. 48). The data points are identified according to information previously exposed in Table 19. A most cemented specimen would present a slightly higher q/p'_{max} value, if the same $\delta\varepsilon_v/\delta\varepsilon_s{}_{,min}$ is considered, than a least cemented sample, indicating the greater contribution of the cohesive parcel to the strength of the former. On the other hand, the least cemented samples have shown a greater scatter around the fitted line mainly due to the tests n. 17, 18 and 19, which were carried out on samples containing 3% of cement.

$$q/p'_{,max} = -0.46\left(\delta\varepsilon_v/\delta\varepsilon_{s\ .min}\right) + 1.78 \qquad (47)$$

$$q/p'_{,max} = -0.51\left(\delta\varepsilon_v/\delta\varepsilon_{s\ .min}\right) + 2.01 \qquad (48)$$

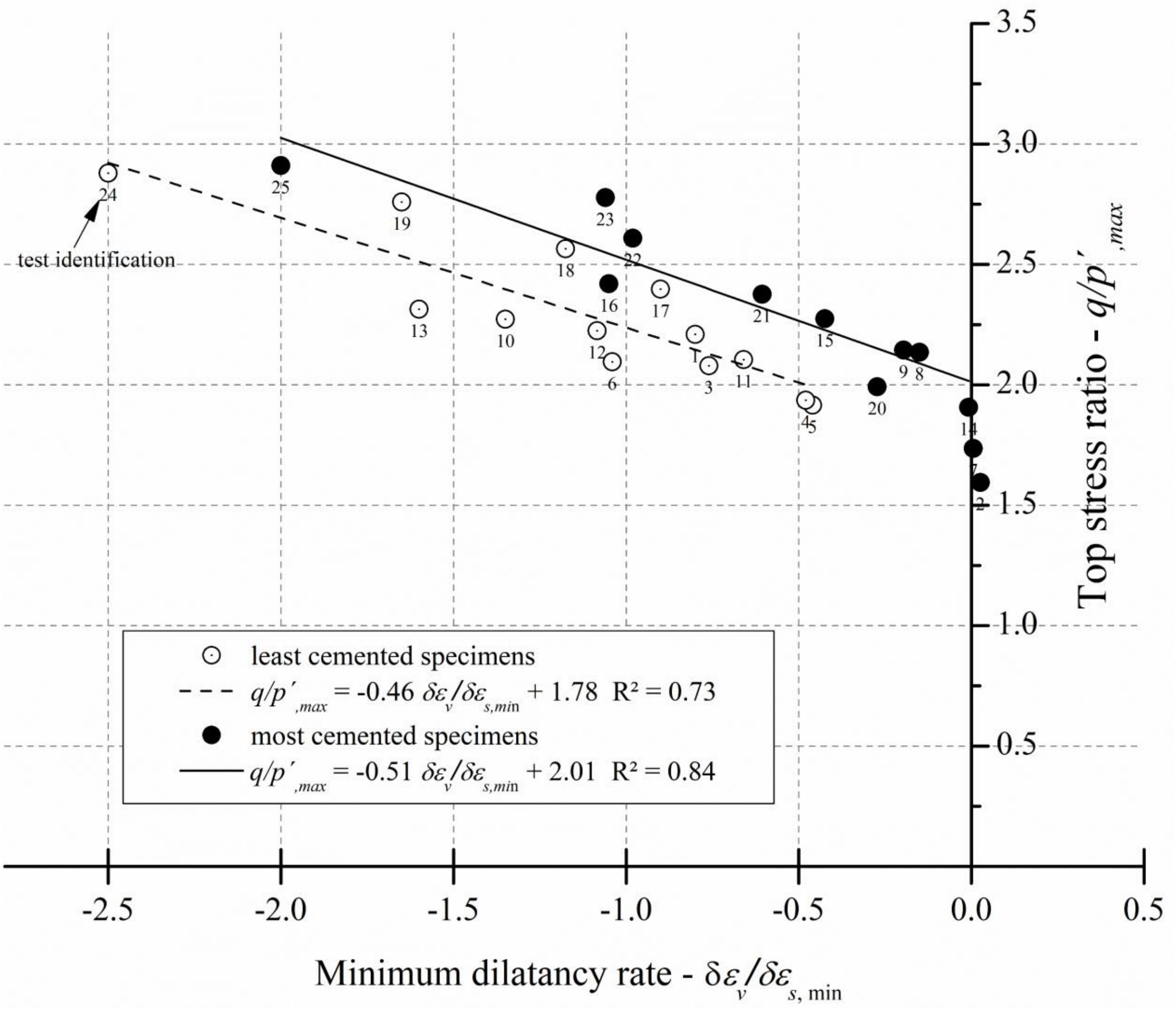

Figure 119 - $\delta\varepsilon_v/\delta\varepsilon_{s,min}$ versus q/p' ratio

A new approach was, thus, proposed dividing the test results between “density-controlled specimens” and “cement-controlled specimens”. The outcomes from tests 17, 18 and 19 were reallocated, whereas the tests 2 and 7 were withdrawn from this analysis because these specimens have not expanded during the shear. As a result, the graphs exhibited in Figure 119 were generated with smaller scatter around the fitted lines for either cement-controlled and density-controlled samples. The cement-controlled (eq. 49) results contemplate the dosages in which the amount of cement varied from 3% to 10%, whereas the majority of the density-controlled samples (eq. 50) were molded using 2% or less of cement. The only exception was test n. 24 (19.04 kN/m³ – 6.5% C).

$$ {q}/{p'}_{,max} = -0.48 \left({\delta\varepsilon_v}/{\delta\varepsilon_s}_{.min} \right) + 2.018 \qquad (49) $$

$$ {q}/{p'}_{,max} = -0.42 \left({\delta\varepsilon_v}/{\delta\varepsilon_s}_{.min} \right) + 1.75 \qquad (50) $$

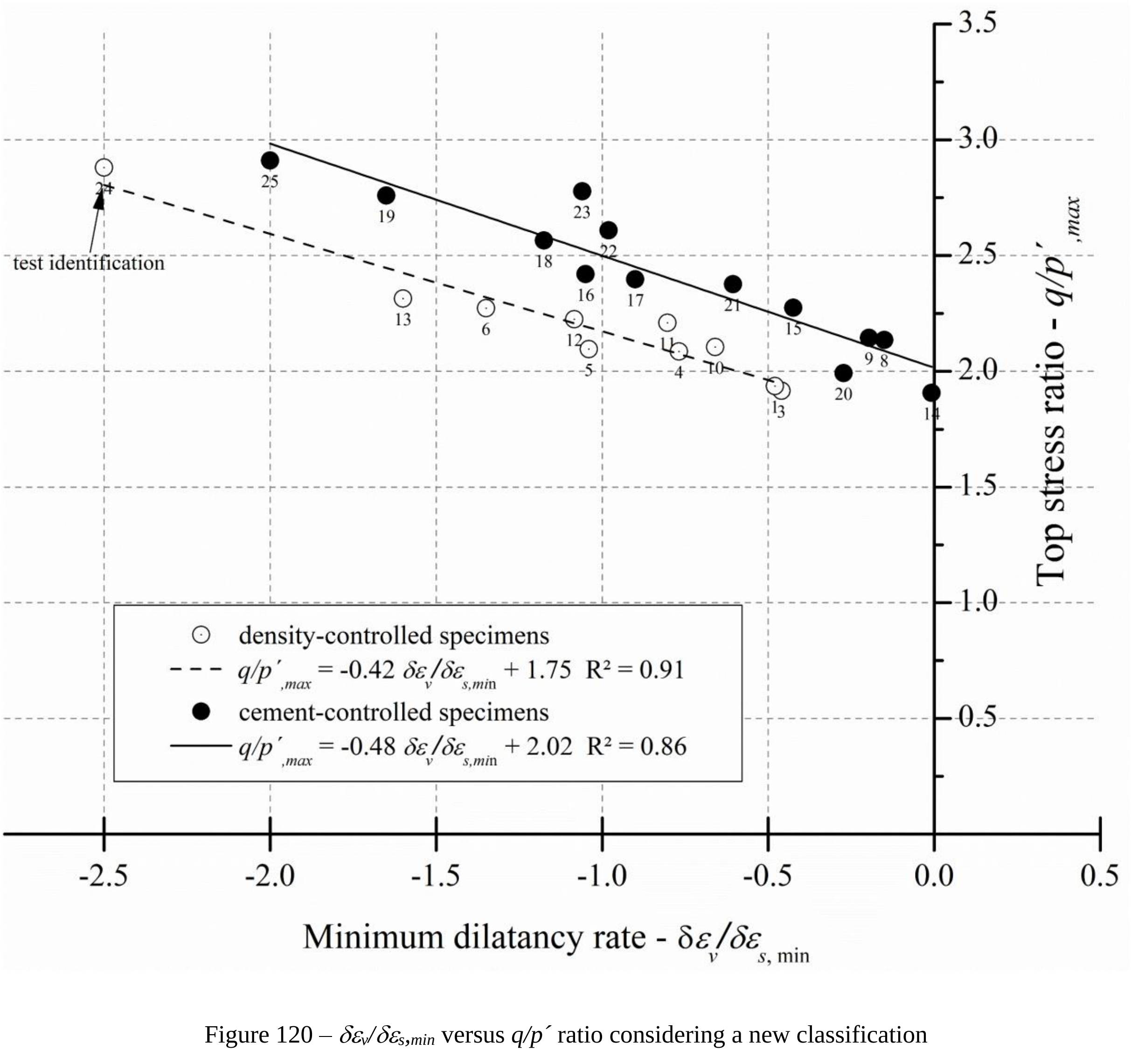

Figure 120 – $\delta\varepsilon_v/\delta\varepsilon_{s,min}$ versus q/p' ratio considering a new classification

The trends depicted in Figure 120 reinforce the fact that the cement content, besides contributing to the cohesive parcel of friction, also alters the dynamics of the volume change behavior by augmenting, in modulus, the dilation rate. For example, test numbers 3 (18.55

kN/m^3 – 1%C), 10 (18.31 kN/m^3 – 2%C) and 17 (18.85 kN/m^3 – 3%C), each one carried out at a confinement of 35 kPa and compacted to very similar dry unit weight values, have presented very different $\delta\varepsilon_v/\delta\varepsilon_{s,min}$ which have diminished with the increment on the cement content. Namely, the addition of 1% of cement has altered $\delta\varepsilon_v/\delta\varepsilon_{s,min}$ from -0.46 to around -0.7 when tests 1 and 10 are compared. When the cement content increases from 2% to 10% (tests n. 10 and 25), this trend is much more perceptible. Both specimens were compacted at dry unit weight of around 18.3 kN/m^3, but the more cemented specimen has exhibited a minimum dilation rate almost 5 times lower than the least cemented one.

At nearly zero dilation rate values, the stress ratio of the cemented samples has tended to values in the range of 1.5 to 2.0 and have not necessarily returned to the behavior of the uncemented soil (M ~ 1.46), as shown in Figure 120, below. As observable, the specimens containing a higher amount of cement have exhibited a greater final q/p' ratio, which may be related to fabrics alteration of the original soil, lumps of cementing particles acting as larger particles and stress localization (CLOUGH *et al.*, 1981; PRIETTO, 2004; LADE & TRADS, 2014). In brief, if a certain amount of cement is used, the shearing conducted at low confinement levels is not able to erase the cement-related alterations on the soil' fabrics. As a reason, the cemented material does not unavoidably return to the stress levels comparable as the obtained for the natural (uncemented) soil, even at higher strains. However, at higher confinement levels, the stress ratio of the most cemented specimens might reduce (or not) to a range similar of the natural soil as the degradation of the bonded structure would be more intense.

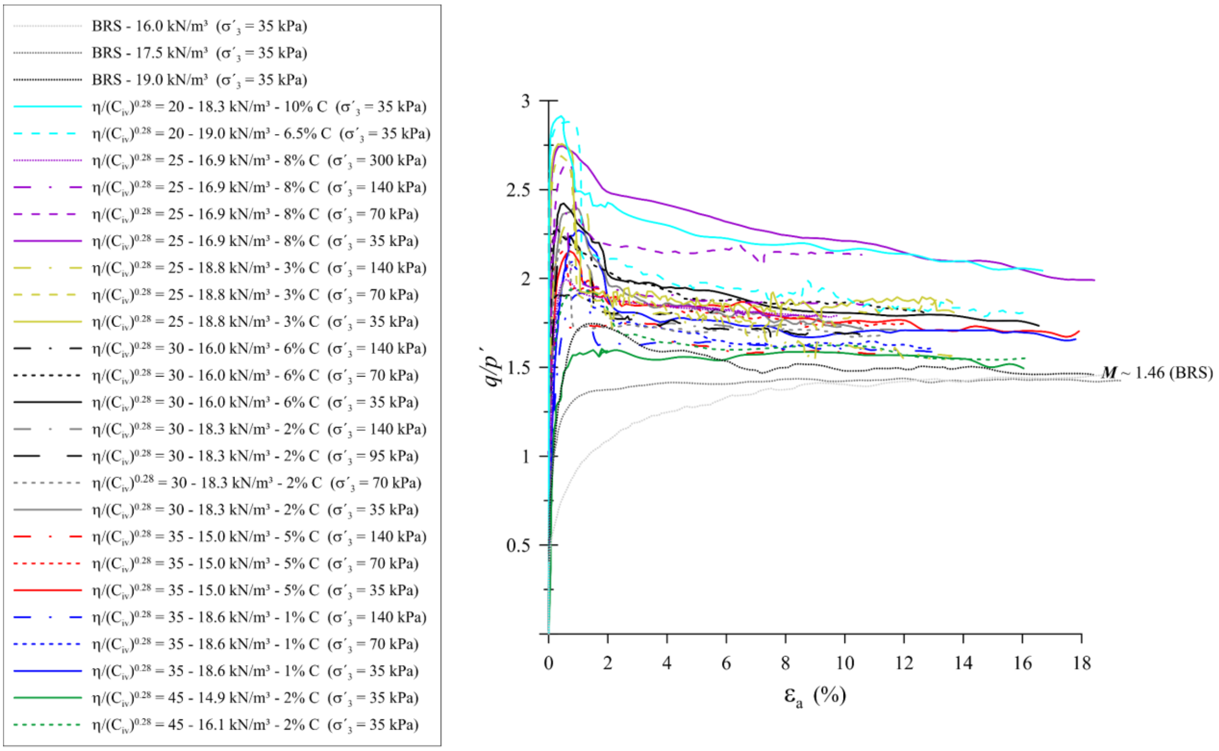

Figure 121 – Stress ratio versus axial strain for all the triaxial tests

Figure 122a resumes the *q/p´*versus ε_a data for the "density-controlled" specimens, whereas Fig. 122b does the same for the "cement-controlled" samples. It is clear that the stress ratio at higher strain levels is relatively lower for the least cemented specimens. Moreover, the increase in the confinement level has generally led to a decrement in the final *q/p´* values for both cases, indicating that the cemented material degradation is proportional to the stress level.

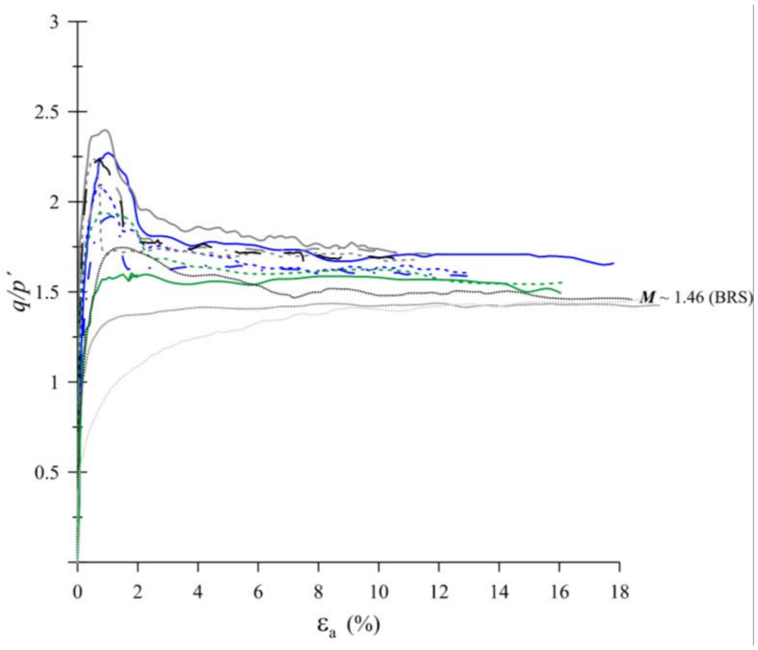

(a)

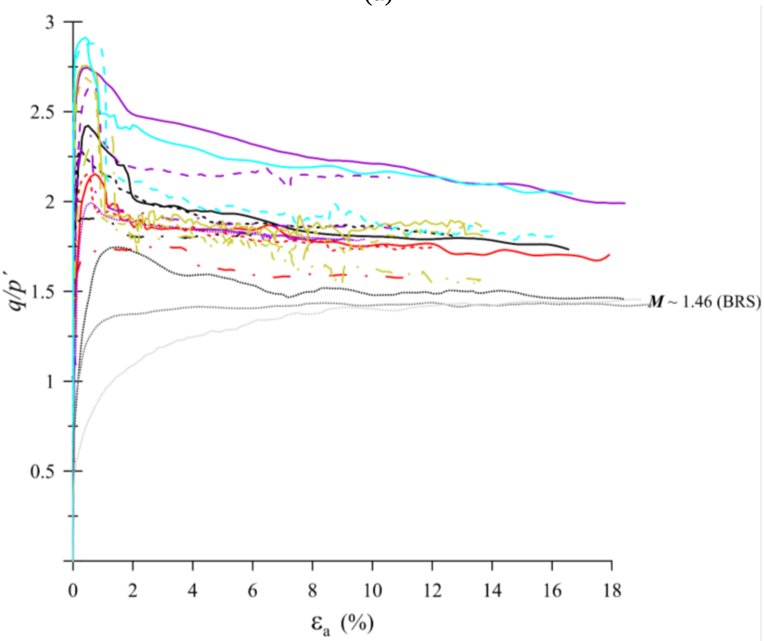

(b)

Figure 122 - Stress ratio versus axial strain for (a) density-controlled specimens (b) cement-controlled specimens

5.5 SCANNING ELECTRON MICROSCOPE TESTS

In order to properly present the scanning electron microscope (SEM) test results, these were discussed in three items. The first contemplates the effect of the cement content, the second comprehends the influence of the dry unit weight, whereas the third discusses the $\eta/(C_{iv})^{0.28}$ impact on the SEM micrographs of the BRS-cement samples.

5.5.1 Effect of the Cement Content

As previously observed in Figure 34 (item 4.1.1), the remolded samples of the Botucatu residual soils present a completely different fabrics when compared to the undisturbed specimen. In the reconstituted sample, the clay particles are randomly distributed and form a clay matrix which covers the larger particles (i.e., quartz grains). As a reason, it is difficult to visualize and identify the effect of cement addition into this soil, especially for low levels of cementation (e.g., KAMRUZZAMAN *et al.*, 2006; BAHMANI *et al.*, 2014). That is, the cement bonds are mixed within the clay matrix and small variations on the amount of cement (e.g., from 1 to 3%) will not be easily perceptible within the SEM micrographs. In this regard, Figure 123 displays the scanning electron microscope (SEM) test micrographs (magnification of 600x) of compacted BRS-cement specimens molded at dry unit weight values varying from 18.7 kN/m³ to 18.3

kN/m³. As this is a narrow range of compacity variation, the effect of different cement contents (0%, 1%, 5% and 10%) on the fabrics of the soil can be reasonably assessed. The yellow squares indicate where the 2500x magnification was applied. These outcomes are exposed in Figure 124.

From the images depicted in Figure 123 (600x), it can be visualized that, as the cement content increases, the cement gel fills the gaps between the kaolinite particles and, as well, the existing voids within the soil. As a reason, the overall fabrics looks more condensed with the increment in the amount of cement. This is clear when comparing the micrographs of Fig. 123a (1% of cement) and Fig. 123d (10% of cement). In the latter, the structure looks much more condensed. These tendencies are corroborated by the micrographs with a greater magnification rate (Figure 124), in which it is noticeable that the cement hydration products fulfill the spaces existing between the kaolinite particles.

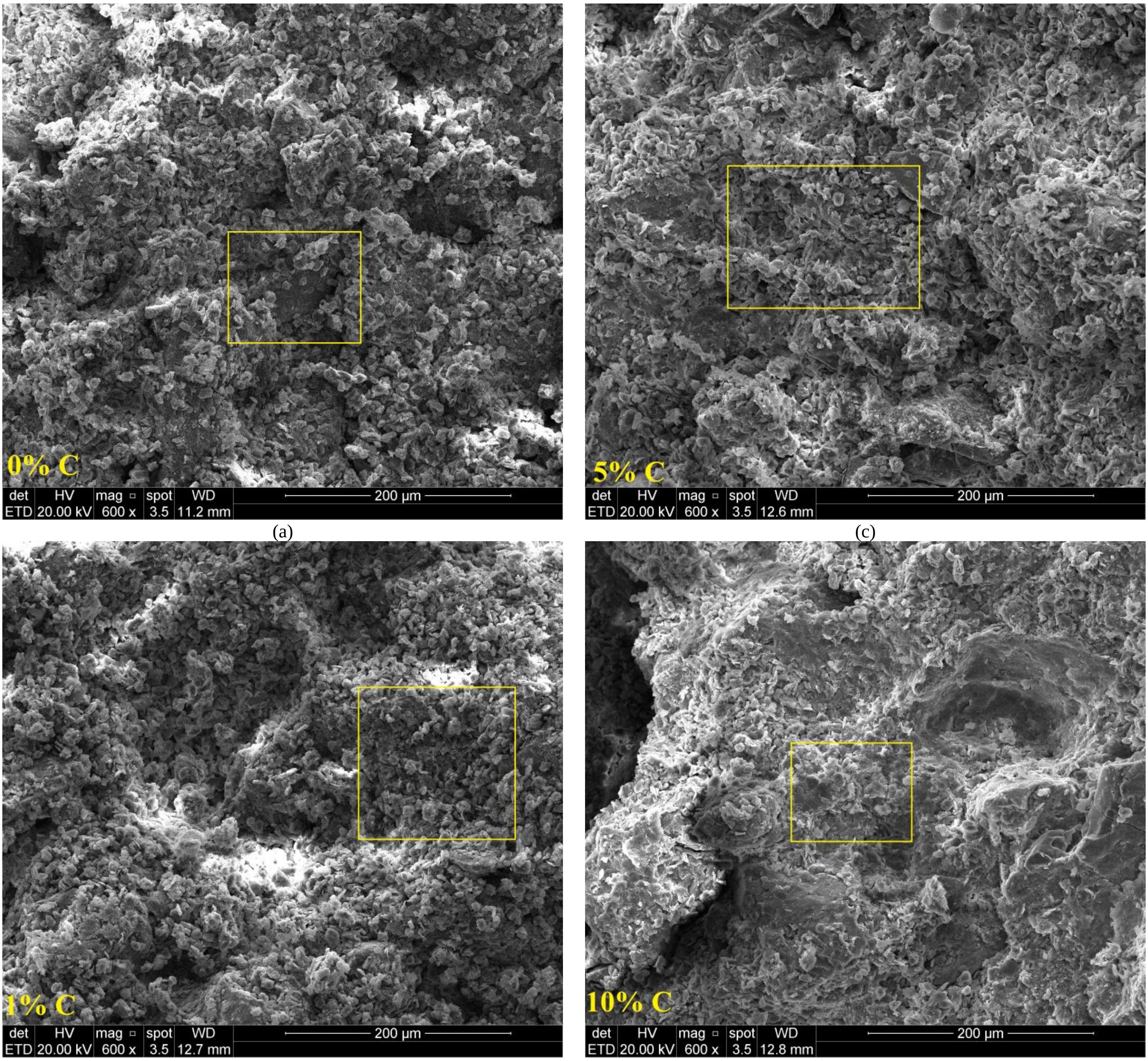

(a) (c)

(b) (d)

Figure 123 – Effect of the cement content magnified 600x (a) 0% (b) 1% (c) 5% (d) 10%

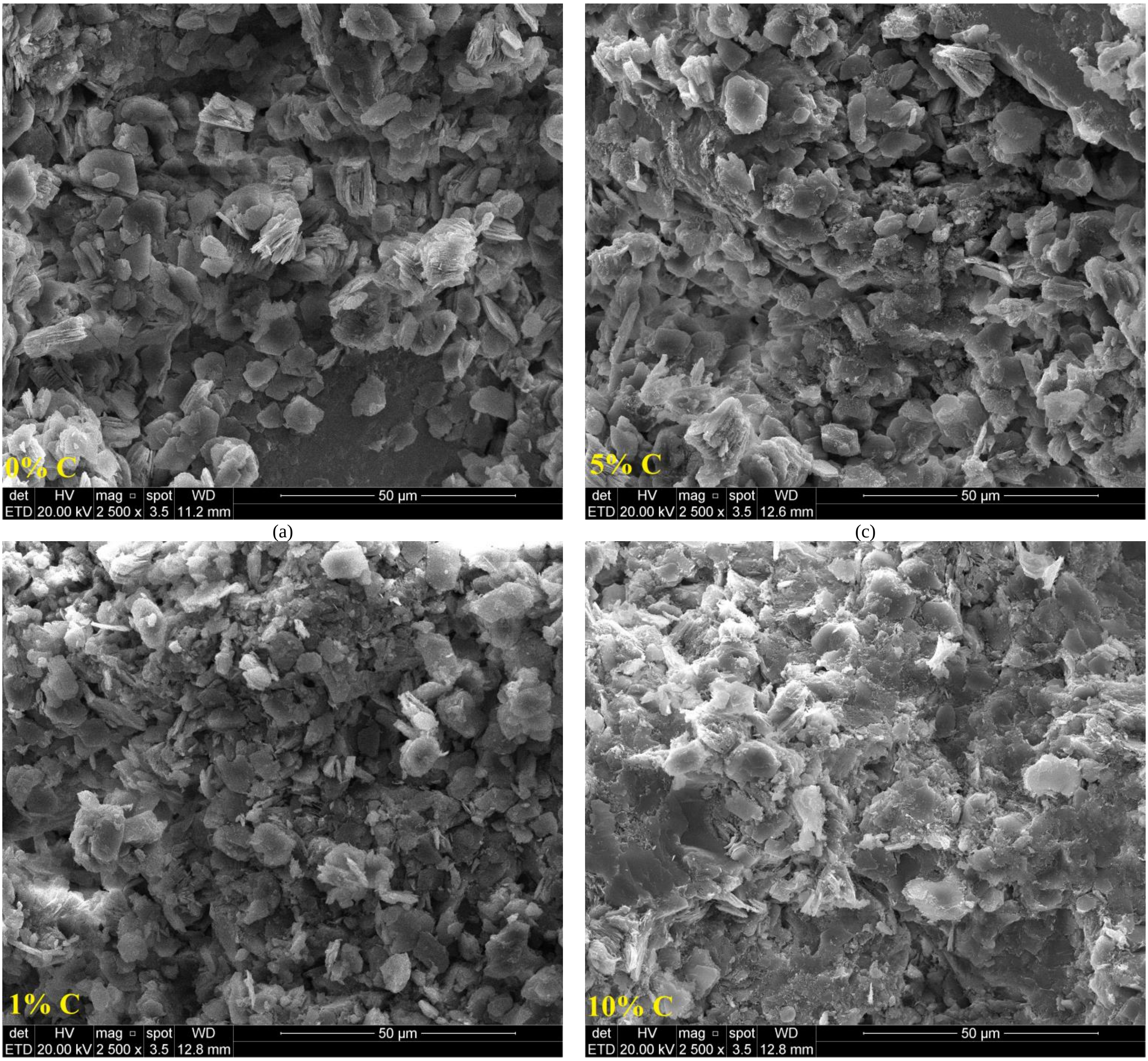

(a) (c)

(b) (d)

Figure 124 - Effect of the cement content magnified 2500x (a) 0% (b) 1% (c) 5% (d) 10%

5.5.2 Effect of the Porosity

In order to visually assess the effect of the porosity on the compacted BRS-cement samples, the same approach as formerly adopted in the previous section was used herein. As a reason, the SEM micrographs of specimens molded using 1% of cement, but having different dry unit weight values (i.e., 14.87 kN/m³, 16.59 kN/m³, 17.53 kN/m³ and 18.55 kN/m³), are shown in Figure 125 (600x magnification) and Figure 126 (2500x magnification). The yellow squares indicate where the zoom was applied for the 2500x micrographs. As the porosity decreases with the increasing dry unit weight, the kaolinite particles which form the clay matrix appear to be disposed in a slightly more condensed state. That is, these particles seem to be a bit closer to each other for higher dry unit weight values. This is noticeable in Figure 126 that exhibits the results obtained with the 2500x magnification, particularly when comparing the results of a wider range of porosity variation: Fig. 123a (14.87 kN/m³) to Fig. 123d (18.55 kN/m³).

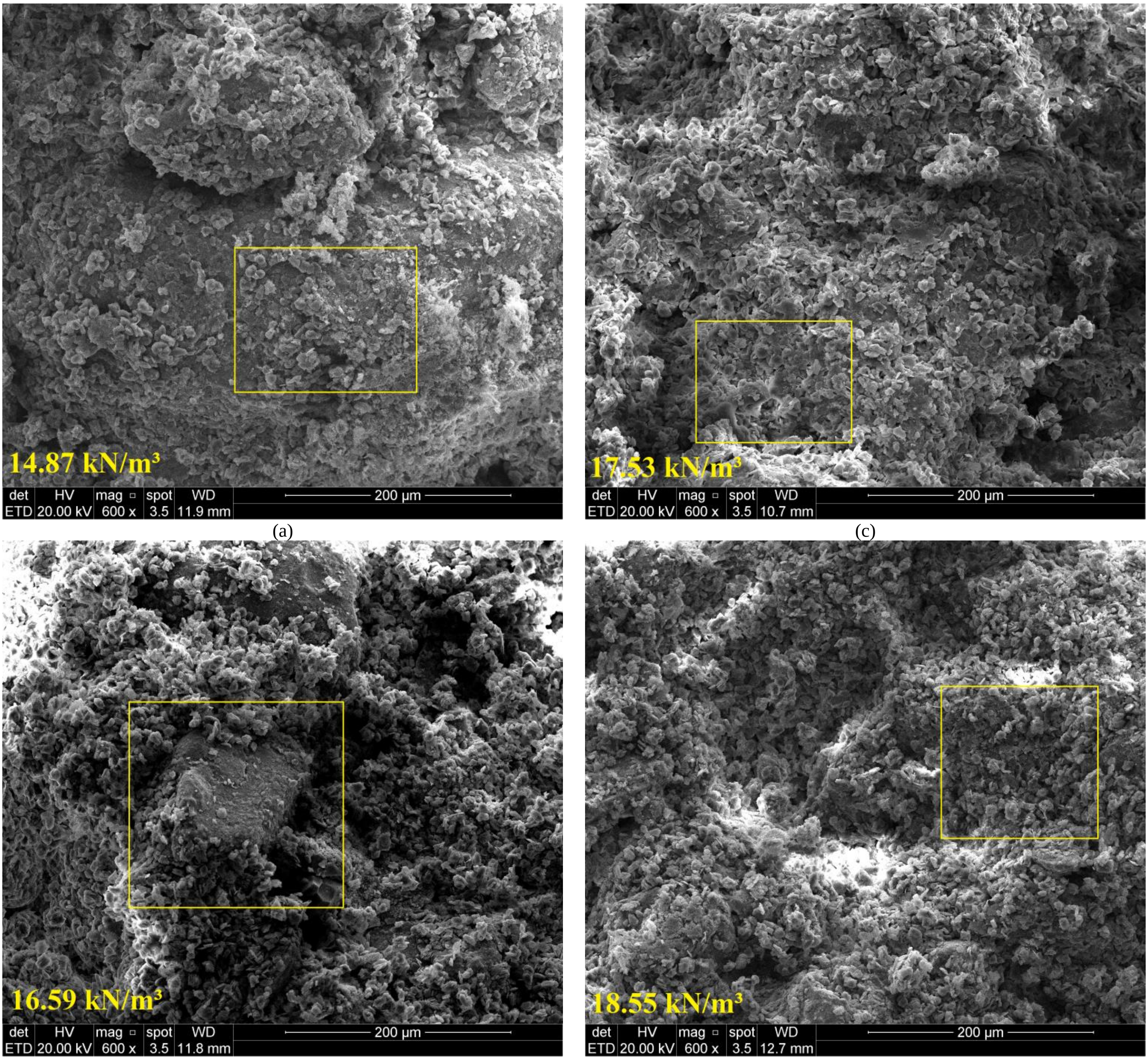

(a) (c)

(b) (d)

Figure 125 - Effect of the compactness magnified 600x (a) 14.87 kN/m³ (b) 16.59 kN/m³ (c) 17.53 kN/m³ (d) 18.55 kN/m³

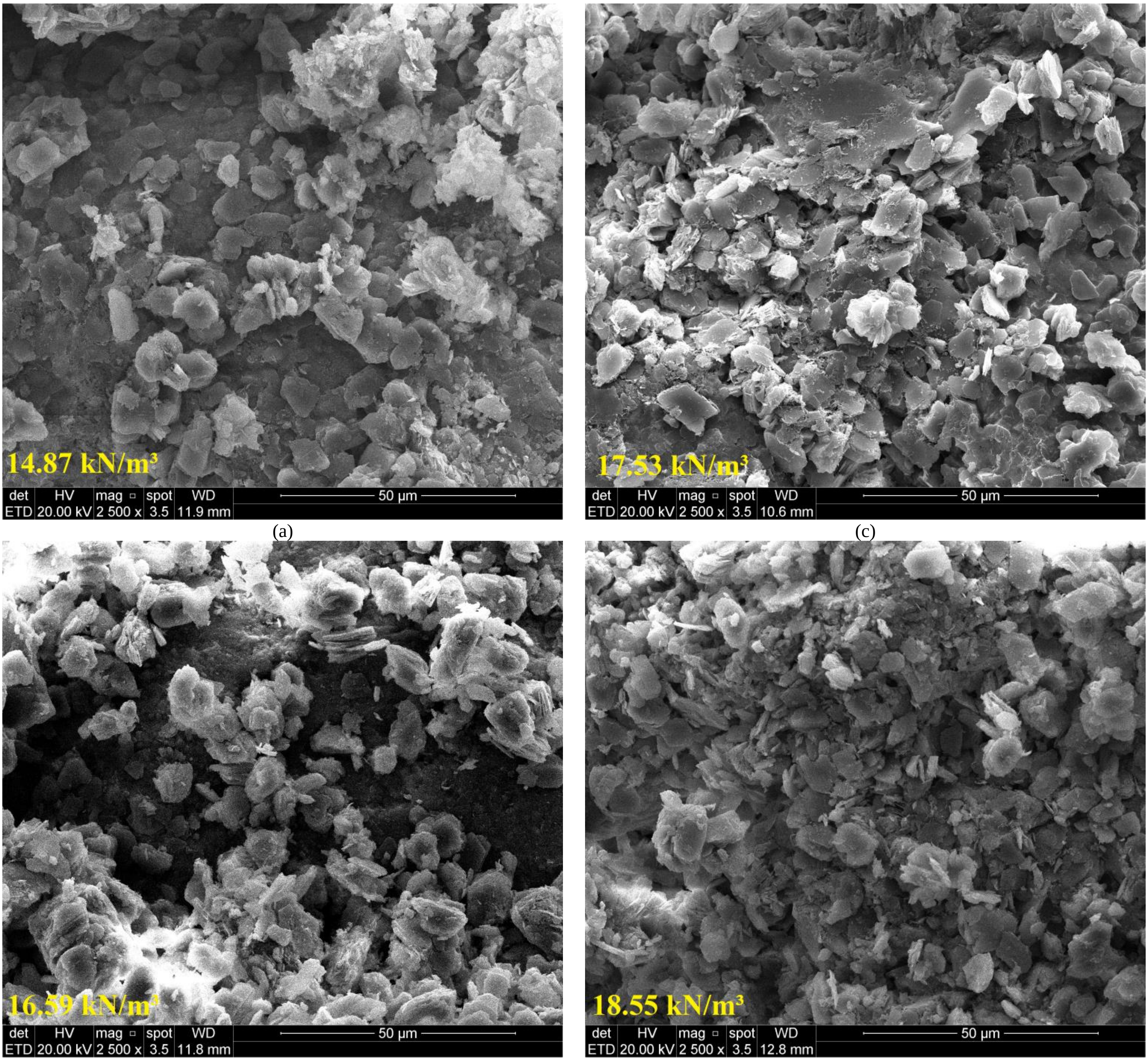

(a) (c)

(b) (d)

Figure 126 - Effect of the compactness magnified 2500x (a) 14.87 kN/m³ (b) 16.59 kN/m³ (c) 17.53 kN/m³ (d) 18.55 kN/m³

5.5.3 Effect of the Adjusted Porosity/Cement Index

The SEM micrographs taken for each one of the tested dosages (see Table 8 at item 3.4) are displayed from Figures 127 to 140. Leastwise, three images having different magnifications rates (600x, 2500x and 5000x) were taken for each tested specimen. In general, fabric differences arising from the dosage's setup, considering the same $\eta/(C_{iv})^{0.28}$ index value, were slightly perceptible and were in accordance to what was discussed in the two previous sections. In brief, the increment in either the amount of cement or in the dry unit weight leads to a more condensed fabrics owing to the creation of a cement matrix that spreads out throughout the clayey matrix, for the first case, or by the decrement on the void's volume in the latter. These occurrences explain the enhancement in the material's performance owing to the decrement in the $\eta/(C_{iv})^{0.28}$ value (e.g., HORPIBULSUK *et al*., 2010). Nonetheless, since one dosage was assembled with a smaller amount of cement and a greater compactness (↓C and ↓η), whereas the other was molded having a higher cement content and a lower density (↑C and ↑η), these differences were visually slight for some $\eta/(C_{iv})^{0.28}$ values, especially amongst the greatest ones ($\eta/(C_{iv})^{0.28} = 45$, 40 and 35). In those, the utilized amounts of cement were relatively small and, when combined with a small dry unit weight value, impedes a proper visualization of its effect on the soil fabrics. Considering lower $\eta/(C_{iv})^{0.28}$ values, made up by lesser porous dosages having greater cement contents, the visual differences arising from the mix design were more evidenced (e.g., Figure 137 and 138, $\eta/(C_{iv})^{0.28} = 22.5$).

The effect of the $\eta/(C_{iv})^{0.28}$ parameter on the soil' fabrics is more evidenced when comparisons are made between distinct dosages molded having different $\eta/(C_{iv})^{0.28}$ values. For example, when comparing the 14.87 kN/m³ - 2%C specimen ($\eta/(C_{iv})^{0.28} = 45$ and Figure 128) to the 17.81 kN/m³ - 8%C sample ($\eta/(C_{iv})^{0.28} = 22.5$ and Figure 138), it is clear that both the increment in the cement content and in the compactness have led to a greater proximity between the soil' particles and, as well, to the development of a more condensed structure due to the higher amount of cement. In addition, it appears that cement contents above 6% were responsible to further alterations in the original soil fabrics. That is, it is visually perceptible the diminishing of pore spaces and a more homogeneous fabrics owing to the presence of greater amounts of cement presented in more compacted samples. Moreover, further fabrics alterations are expected for higher curing periods (e.g., MITCHEL & EL JACK, 1966 HORPIBULSUK *et al*., 2010).

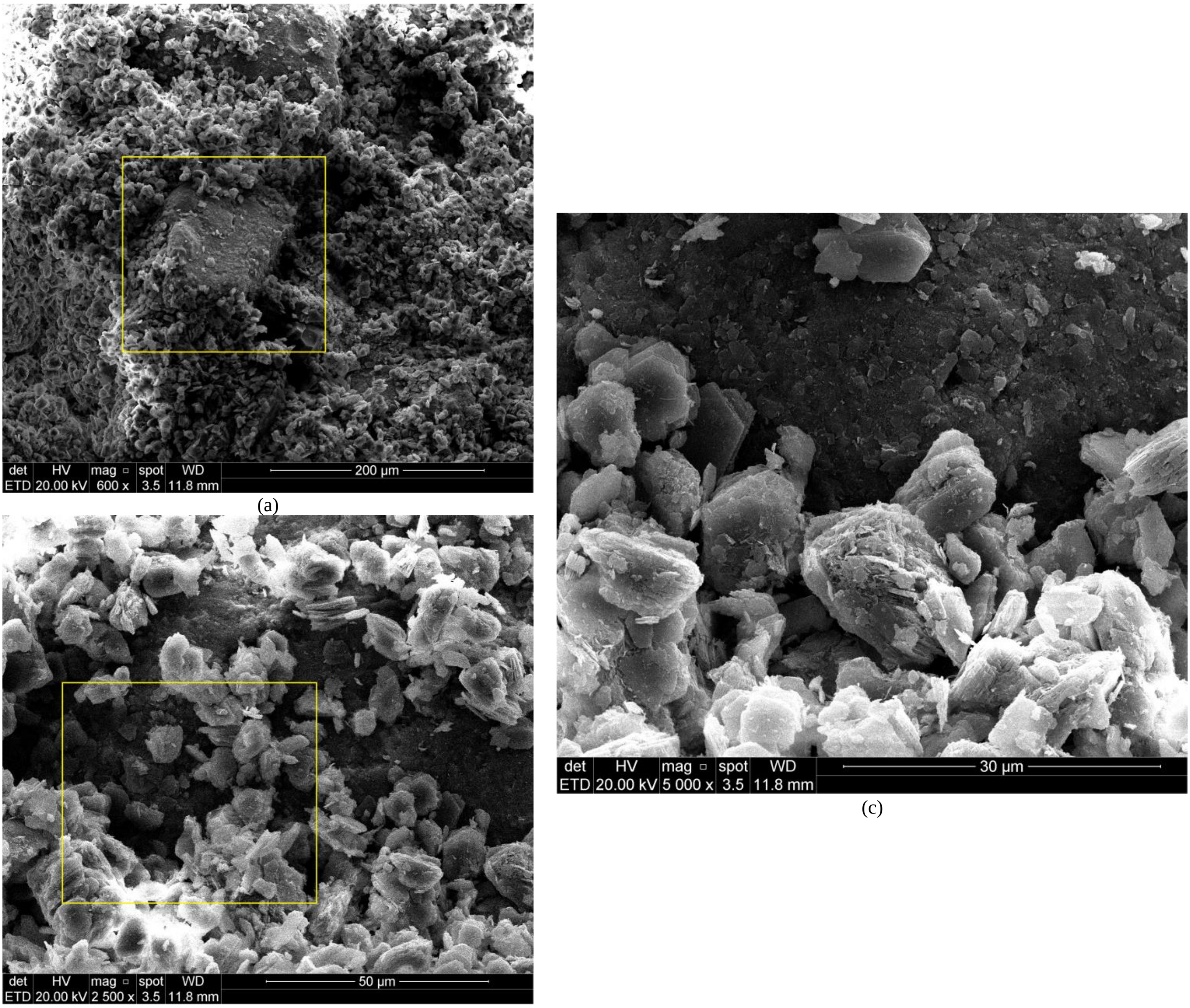

(a)

(b)

(c)

Figure 127 – SEM images for $\eta/(C_{iv})^{0.28}$ = 45, 16.59 kN/m³ - 1%C and magnifications of (a) 600x (b) 2500x (c) 5000x

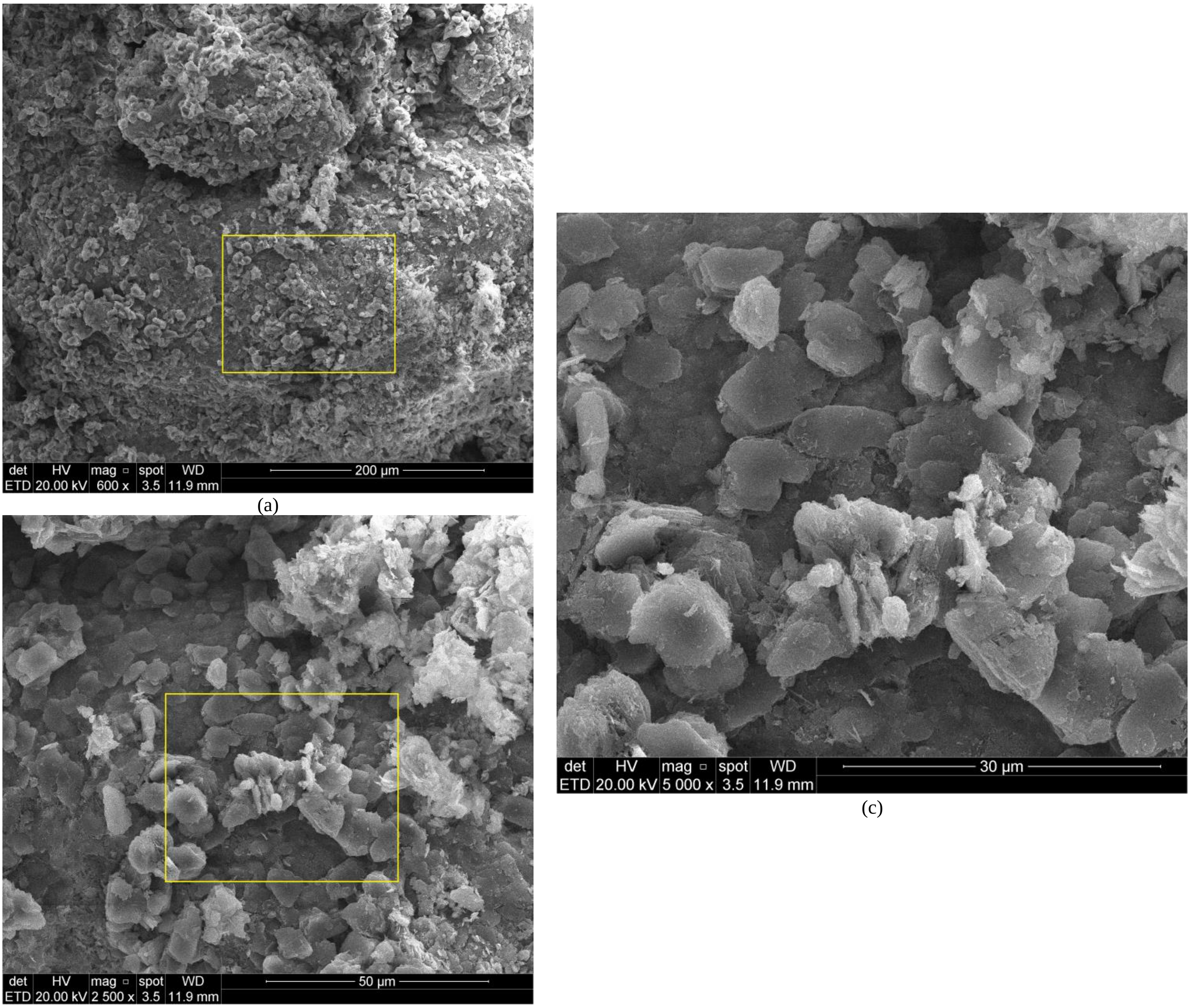

(a)

(b)

(c)

Figure 128 – SEM images for $\eta/(C_{iv})^{0.28}$ = 45, 14.87 kN/m³ - 2%C and magnifications of (a) 600x (b) 2500x (c) 5000x

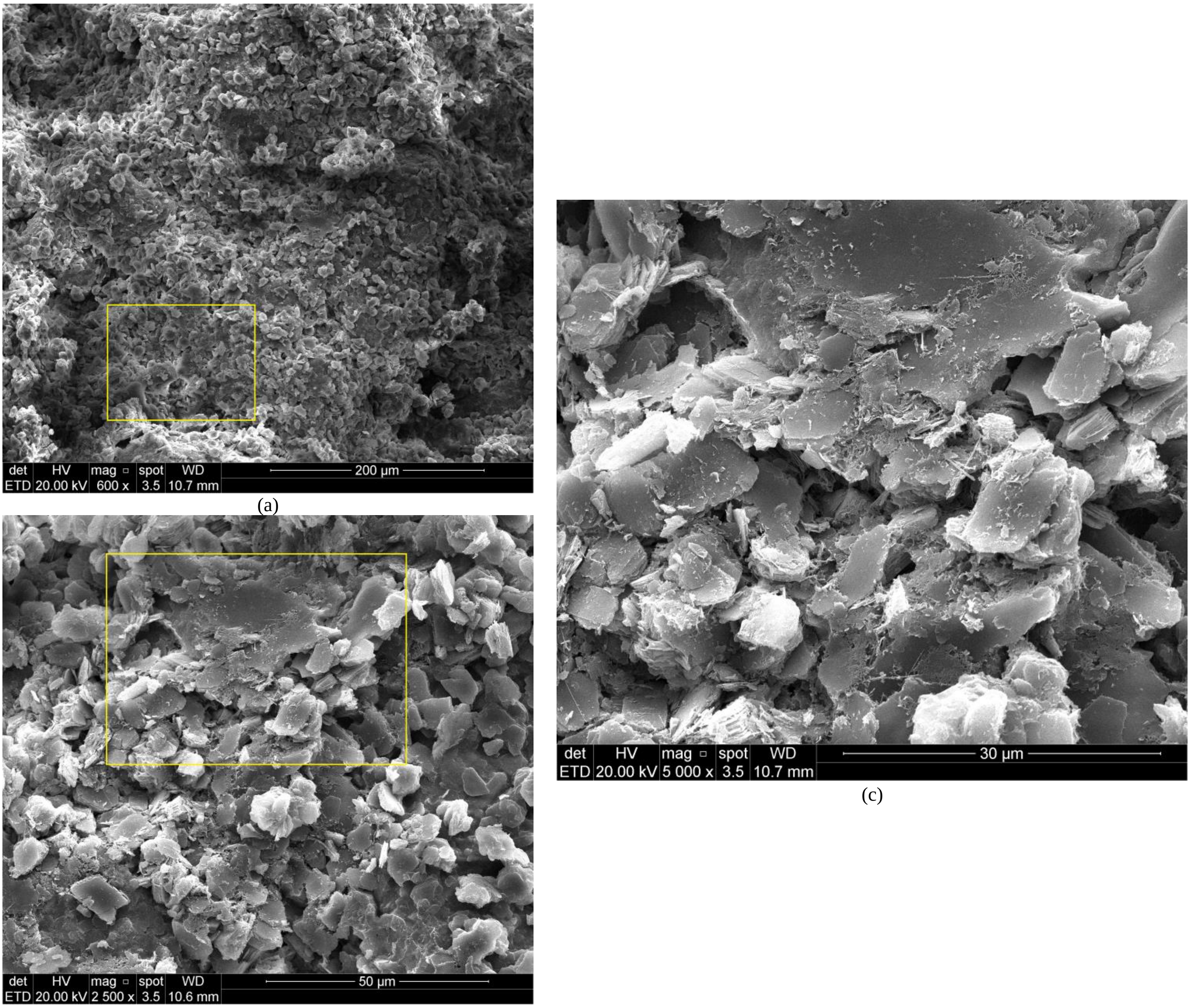

(a)

(b)

(c)

Figure 129 – SEM images for $\eta/(C_{iv})^{0.28}$ = 40, 17.53 kN/m³ - 1%C and magnifications of (a) 600x (b) 2500x (c) 5000x

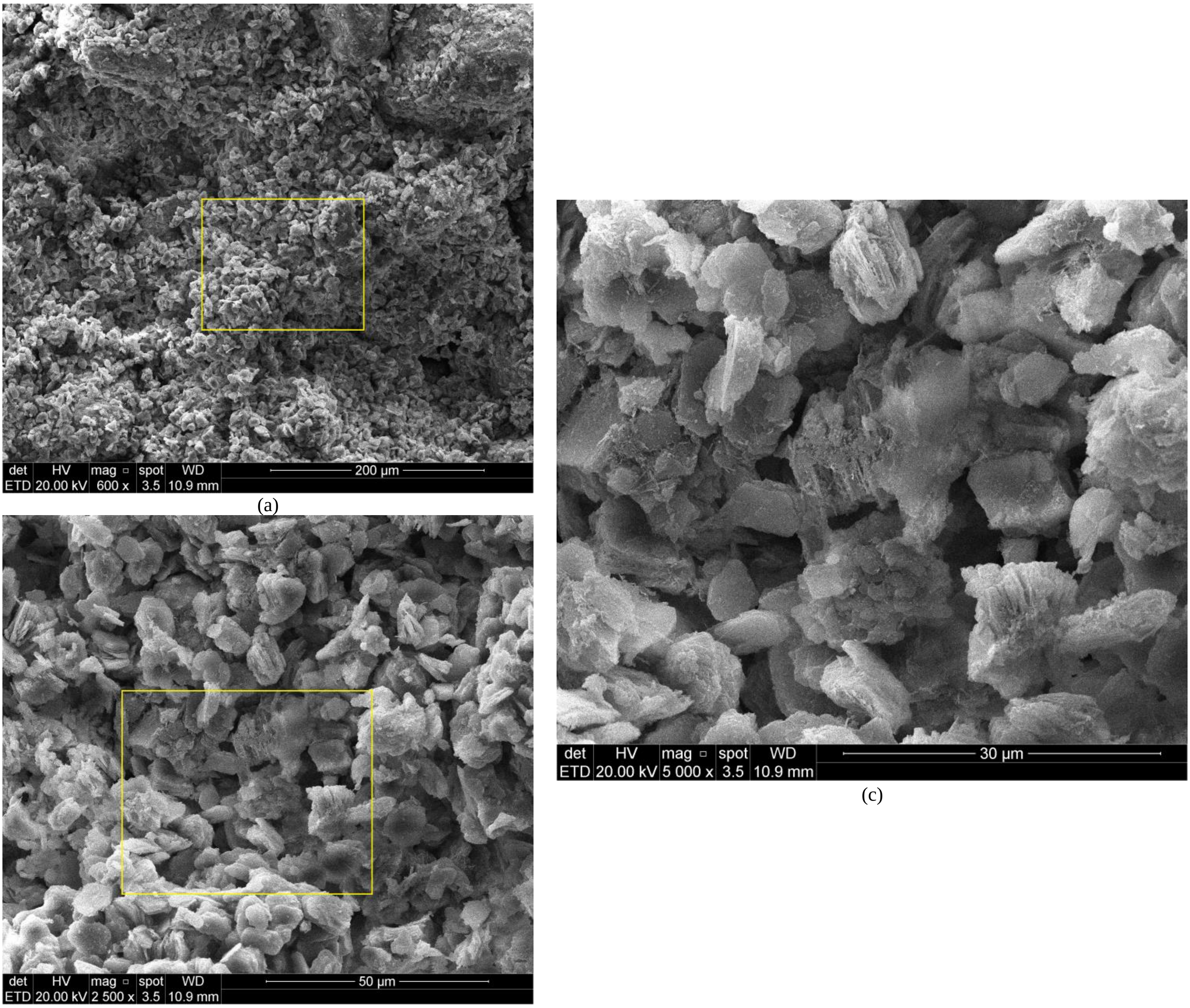

(a)

(b)

(c)

Figure 130 – SEM images for $\eta/(C_{iv})^{0.28}$ = 40, 14.96 kN/m³ - 3%C and magnifications of (a) 600x (b) 2500x (c) 5000x

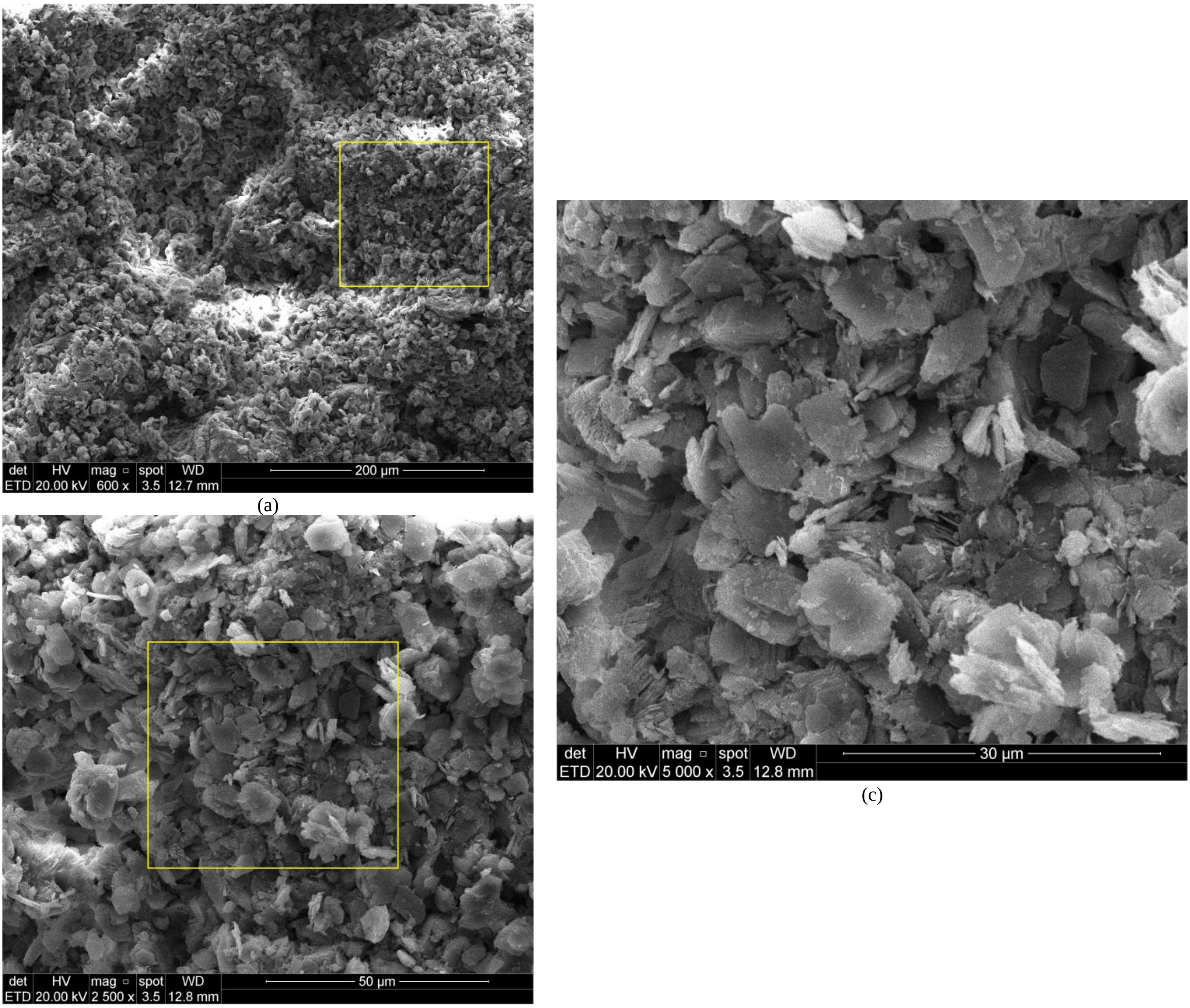

(a)

(b)

(c)

Figure 131 – SEM images for $\eta/(C_{iv})^{0.28}$ = 35, 18.55 kN/m³ - 1%C and magnifications of (a) 600x (b) 2500x (c) 5000x

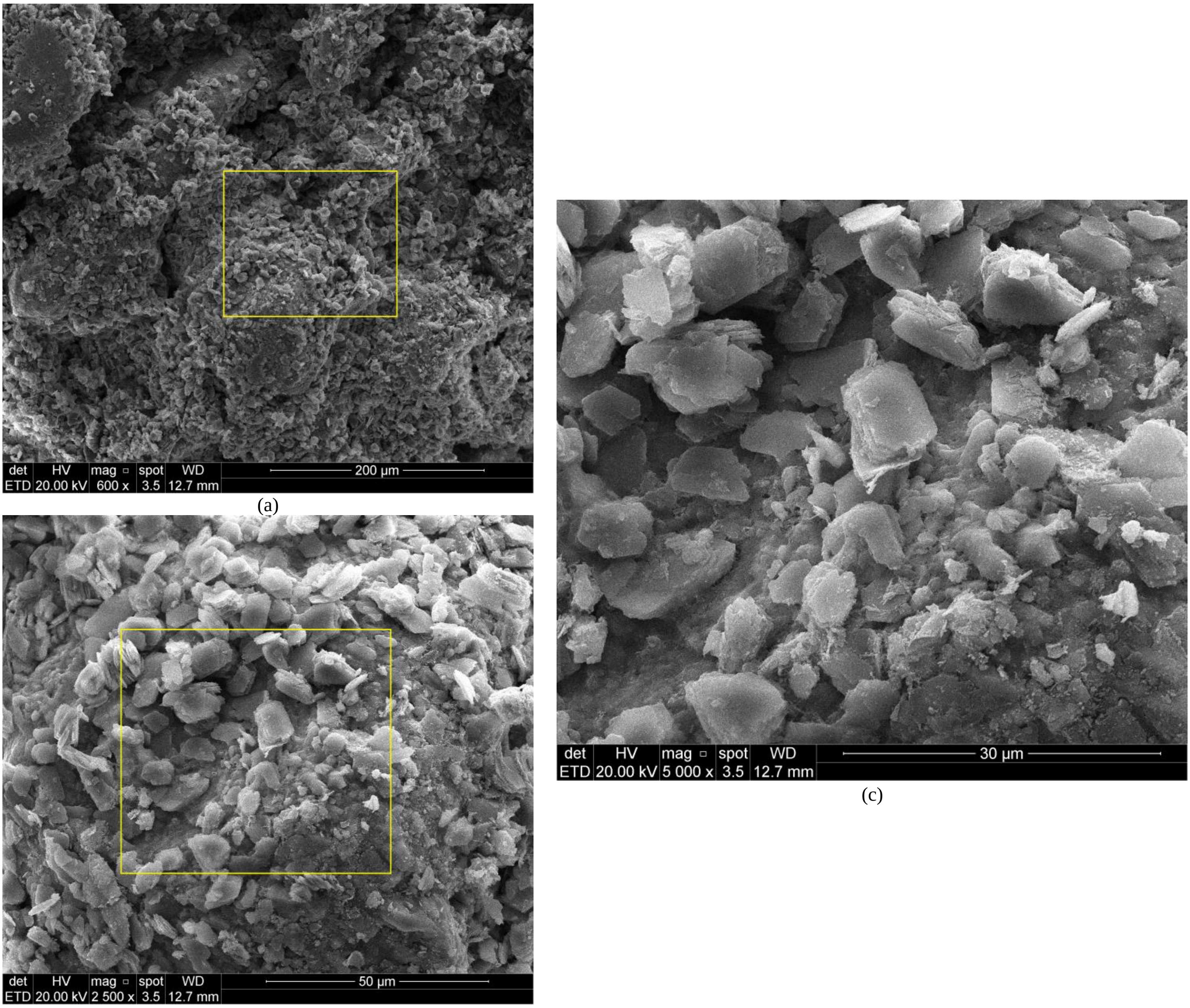

(a)

(b)

(c)

Figure 132 – SEM images for $\eta/(C_{iv})^{0.28}$ = 35, 14.96 kN/m³ - 5%C and magnifications of (a) 600x (b) 2500x (c) 5000x

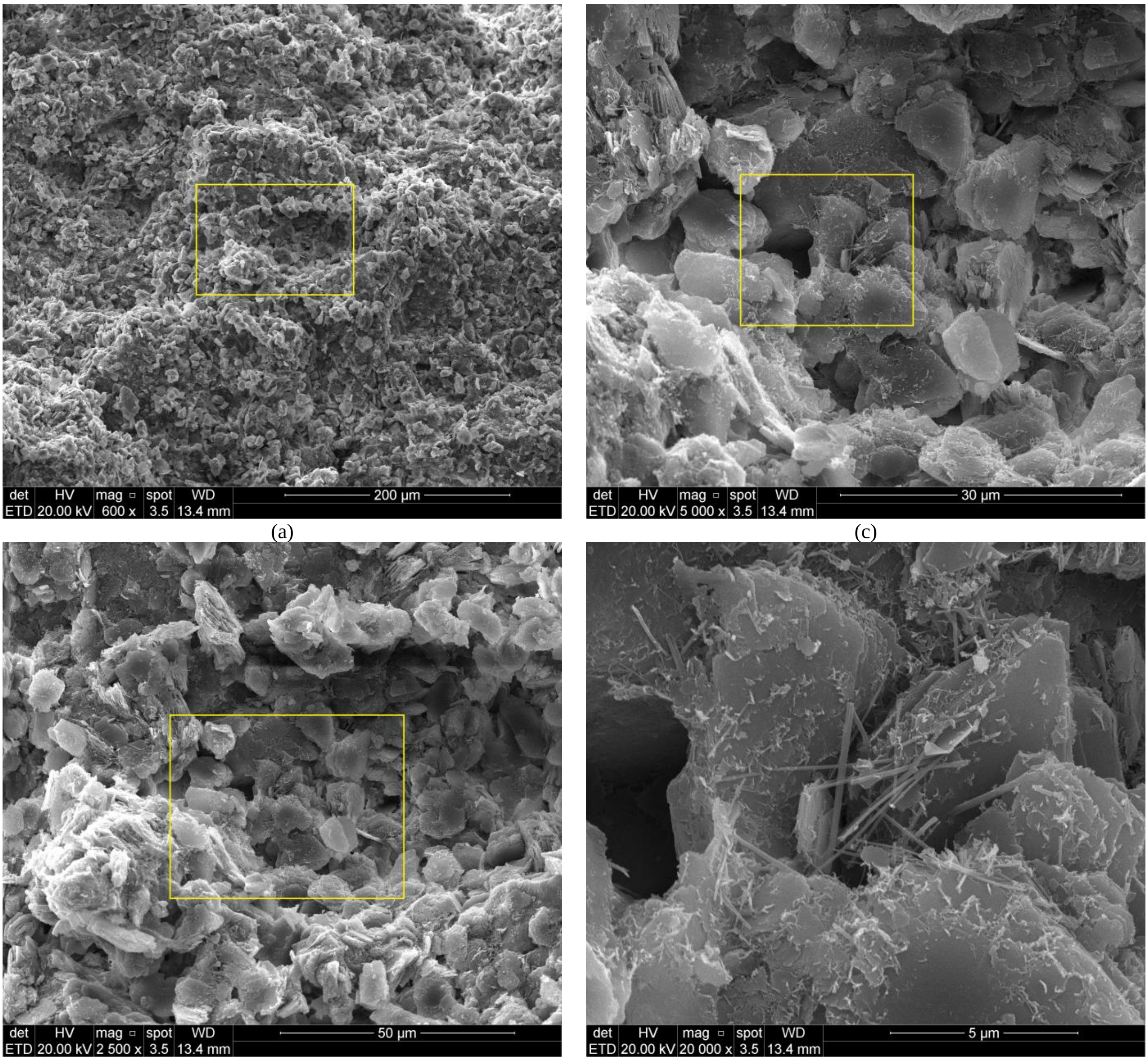

(a) (c)

(b) (d)

Figure 133 – SEM images for $\eta/(C_{iv})^{0.28}$ = 30, 18.31 kN/m³ - 2%C and magnifications of (a) 600x (b) 2500x (c) 5000x (d) 20000x

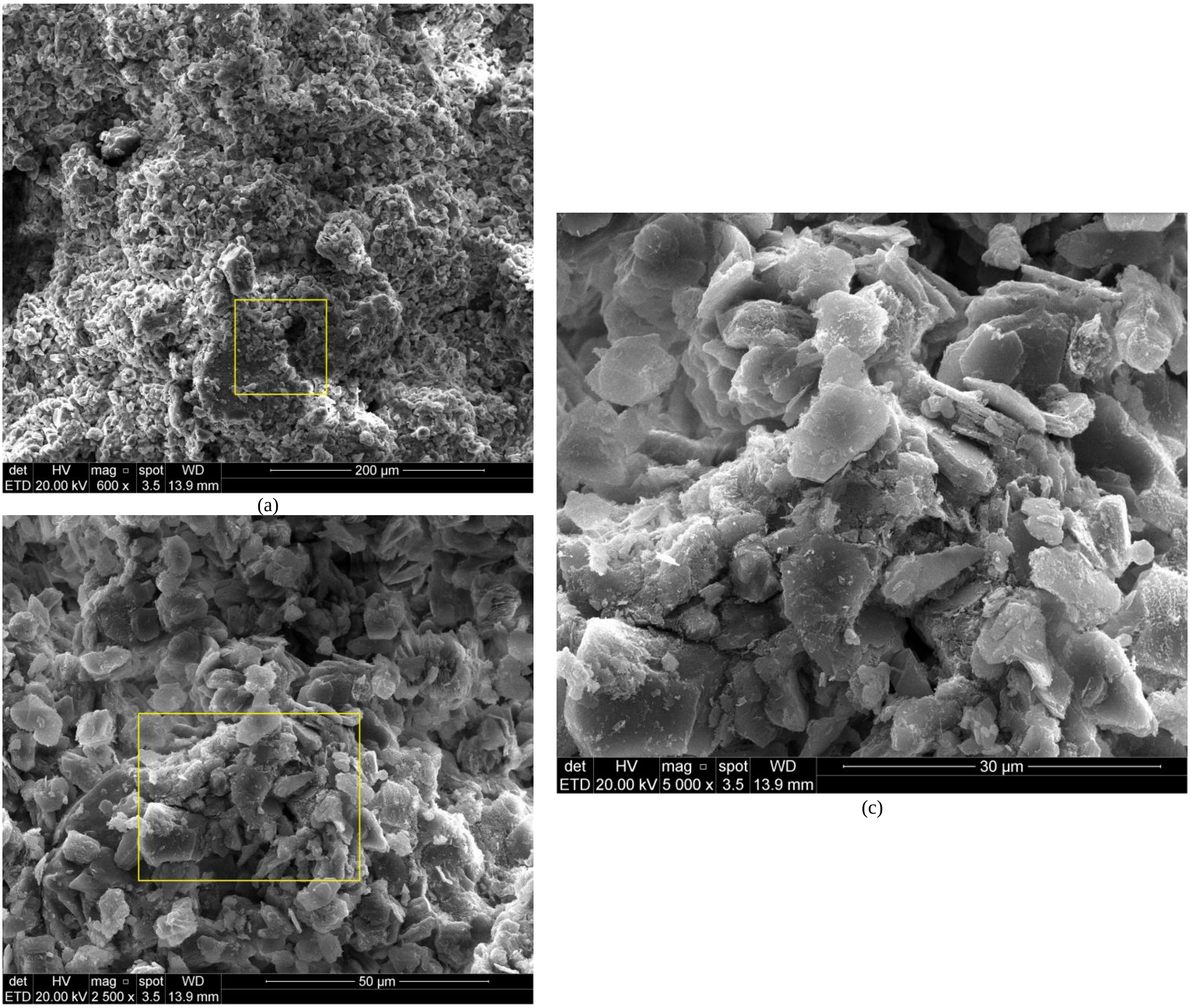

(a)

(b)

(c)

Figure 134 – SEM images for $\eta/(C_{iv})^{0.28}$ = 30, 15.96 kN/m³ - 6%C and magnifications of (a) 600x (b) 2500x (c) 5000x

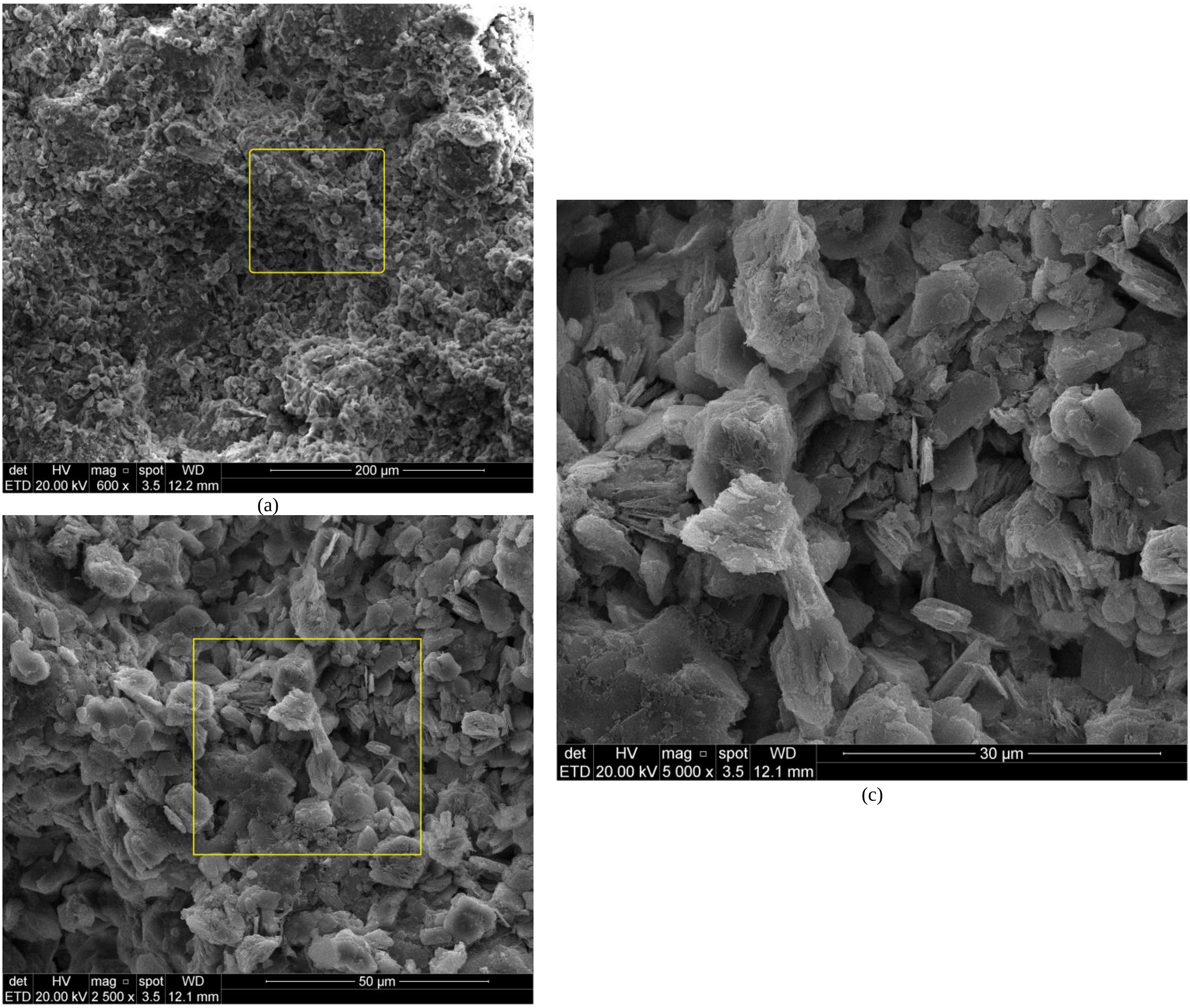

(a)

(b)

(c)

Figure 135 – SEM images for $\eta/(C_{iv})^{0.28}$ = 25, 18.85 kN/m³ - 3%C and magnifications of (a) 600x (b) 2500x (c) 5000x

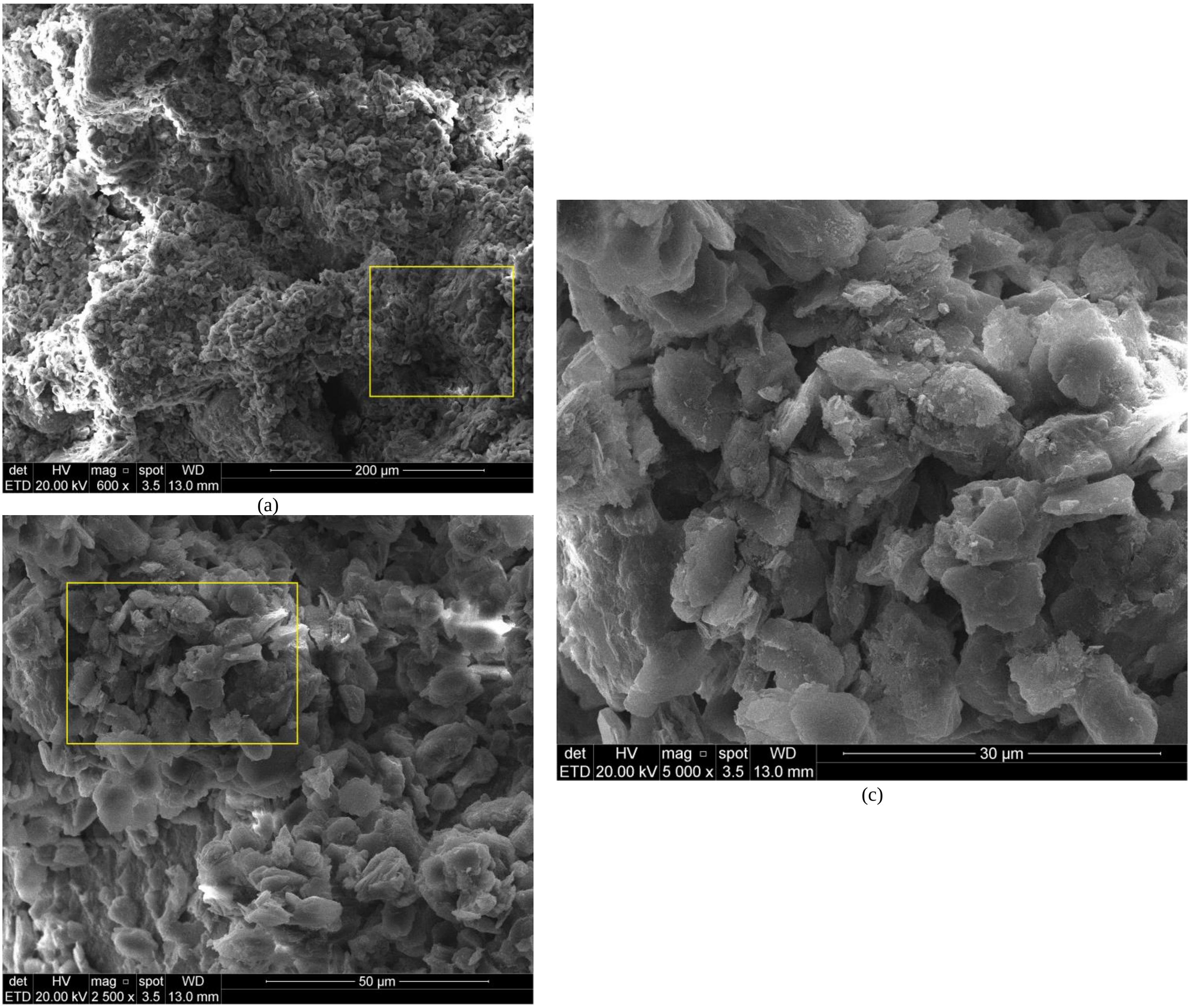

(a)

(b)

(c)

Figure 136 – SEM images for $\eta/(C_{iv})^{0.28} = 25$, 16.94 kN/m³ - 8%C and magnifications of (a) 600x (b) 2500x (c) 5000x

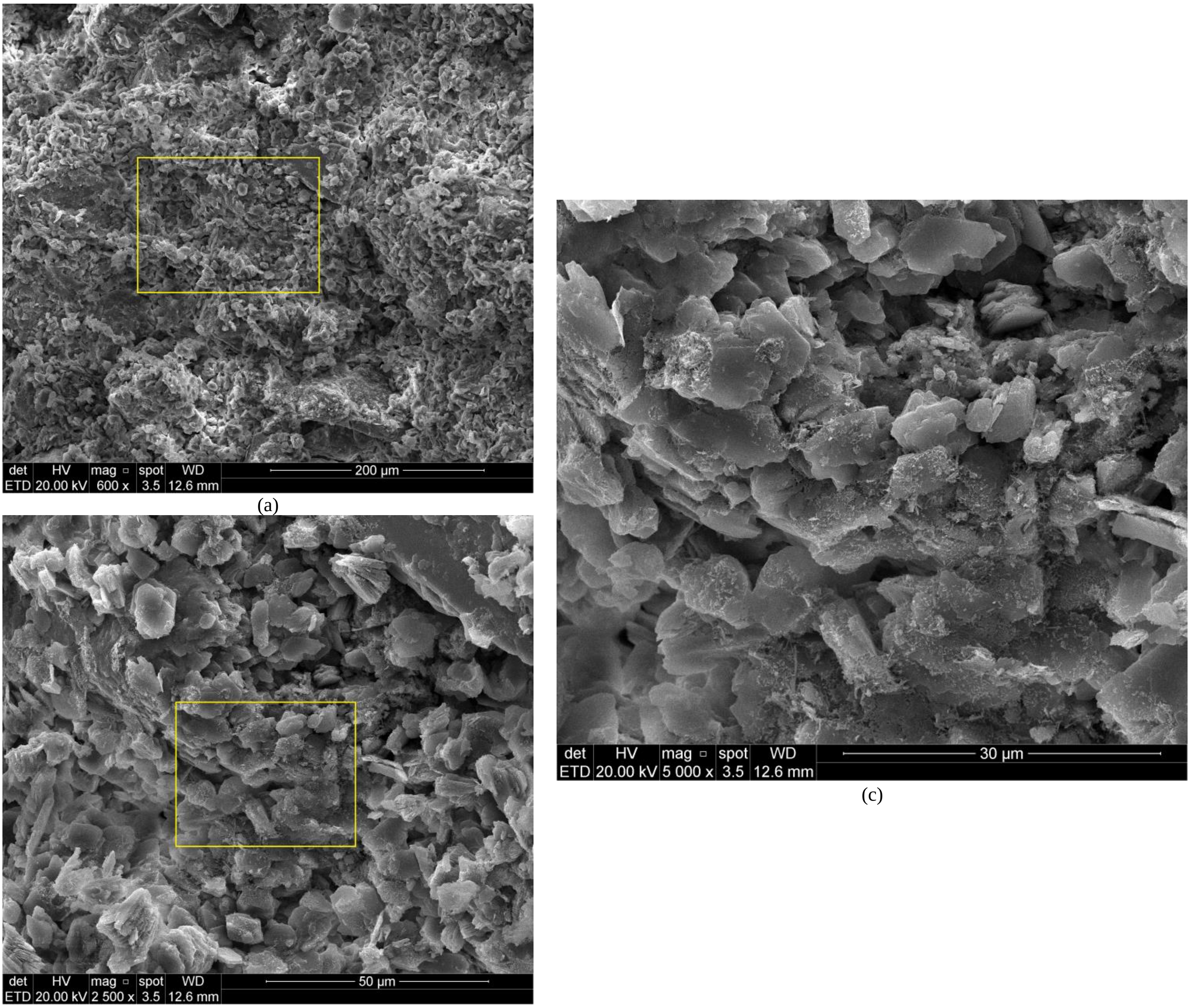

(a)

(b)

(c)

Figure 137 – SEM images for $\eta/(C_{iv})^{0.28}$ = 22.5, 18.67 kN/m³ - 5%C and magnifications of (a) 600x (b) 2500x (c) 5000x

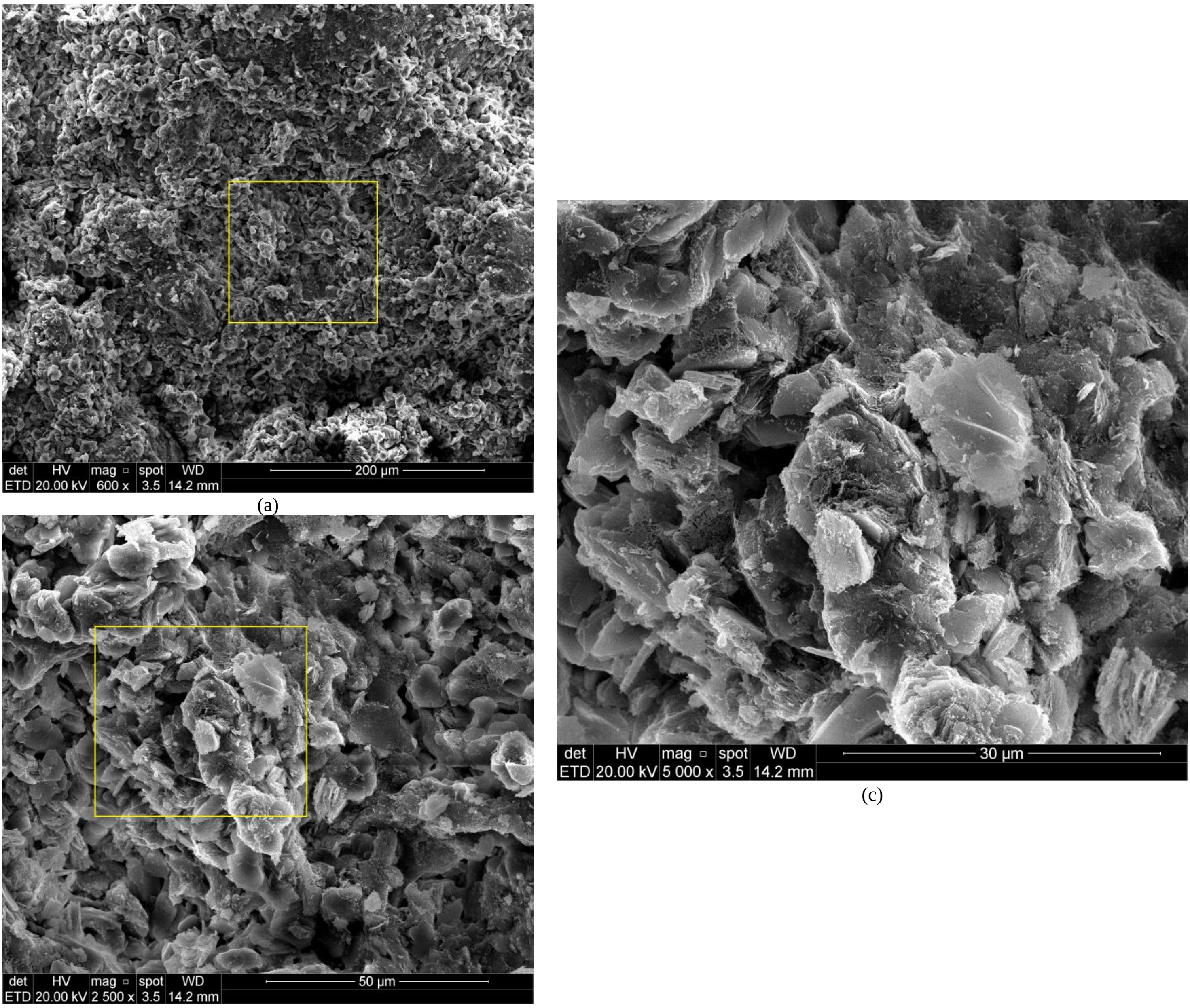

(a)

(b)

(c)

Figure 138 – SEM images for $\eta/(C_{iv})^{0.28} = 22.5$, $17.81\ \mathrm{kN/m^3}$ - 8%C and magnifications of (a) 600x (b) 2500x (c) 5000x

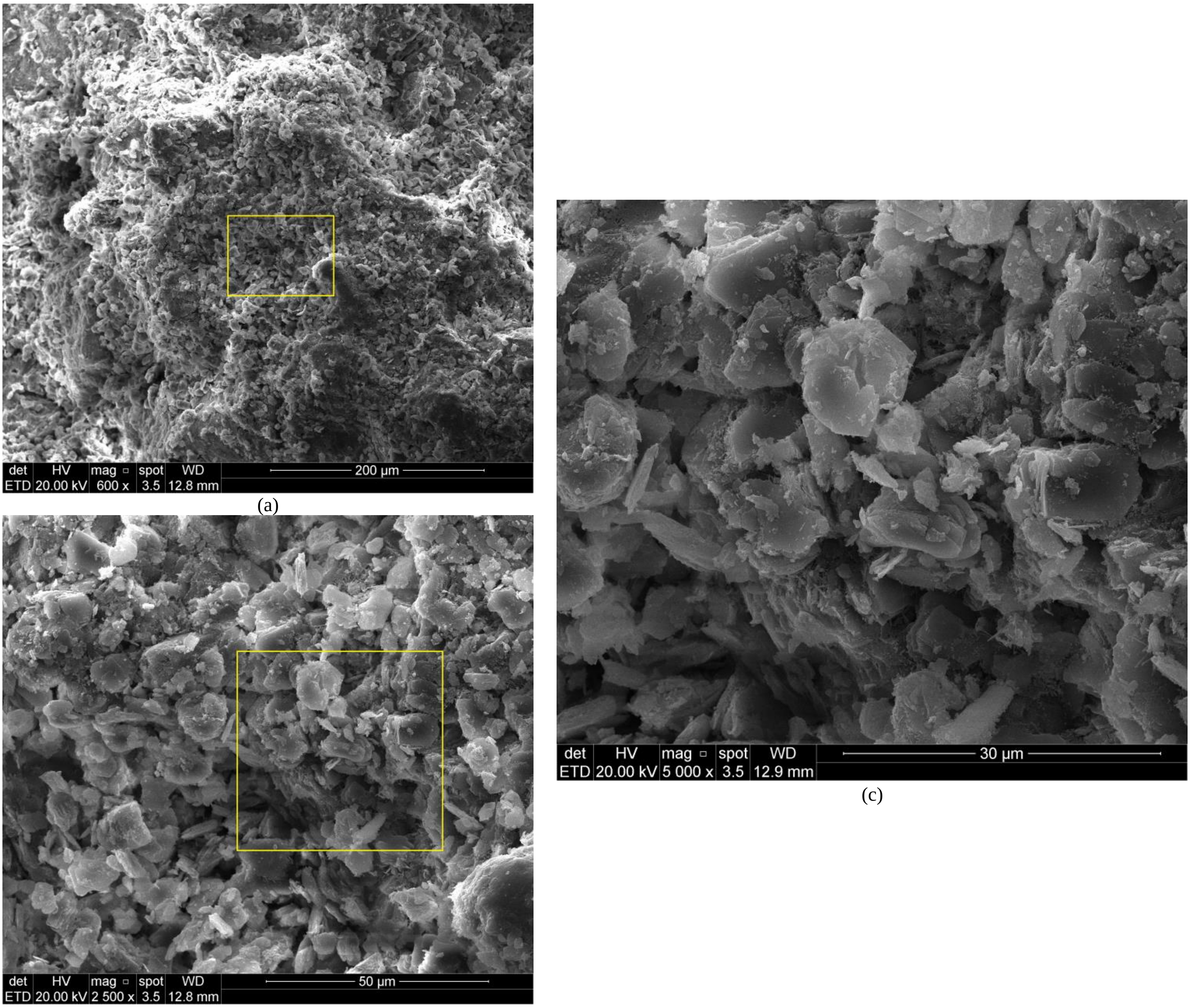

(a)

(b)

(c)

Figure 139 – SEM images for $\eta/(C_{iv})^{0.28} = 20$, 19.04 kN/m³ - 6.5%C and magnifications of (a) 600x (b) 2500x (c) 5000x

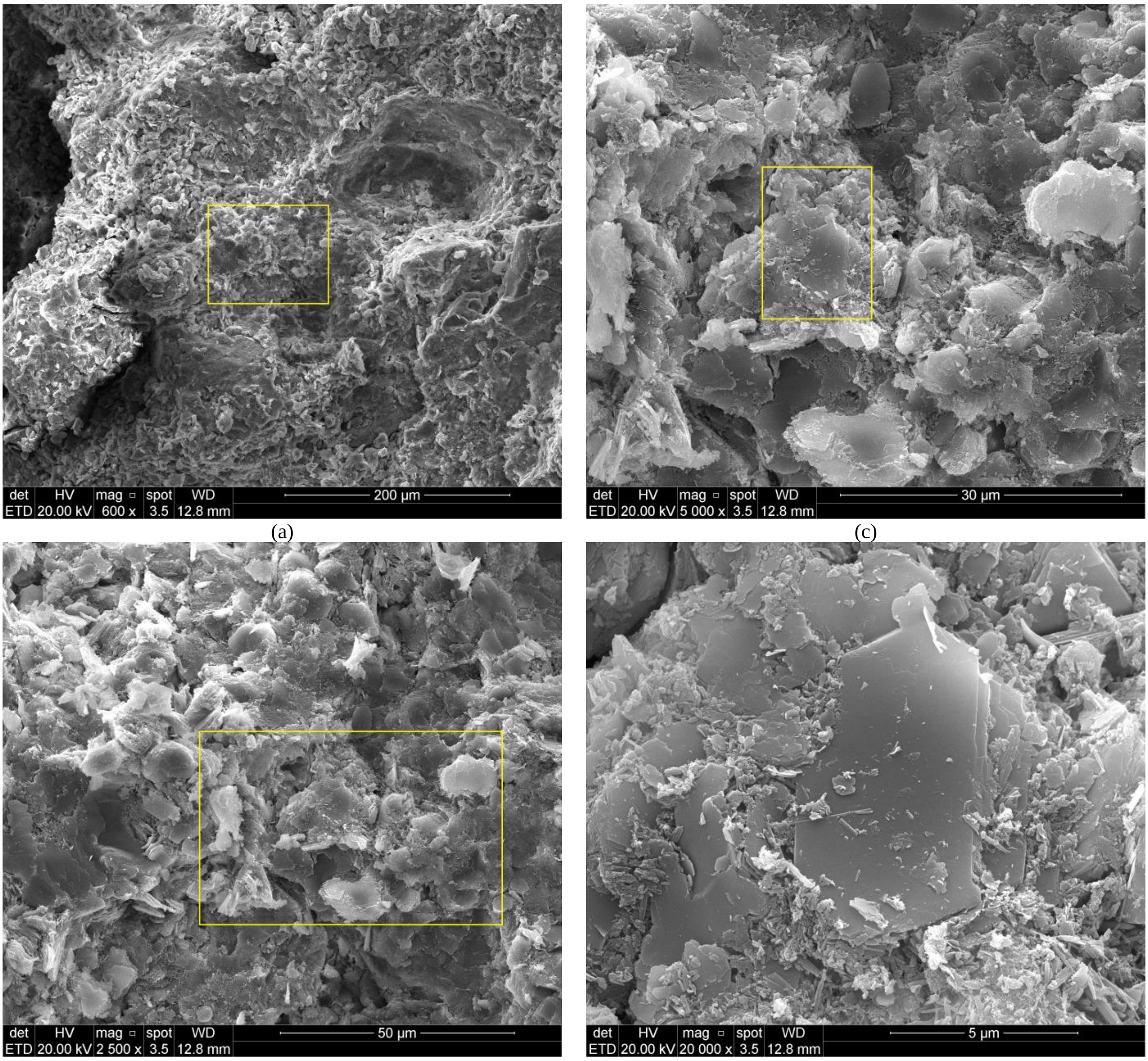

(a) (c)

(b) (d)

Figure 140 – SEM images for $\eta/(C_{iv})^{0.28}$ = 20, 18.32 kN/m³ - 10%C and magnifications of (a) 600x (b) 2500x (c) 5000x (d) 20000x

5.6 MERCURY INTRUSION POROSIMETRY TESTS

The cumulative pore volume distribution and the incremental pore volume distributions are plotted in Figures 141, 142 and 143, and each figure contains the results of a single $\eta/(C_{iv})^{0.28}$ value. The first distribution is the relationship between the sum of pore volume increments (ΔV_i), divided by the cumulative pore volume (V_{cum}), to the pore diameter (d_p), whereas the second relates the pore volume increments (ΔV_i) to d_p. The cumulative distribution is basically an integral and indicates a higher concentration of pore volumes for steeper regions in the V_{cum} versus d_p plot. The incremental pore volume distribution, in turn, basically assigns a determined pore volume increment to a specific pore radius, resembling a histogram. The boundaries between the macropores (d_p > 50nm), mesopores (50 nm > d_p > 3 nm) and micro/super micro (d_p < 3 nm) were based on the unified pore size classification proposed by Zdravkov *et al.* (2007).

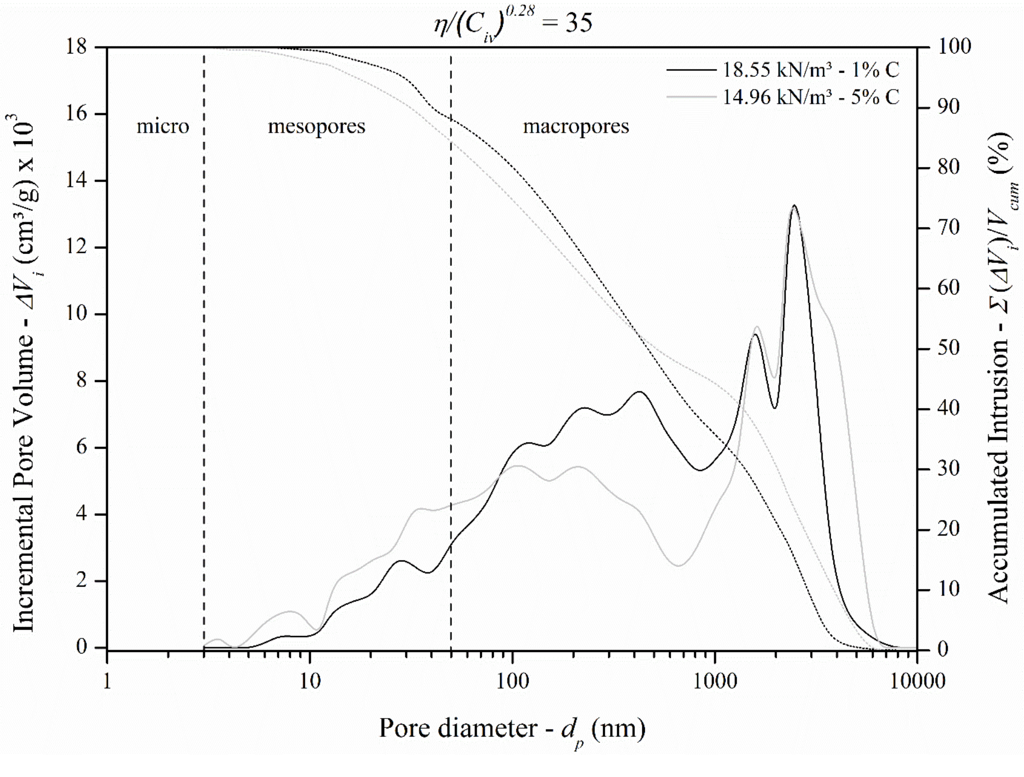

Figure 141 – Incremental PSD and acumulated intrusion for $\eta/(C_{iv})^{0.28}$ = 35

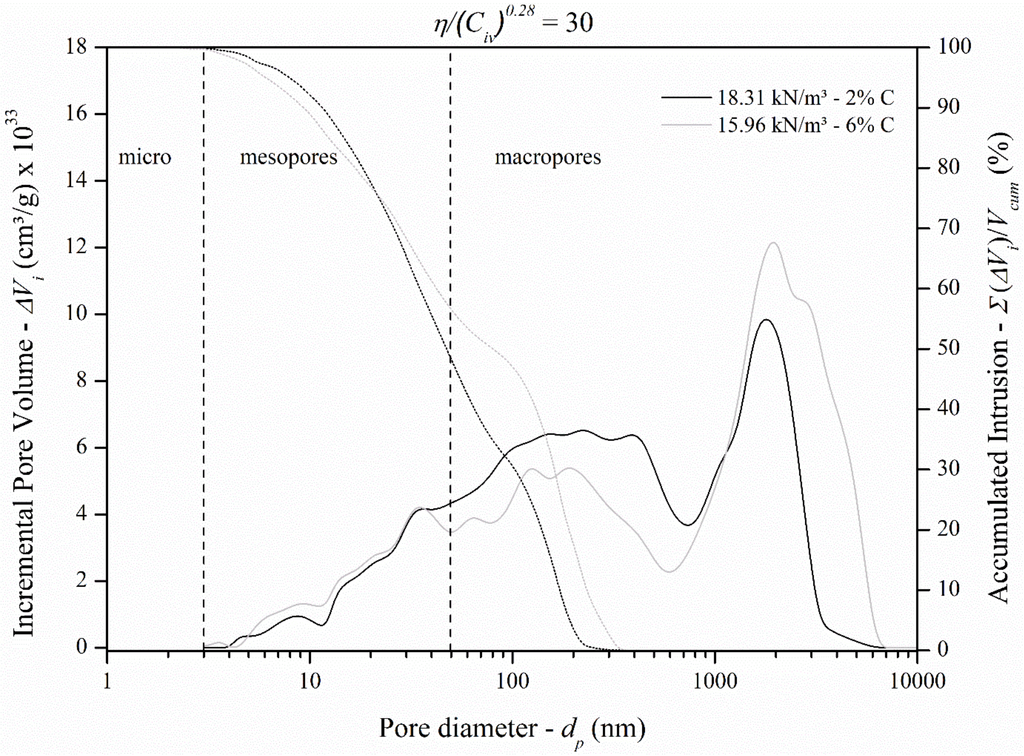

Figure 142 - Incremental PSD and acumulated intrusion for $\eta/(C_{iv})^{0.28} = 30$

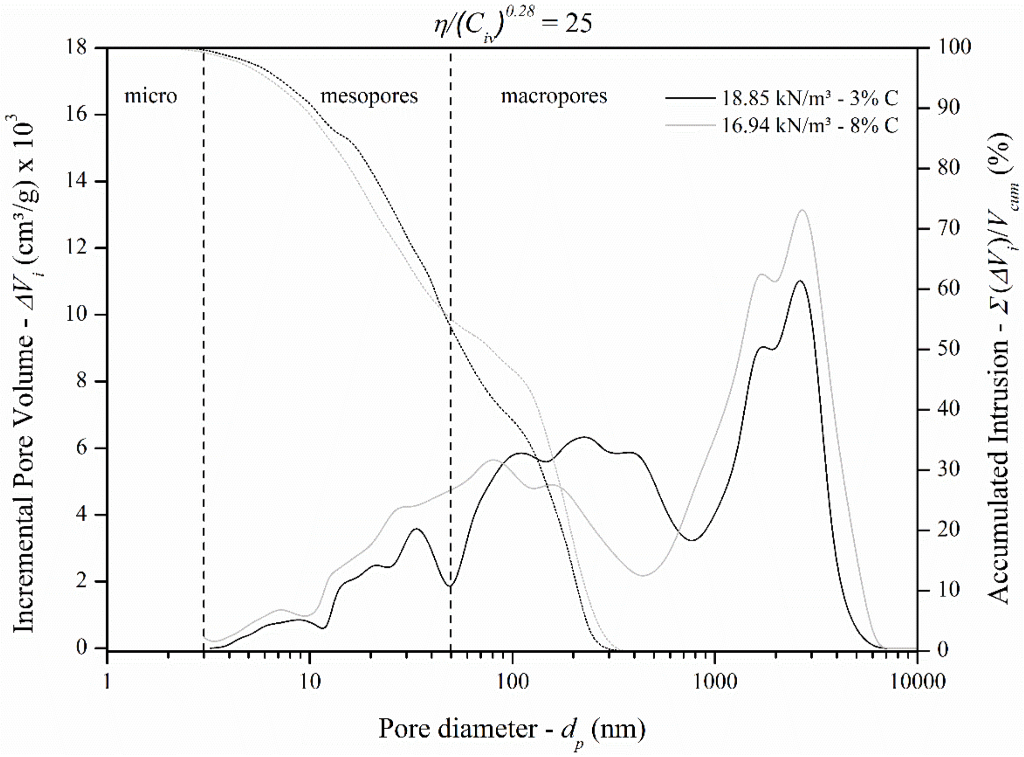

Figure 143 - Incremental PSD and acumulated intrusion for $\eta/(C_{iv})^{0.28} = 25$

From the results presented above, all the tested specimens have exhibited a prominent peak within the macropores region (d_p around 2000-3000 nm), which slightly increases with the increment in the cement content (and increase of porosity) when the results within the same $\eta/(C_{iv})^{0.28}$ value are compared. This trend might be related to the filling of the pores with cement hydration products. Moreover, the most cemented and least dense specimens, considering the same adjusted porosity/cement index, have presented sensible lower ΔV_i values in the range of around 60 nm < d_p < 700 nm. Nonetheless, the overall forms of the incremental distributions were roughly the same, despite the tested dosage and the adopted $\eta/(C_{iv})^{0.28}$. That is, an apparent predominance of pore-sizes in the macropores region, especially for the most cemented specimens within each adjusted porosity/cement index values.

An alternative form of presenting the PSD results is by plotting the incremental pore volume distribution as a function of the pore diameter ($-\Delta V_i/\Delta d_p$ versus d_p). This is a differential pore volume distribution which can be interpreted as a pore volume density and does not present the disadvantage of apparently overemphasizing larger pore volumes as happens in the incremental distribution (MEYER & KLOBES, 1999). In the latter, this occurs because the ordinate values are dependent upon experimental point spacing, thus larger d_p intervals will accumulate greater pore volumes. In this regard, Figures 144, 145 and 146 present the incremental pore volume distributions for the tested specimens and each figure is relative to a single $\eta/(C_{iv})^{0.28}$ value. The volume of pores within certain pore diameter range ($d_{p,a} - d_{p,b}$) can be determined as the area under the curve if a linear d_p-axis is used. In other words, it is the integral between points $d_{p,a}$ and $d_{p,b}$.

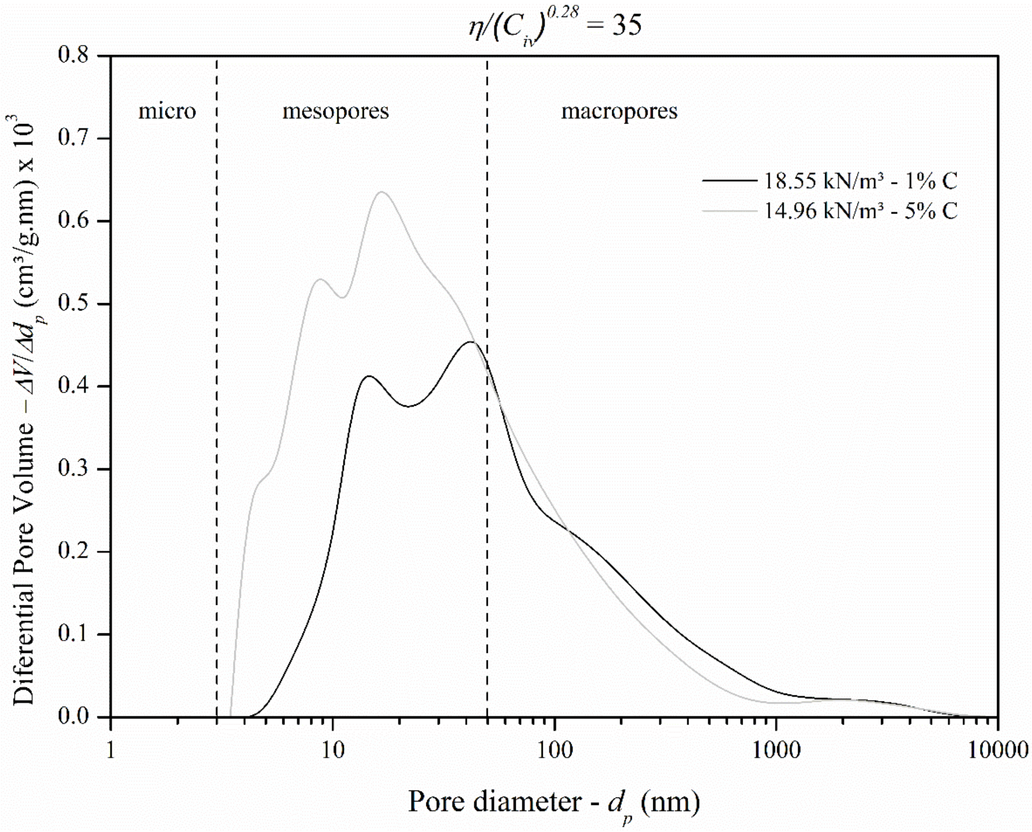

Figure 144 - Differential pore volume distribution for $\eta/(C_{iv})^{0.28} = 35$

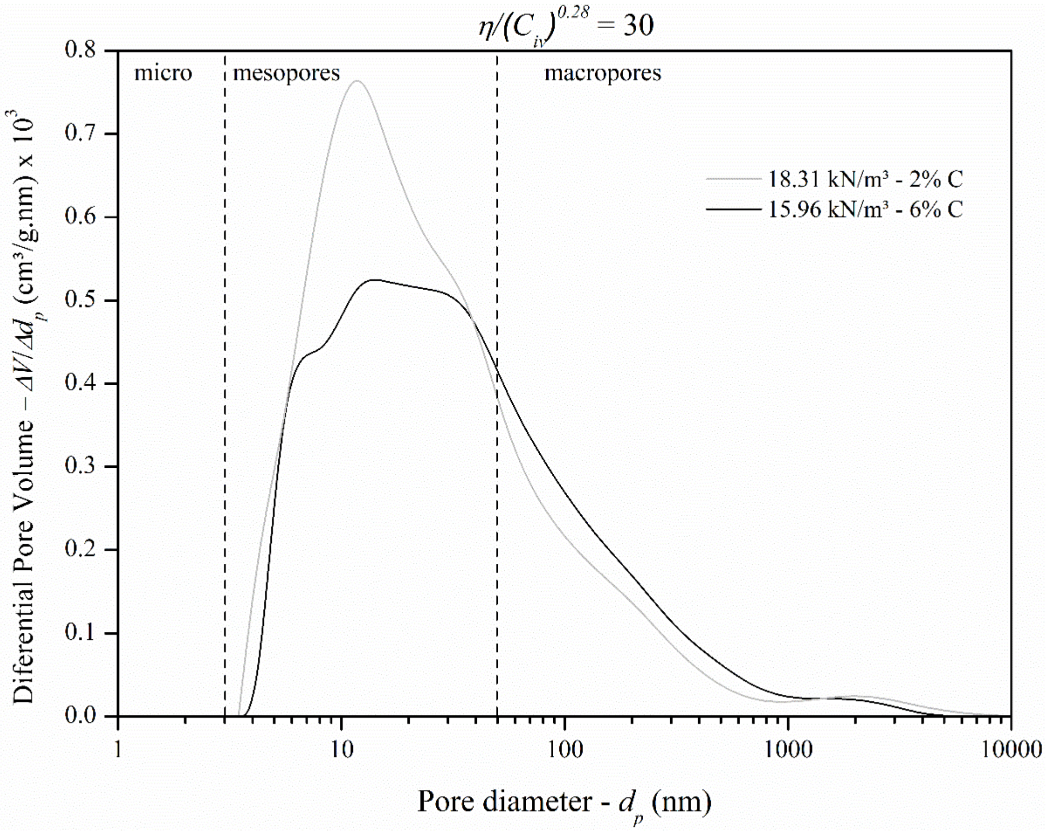

Figure 145 - Differential pore volume distribution for $\eta/(C_{iv})^{0.28} = 30$

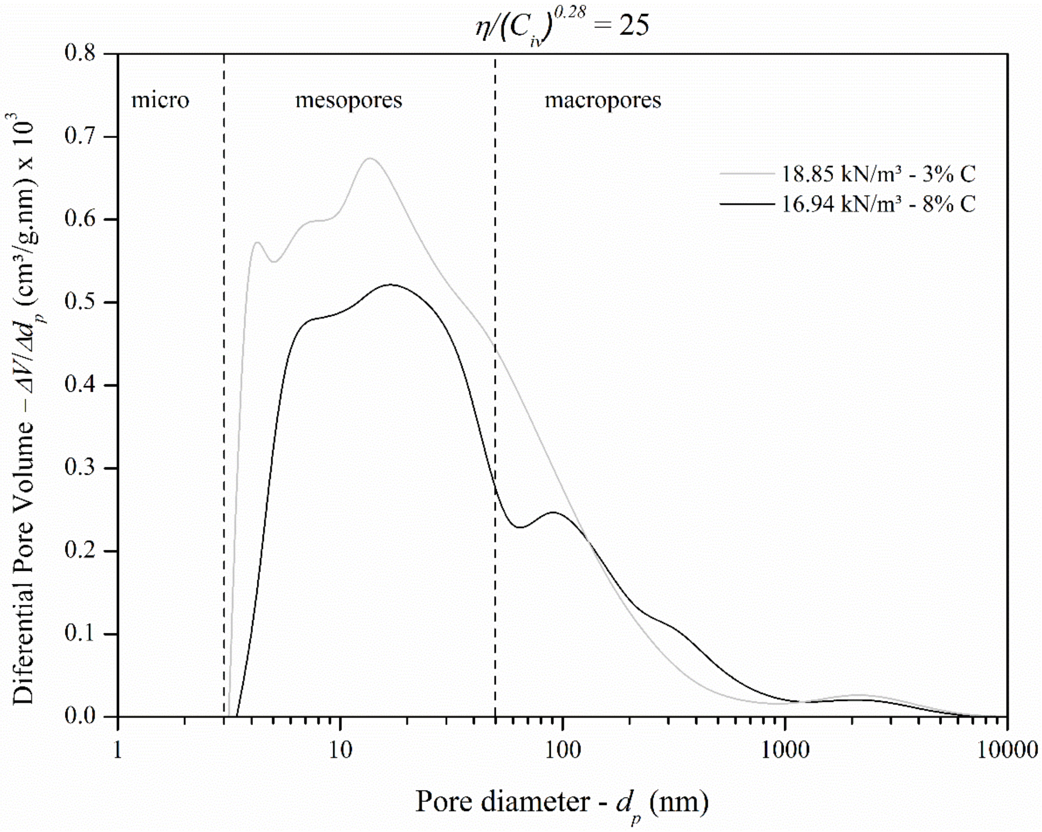

Figure 146 - Differential pore volume distribution for $\eta/(C_{iv})^{0.28} = 25$

From the differential pore volume outcomes, it is clear that, within the same $\eta/(C_{iv})^{0.28}$ value, the least dense and most cemented specimens presented considerably greater volumes of mesopores (50 nm > d_p > 3 nm). Yet, in the macropores zone, this has not occurred since the total volume of macropores was nearly the same considering the two opposite dosages. This effect is probably related to the increment in the compactness of the medium that contributed to diminish the mesopore volumes and, as well, the overall volume of pores. In addition, it is possible that the cement hydration products present a higher concentration of small pores, located in the mesopore region.

Since the dosages 18.55 kN/m³ - 1%C ($\eta/(C_{iv})^{0.28} = 35$), 18.31 kN/m³ - 2%C ($\eta/(C_{iv})^{0.28} = 30$) and 18.85 kN/m³ - 3%C ($\eta/(C_{iv})^{0.28} = 25$) present similar molding porosity values, in the order of 30%, it is reasonable to compare the PSD outcomes of these specimens in order to evaluate the effect of the cement addition on the pore distribution of these samples. In this regard, Figure 147 presents the incremental pore volume distribution, whereas Figure 148 exhibits the differential pore volume distribution for these samples.

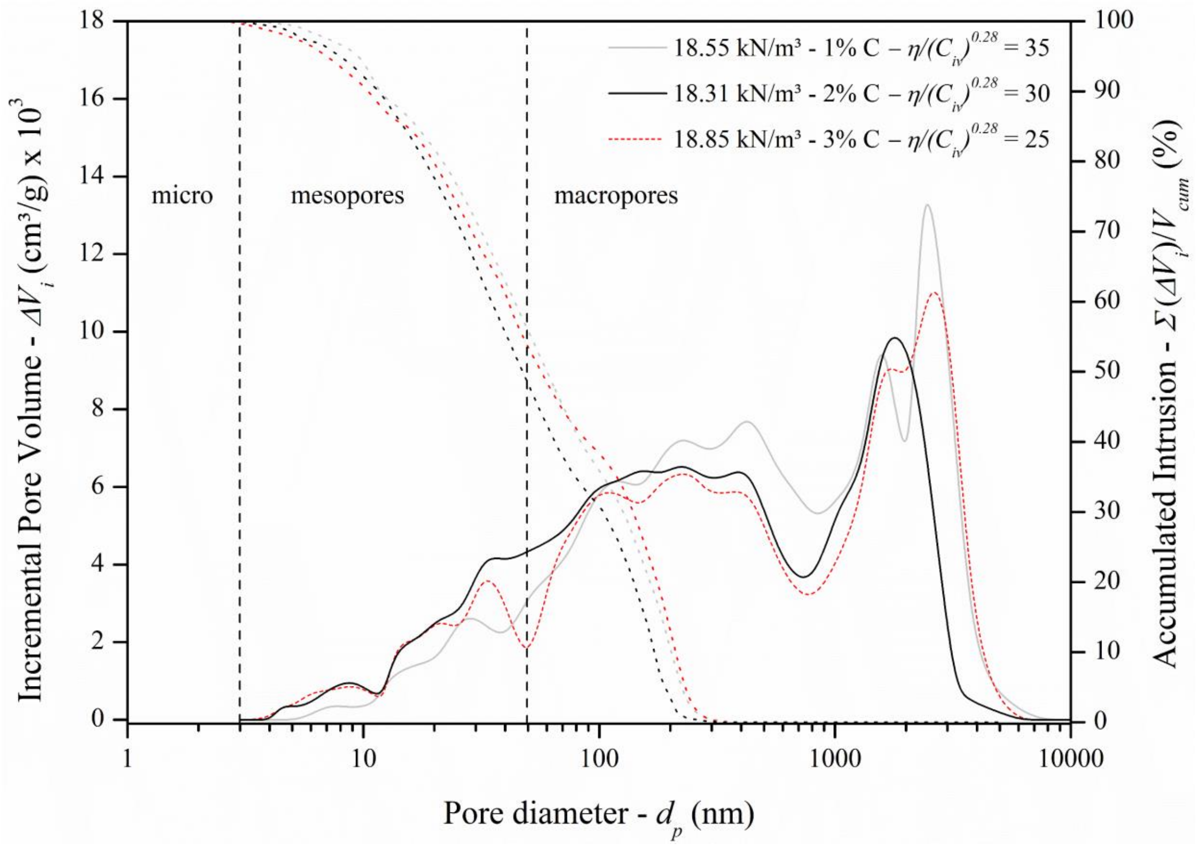

Figure 147 Incremental PSD and acumulated intrusion for multiple dosages

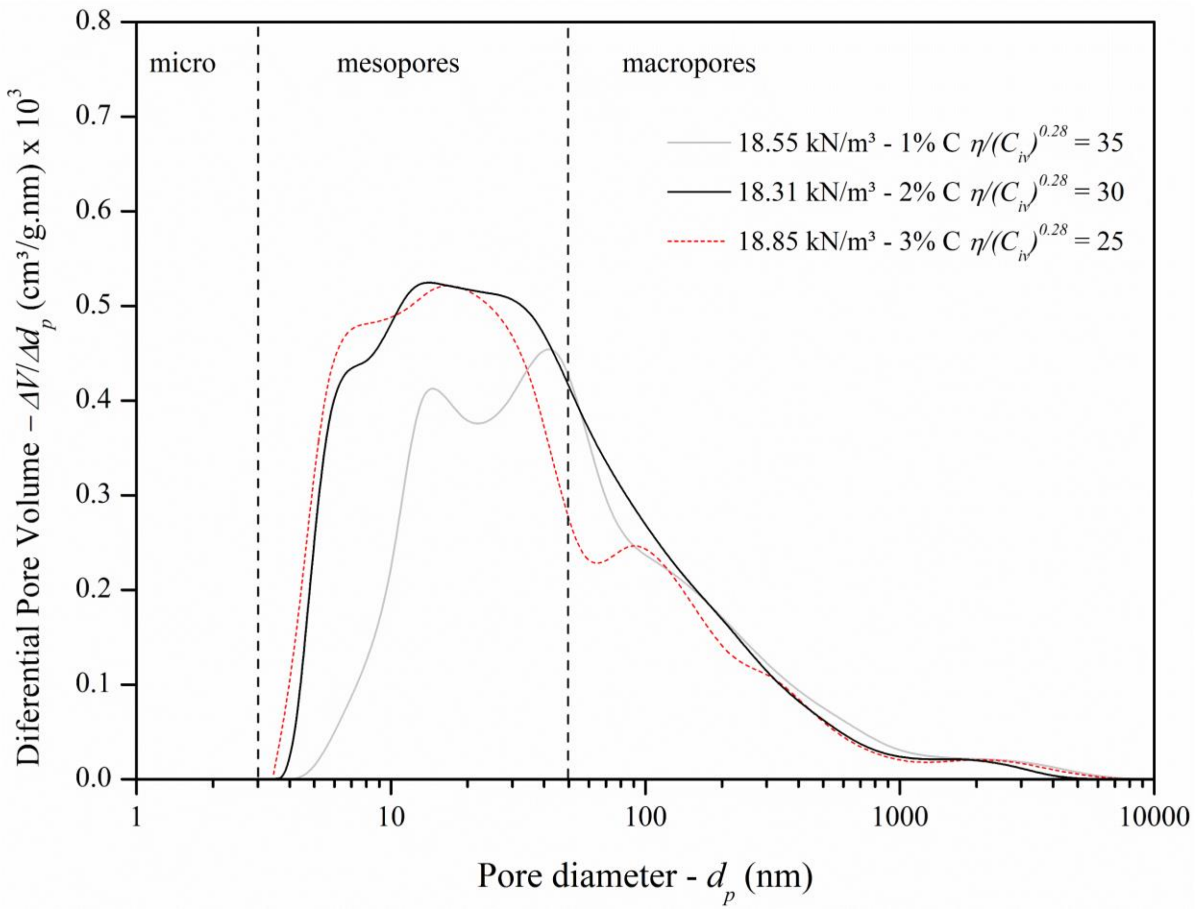

Figure 148 - Differential pore volume distribution for multiple dosages

In the incremental pore volume distribution, certain pore volume (ΔV_i) is attributed to a specific pore diameter (d_p), meaning that a greater volume of pores is assigned to a determined diameter if a well-defined peak is visible. Thus, in general, the increment in the cement content has implied a decrement on the size of the peaks in the macropores region which may indicates that the larger pores were occupied by cement hydration products. Despite this difference, the overall response was very similar. The differential pore volumes results are in consonance to what was demonstrated by the ΔV_i versus d_p plot. In essence, the volume of macropores has slightly decreased owing to the addition of cement, whereas the opposite was verified in the mesopore region. That is, it seems that the increase on the amount of cement has led to a slightly augment on the volume of mesopores.

6 CONCLUSIONS

The conclusions are presented in three parts. First, a summary of the main results is graphically exposed. Next, the main conclusions relative to the data obtained in the present work is presented in topics. Finally, suggestions for further research are given.

6.1 SUMMARY OF MAIN RESULTS

All the data relative to the initial shear modulus tests, unconfined compressive strength tests and durability tests were summarized into contour plots that relate the tested dosages (i.e., dry unit weight and amount of cement) to a mean value of the obtained mechanical response that is depicted as the contour line. Zones relative to the adopted $\eta/(C_{iv})^{0.28}$ values were highlighted and are separated by the contour lines. In brief, this is a simple graphical manner to summarize all the data into a single graph, facilitating the overall comprehension of the results.

Initial Shear Modulus

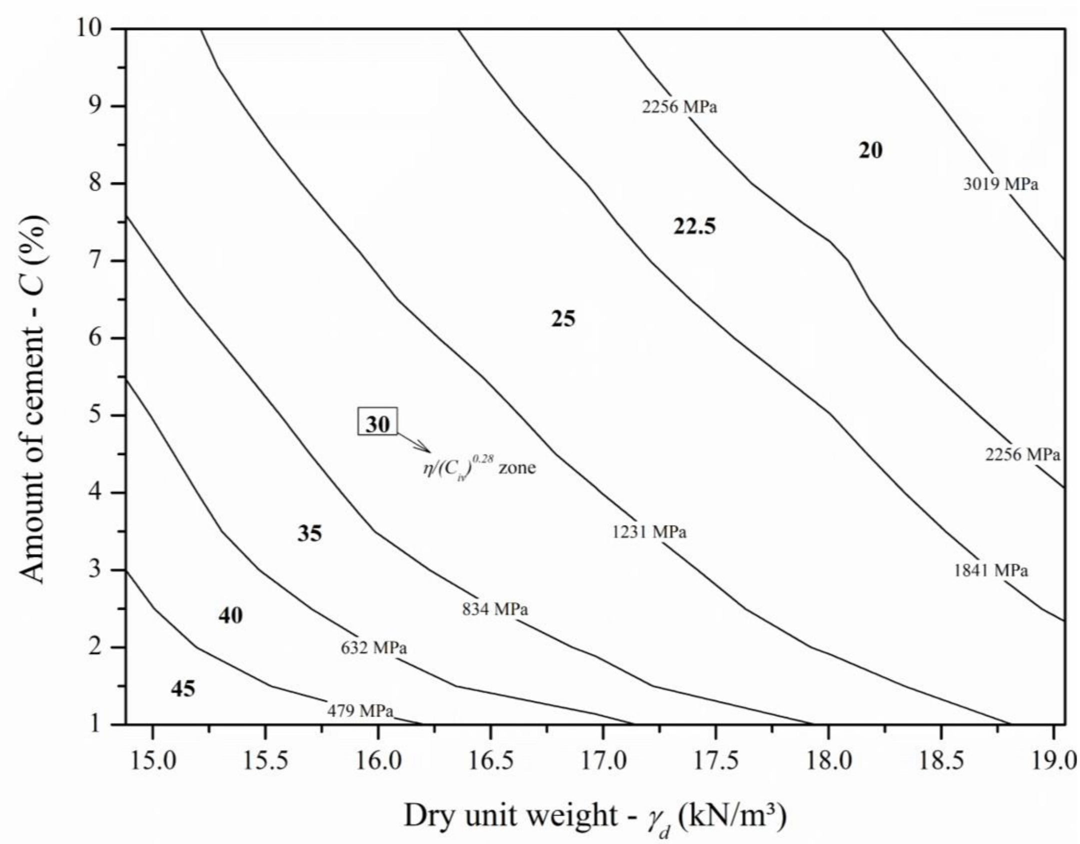

Unconfined Compressive Strength

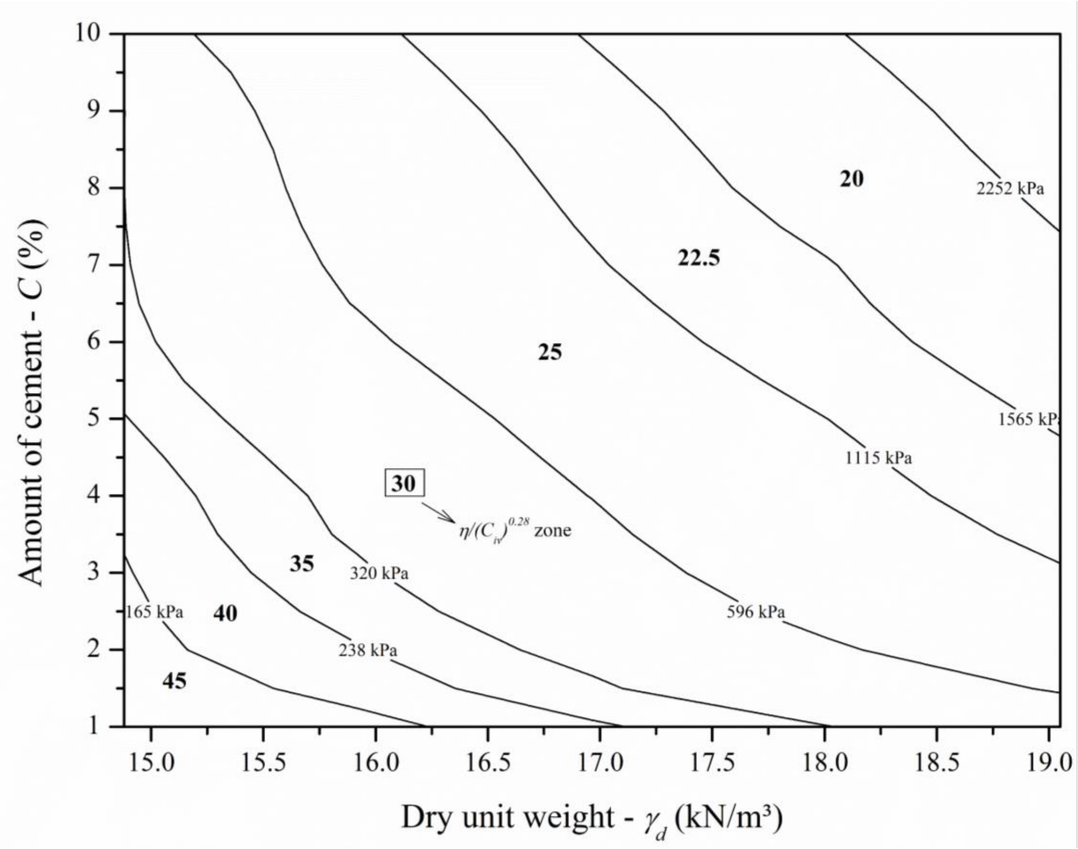

Durability

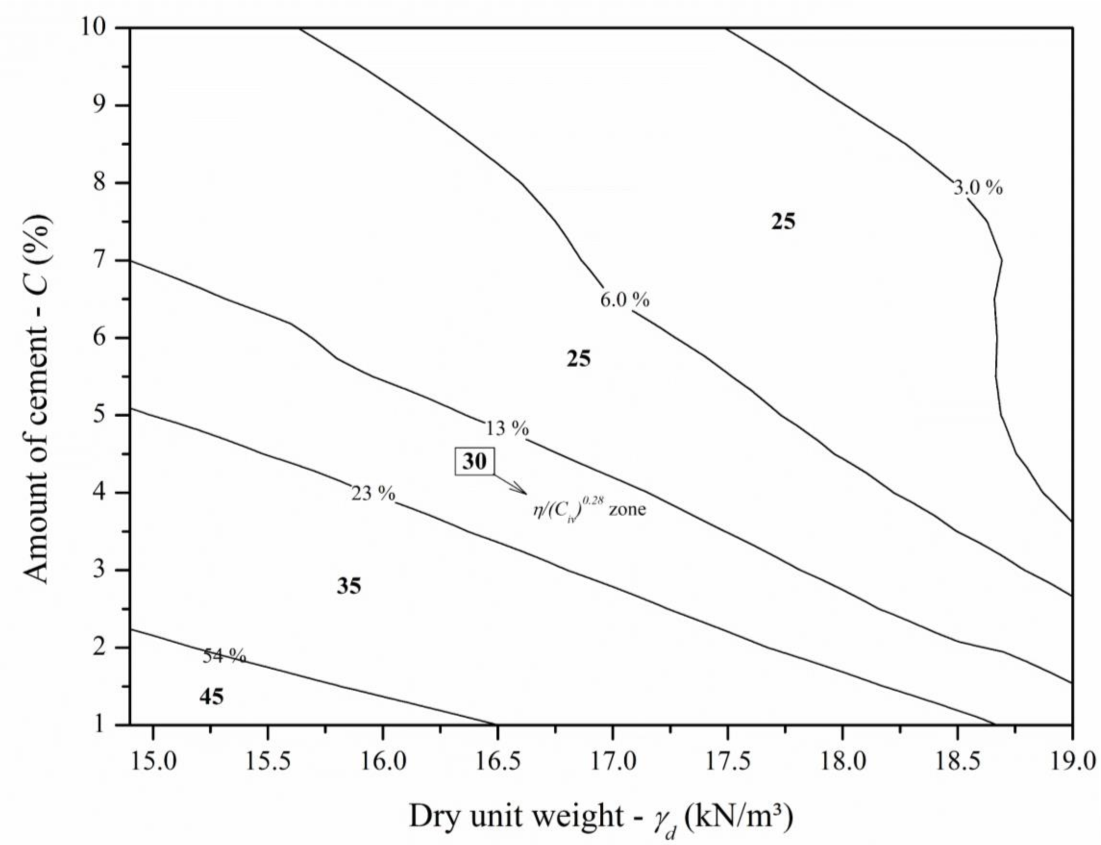

6.2 SUMMARY OF MAIN CONCLUSIONS

This thesis intended to produce an experimental contribution relative to the comprehension of the role of the dosage, considering the same $\eta/(C_{iv})^{0.28}$ value, on the mechanical response of a cemented clayey sand. Particularly, initial shear modulus tests, unconfined compressive strength tests and durability tests provided a valuable amount of data in order to the fulfill this work's purpose. Following, triaxial tests have given valuable insights which have helped to explain the mechanisms of strength mobilization for different dosages assembled at the same $\eta/(C_{iv})^{0.28}$ index value and, as well, have indicated certain boundaries for the usefulness of the $\eta/(C_{iv})^{0.28}$ parameter. Thus, considering the **boundaries** of the present research, with highlight to either the materials utilized herein and test conditions, the following conclusions can be drawn within the results of each test method

Initial Shear Modulus Results

The initial shear modulus was properly related to the adjusted porosity/cement index value, regardless of the adopted dosage. Moreover, a good agreement between the theoretical derivation proposed by Diambra *et al*. (2019) and the measured stiffness values for the BRS-cement specimens was gathered. This reinforces the value of the internal adjustment exponent (equals to 0.28), responsible to conciliate the relative importance of the compactness and the amount of cement, which was utilized herein.

Unconfined Compressive Strength Results

Irrespective of the adopted mix design within each adjusted porosity/cement index value, a unique power-type relationship was obtained when correlating the unconfined compression strength results and the $\eta/(C_{iv})^{0.28}$ parameter. This have occurred even when the outcomes of statistically unequal dosages were computed. Therefore, it is believed that such index is adequate to address the unconfined compressive strength of BRS-cement samples, even when several dosages are molded at the same $\eta/(C_{iv})^{0.28}$ value. In addition, the results from present study were in accordance to the theoretical model proposed by Diambra *et al*. (2017).

Durability Test Results

As observed for the stiffness and strength data, the durability test results could be properly correlated to the $\eta/(C_{iv})^{0.28}$ regardless of the adopted dosage. Moreover, within the same $\eta/(C_{iv})^{0.28}$, the dosage has exerted a negligible effect on the durability response of the tested specimens.

Triaxial Test Results

A good agreement between the top deviatoric stress and the $\eta/(C_{iv})^{0.28}$ index value was obtained when the two lowest confining pressures were used (σ'_3 = 35 and 70 kPa). However, the stress-strain response and the volume change behavior up to the peak (and after) were not necessarily similar when comparing the outcomes of two distinct dosages molded at the same adjusted/porosity cement index value. It is believed that, within equal $\eta/(C_{iv})^{0.28}$ values and for low confinement levels, the strength related to the cement parcel (in the most porous specimen) is compensated by the higher degree of interlocking and, consequently, greater dilatancy rate observed in the least porous sample. For higher confinement pressures and for specific

$\eta/(C_{iv})^{0.28}$ values, this may not occur as demonstrated for some tests conducted at $\sigma'_3 = 140$ kPa. In these, the strength of the most cemented and most porous specimens was associated to the cement and, as well, to a purely frictional component because the higher confinement pressure was sufficient to inhibit the occurrence of expansion ($\eta/(C_{iv})^{0.28} = 30$ and 35, being the volume change fully compressive. Thus, the effective stress parameters (ϕ_{peak}' and c') cannot be fully associated to the $\eta/(C_{iv})^{0.28}$ when very distinct dosages, having the same initial $\eta/(C_{iv})^{0.28}$, are compared. In other words, ϕ_{peak}' and c' cannot be related to the $\eta/(C_{iv})^{0.28}$ due to the dosage-dependence of the strength mobilization mechanisms.

Scanning Electron Microscope Tests

In general, the effects on the soil fabrics of both the increase in the cement content and increment in the dry unit weight could be visually perceived in the SEM micrographs. Thus, the more cemented and dense specimens, which have presented a greater mechanical performance, have exhibited a more condensed structure owing to the development of a cement matrix in a less porous environment.

Mercury Intrusion Porosimetry Tests

The mercury intrusion porosimetry tests have marginally contributed to the understanding of the role of the $\eta/(C_{iv})^{0.28}$ on the mechanical response of the compacted BRS-cement mixtures. In general, no major differences on the pore size distributions of the tested specimens were perceived. In addition, within each $\eta/(C_{iv})^{0.28}$ value, it was only possible to attest a change in the volume of the mesopores amongst the most cemented specimens. Such results indicate that this technique is not the most indicated if the adjusted/porosity cement index needs to be further explained by microstructural means.

The $\eta/(C_{iv})^{0.28}$ index

The adjusted porosity/cement index value has proved to be useful in modelling the initial shear modulus (G_0), the unconfined compressive strength (q_u), the split tensile strength (q_t), the durability response and top deviatoric stress (q_{max}) for low confinement levels when distinct dosages, molded at the same $\eta/(C_{iv})^{0.28}$ index value, are compared. It has been shown that q_{max} can be reasonably estimated using q_u and, thus, using the $\eta/(C_{iv})^{0.28}$ index for low confining pressures ($\sigma'_3 < 140$ kPa). It seems that for the greater $\eta/(C_{iv})^{0.28}$ values (greater than 30) the compactness exerts a major influence in the behavior, whereas the cement dominates the response for the smaller $\eta/(C_{iv})^{0.28}$ values. In addition, the chosen internal exponent equals to 0.28 has shown to be in consonance with the existing theoretical derivations (e.g. DIAMBRA *et al*., 2017, 2019).

6.3 SUGGESTIONS FOR FUTURE RESEARCH

A list of suggestions is provided in this item with the intention to enlarge the comprehension and enrich the discussion of the role of the adjusted porosity/cement index on the behavior of cemented soils. As a reason, each topic is briefly explained.

Effect of cement type. Even though ordinary Portland cement was used in this work, it would be important to carry out similar research using a “greener” alternative binder such as an alkali-activated binder, for example.

Employment of a distinct soil. This thesis was carried out using a clayey sand named Botucatu Residual Soil which possess a few peculiarities that were discussed herein. The conduction of a similar research program, using a different geomaterial, would be interesting to assess the role of the soil on the approach that was used in the present work.

Effect of stress paths for triaxial testing. Regarding low confinement pressures, the peak-stress values were similar considering the conventional compression triaxial tests (constant σ'_3 during shearing) for different dosages molded at the same $\eta/(C_{iv})^{0.28}$ value. It would be interesting to conduct triaxial tests for different stress-paths (e.g., compression unloading and extension loading) using the same approach (i.e., same $\eta/(C_{iv})^{0.28}$ value and different dosages) to check how the material would behave as the cement bonds would probably degrade in a different manner, affecting the strength and stiffness results.

Effect of the intermediate stress. Cubic cell tests could be carried out, following a similar experimental program, in order to assess the effect of the intermediate stress on the strength of the tested specimens. The influence of the direction of the principal stresses could be, as well, evaluated.

Effect of cyclic loading. The analysis of strength and stiffness degradation owing to cyclic loading would be interesting if conducted as a function of the $\eta/(C_{iv})^{0.28}$ value. Namely, how would different dosages, molded using the same $\eta/(C_{iv})^{0.28}$ value, behave under the same cyclic loading conditions?

Effect of fibers addition. The addition of a certain amount of polyproline fibers could influence in a different manner (or not) the response of different dosages assembled at the same $\eta/(C_{iv})^{0.28}$ value. Thus, it would be interesting to evaluate this issue.

Additional microstructure characterization. It would be important to characterize the microstructure of the BRS-cement specimens using other testing methods than scanning electron microscope and mercury intrusion porosimetry. These techniques have proven to be qualitatively useful, but have not revealed much about the role $\eta/(C_{iv})^{0.28}$ index itself. In other words, they were not sufficient to explain major differences related to different dosages assembled at the same $\eta/(C_{iv})^{0.28}$ value, for example.

REFERENCES

ABELL, A. B.; WILLIS, K. L.; LANGE, D. A. Mercury intrusion porosimetry and image analysis of cement-based materials. **Journal of Colloind and Interface Science**, v. 211(1), p. 39-44, 1999.

AMERICAN SOCIETY FOR TESTING AND MATERIALS (ASTM). **ASTM D 559**: standard test methods for wetting and drying compacted soil-cement mixtures. Philadelphia, 2015.

AMERICAN SOCIETY FOR TESTING AND MATERIALS (ASTM). **ASTM D 560**: standard test methods for freezing and thawing compacted soil-cement mixtures. Philadelphia, 2016.

AMERICAN SOCIETY FOR TESTING AND MATERIALS (ASTM). **ASTM D 558M**: standard test methods for moisture-density (unit weight) relations of soil-cement mixtures. Philadelphia, 2019a.

AMERICAN SOCIETY FOR TESTING AND MATERIALS (ASTM). **ASTM D 4972**: standard test methods for pH of soils. Philadelphia, 2019b.

AMERICAN SOCIETY FOR TESTING AND MATERIALS (ASTM). **ASTM D 8295**: standard test method for determination of shear wave velocity and initial shear modulus in soil specimens using bender elements. Philadelphia, 2019c.

AMERICAN SOCIETY FOR TESTING AND MATERIALS (ASTM). **ASTM D 7181**: standard test methods for consolidation drained triaxial compression test for soil. Philadelphia, 2020.

ASSOCIAÇÃO BRASILEIRA DE NORMAS TÉCNICAS (ABNT). **NBR 6508**: grãos de solos que passam na peneira de 4,8 mm - Determinação da massa específica. Rio de Janeiro, 1984.

ASSOCIAÇÃO BRASILEIRA DE NORMAS TÉCNICAS (ABNT). **NBR 6459**: determinação do limite de liquidez. Rio de Janeiro, 2016.

ASSOCIAÇÃO BRASILEIRA DE NORMAS TÉCNICAS (ABNT). **NBR 7180**: determinação do limite de plasticidade. Rio de Janeiro, 2016.

ASSOCIAÇÃO BRASILEIRA DE NORMAS TÉCNICAS (ABNT). **NBR 7181**: análise granulométrica de solos. Rio de Janeiro, 2018.

ASSOCIAÇÃO BRASILEIRA DE NORMAS TÉCNICAS (ABNT). **NBR 7182**: solo – ensaio de compactação. Rio de Janeiro, 2020.

ATKINSON, J. H. Non-linear soil stiffness in routine design. **Géotechnique**, v. 50(5), p. 487–508, 2000. **https://doi.org/10.1680/geot.2000.50.5.487**

ATKINSON, J. **The mechanics of soils and foundations**. London: Taylor and Francis, 2007.

BAHMANI, S. H.; HUAT, B. B. K.; ASADI, A.; FARZADNIA, N. Stabilization of residual soil using SiO_2 nanoparticles and cement. **Construction and Building Materials,** v. 64(1), p. 350-359, 2014. **http://dx.doi.org/10.1016/j.conbuildmat.2014.04.086**

BALDOVINO, J. de J. A.; IZZO, R. L. dos S.; PEREIRA, M. D.; ROCHA, E. V. de G.; ROSE, J. L.; BORDIGNON, V. R. Equations controlling tensile and compressive strength ratio of sedimentary soil-cement mixtures under optimal compaction conditions. **Journal of Materials in Civil Engineering**, v. 32(1), p. 04019320, 2020a. **https://doi.org/10.1061/(asce)mt.1943-5533.0002973**

BALDOVINO, J. de J. A.; IZZO, R. L. dos S.; ROSE, J. L. Effects of freeze–thaw cycles and porosity/cement index on durability, strength and capillary rise of a stabilized silty soil under optimal compaction conditions. **Geotechnical and Geological Engineering,** v. 39(1), p. 481-498, 2020b. **https://doi.org/10.1007/s10706-020-01507**

BECKETT, C.; CIANCIO, D. Effect of compaction water content on the strength of cement-stabilized rammed earth materials. **Canadian Geotechnical Journal,** v. 51(5), p. 583-590, 2014. **https://doi.org/10.1139/cgj-2013-0339**

BEEN, K. JEFFERIES, M. Soil liquefaction: a critical state approach. Boca Raton: CRC Press, 2019.

BEHNOOD, A. Soil and clay stabilization with calcium- and non-calcium-based additives: A state-of-the-art review of challenges, approaches and techniques. **Transportation Geotechnics**, v. 17(A), p. 14-32, 2018. **https://doi.org/10.1016/j.trgeo.2018.08.002**

BERGSTRÖM, S. G. Curing temperature, age and strength of concrete. **Magazine of Concrete Research**, v. 5(14), p. 61–66, 1953. **https://doi.org/10.1680/macr.1953.5.14.61**

BHATTACHARJEE, B. Influence of pore size distribution on the properties of a stabilized soil cement system. In: FOURTH GEO-CHINA INTERNATIONAL CONFERENCE, 2016. **Proceedings**…Reston: American Society of Civil Engineers, 2016, p. 53-60. **https://doi.org/10.1061/9780784480069.007**

BISHOP, A. W. The strength of soils as engineering materials. Géotechnique, v. 16(2), p. 91–130, 1966. **https://doi.org/10.1680/geot.1966.16.2.91**

BOLTON, M. D. The strength and dilatancy of sands. **Géotechnique**, v. 36(1), p. 65–78, 1986. **https://doi.org/10.1680/geot.1986.36.1.65**

BORTOLOTTO, M. S. **Bender elements, ultrasonic pulse velocity, and local gauges for the analysis of stiffness degradation of an artificially cemented soil**. 2017. 180 f. Dissertação (Mestrado em Engenharia) – Programa de Pós Graduação em Engenharia Civil, Universidade Federal do Rio Grande do Sul, Porto Alegre, 2017.

BOX, G.; HUNTER, J. S.; HUNTER, W. G. **Statistics for experimenters: design, innovation and discovery**. 2nd edition. Hoboken: Wiley-Interscience, 2005.

BRESSANI, M. B. Experimental properties of bonded soils. 1990. 459 f. Thesis (Doctor of Philosophy) – Faculty of Engineering, University of London - Imperial College of Science Technology and Medicine, London, 1990.

CARDOSO, R. Porosity and tortuosity influence on geophysical properties of an artificially cemented sand. **Engineering Geology**, v. 211(1), p. 197-207, 2016. **http://dx.doi.org/10.1016/j.enggeo.2016.07.009**

CARDOSO, R. Influence of water-cement ratio on the hydraulic behavior of an artificially cemented sand. **Geotechnical Geological Engineering**, v. 35(4), p. 1513-1527, 2017. **10.1007/s10706-017-0190-3**

CARDOSO, R. RIBEIRO, D; NÉRIE, R. Bonding effect on the evolution with curing time of compressive and tensile strength of sand-cement mixtures. **Soils and Foundations**, v. 57(4), p. 655-668, 2017. **https://doi.org/10.1016/j.sandf.2017.04.006**

CARRETTA, M. da S. **Comportamento de um solo residual levemente cimentado:** estimativa de capacidade de carga para estacas submetidas a esforços transversais. 2018. 180 f. Dissertação (Mestrado em Engenharia) – Programa de Pós Graduação em Engenharia Civil, Universidade Federal do Rio Grande do Sul, Porto Alegre, 2018.

CARRETTA, M. da S.; CRISTELO, N.; FESTUGATO, L. MIGUEL, G. D.; CONSOLI, N. C. Experimental assessment of the small-strain response of residual soil under monotonic and cyclic loading. **Proceedings of the Institution of Civil Engineers - Geotechnical Engineering**, p. 1-14, 2021. https://doi.org/10.1680/jgeen.20.00073 (ahead of press)

CASCANTE, G.; SANTAMARINA, J. Interparticle contact behavior and wave propagation. **Journal of Geotechnical Engineering**, v. 122(10), p. 831–839, 1996. **https://doi.org/10.1061/(asce)0733-9410(1996)122:10(831)**

CHANDLER, R.; CRILLY, M.; SMITH, M. A low-cost method of assessing clay desiccation for low-rise buildings. **Proceedings of the Institution of Civil Engineers - Civil Engineering**, v. 92(2), p. 82–89, 1992. **https://doi.org/10.1680/icien.1992.18771**

CHANG, T.; WOODS, R. D. Effect of particle contact bond on shear modulus. **Journal of Geotechnical Engineering**, v. 118(8), p. 1216-1233, 1992. **https://doi.org/10.1061/(asce)0733-9410(1992)118:8(1216)**

CHARLES, J. A. Ground improvement: the interaction of engineering science and experience-based technology**. Géotechnique**, v. 52(7), p. 527-532, 2002. **https://doi.org/10.1680/geot.2002.52.7.527**

CLARE, K. E.; POLLARD, A. E. The effect of curing temperature on the compressive strenght of soil-cement mixtures. **Géotechnique,** v. 4(3), p. 97–106, 1954. https://doi.org/10.1680/geot.1954.4.3.97

CLARE, K. E.; POLLARD, A. E. The relationship between compressive strength and age for soils stabilized with four types of cement. **Magazine of Concrete Research**, v. 3(8), p. 57–64, 1951. **https://doi.org/10.1680/macr.1951.3.8.57**

CLAYTON, C. R. I. Stiffness at small strains: research and practice. **Géotechnique**, v. 61(1), p. 5-37. **https://doi.org/10.1680/geot.2011.61.1.5**

CLAYTON, C. R. I.; KHATRUSH, S. A. A. A new device for measuring local axial strains on triaxial specimens. Géotechnique, v. 36(4), p. 593-597, 1986. **https://doi.org/10.1680/geot.1986.36.4.593**

CLOUGH, G. W.; SITAR, N.; BACHUS, R. C. Cemented sands under static loading. **Journal of Geotechnical Engineering Division,** v. 107, p. 799-817, 1981.

COLLIER, N. C.; SHARP, J. H.; MILESTONE, N. B.; HILL, J.; GODFREY, I. H. The influence of water removal techniques on the composition and microstructure of hardened cement pastes. **Cement and Concrete Research**, v. 38(1), p. 737-744, 2008. **10.1016/j.cemconres.2008.02.012**

COLLINS, I. F.; MUHUNTHAN, B. On the relationship between stress-dilatancy, anisotropy, and plastic dissipation for granular materials**. Géotechnique**, v. 53(7), p. 611–618, 2003. **https://doi.org/10.1680/geot.2003.53.7.61**

CONSOLI, N. C.; PRIETTO, P. D. M.; ULBRICH, L. A. Influence of fiber and cement addition on behavior of sandy soil. **Journal of Geotechnical and Geoenvironmental Engineering**, v. 124(12), p. 1211–1214, 1998. **https://doi.org/10.1061/(asce)1090-0241(1998)124:12(1211)**

CONSOLI, N. C.; PRIETTO, P. D. M.; ULBRICH, L. A. The behaviour of a fibre-reinforced cemented soil**. Proceedings of the Institution of Civil Engineers - Ground Improvement**, v. 3(1), p. 21–30, 1999. **https://doi.org/10.1680/gi.1999.030103**

CONSOLI, N. C.; ROTTA, G. V.; PRIETTO, P. D. M. Influence of curing under stress on the triaxial response of cemented soils. **Géotechnique,** v. 50(1), p. 99-105, 2000. **https://doi.org/10.1680/geot.2000.50.1.99**

CONSOLI, N. C.; PRIETTO, P. D. M.; CARRARO, J. A. H.; HEINECK, K. S. Behavior of compacted soil-fly ash-carbide lime mixtures. **Journal of Geotechnical and Geoenvironmental Engineering,** v. 127 (9), p. 774 – 782, 2001

CONSOLI, N. C.; ROTTA, G. V.; PRIETTO, P. D. M. Influence of curing under stress on the triaxial response of cemented soils**. Géotechnique**, v. 52(5), p. 382–384, 2002. **https://doi.org/10.1680/geot.52.5.382.38705**

CONSOLI, N. C.; ROTTA, G. V.; PRIETTO, P. D. M. Yielding–compressibility–strength relationship for an artificially cemented soil cured under stress**. Géotechnique**, v. 56(1), p. 69–72, 2006. **https://doi.org/10.1680/geot.2006.56.1.69**

CONSOLI, N. C.; FOPPA, D.; FESTUGATO, L.; HEINECK, K. S. Key Parameters for Strength Control of Artificially Cemented Soils. **Journal of Geotechnical and Geoenvironmental Engineering**, v. 133(2), p. 197–205, 2007a. **https://doi.org/10.1061/(asce)1090-0241(2007)133:2(197)**

CONSOLI, N. C.; ROTTA, G. V.; FOPPA, D.; FAHEY, M. Mathematical model for isotropic compression behaviour of cemented soil cured under stress. **Geomechanics and Geoengineering**, v. 2(4), p. 269-280, 2007b. **https://doi.org/10.1080/17486020701618337**

CONSOLI, N. C.; VIANA DA FONSECA, A.; CRUZ, R. C.; HEINECK, K. S. Fundamental parameters for the stiffness and strength controlo f artificially cemented sand. **Journal of Geotechnical and Geoenvironmental Engineering,** v. 135(9), p. 1347–1353, 2009. **https://doi.org/10.1061/(asce)gt.1943-5606.0000**

CONSOLI, N. C.; CRUZ, R. C.; FLOSS, M. F.; FESTUGATO, L. Parameters controlling tensile and compressive strength of artificially cemented sand. **Journal of Geotechnical and Geoenvironmental Engineering**, v. 136(5), p. 759-763, 2010. **https://doi.org/10.1061/(asce)gt.1943-5606.0000278**

CONSOLI, N. C.; DALLA ROSA, A.; CORTE, M. B.; LOPES JR., L da S.; CONSOLI, B. S. Porosity-cement ratio controlling strength of artificially cemented clays. **Journal of Materials in Civil Engineering**, v. 23(8), p. 1249–1254, 2011. **https://doi.org/10.1061/(asce)mt.1943-5533.0000283**

CONSOLI, N. C.; FONSECA, A. V. da; SILVA, S. R.; CRUZ, R. C.; FONINI, A. Parameters controlling stiffness and strength of artificially cemented soils**. Géotechnique**, 62(2), p. 177–183, 2012a. **https://doi.org/10.1680/geot.8.p.084**

CONSOLI, N. C.; CRUZ; R. C.; da FONSECA, A. V.; COOP, M. R. Influence of cement-voids ratio on stress-dilatancy behavior of artificially cemented sand. **Journal of Geotechnical and Geoenvironmental Engineering**, v. 138(1), p. 100-109, 2012b. 10.1061/(ASCE)GT.1943-5606.0000565.

CONSOLI, N. C; VAZ FERREIRA, P. M.; TANG, C. S.; MARQUES, S. F. V.; FESTUGATO, L.; CORTE, M. B. A unique relationship determining strength of silty/clayey soils – Portland cement mixes. **Soils and Foundations**, v. 56(6), p. 1082–1088, 2016. **https://doi.org/10.1016/j.sandf.2016.11.011**

CONSOLI, N. C.; MARQUES, S. F. V.; FLOSS, M. F.; FESTUGATO, L. Broad-spectrum empirical correlation determining tensile and compressive strength of cement-bonded clean granular sand. **Journal of Materials in Civil Engineering**, v. 29(6), p. 06017004, 2017a. **https://doi.org/10.1061/(asce)mt.1943-5533.0001858**

CONSOLI, N. C.; da SILVA, A. P.; NIERWINSKI, H. P; SOSNOSKI, K. Durability and strength of fiber-reinforced compacted gold tailings-cement blends. **Geotextiles and Geomembranes**, v. 45(2), p. 98–102, 2017b. **https://doi.org/10.1016/j.geotexmem.2017.01.001**

CONSOLI, N. C.; da SILVA, A. P.; NIERWINSKI, H. P; SOSNOSKI, K. Durability, strength, and stiffness of compacted gold tailings – cement mixes. **Canadian Geotechnical Journal**, v. 55(4), p. 486–494, 2018a. **https://doi.org/10.1139/cgj-2016-0391**

CONSOLI, N.C.; HOCH, B. Z.; FESTUGATO, L.; DIAMBRA, A.; IMBRAIM, E.; da SILVA, J. K. Compacted chalk putty–cement blends: mechanical properties and performance. **Journal of Materials in Civil Engineering**, v. 30(2), p. 04017266, 2018b. **https://doi.org/10.1061/(asce)mt.1943-5533.0002141**

CONSOLI, N. C.; TOMASI, L. F. The impact of dry unit weight and cement content on the durability of sand–cement blends. **Proceedings of the Institution of Civil Engineers - Ground Improvement**, v. 171(2), p. 96–102, 2018. **https://doi.org/10.1680/jgrim.17.00034**

CONSOLI, N. C.; CARRETA, M da S.; LEON, H. B.; SCHEUERMANN FILHO, H. C.; TOMASI, L. F. Strength and stiffness of ground waste glass-carbide lime blends. **Journal of Materials in Civil Engineering**, v. 31(10), p. 06019010, 2019a. **https://doi.org/10.1061/(asce)mt.1943-5533.0002862**

CONSOLI, N. C.; SALDANHA, R. B.; SCHEUERMANN FILHO, H. C. Short-and long-term effects of sodium chloride on strength and durability of coal fly ash stabilized with carbide lime. **Canadian Geotechnical Journal,** v. 56(12), p. 1929-1939, 2019b. **https://doi.org/10.1139/cgj-2018-0696**

COOP, M. R.; ATKINSON, J. H. The mechanics of cemented carbonate sands. **Géotechnique,** v. 44(3), p. 533-537, 1993. **https://doi.org/10.1680/geot.1994.44.3.533**

COOP, M. R.; WILSON, S. M. Behavior of hydrocarbon reservoir sands and sandstones. **Journal of Geotechnical and Geoenvironmental Engineering**, v. 129(11), p. 1010-1019, 2003. 10.1061/~ASCE!1090-0241~2003!129:11~1010!

CÔRREA, B. R. S.; SCHEUERMANN FILHO, H. C.; MATTOS, J. R. G.; CONSOLI, N. C. Compacted ground glass particles—carbide lime blends: an environment friendly material. **Geotechnical and Geological Engineering**, 2021. **https://doi.org/10.1007/s10706-021-01689-z**. (ahead of print)

CORTE, M. B. **Desenvolvimento de equipamento para ensaios Simple Shear,** 2016. 177 f. Dissertação (Mestrado em Engenharia) – Programa de Pós Graduação em Engenharia Civil, Universidade Federal do Rio Grande do Sul, Porto Alegre, 2016.

CORTE, M. B.; FESTUGATO, L; CONSOLI, N. C. Development of a cyclic simple shear apparatus. **Soils and Rocks**, 2017, v. 40(3), p. 279-289, 2017.

CORTE, M. B. **Response of lightly cemented sand under multiaxial loading conditions** 2020. 259 f. Tese (Doutorado em Engenharia) – Programa de Pós Graduação em Engenharia Civil, Universidade Federal do Rio Grande do Sul, Porto Alegre, 2020.

CROFT, J. B. The influence of soil mineralogical composition on cement stabilization. **Géotechnique**, v. 17, p. 119-134, 1967.

CRUZ, R. C. **Influência de parâmetros fundamentais na rigidez, resistência e dilatância de uma areia artificialmente cimentada**. 2008. 216 f. Tese (Doutorado em Engenharia) – Programa de Pós Graduação em Engenharia Civil, Universidade Federal do Rio Grande do Sul, Porto Alegre, 2008.

CUCCOVILLO, T.; COOP, M. R. On the mechanics of structured sands. **Géotechnique,** v. 49(6), p. 741-760, 1999. **https://doi.org/10.1680/geot.1999.49.6.741**

DALLA ROSA, F. Comportamento mecânico de um solo cimentado curado sob tensão em ensaios triaxiais. 2006. 103 f. Dissertação (Mestrado em Engenharia) – Programa de Pós Graduação em Engenharia Civil, Universidade Federal do Rio Grande do Sul, Porto Alegre, 2006

De JOSSELIN De JONG, G. Rowe's stress—dilatancy relation based on friction. **Géotechnique**, v. 26(3), p. 527–534, 1976. **https://doi.org/10.1680/geot.1976.26.3.527**

DE PAULA, T. M.; CONSOLI, N. C.; FESTUGATO, L. FAVRETTO, F.; DARONCO, J. V. L. Behaviour of fibre-reinforced cemented sand under flexural tensile stress. **E3S Web of Conferences**, v. 92(1), p. 12005, 2019. **https://doi.org/10.1051/e3sconf/20199212005**

DEMPSEY, B. J.; THOMPSON, M. R. Durability properties of soil-lime mixtures. **Highway Research Board,** n. 235, p. 61 – 75, 1968.

DIAMBRA, A.; FESTUGATO, L.; IBRAIM, E.; PECCIN, A.; CONSOLI, N. C. Modelling tensile/compressive strength ratio of artificially cemented clean sand. **Soils and Foundations,** v. 58(1), p. 199-211, 2018. **https://doi.org/10.1016/j.sandf.2017.11.011**

DIAMBRA, A.; IBRAIM, E.; CONSOLI, N. C.; FESTUGATO, L. Theoretical derivation of artificially cemented granular soil strength. **Journal of Geotechnical and Geoenvironmental Engineering,** v. 143(5), p. 1-9, 2017. **https://doi.org/10.1061/(ASCE)GT.1943-5606.0001646**

DIAMBRA, A.; FESTUGATO, L.; CORTE, M. B. Stiffness of artificially cemented sands: insight on characterisation through empirical power relationships. **Road Materials and Pavement Design**, p. 1-11, 2019. **https://doi.org/10.1080/14680629.2019.1705379**

DIAMOND, S. Mercury porosimetry: an inappropriate method for the measurement of pore size distributions in cement-based materials. **Cement and Concrete Research**, v. 30(1), p. 1517-1525, 2000. **https://doi.org/10.1016/S0008-8846(00)00370-7**

DOS SANTOS, A. P. S.; CONSOLI, N. C.; HEINECK, K. S.; COOP, M. R. High-Pressure isotropic compression tests on fiber-reinforced cemented sand. **Journal of Geotechnical and Geoenvironmental**, v. 136(6), p. 885-890, 2010. **https://doi.org/10.1061/(ASCE)GT.1943-5606.0000300**

EKINCI, A.; SCHEUERMANN FILHO, H. C.; CONSOLI, N. C. Copper slag–hydrated lime–Portland cement stabilised marine-deposited clay. **Proceedings of the Institution of Civil Engineers - Ground Improvement**, p. 1-13, 2021. **https://doi.org/10.1680/jgrim.18.00123**. (ahead of print)

ESCALANTE-GARCIA, J. I.; SHARP, J. H. The effect of temperature on the early hydration of Portland cement and blended cements. **Advances in Cement Research**, v. 12(3), p. 121–130, 2000. **https://doi.org/10.1680/adcr.2000.12.3.121**

FEARON, R. E.; COOP, M. R. Reconstitution: what makes an appropriate reference material? **Géotechnique**, v. 50(4), p. 471-477, 2000. **https://doi.org/10.1680/geot.2000.50.4.471**

FEDA, J. **Mechanics of Particulate Materials**. New York: Elsevier, 1982.

FERNANDEZ, A. L.; SANTAMARINA, J. C. Effect of cementation on the small-strain parameters of sands. **Canadian Geotechnical Journal**, v. 38(1), p. 191-199, 2001. **https://doi.org/10.1139/cgj-38-1-191**

FESTUGATO, L. **Comportamento de hidratação e resposta cisalhante cíclica de resíduo de mineração cimentado reforçado com fibras.** 2011. 221 f. Tese (Doutorado em Engenharia) – Programa de Pós Graduação em Engenharia Civil, Universidade Federal do Rio Grande do Sul, Porto Alegre, 2011.

FESTUGATO, L.; FOURIE, A.; CONSOLI, N. C. Cyclic shear response of fibre-reinforced cemented paste backfill. **Géotechnique Letters**, v. 3(1), p. 5-12, 2013. **https://doi.org/10.1680/geolett.12.00042**

FLOSS, M. F. **Parâmetros de controle da resistência e rigidez de solos granulares artificialmente cimentados**. 2012. 183 f. Tese (Doutorado em Engenharia) – Programa de Pós Graduação em Engenharia Civil, Universidade Federal do Rio Grande do Sul, Porto Alegre, 2012.

FONINI, A. **Comportamento mecânico de uma areia cimentada:** análise experimental e micromecânica. 2012. 209 f. Tese (Doutorado em Engenharia) – Programa de Pós Graduação em Engenharia Civil, Universidade Federal do Rio Grande do Sul, Porto Alegre, 2012.

FOPPA, D. **Analise de variáveis-chave no controle da resistência mecânica de solos artificialmente cimentado**. 2005. 144 f. Dissertação (Mestrado em Engenharia) – Programa de Pós Graduação em Engenharia Civil, Universidade Federal do Rio Grande do Sul, Porto Alegre, 2005.

FOPPA, D. **Novo método para cálculo da capacidade de carga de fundações superficiais assentes sobre camada de reforço em solo cimento**. 2016. 229 f. Tese (Doutorado em Engenharia) – Programa de Pós Graduação em Engenharia Civil, Universidade Federal do Rio Grande do Sul, Porto Alegre, 2016.

GAO, J. P-values – a chronic conundrum. **BMC Medical Research Methodology**, v. 20(1). **https://doi.org/10.1186/s12874-020-01051-6**

GIBSON, E. W. The role of p-values in judging the strength of evidence and realistic replication expectations. **Statistics in Biopharmaceutical Research,** v. 13(1), p. 6-18. **https://doi.org/10.1080/19466315.2020.1724560**

GIESCHE, H. Mercury porosimetry: a general (practical) overview. **Part. Part. Syst. Charact.**, v. 23, p. 1-11, 2006.

HARDIN, B. O. The nature of stress-strain behavior of soils. In: FROM VOLUME I OF EARTHQUAKE ENGINEERING AND SOIL DYNAMICS-PROCEEDINGS OF ASCE GEOTECHNICAL ENGINEERING DIVISION SPECIALITYCONFERENCE, 1978, Pasadena, California: **Proceedings…** New York: Geotechnical Engineering Division of ASCE, 1978, p. 3-90.

HEAD, K. H. **Manual of soil laboratory testing volume 3**: effective stress. Chichester: John Wiley and Sons, 1998.

HEINECK, K. S. **Estudo da influência de cimentação induzida sob tensão**. 1998. 118 f. Dissertação (Mestrado em Engenharia) – Programa de Pós Graduação em Engenharia Civil, Universidade Federal do Rio Grande do Sul, Porto Alegre, 1998.

HENZINGER, C; SCHÖMING, P. Prognose der Festigkeitsentwicklung zementbehandelter Böden mit dem Porosity/Binder-Index. **Geotechnik**, v. 43(1), p. 14-25, 2020. **https://doi.org/10.1002/gete.201900017**

HERZOG, A.; MITCHELL, J. K. Reactions Accompanying stabilization of clay with cement. Highway Research Board, v. 36, p. 146-170, 1963.

HO, L. S.; NAKARAI, K.; EGUCHI, K; OGAWA, Y. Difference in Strength Development between cement-treated sand and mortar with various cement types and curing temperatures. **Materials**, v. 13(21), p. 4999, 2020. **https://doi.org/10.3390/ma13214999**

HOCH, B. Z. Misturas de chalk com cimento: estudo da rigidez, resistência e durabilidade. 2017. 146 f. Dissertação (Mestrado em Engenharia) – Programa de Pós Graduação em Engenharia Civil, Universidade Federal do Rio Grande do Sul, Porto Alegre, 2017.

HORPIBULSUK, S.; RACHAN, R.; CHINKULKIJNIWAT, A.; RAKSACHON, Y.; SUDDEPONG, A. Analysis of strength development in cement-stabilized silty clay from microstructural considerations. **Construction and Building Materials** v. 24(10), p. 2011-2021, 2010 **https://doi.org/10.1016/j.conbuildmat.2010.03.011**

IMSEEH, W. G.; ALSHIBI, K. A.; AL-RAOUSH, R. I. Discrepancy in the critical state void ratio of poorly graded sand due to shear strain localization. **Journal of Geotechnical and Geoenvironmental Engineering**, v. 146(8), p. 04020066, 2020.

INGLES, O. G.; METCALF, J. B. **Soil Stabilization**: principles and practices. Sidney: Butterworths, 1972. Geologia Croatica, v. 68(2), p. 139-145, 2015.

IVANIĆ, M.; VDOVIĆ, N., BARRETO, S. de B.; BERMANEC, V.; SONDI, I. Mineralogy, surface properties and electrokinetic behavior of kaolin clays derived from naturally occurring pegmatite and granite deposits.

JARDINE, R. J. J. Some observations on the kinematic nature of soil stiffness. **Soils and Foundations,** v. 32(2), p. 111-124, 1992.

JOHANN, A. D. R. Metodologias para a previsão do comportamento mecânico e para a análise da variação da porosidade de um solo siltoso tratado com cal em diferentes tempos de cura. 2013. 271 f. Tese (Doutorado em Engenharia) – Programa de Pós Graduação em Engenharia Civil, Universidade Federal do Rio Grande do Sul, Porto Alegre, 2013.

KAMRUZZAMAN, A. H. M.; CHEW, S. H.; LEE, F. H. Microstructure of cemented-treated Singapore marine clay. **Proceedings of the Institution of Civil Engineers – Ground Improvement**, v. 10(3), p. 113-123, 2006. **https://doi.org/10.1680/grim.2006.10.3.113**

KHAJEH, A.; MOLA-ABASI, H.; NADERI, S. S. Parameters controlling tensile strength of zeolite-cemented sands. **Scientia Iranica,** v. 26(1), p. 213-233, 2019. **https://doi.org/10.24200/sci.2017.4585**

LA ROCHELLE, P.; LEROUEIL, S.; TRAK, B.; BLAIS-LEROUX, L.; TAVENAS, F. Observational approach to membrane and area corrections in triaxial tests. In: ADVANCED TRIAXIAL TESTING OF SOIL AND ROCK, West Coshohocken, PA: ASTM International, p. 715-731. **https://doi.org/10.1520/STP29110S**

LADD, R. S. Preparing test specimens using undercompaction. **Geotechnical Testing Journal**, v. 1(1), 16-23, 1978. **https://doi.org/10.1520/gtj10364j**

LADE, P. V. **Triaxial testing of soils**. Chichester: Wiley Blackwell, 2016.

LADE, P. V.; OVERTON, D. D. Cementation effects on frictional materials. **Journal of Geotechnical Engineering,** v. 115(10), p. 1373-1387, 1989.

LADE, P. V.; TRADS, N. The role of cementation in the behaviour of cemented soils. **Geotechnical Research**, v. 1(4), p. 111-132, 2014. **https://doi.org/10.1680/gr.14.00011**

LARNACH, W. J. Relationship between dry density, voids/cement ratio and strength of soil-cement mixtures. **Civil Engineering and Public Works Reviews,** v. 55(648), p. 903-905, 1960.

LEE, S.; LEE, D. K. What is the proper way to apply the multiple comparison test? **Korean Journal of Anesthesiology**, v. 71(5), p. 353–360, 2018. **https://doi.org/10.4097/kja.d.18.00242**

LEE, J. K.; SHANG, J. Q. Micropore structure of cement-stabilized gold mine tailings. **Minerals**, v. 8(3), p. 1-9, 2018. **https://doi.org/10.3390/min8030096**

LEON, H. B. **O índice porosidade/teor volumétrico de cimento (η/Civ) como um parâmetro de estado para areias cimentadas**. 2018. 132 f. Dissertação (Mestrado em Engenharia) – Programa de Pós Graduação em Engenharia Civil, Universidade Federal do Rio Grande do Sul, Porto Alegre, 2018.

LEROUEIL, S. VAUGHAN, P. R. The general and congruent effects of structure in natural soils and weak rocks. **Géotechnique,** v. 40(3), p. 467-488, 1990. **https://doi.org/10.1680/geot.1990.40.3.467**

LIU, S. Y.; ZHANG, D. W.; LIU, Z. B.; DENG, Y. F. Assessment of unconfined compressive strength of cement stabilized marine clay. **Marine Georesources and Geotechnology**, v. 26(1), p. 19-35, 2008. **https://doi.org/10.1080/10641190801937916**

LO, S. R.; WARDANI, S. P.R. Strength and dilatancy of a silt stabilized by a cement and fly ash mixture. **Canadian Geotechnical Journal**, v. 39(1), p. 77–89, 2002. **https://doi.org/10.1139/t01-062**

MACCARINI, M. Laboratory studies of a weakly bonded artificial soil. 1987. 334 f. Thesis (Doctor of Philosophy) – Faculty of Engineering, University of London - Imperial College of Science Technology and Medicine, London, 1987.

MAGHOUS, S.; CONSOLI, N. C.; FONINI, A.; DUTRA, V. F. P. A theoretical experimental approach to elastic and strength properties of artificially cemented sand. **Computer and Geotechnics**, v. 62, p. 40-60, 2014. **http://dx.doi.org/10.1016/j.compgeo.2014.06.0**

MALANDRAKI, V.; TOLL, D. Drained probing triaxial tests on a weakly bonded artificial soil. **Géotechnique**, v. 50(2), p. 141-151, 2000. **https://doi.org/10.1680/geot.2000.50.2.141**

MALANDRAKI, V.; TOLL, D. G. The definition of yield for bonded materials. **Geotechnical and Geological Engineering**, v. 14(1), p. 67–82, 1996. **https://doi.org/10.1007/BF00431235**

MARINHO, F. A. M. A técnica do papel filtro para medida de sucção. In: ENCONTRO SOBRE SOLOS NÃO SATURADOS, 1995, Porto Alegre. **Anais...** Porto Alegre: CPGEC/CNPQ/FINESP/FAPERGS/ABMS, 1995, p. 111-125.

MARQUES, S. F. V. **Comportamento de uma areia artificialmente cimentada até altas tensões de confinamento.** 2016. 239 f. Tese (Doutorado em Engenharia) – Programa de Pós Graduação em Engenharia Civil, Universidade Federal do Rio Grande do Sul, Porto Alegre, 2016.

MARTINS, F. B. Investigação do comportamento mecânico de um solo naturalmente estruturado. 2001. 303 f. Tese (Doutorado em Engenharia) – Programa de Pós Graduação em Engenharia Civil, Universidade Federal do Rio Grande do Sul, Porto Alegre, 2001.

MARTINS, F. B.; FERREIRA, P. M. V.; FLORES, J. A. A. F.; BRESSANI, L. A.; BICA, A. V. D. Interaction between geological and geotechnical investigations of a sandstone residual soil. **Engineering Geology**, v. 78(1), p. 1-9, 2005. **10.1016/j.enggeo.2004.10.003**

McHUGH, M. L. Multiple comparison analysis testing in ANOVA. **Biochemia Medica**, v. 21(3), p. 203-209, 2011. **https://doi.org/10.11613/bm.2011.029**

MEYER, K.; KLOBES, P. Comparison between different presentations of pore size distribution in porous materials. **Fresenius Journal of Analytical Chemistry**, v. 363(1), p. 174-178, 1999.

MITCHELL, J. K.; EL JACK, S. A. The Fabric of Soil-Cement and Its Formation. **Clays and Clay Minerals**, v. 14(1), p. 297-305, 1966. **https://doi.org/10.1346/ccmn.1966.0140126**

MITCHELL, J. K.; JARDINE F. M. **A guide to ground treatment.** London: CIRIA, 2002. Technical Report C573.

MITCHELL, J. K.; SOGA, K. **Fundamentals of Soil Behavior.** 3 ed. Hoboken: John Wiley and Sons, 2005.

MOH, Z. Reactions of soil minerals with cement and chemicals. **Highway Research Board**. v. 86, p. 39-60, 1965.

MOLA-ABASI, H.; KHAJEH, A.; NADERI, S. S. Variables controlling tensile strength of stabilized sand with cement and zeolite. **Journal of Adhesion Science and Technology**, v. 32(9), p. 947–962, 2017. **https://doi.org/10.1080/01694243.2017.1388052**

MOONEY, A.; VIGGIANI, M. G. A unique critical state for sand? **Journal of Geotechnical and Geoenvironmental Engineering**, v. 124(11), p 1100-1108, 1998.

MONTGOMERY, D. **Design and analysis of experiments.** 8th edition**.** Hoboken: John Wiley and Sons, 2013.

MOREIRA, E. B.; BALDOVINO, J. A.; ROSE, J. L.; IZZO, L dos S. R. Effects of porosity, dry unit weight, cement content and void/cement ratio on unconfined compressive strength of roof tile waste-silty soil mixtures. **Journal of Rock Mechanics and Geotechnical Engineering**, v. 11(2), p. 369-378, 2019. **https://doi.org/10.1016/j.jrmge.2018.04.015**

MUHUNTHAN, B.; OLCOTT, D. Elastic energy and shear work. Geotechnique, v. 52(7), p. 541–544, 2002. **https://doi.org/10.1680/geot.2002.52.7.541**

NUÑEZ, W. P. **Estabilização físico-química de um solo residual de arenito Botucatu, visando seu emprego na pavimentação.** 1991. 150 f. Dissertação (Mestrado em Engenharia) – Programa de Pós Graduação em Engenharia Civil, Universidade Federal do Rio Grande do Sul, Porto Alegre, 1991.

ODLER, I. Hydration, setting and hardening of Portland cement. In: HEWLETT, P. C. (Org.). **Lea´s Chemistry of Cement and Concrete**. 4 ed. Amsterdam: Butterworth Heinemann, 2004, p. 241 – 297.

PORTLAND CEMENT ASSOCIATION (PCA). **Soil-cement laboratory handbook**. Skokie: PCA, 1995.

PRIETTO, P. D. M. **Estudo do comportamento mecânico de um solo artificialmente cimentado**. 1996. 147 f. Dissertação (Mestrado em Engenharia) – Programa de Pós Graduação em Engenharia Civil, Universidade Federal do Rio Grande do Sul, Porto Alegre, 1996.

PRIETTO, P. D. M. **Resistência e dilatância de solos cimentados:** uma abordagem teórico-experimental. 2004. 229 f. Tese (Doutorado em Engenharia) – Programa de Pós Graduação em Engenharia Civil, Universidade Federal do Rio Grande do Sul, Porto Alegre, 2004.

RAD, N. S.; CLOUGH, G. W. **The influence of cementation of the static and dynamic behavior of sands.** Stanford: University of Stanford – Department of Civil and Environmental Engineering, 1982. Report No. 59.

RANAIVOMANANA, H.; RAZAKAMANANTSOA, A. Toward a better understanding of the effects of cement treatment on microstructural and hydraulic properties of compacted soils. **MATEC Web of Conferences**, v. 163, 06007, 2018. **https://doi.org/10.1051/matecconf/201816306007**

REYNOLDS, O. On the dilatancy of media composed of rigid particles in contact. **The London, Edinburgh and Dublin Philosophical Magazine and Journal of Science**, v. 20(5), p. 469-481, 1885.

RIBEIRO, D.; NÉRI, R.; CARDOSO, R. Influence of water content in the UCS of soil-cement mixtures for different cement dosages. **Procedia Engineering**, v. 143(1), p. 59-66, 2016. **https://doi.org/10.1016/j.proeng.2016.06.008**

RINALDI, V. A.; SANTAMARINA, J. C. C. Cemented soils: small strain stiffness. **Deformational Characteristics of Geomaterials**, v. 1(1), p. 267–273, 2008.

RIOS, S.; VIANA DA FONSECA, A.; BAUDET, B. A. Effect of the Porosity/Cement Ratio on the Compression of Cemented Soil. **Journal of Geotechnical and Geoenvironmental Engineering**, v. 138(11), p. 1422–1426, 2012. **https://doi.org/10.1061/(ASCE)GT.1943-5606.0000698**

RIOS, S.; VIANA da FONSECA, A.; CONSOLI, N. C.; FLOSS, M.; CRISTELO, N. Influence of grain size and mineralogy on the porosity/cement ratio. **Géotechnique Letters**, v. 3(3): 130–136, 2013, https://doi.org/10.1680/geolett.13.00003

ROSCOE, K. H.; SCHOFIELD, A. N. Mechanical behavior of an idealized “wet-clay”. In: EUROPEAN CONFERENCE ON SOIL MECHANICS AND FOUNDATION ENGINEERING, 3., 1963, Wiesbaden, **Proceedings…** 1963. P. 47-54.

ROTTA, G. V. **Cimentação introduzida sob tensão**: compreendendo a importância do índice de vazios de formação da estrutura no comportamento mecânico de solos cimentados. 2000. 134 f. Dissertação (Mestrado em Engenharia) – Programa de Pós Graduação em Engenharia Civil, Universidade Federal do Rio Grande do Sul, Porto Alegre, 2000.

ROTTA, G. V. **Plastificação de um solo cimentado curado sob tensão**. 2005. 152 f. Tese (Doutorado em Engenharia) – Programa de Pós Graduação em Engenharia Civil, Universidade Federal do Rio Grande do Sul, Porto Alegre, 2005.

ROTTA, G. V.; CONSOLI, N. C.; PRIETTO, P. D. M.; COOP, M. R.; GRAHAM, J. Isotropic yielding in an artificially cemented soil cured under stress. **Géotechnique**, v. 53(5), p. 493-501, 2003. **https://doi.org/10.1680/geot.2003.53.5.493**

ROWE, P. W. The stress-dilatancy relation for static equilibrium of an assembly of particles in contact**. Proceedings of the Royal Society of London. Series A. Mathematical and Physical Sciences,** v. 269(1339), p. 500–527, 1962. **https://doi.org/10.1098/rspa.1962.0193**

ROWE, P. W.; PARKIN, A. K. The relationship between the shear strength of sands in triaxial compression, plane strain and direct shear. Géotechnique, v. 20(1), p. 113–115, 1970. **https://doi.org/10.1680/geot.1970.20.1.113**

SALDANHA, R. B.; CONSOLI, N. C. Accelerated mix design of lime stabilized materials. **Journal of Materials in Civil Engineering,** v. 28(3), 2016. **https://doi.org/10.1061/(asce)mt.1943-5533.0001437**

SALDANHA, R. B.; SCHEUERMANN FILHO, H. C.; MALLMANN, J. E. C.; CONSOLI, N. C.; REDDY, K. R. Physical-mineralogical-chemical characterization of carbide lime: an environment-friendly chemical additive for soil stabilization. Journal of Materials in Civil Engineering, v. 30(6), p. 1-7, 2018.

SALDANHA, R. B.; SCHEUERMANN FILHO, H. C.; RIBEIRO, J. L. D.; CONSOLI, N. C. Modelling the influence of density, curing time, amounts of lime and sodium chloride on the durability of compacted geopolymers monolithic walls. **Construction and Building Materials**, v. 136, p. 65-72. **https://doi.org/10.1016/j.conbuildmat.2017.01.023**

SALVATORE, E.; MODONI G.; ANDÒ, E.; ALBANO, M.; VIGGIANI, G. Determination of the critical state of granular materials with triaxial tests. **Soils and Foundations**, v. 57, p. 733-744, 2017. **https://doi.org/10.1016/j.sandf.2017.08.005**

SARAYA, M. E. I. Stopping of cement hydration by various methods. **HBRC Journal**, v. 6(2), p. 46-58, 2010.

SATO, A.; NISHIMOTO, S.; SUZUKI, T. Relationship between curing temperature and strength of stabilized soil. In: 13th INTERNATIONAL CONFERENCE ON COLD REGIONS ENGINEERING. **Proceedings**…Reston: American Society of Civil Engineers, 2006, p. 1-10. **https://doi.org/10.1061/40836(210)41**

SCHEUERMANN FILHO, H. C.; SACCO, R. L.; CONSOLI, N. C. The effect of grain size of ground glass particles on the strength of green stabilized sand. **Soils and Rocks**, v. 43(4), p. 669-677, 2020. **https://doi.org/10.28927/SR.434669**

SCHEUERMANN FILHO, H. C.; SALDANHA, R. B.; da ROCHA; C. G.; CONSOLI, N. C. Sustainable binders stabilizing dispersive clay. **Journal of Materials in Civil Engineering**, v. 33(3), 2021. **https://doi.org/10.1061/(ASCE)MT.1943-5533.0003595**

SCHNAID, F.; PRIETTO, P. D. M.; CONSOLI, N. C. Characterization of cemented sand in triaxial compression. **Journal of Geotechnical and Geoenvironmental Engineering**, v. 127(10), p. 857-868, 2001. https://doi.org/10.1061/(ASCE)1090-0241(2001)127:10(857)

SHARMA, S. S.; FAHEY, M. Degradation of Stiffness of cemented calcareous soil in cyclic triaxial tests**. Journal of Geotechnical and Geoenvironmental Engineering**, v. 129(7), p. 619–629, 2003. **https://doi.org/10.1061/(asce)1090-0241(2003)129:7(619)**

SHIHATA, S. A.; BAGHDADI, Z. A. Long-term strength and durability of soil cement. **Journal of Materials in Civil Engineering**, v. 13(3), p. 161–165, 2001. **https://doi.org/10.1061/(ASCE)0899-1561(2001)13:3(161)**

STRACKE, F.; JUNG, J. G.; KORF, E. P.; CONSOLI, N. C. The influence of moisture content on tensile and compressive strength of artificially cemented sand. **Soils and Rocks**, v. 35(3), p. 303-308, 2012.

SUDDEEPONG, A.; INTRA, A.; HORPIBULSUK, S.; SUKSIRIPATTANAPONG, C.; ARULRAJAH, A.; SHEN, J. Durability against wetting-drying cycles for cement-stabilized reclaimed asphalt pavement blended with crushed rock. Soils and Foundations, v. 58(2), p. 333-343, 2018. **https://doi.org/10.1016/j.sandf.2018.02.017**

TAYLOR, H. F. W. **Cement Chemistry**. 2 ed. London: Thomas Telford, 1997.

TOMASI, L. F. **Comportamento mecânico de resíduo de mineração estabilizado com cimento**. 2018. 151 f. Dissertação (Mestrado em Engenharia) – Programa de Pós Graduação em Engenharia Civil, Universidade Federal do Rio Grande do Sul, Porto Alegre, 2018.

TREZZA, M. A. Hydration study of ordinary Portland cement in the presence of zinc ions. **Materials Research**, v. 10(4), p. 331-334, 2007.

TRHLÍKOVÁ, J.; MAšÍN, D.; BOHÁč, J. Small-strain behaviour of cemented soils. **Géotechnique**, v.62(10), p. 943-947, 2012. **https://doi.org/10.1680/geot.9.p.100**

URAL, N. The significance of scanning electron microscopy (SEM) analsysis on the microstructure of improved clay: an overview. **Open Geosciences**, v.13(1), p. 197-218, 2020.

VAUGHAN, P. R.; MACCARINI, M.; MOKHTAR, S. M. Indexing the engineering properties of residual soil. **Quarterly Journal of Engineering Geology**, v. 21(1), p. 69–84, 1988. **https://doi.org/10.1144/gsl.qjeg.1988.021.01.05**

VIGGIANI, G.; ATKINSON, J. H. Stiffness of fine-grained soil at very small strains. **Géotechnique**, v. 45(2), p. 249-265, 1995.

WILD, S.; ARABI, M.; ROWLANDS, G. O. Relation between pore size distribution, permeability, and cementitious gel formation in cured clay-lime systems. **Materials Science and Technology (United Kingdom)**, v. 3(12), p. 1005-1011. 1987. **https://doi.org/10.1179/mst.1987.3.12.1005**

WINSLOW, D. N.; LOVELL, C. W. Measurements of pore size distributions in cements, aggregates and soils. **Powder Technology**, v. 29(1), p. 151-165, 1981. **https://doi.org/10.1016/0032-5910(81)85013-9**

WINTER, D. Resistência, rigidez, e durabilidade de solos arenosos estabilizados com materiais mais sustentáveis. 2018. 166 f. Tese (Doutorado em Engenharia) – Programa de Pós Graduação em Engenharia Civil, Universidade Federal do Rio Grande do Sul, Porto Alegre, 2018.

WROTH, C. P.; BASSETT, R. H. A stress-strain relationship for the shearing behaviour of a sand. **Géotechnique**, 15(1), p. 32–56, 1965. **https://doi.org/10.1680/geot.1965.15.1.32**

YAO, K.; LI, N.; CHEN, D. H.; WANG, W. Generalized hyperbolic formula capturing curing period effect on strength and stiffness of cemented clay. **Construction and Building Materials**, v. 199(1), p. 63-71. **https://doi.org/10.1016/j.conbuildmat.2018.11.288**

YU; Hai-Sai. **Plasticity and geotechnics.** New York: Springer, 2006.

YUN, T. S.; SANTAMARINA, J. C. Decementation, softening, and collapse: changes in small-strain shear stiffness in k_0 loading. **Journal of Geotechnical and Geoenvironmental Engineering**, v. 131(3), p. 350-358, 2005. **https://doi.org/10.1061/(ASCE)1090-0241(2005)131:3(350)**

YU, C.; WANG, H.; ZHOUG, A.; CAI, X.; WU, Z. Experimental study on strength and microstructure of cemented soil with different suctions. **Journal of Materials in Civil Engineering**, v. 31(6), p. 04019082, 2019. **10.1061/(ASCE)MT.1943-5533.0002717**

ZDRAVKOV, B. D.; CERMÁK, J. J.; SEFARA, M, JANKU, J. Pore classification in the characterization of porous materials: a perspective. **Central European Journal of Chemistry**, v. 5(2), p. 385-395. **10.2478/s11532-007-0017-9**

ZHANG, R. J.; LU, Y. T.; TAN, T. S.; PHOON, K. K.; SANTOSO, A. M. Long-term effect of curing temperature on the strength behavior of cement-stabilized clay. **Journal of Geotechnical and Geoenvironmental Engineering,** v. 140(8), p. 04014045, 2014. **https://doi.org/10.1061/(asce)gt.1943-5606.0001144**

ZHANG, R.; QIAO, Y.; ZHENG, J.; DONG, C. A method for considering curing temperature effect in mix proportion design of mass cement-solidified mud at high water content. **Acta Geotechnica**, v. 16(1), p. 279-301, 2020. **https://doi.org/10.1007/s11440-020-00961-5**

ZHANG, X.; ZHU, Z. Study on the relationship between microstructure and strength of stabilized/solidified silt. **International Journal of Structural and Civil Engineering**, v. 7(1), p. 65-71, 2018. **https://doi.org/10.18178/ijscer.7.1.65-71**

ZHANG, Z. TAO, M. Durability of cement stabilized low plasticity soils. **Journal of Geotechnical and Geoenvironmental Engineering**, v. 134(2), p. 203-213, 2008. **https://doi.org/10.1061/(asce)1090-0241(2008)134:2(203)**

APPENDIX A – DATA USED FOR THE INITIAL SHEAR MODULUS MODEL

Dosage	ν	C_{iv}	η	C (%)	T	λ	$p_e´$	$p^*_e´$	$p_e´/p^*_e´$	$G_{0\,(kPa)}$	$G_{0,p}$	$G_0/p_e´$	$\eta/(C_{iv})^b$
5	1,588799	0,78143	37,05938	1,5	2,0043	0,067	493,4923	189,0111	2,610917	706830,3	710435,2	154573,1	39,46567
	1,586725	0,782451	36,9771	1,5	2,0043	0,067	509,0088	194,954	2,610917	728376,8	716842,1	157861,3	39,36493
	1,591791	0,779961	37,17769	1,5	2,0043	0,067	471,9386	180,7559	2,610917	716658,8	701293,8	158765,3	39,61067
11	1,4472	1,139136	30,90104	2	2,0116	0,067	4554,563	1564,354	2,911466	1420408	1432282	168289,1	29,8911
	1,449934	1,136988	31,03134	2	2,0116	0,067	4372,441	1501,8	2,911466	1410825	1415431	169143,6	30,03159
	1,45879	1,130086	31,45003	2	2,0116	0,067	3831,06	1315,853	2,911466	1348841	1362202	168031,5	30,48411
15	1,429083	1,71622	30,02504	3	2,0262	0,067	7421,97	2050,077	3,620337	1862625	1848165	204038,4	26,16069
	1,416236	1,731788	29,39029	3	2,0262	0,067	8990,661	2483,377	3,620337	1928947	1953844	199874,7	25,54872
	1,41579	1,732334	29,36803	3	2,0262	0,067	9050,76	2499,977	3,620337	1967431	1957622	203468,9	25,52732

APPENDIX B – STIFFNESS PROPERTIES IN THE TRIAXIAL TESTS

$\eta/(C_{iv})^{0,28}$	Mix Design	σ'_3	P$_1$		P$_2$		E_{sec} (MPa)		
			ε_a (%)	q (kPa)	ε_a (%)	q (kPa)	$\varepsilon_a = 0,1\%$	ε_a (peak)	$\varepsilon_a = 1,0\%$
45	16,1 kN/m³ - 1% C	35	0,03	60	0,3	158	98	27	20
	14,9 kN/m³ - 2%C	35	0,08	33	0,08	33	38	7	10
35	18,6 kN/m³ - 1%C	35	0,08	65	0,8	332	62	38	33
		70	0,07	120	0,65	478	150	69	45
		140	0,07	163	0,55	602	250	70	75
	15,0 kN/m³ - 5%C	35	0,08	101	0,8	252	120	40	33
		70	0,08	312	0,5	525	315	55	45
		140	0,07	370	0,3	540	400	23	75
30	18,3 kN/m³ - 2%C	35	0,075	155	0,5	520	108	59	40
		70	0,15	292	0,45	606	200	120	28
		140	0,06	335	0,43	747	400	94	100
	16,0 kN/m³ - 6%C	35	0,04	153	0,5	550	110	97	48
		70	0,035	337	0,3	667	400	266	50
		140	0,03	340	0,3	733	600	164	100
25	18,8 kN/m³ - 3%C	35	0,03	335	0,3	1260	690	329	26
	16,9 kN/m³ - 8%C	35	0,06	715	0,45	1540	750	340	120
20	19,0 kN/m³ - 6,5%C	35	0,06	1115	0,45	2754	1300	404	23
	18,3 kN/m³ - 10%C	35	0,15	2510	0,5	3300	2000	715	95